May 2019

Determining Wind Turbine Drivetrain Test Bench Capability to Replicate Dynamic Loads: Evaluation Methods and Their Validation

Philippe Giguère
Clemson University, philippegiguere@charter.net

DETERMINING WIND TURBINE DRIVETRAIN TEST BENCH CAPABILITY TO REPLICATE DYNAMIC LOADS: EVALUATION METHODS AND THEIR VALIDATION

A Dissertation
Presented to
the Graduate School of
Clemson University

In Partial Fulfillment
of the Requirements for the Degree
Doctor of Philosophy
Mechanical Engineering

---

by
Philippe Giguère
May 2019

Accepted by:
Dr. John R. Wagner, Committee Chair
Dr. Richard S. Figliola
Dr. Gregory M. Mocko
Dr. Edward R. Collins

ABSTRACT

Wind turbine drivetrain test facilities are impressive laboratories that offer a controlled environment to test the response of drivetrains under design and conditions. The stochastic nature of the wind results in highly dynamic loads and this is reflected in the design standards and certification process of wind turbines. A wide range of wind conditions and turbine operating states are prescribed as design load cases. The design process of a wind turbine yields thousands of time series of fluctuating forces, bending moments and speed to cover these design load cases. The capability of a test bench to replicate such dynamic loads has been the subject of this research at Clemson University in cooperation with GE Renewable Energy.

This collaborative research project used the 7.5-MW test bench of Clemson University to test two multi-MW drivetrain designs used on GE onshore wind turbines. This testing provided the first demonstration that the design load cases that typically drive the design of wind turbine drivetrains can be replicated on a test bench with an acceptable accuracy. The acceptance threshold for the accuracy was found to vary depending on the specific loads. The yaw and nodding bending moments are most critical to replicate accurately due to being generally much larger than the forces, and the measurement error of the load application unit of the test bench was demonstrated to be an appropriate threshold based on multibody simulations. The dynamic response of one of the drivetrains tested was simulated using inputs to the model with and without the measured tracking error. This is the error between the loads commanded to the test bench and the loads that are measured at the point of application. For the drivetrain displacements considered, the multibody simulations quantified the impact of the tracking error on the displacements

to be within 11% of the peak displacement. Most displacements were within 2.6%-3.1% of the peak displacement on average.

Multibody simulations were also used to quantify the impact of a cross-coupling effect between forces and bending moments that occurs when the load application unit of the test bench applies loads dynamically. The impact on the dynamic response of the drivetrain from the cross-coupling was found to be generally small and acceptable despite significant tracking error on the forces. The testing also served as experimental verification of a novel method for the early assessment of the capability of a test bench to replicate dynamic loads. The identification of load time series that should be replicated with an acceptable level of accuracy and those that are likely beyond the capability of the test bench was validated.

A new avenue of research in the wind energy sector has been initiated, and several recommendations are proposed for growing the knowledge base and the role of test benches for design certification purposes.

DEDICATION

To my wife Barbara and late Dr. Andrei Mander.

ACKNOWLEDGMENTS

This research was sponsored by the Clemson University Restoration Institute (CURI) for four years and I am thankful to have been given the opportunity to define and pursue the research documented in this dissertation.

Several circumstances had to happen for this research to take place and they somehow did. A chance encounter with Mr. Paul Meyers (GE retired) set the wheels in motion to this research and I thank Paul for making me aware of the graduate assistantship opportunity focused on the utilization of Clemson's wind turbine drivetrain test benches. The foresight of Dr. Nick Rigas and late Dr. Andrei Mander from Clemson University opened the door to a non-traditional student and provided freedom. They have my gratitude. Mr. Mark Johnson and Mr. Paul Judge for GE Renewable Energy made the essential support from GE possible. Herr Hartmut Scholte-Wassink, Dr. Tom Fric, Dr. Anurag Gupta, Mr. Darren Danielsen, and Dr. Ed Hall honored the commitment made by Mark and allowed the continuation of this research to the end. I thank these GE leaders for supporting this highly unusual arrangement.

I want to express my gratitude to my adviser, Dr. John Wagner, who understood how to advise a non-traditional student and always saw a bright side even when progress was slower than planned due to the demands of my employment at GE Renewable Energy. Dr. Wagner was most patient and understanding in advising this research.

I also thank my committee members, Dr. Richard Figliola and Dr. Greg Mocko from the Mechanical Engineering Department, and Dr. Randy Collins from the Electrical and Computer Engineering Department. Special thanks to Dr. Collins for taking over the late Dr. Andrei Mander who I miss dearly.

I thank Dr. Curtiss Fox from the Energy Innovation Center of Clemson University for being supportive of this research and fostering a cooperative environment with GE Renewable Energy.

I was fortunate to be surrounded with talented engineers who were always willing to help. I am particularly grateful to Dr. Amin Bibo from the Energy Innovation Center of Clemson University who helped in countless ways including challenging my thinking and offering alternative views. His predecessor, Dr. Ryan Schkoda, also provided valuable support. I also want to thank Dr. Meghashyam Panyam and Mr. Konstantin Bulgakov, also from the Energy Innovation Center of Clemson University, for running the test bench outside of normal operating hours during my tests. Dr. Bibo and Dr. Panyam provided the Simpack model used in this research, which was very much appreciated.

The publication of my research required internal reviews at GE and I want to acknowledge the support I received from five GE colleagues: Mr. David Crichton, Mr. Jim Madge, Mr. Brandon Gerber, Mr. Jim Davidson, and Mr. Robert Huck. I thank them for diligently reviewing my publications. Dave, Jim, and Brandon are Chief Engineers at GE Renewable Energy and they are among the best engineers I have worked with. I am thankful for their input. I want to also acknowledge the support I received from the late Bill Holley, who was another Chief Engineer at GE Renewable Energy.

My thanks also goes to Dr. Gerard from the Mathematical Sciences Department at Clemson University for his guidance with the analysis of my test data, and to Mr. Andrew Edmunds for welcoming me in the office space of the Risk Engineering and System Analytics (RESA) Center of Clemson University. The office of RESA provided a perfect environment to write the bulk of this dissertation.

TABLE OF CONTENTS

Page

Table of Contents (Continued)

Page

Table of Contents (Continued)

Page

LIST OF TABLES

List of Tables (Continued)

LIST OF FIGURES

List of Figures (Continued)

Figure Page

List of Figures (Continued)

Figure Page

List of Figures (Continued)

Figure Page

List of Figures (Continued)

Figure Page

List of Figures (Continued)

Figure Page

List of Figures (Continued)

Figure Page

List of Figures (Continued)

Figure Page

List of Figures (Continued)

Figure Page

List of Figures (Continued)

Figure Page

NOMENCLATURE

Symbol	Description [units]
CI	Confidence interval
Cov	Coverage error
CR	Capability ratio
DLC	Design loads coverage
FF	Feed-forward
Fr	Resultant shear force [kN]
Fx	Vertical shear force, positive downwards [kN]
Fy	Lateral shear force, positive to the right side of turbine facing wind [kN]
Fz	Axial shear force, positive along wind direction [kN]
HIL	Hardware-in-the-loop
IEA	International Energy Agency
IEC	International Electromechanical Commission
J	Maximum number of time steps
Q	Magnitude of LAU input [kN or kNm]
Qt	Truncated magnitude of LAU input [kN or kNm]
$\dot{Q}$	Ramp rate of LAU input [kN/s or kNm/s]
LAU	Load application unit
LSrpm	Rotational speed of the test bench [rpm]
M	Measurement
Mr	Resultant bending moment [kNm]
ms	Millisecond

Nomenclature (Continued)

Symbol	Description [units]
Mx	Yaw bending moment, positive is CW direction [kNm]
My	Tilt bending moment, positive is CCW direction [kNm]
Mz	Torque, positive is CW direction [kNm]
NO	Normal operation
NR	Non-rotating
RR	Ramp rate
SD	Shut down
Spd	Rotational speed of the test bench [rpm]
s	Second
T_d	Feed-forward gain
TP	Test profile
t	Time [sec]

Superscript	Description
±	Test profile corresponding to maximum (+) and minimum (–) magnitude of a given load

Subscript	Description
i	Index representing the LAU inputs
j	Index representing time (time step)
L	Test bench limit
m	Magnitude [force or moment]
rr	Ramp rate [force or moment /sec]

CHAPTER ONE

INTRODUCTION

The wind industry has experienced large growth over the last two decades throughout the world. This growth has occurred in both the number of installed onshore and offshore wind turbines, as well as their physical size. The global wind power capacity has increased nearly 24 fold since 2001 [1]. A 1.5-MW wind turbine, which was considered large in 2001, is now on the small end of utility scale wind turbines with most new wind turbines have a rated power in the 2-3 MW range. Advancements in wind turbine technology has played a key role in this growth, and large financial investments in ground-based testing facilities have been made to further drive improvements. In particular, several drivetrain/nacelle testing facilities have been developed over the last 7 years [3-8] to test large multi-MW wind turbines. Table 1.1 summarizes these test facilities and offers references providing more details on their specific test benches, which are also referred to as test rigs. The drivetrain of a wind turbine is often tested within the entire nacelle.

Testing in a laboratory environment offers the obvious advantage of controlling the loads that are applied to the mechanical drivetrain whereas a wind turbine prototype is subject to stochastic loads. This is particularly important because the certification of new designs will generally include load cases that cannot be readily duplicated in the field. A test bench provides the opportunity to test these load cases, which may drive the design of the drivetrain components. Fluctuating loads from turbulent wind conditions can also drive the design of drivetrain components. The range of fluctuations that can be applied by a test bench depends on its underlying dynamic capability and the properties of the drivetrain being tested.

Table 1.1: Recent wind turbine nacelle/drivetrain test facilities.

Facility	Resources	Location
Center for Wind-Power Drives	4 MW Test Rig [2,3]	Aachen, Germany
Clemson University	7.5-MW and 15 MW Test Benches [4]	N. Charleston, SC, USA
Fraunhofer Institute for Wind Energy	10-MW Dynamic Nacelle Testing Laboratory [5]	Bremerhaven, Germany
Lindoe Offshore Renewables Center	Nacelle Mechanical Test Dock (10-MW) [6]	Munkebo, Denmark
National Renewable Energy Laboratory	5-MW Dynamometer [7]	Golden, CO, USA
ORE Catapult National Renewables Energy Center	15-MW Test Bench [8]	Blyth, U.K.

For the case of validating a new drivetrain design and the models used in their design, the loads that drove the design of the drivetrain components are of particular interest. If the purpose of testing is to investigate a component degradation and/or failure, the loads of interest are those covering the range corresponding to the operational conditions preceding the anomaly. Another example for using a drivetrain test bench is to test a design change in which case the loads of interest may be the design loads or the loads that preceded an event resulting in a failure. Independent of the reason to test, the selected test bench should have the capability to replicate the loads of interest with minimum tracking error, i.e., small differences between the loads the test bench applies and the commanded loads.

The loads of interest can be defined in terms of magnitude and rate of change as a function of time. If a test bench has greater capability than the magnitude and ramp rate time series of the loads of interest, the tracking error should only reflect the performance of the test bench controller. Otherwise, the tracking error also reflects the additional error due to the hardware limitation of the test bench.

1.1 Literature review

The capability of a test bench refers to having the hardware and software control algorithms to replicate the desired loads onto the drivetrain. The International Energy Agency (IEA) published a compilation of testing centers for wind turbine blades and nacelles [9] as part of its Wind Task 35, which focused on ground based testing for wind turbines and their components. This compilation provides a summary of the capabilities of public and private testing centers for wind turbine drivetrains/nacelles. Included in this summary are the maximum power and torque of the motor drive, the maximum forces and bending moments that the test bench can apply to the test article, and a binary evaluation of the availability to emulate the wind and the grid real-time. The testing facilities listed in Table 1.1, which are the most recent public facilities, are included in the IEA Wind Task 35 compilation, which dates to May 2016. In terms of determining the capability of a test bench to replicate loads of interest, this compilation from IEA Wind Task 35 can be useful when testing static loads, but it is insufficient to evaluate the capability of a test bench to replicate dynamic loads. There is no quantification of the rate at which the torque, moments, forces, and speed can be varied. This is likely due to this information being deemed proprietary by the different test bench operators. The IEA Wind Task 35 summary document [9] includes the statement that some capabilities are confidential and not meant for publication.

The first and only attempt of quantifying the capability of a test bench to replicate dynamic loads appears to be the work of Leupold from the Center for Wind Power Drives at the University of Aachen in Germany. Specifically, Leupold modeled the capability of the 4-MW test bench at the University of Aachen [2,3] to apply dynamic loads using co-simulation with the multibody simulation software Simpack and Matlab/Simulink. The

structural components of the test bench and the test article were modeled with Simpack, and Matlab/Simulink was used to model the controller of the test bench. The hydraulics of the test bench were modeled using the AmeSim software. The AmeSim model was imported into Matlab/Simulink such that the co-simulations were done with Simpack and Matlab/Simulink. The modeling results were compared with experiments in which the LAU replicated dynamic loads to a reaction frame in lieu of having a drivetrain connected to the test bench. Dynamic loads applied in the form of sine waves of different amplitudes and frequencies were commanded by the test bench controller. No experiment was conducted with a drivetrain installed on the test bench. Accordingly, the co-simulation model could only be validated with the six piston pairs of the LAU being operated in position control. The agreement of the modeling results with experiments when comparing frequency spectra were mixed. Specifically, the agreement was good at low frequencies after which the agreement deteriorated. Two lessons learned from the work of Leopold were that the test bench controller must be modeled, and modeling the friction in the piston is important to achieve a good agreement between the model and the experimental results. This work of Leupold has not been presented at a conference nor published in a Journal. The only documentation is in a master thesis at the University of Aachen in German that has not been released publicly. A request for this thesis made to the author was not granted. Therefore, no public records of the work of Leupold could be obtained, and the information communicated above is solely based on a personal communication (S. Leupold and S. Reisch, Research Associate and Scientific Assistant, RWTH, Aachen University, Germany, personal communication, March 20, 2017). Nevertheless, this early work of Leupold indicates an interest in testing a wind turbine drivetrain with dynamic loads and suggests one approach to determine the capability of a test bench to replicate dynamics loads.

Beside the work of Leupold, the European Project for procedures to test and measure wind energy systems (PROTEST) [10] offers a comprehensive set of recommendations for modeling mechanical components and validating the models. However, the focus is on using wind turbine prototypes for measurements. The use of a drivetrain test bench does not appear to have been considered, which is not surprising given that this work preceded the expansion of wind turbine drivetrain test facilities and creation of most of the facilities listed in Table 1.1. Nevertheless, the PROTEST project also defined new design load cases for mechanical components that can be considered when testing a drivetrain design on a test bench. The PROTEST project has a website providing more details about the project [11].

Relevant to this research are the development of controls methods for wind turbine test benches [12-18], which are important for minimizing tracking error, and modeling capability [19-23]. Measurements made on wind turbine drivetrain test benches have been used to validate models [24-28], and modeling has been used to investigate the change in drivetrain dynamic response from the different boundary conditions between a test-bench setup vs. a field turbine [29]. This change is referred to as the effect of abstraction, which was found to induce frequency content in the range of 5-6 Hz under ideal test bench conditions that can be mitigated with filtering the inputs loads to the LAU [29]. The effect of abstraction has been discussed within the IEA Wind Task 35 with the conclusion that most of the 29 abstractions identified can be mitigated [30]. Overall, IEA Wind Task 35 concluded that results from a test bench are expected to be comparable to in-field conditions, which is rightfully stated as a major requirement for valuable test procedures of wind turbine drivetrains/nacelles [31]. Another outcome of IEA Wind Task 35 was the creation of a framework of test load cases to be applied to the main shaft of

the drivetrain [31]. These test load cases refer to the IEC 61400-1 design load cases (DLCs), which are described in Section 1.4 of this dissertation. This research is directly applicable to the work of IEA Wind Task 35, but it was closed in Oct. 2017.

Another area of research with wind turbine drivetrain/nacelle test benches is the development of hardware-in-the-loop (HIL) testing strategies [32-36]. In brief, HIL consists of coupling the test bench and the full-scale drivetrain/nacelle including the wind turbine controller to a simulation system that models the wind and missing wind turbine components (rotor and full1-length tower) in order to emulate field conditions. The wind model in a HIL testing arrangement yields dynamic inputs to the LAU of the test bench, and thus this research is complementary to HIL development.

Overall, the review of the literature indicates that the research has focused on the drivetrain/nacelle test benches themselves, which is not surprising considering that these ground-based testing facilities are relatively new. The utilization of these facilities is gaining greater acceptance. Wind turbine manufacturers have announced plans to test their latest designs on a wind turbine test bench [37-39] and a wind turbine drivetrain test bench was recently used to investigate a new condition monitoring system [40]. The surveyed literature does not provide guidance for determining the capability of a test bench to replicate dynamics loads. This statement was corroborated by several participants at the Wind Power Drives conference held in Aachen Germany on March 7-8, 2017. Furthermore, the only known indication of dynamic capability of a wind turbine drivetrain/nacelle test bench is that of Clemson's 7.5-MW test bench from this research [41-44]. This outcome from the literature review points to the opportunity to charter a new research and development area for wind turbine drivetrain test benches. This research took aim at this opportunity.

1.2 Motivation

As it will be explained in Section 1.4, most wind turbine design conditions result in dynamic loads and thus replicating these loads using a test bench is important and the motivation for this research is twofold. First, a wind turbine manufacturer should be able to know *a priori* what design loads of a drivetrain of interest can be replicated with a given test bench. At this time, no documented method is available to do such evaluation per the surveyed literature. Second, wind turbine manufacturers and drivetrain test bench operators should know the level of accuracy that is needed for replicating design loads and there is no guideline available.

The first motivation of not having a method for evaluating the capability of a test bench to replicate loads of interest mainly relates to the early identification of any shortcoming in capability. Any deficiency can then be addressed jointly by the wind turbine manufacturer and the test bench operator. Given the significant cost of testing on a full-scale wind turbine drivetrain test bench, informed decisions can be made using a validated methodology.

The second motivation of not having defined targets for the accuracy of the actual loads applied by the LAU as compared with the commanded loads to the LAU is critical for empowering informed decisions. The interpretation of results from an evaluation method for the capability of a test bench to replicate design loads without defined accuracy targets is subjective and may drive the cost of testing to an unnecessary level. This type of scenario can be avoided with demonstrated guidelines.

The use of a wind turbine test bench for replicating dynamic loads is in its infancy and this research is a first attempt to close the gap between this maturity level and the

expectations of the IEC 61400-1 standard [45]. The IEC 61400-1 standard defines design load cases that are primarily dynamic rather than static. There is certainly merit in testing drivetrains under static loads, however, the motivation of this research is to promote testing under dynamic loads.

1.3 General description of a wind turbine drivetrain test bench

A schematic of a typical wind turbine drivetrain test bench setup is shown in Fig. 1.1. The drivetrain, which is referred to as the test article in the remaining of this document, is connected to the test bench and to the ground using machined parts referred to as the adapters. These adapters are typically specifically designed for a test article. The test bench consists of several components: one or multiple motors, a gearbox, and a load application unit (LAU). The load application unit applies non-torque loads to the test article at the point of application, which is indicated with a red circle in Fig. 1.1. The design of a test bench typically includes adjustments to accommodate drivetrain tilt angles. Note that some test benches do not have a load application unit because they only apply torque loads to the test article, and others are direct drive and have no gearbox. This research is relevant to test benches that can apply both non-torque and torque loads.

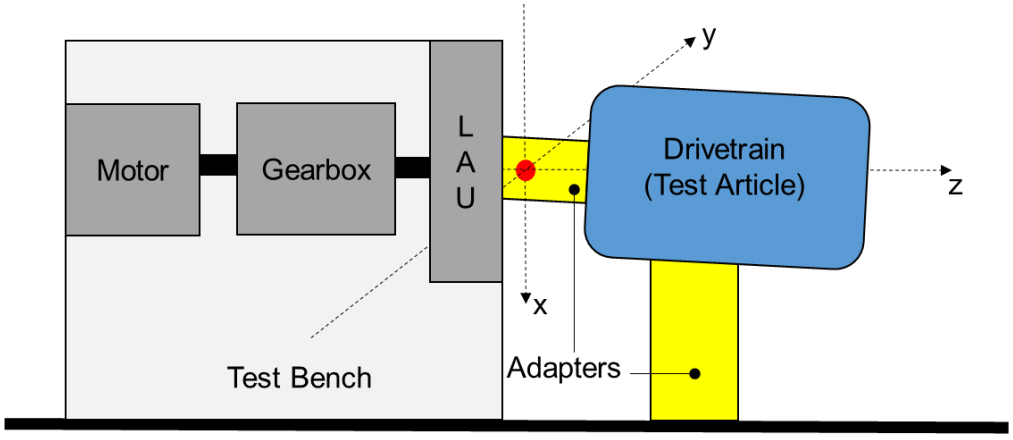

Figure 1.1: Typical wind turbine drivetrain test bench schematic.

The load application unit is designed with a targeted range of non-torque loads, torque, and rotational speeds to accommodate wind turbines of a particular size. The desired capability to change the loads and speed as a function of time (ramp rates) is an important design driver of the overall test bench. The supporting hardware of a test bench yields limits for both loads magnitude and the ramp rate of the loads over time. The test article itself influences the maximum and minimum loads magnitude and ramp rate that a test bench can achieve, but this is a limitation of the drivetrain design, and not of the test bench. For a given load (e.g., the vertical force, Fx), the capability of the test bench for the magnitude and ramp rate, without consideration to the test article, defines the nominal capability of a test bench. The stiffer the test article, the closer the test bench capability for that test article is to the nominal capability. The nominal test bench capability for magnitude is typically defined by assuming an infinitively stiff drivetrain. For the ramp rate, the nominal test bench capability is also influenced by the test bench controller. The change in loads must be done in a stable manner and the nominal capability for the ramp rate can be based on demonstrated capability with other drivetrain designs. All test benches listed in Table 1.1 should have a certain level of demonstrated dynamic capability. Given that the test bench controller can be tuned, the ramp rate limits often have greater growth potential than the limits on the load magnitudes. Accordingly, the capability of a test bench refers to nominal capability, which is defined using a limit on magnitude and ramp rate for the quantities listed in Table 1.2.

The magnitude and ramp rate limits defining the nominal capability of the test bench are implemented in its controller to protect the test bench. During a test, the controller commands the non-torque loads (Fx, Fy, Fz, Mx, and My) and either the torque (Mz) or the speed (Spd) depending on the control approach used with the test bench.

Specifically, a total of six time series are prescribed concurrently giving one test profile, and all test profiles are subject to the limits defining the nominal test bench capability.

Table 1.2: Generic test bench nominal capability.

LAU Input	Magnitude Limit	Ramp Rate Limit
Fx	$\pm Fx_L$	$\pm Fx_{rrL}$
Fy	$\pm Fy_L$	$\pm Fy_{rrL}$
Fz	$\pm Fz_L$	$\pm Fz_{rrL}$
Mx	$\pm Mx_L$	$\pm Mx_{rrL}$
My	$\pm My_L$	$\pm My_{rrL}$
Mz	$\pm Mz_L$	$\pm Mz_{rrL}$
Spd	Spd_L	$\pm Spd_{rrL}$

The nominal capability of a test bench can be compared with the test profiles of interest for a particular wind turbine drivetrain, which are referred to as the design loads. This comparison provides two useful metrics to plan a test campaign, namely the test bench coverage and the test bench capability ratio. Before describing a method for evaluating the loads coverage of a test bench and its capability ratio, an overview of the load cases that must be considered in the design of a wind turbine is presented. These design load cases yield the test profiles of interest.

1.4 Wind turbine design load cases

The design loads (forces and bending moments) of a wind turbine are calculated loads from various operational conditions and situations defined by certification standards. Most wind turbine designs are certified to the IEC standards [45] and/or Germanisher Lloyd (GL) requirements [46], and the operational conditions and situations are referred to load cases. The IEC 61400-1 standard [45] defines a total of 22 load cases covering both fatigue and extreme loading. Each of the load cases includes variants covering different internal conditions of the wind turbine (operating states) and external conditions replicated on the wind turbine. The operating state is either normal power production or

operation with a particular fault of the turbine itself (e.g., failure of the blade pitch system), or a fault of the electrical grid. All load cases and their variants (subcases) typically amounts to over 10,000 simulations carried out using a model representing the wind turbine and its controls system. The resulting loads from simulations (simulated loads) of extreme load cases are scaled by a partial load safety factor of 1.1, 1.35, or 1.5 depending on the load case [45] to obtain the design loads. Fatigue loads are not scaled, and thus design loads are the same as simulated loads for fatigue.

The load cases are 1-10 minutes long. A representative example of a load time series relevant to the drivetrain and the corresponding time series of the ramp rates are given in Fig. 1.2. Both the load magnitudes and the ramp rate have been normalized due to the proprietary nature of these data. The time step in this example is 40 ms, and both the positive and negative loads are of interest. Accordingly, there is typically at least two test profiles of interest for each LAU input except for speed. The ability of a test bench to apply a time series such as that shown in Fig. 1.2 is the question being addressed and metrics called coverage error and capability ratio are used for that purpose.

The load cases required by the IEC covers the following situations:

- Power production under normal operation with either typical or extreme turbulence, or subject to an extreme change in wind direction or wind shear.
- Power production with the wind turbine experiencing a fault (several must be modeled) or a grid-loss event under normal wind conditions. The load case specific to internal or external electrical faults calls for combining such a fault with an extreme wind gust.
- Startup of the wind turbine.
- Normal and emergency shutdown of the wind turbine.

- Parked or idling wind turbine subjected to an extreme wind gust having a recurrence period of 50-years (no internal or external fault) or 1-year (with a grid-loss event).
- Parked or idling wind turbine with fault conditions subjected to an extreme wind gust having a recurrence period 1-year.
- Transport, assembly, maintenance, and repair of the wind turbine.

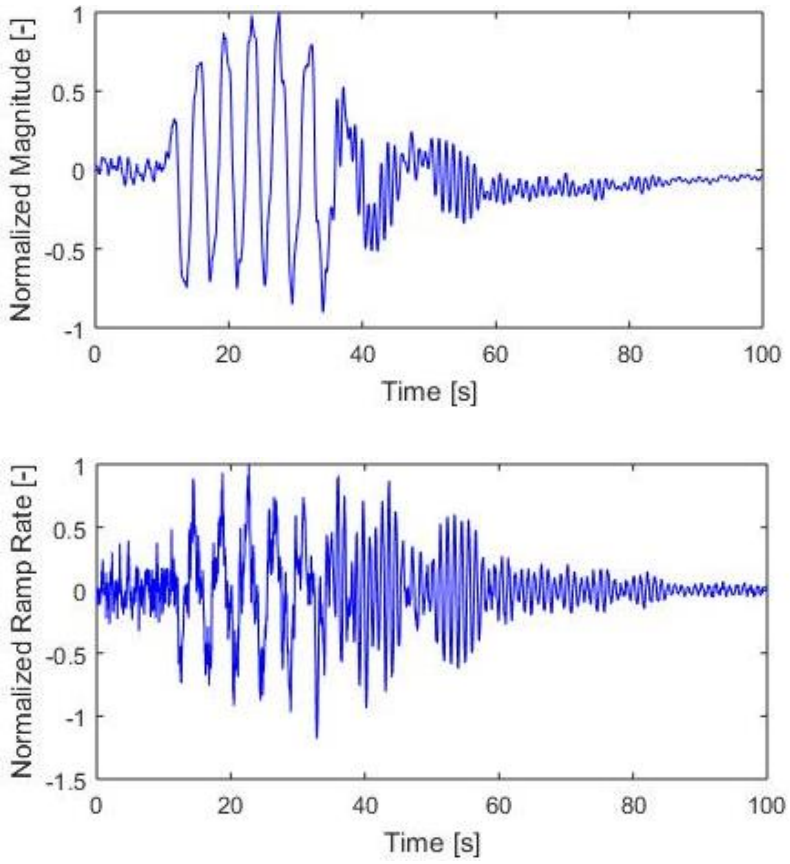

Figure 1.2: Example input load time series for magnitude (top) and ramp rate (bottom).

These situations cover multiple load cases with each load case and their variants having to be simulated under a large range of conditions. Table 1.3 gives the number of

IEC load cases [45] corresponding to each of the situations described above and a representative number of simulations. Each simulation provides time series of the various loads on the wind turbine, such as those important to the drivetrain.

The relative importance of the different load cases depends on their respective impact on the design of the wind turbine. Some of the load cases may drive the design of several components whereas other load cases may have no impact on the design at all. For example, the loads during startup are rarely driving the design of wind turbine components while loads from an internal or external fault to the wind turbine occurring at maximum power production often drive the design of several components. Of most relevance for wind turbine drivetrains are the hub centered loads with stationary (non-rotating) coordinate frame. These are the loads used as input to the test bench LAU.

Table 1.3: Number of IEC design load cases and corresponding number of simulations.

Load Case Description	Number of Load Cases	Number of Simulations
Normal Power Production	5	2250
Power Production with Fault (Turbine or Grid)	4	2100
Startup	3	3
Normal Shutdown	2	39
Emergency Shutdown	1	36
Parked/Idling in Storm	4	326
Parked/Idling in Storm with (turbine) Fault	1	570
Transport, Assembly, Maintenance, Repair	2	7500

1.5 Dissertation outline

The organization of this dissertation reflects the progression of this research per the proposal presented in April 2017.

Chapter Two presents a method for evaluating the capability of a wind turbine drivetrain test bench to replicate dynamic loads using limited information that is typically available early in the planning phase of a test campaign. This method is demonstrated in

Chapter Three using a case study using a 2.3-MW utility-scale wind turbine and the 7.5-MW test bench of Clemson University. Chapter Three also includes a description of this test bench and the 2.3-MW drivetrain.

The results from the case study were compared with measurements and this comparison is presented in Chapter Four, which provides a detailed account of the first experimental verification of the evaluation method. Chapter Four also presents improvements to the methodology and its application to another drivetrain design.

This research relied on modeling to complement the experiments using multibody simulations. The scope and results of the simulations are presented in Chapter Five.

Chapter Six describes the second experimental verification performed as part of this research using the same test bench but a different wind turbine drivetrain. The experimental results for a 3.2-MW drivetrain are presented in a similar way to the results from the tests performed with the 2.3-MW drivetrain. Several comparisons of the results from both drivetrains are made and results from analysis with the aggregated data from both drivetrains are also presented.

The conclusions and recommendations from this research are presented in Chapter Seven, which also includes a summary of contributions. The recommendations are subdivided into research directions and design certification opportunities for wind turbine drivetrain/nacelle test benches.

CHAPTER TWO

EVALUATION METHODOLOGY

Testing on a test bench is done to validate a drivetrain design in a controlled manner. The ability of a test bench to apply the design loads of the test article (drivetrain) is an expectation of wind turbine manufacturers. How much of that expectation can be met by a test bench is relevant in both the planning stage and execution of a test campaign. A method is presented to quantify the test bench coverage of the test profiles of interest and the corresponding excess or deficit in capability. The results of the method are test bench and test article specific, but the method is applicable to any test bench and test article. An application of this method is presented in Chapter Three.

As previously mentioned, the actual loading magnitude and ramp rate limits that can be replicated on a test article depends on the stiffness of that test article. The original intent of the test bench coverage metric is to communicate the capability of the test bench for a fully stiff drivetrain. This approach reflects that the stiffness of a drivetrain or lack thereof is a limitation of the test article, not of the test bench. Furthermore, the stiffness of the test article is quantified during a drivetrain test, and thus determining the test bench coverage error prior to the actual test will always have some level of uncertainty.

Figure 2.1 gives the inputs and the outputs to the evaluation method. The drivetrain design loads are defined in terms of time series of the loads and speed that the LAU must apply to the test article. Several test profiles are to be evaluated and they are processed separately. The test bench nominal capability as previously defined are also input to the method.

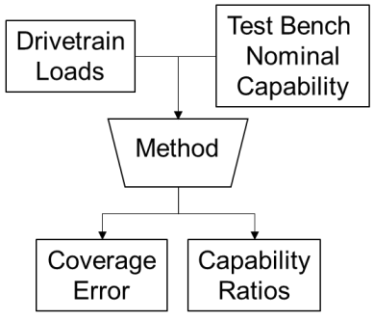

Figure 2.1: Inputs and outputs of the evaluation method.

There are three complementary evaluation metrics for quantifying the capability of a test bench for each LAU input of a test profile.

- Test bench coverage error (Cov)
- Test bench capability ratio for magnitude (CRm)
- Test bench capability ratio for ramp rate (CRrr)

The Cov is expressed as an RMS error from comparing a test profile, such as the example from Fig. 2, against the nominal test bench limits. This is done for every time step of the time series and the test bench is said to fully cover a test profile when the coverage RMS error is zero. An alternative way for stating this outcome is that the test bench has 100% coverage of the test profile, which was the terminology used with the original definition of the test bench coverage metric [42]. More details on the calculations of Cov including the basis for changing the definition are given in Section 2.1.

The test bench capability ratio aims to capture excess capability to complement the metric of Cov. Multiple test profiles having a coverage error of zero will have different level of excess capability that is not captured by Cov. The capability ratio can also indicate a shortcoming in test bench capability. This metric is to be calculated for the magnitude

of the LAU inputs and also for the corresponding ramp rates. The calculations of the capability ratios is presented in Section 2.2.

2.1 Test bench coverage error

The test bench coverage error is a RMS calculation in which the time series of each LAU inputs of a test profile is evaluated against the nominal test bench capability. The RMS is calculated between the test profile of interest and the same profile after being truncated (if applicable) to the test bench limits both in terms of magnitude and ramp rate. The extent of the truncation, if any, must take into consideration that the ramp rate for the following time step must be recalculated when the magnitude of a given LAU input falls outside the nominal test bench limits, and vice-versa when the ramp rate exceeds the test bench limit. The steps involved to obtain the truncated test profile are described below.

The first step is to calculate the ramp rate of each input to the LAU. Defining the inputs to the LAU as Q_i, the ramp rates as $\dot{Q}_i$, the time step as Δt, and using the index j for time, the ramp rate of the LAU inputs is expressed as:

$$\dot{Q}_{ij}^{\pm} = \frac{Q_{i(j+1)}^{\pm} - Q_{ij}^{\pm}}{\Delta t} \tag{2.1}$$

The ± superscript in Eq. 2.1 reflects that both the test profile yielding the maximum (+) value of an LAU input and that for the minimum (–) value are both of interest except for speed. The time step is typically in milliseconds and refer to Table 1.2 for the LAU inputs.

The second step is to compare the magnitude and ramp rate value of the LAU inputs at each time step with the nominal test bench limits and truncate the test profile when the limits are exceeded. This comparison is done for each LAU input separately.

Defining the test bench limits of the LAU inputs as $Q_{i\mathrm{L}}$ for the magnitude and $\dot{Q}_{i\mathrm{L}}$ for the ramp rate, the truncated magnitude and ramp rate of each LAU input at every time step (Qt_{ij} and $\dot{Q}t_{ij}$, respectively) can be obtained using Eqs. 2.2-2.5. The upper bound on i is for the six LAU inputs and J is the number of time steps of the test profile.

$$Qt_{ij}^{\pm} = \begin{bmatrix} Q_{ij}^{\pm} < -Q_{i\mathrm{L}} \rightarrow -Q_{i\mathrm{L}} \text{ ; for } i = 1, \dots, 6 \text{ and } j = 0, \dots, J \\ Q_{ij}^{\pm} > Q_{i\mathrm{L}} \rightarrow Q_{i\mathrm{L}} \text{ ; for } i = 1, \dots, 6 \text{ and } j = 0, \dots, J \end{bmatrix} \tag{2.2}$$

$$\dot{Q}t_{ij}^{\pm} = \begin{bmatrix} Q_{ij}^{\pm} < -Q_{i\mathrm{L}} \rightarrow \frac{-Q_{i\mathrm{L}} - Q_{ij}^{\pm}}{\Delta t} \text{ ; for } i = 1, \dots, 6 \text{ and } j = 0, \dots, J \\ Q_{ij}^{\pm} > Q_{i\mathrm{L}} \rightarrow \frac{Q_{i\mathrm{L}} - Q_{ij}^{\pm}}{\Delta t} \text{ ; for } i = 1, \dots, 6 \text{ and } j = 0, \dots, J \end{bmatrix} \tag{2.3}$$

$$Qt_{ij}^{\pm} = \begin{bmatrix} \dot{Q}_{ij}^{\pm} < -\dot{Q}_{i\mathrm{L}} \rightarrow Q_{ij}^{\pm} + \left(-\dot{Q}_{i\mathrm{L}} \cdot \Delta t\right) \text{ ; for } i = 1, \dots, 6 \text{ and } j = 0, \dots, J \\ \dot{Q}_{ij}^{\pm} > \dot{Q}_{i\mathrm{L}} \rightarrow Q_{ij}^{\pm} + \dot{Q}_{i\mathrm{L}} \cdot \Delta t \text{ ; for } i = 1, \dots, 6 \text{ and } j = 0, \dots, J \end{bmatrix} \tag{2.4}$$

$$\dot{Q}t_{ij}^{\pm} = \begin{bmatrix} \dot{Q}_{ij}^{\pm} < -\dot{Q}_{i\mathrm{L}} \rightarrow -\dot{Q}_{i\mathrm{L}} \text{ ; for } i = 1, .., 6 \text{ and } j = 0, \dots, J \\ \dot{Q}_{ij}^{\pm} > \dot{Q}_{i\mathrm{L}} \rightarrow \dot{Q}_{i\mathrm{L}} \text{ ; for } i = 1, .., 6 \text{ and } j = 0, \dots, J \end{bmatrix} \tag{2.5}$$

Once the magnitude and ramp rate at each time are within the test bench limit, the truncated test profile is compared with the original test profile to calculate the coverage error (Cov) using Eq. 2.6, which is an RMS value.

$$\mathrm{Cov}_{Q_i}^{\pm} = \sum_{j=1}^{J} \sqrt{\frac{1}{J}\left(Qt_{ij}^{\pm} - Q_{ij}^{\pm}\right)} \tag{2.6}$$

This definition of the coverage metric has the advantage of being directly comparable to the tracking error between the commanded test profile to the test bench LAU and the measured LAU inputs to the test article, which is expressed as RMS and peak values. The original definition of Cov [42] was in percent as in the percentage of time steps of the test profiles that are different from the original test profile. Such binary

assessment is not practical with measurement data and does not capture quantify of the differences. Accordingly, the use of percent for Cov was abandoned for an RMS value. Note that the Cov could also be formulated as a peak error, but this was not deemed necessary.

It is important to note that a non-zero Cov error is by no mean a show stopper as explained in Section 2.3.2.

2.2 Test bench capability ratio

The test bench capability ratio, CR, is simply the test bench limit of a given LAU input divided by the peak value of that LAU input over the test profile as indicated in Eqs. 2.7-2.12. A $CR < 1$ represents a deficit in test bench capability and $CR > 1$ indicates excess capability.

$$CR_{Q_i}^{\pm} = \max\left[\max\left(\frac{Q_{i\mathrm{Lmax}}}{Q_{i\mathrm{max}}^{\pm}}\right) \text{ v } \min\left(\frac{Q_{i\mathrm{Lmin}}}{Q_{i\mathrm{min}}^{\pm}}\right)\right] \tag{2.7}$$

$$CR_{\dot{Q}_i}^{\pm} = \max\left[\max\left(\frac{\dot{Q}_{i\mathrm{Lmax}}}{\dot{Q}_{i\mathrm{max}}^{\pm}}\right) \text{ v } \min\left(\frac{\dot{Q}_{i\mathrm{Lmin}}}{\dot{Q}_{i\mathrm{min}}^{\pm}}\right)\right] \tag{2.8}$$

with

$$Q_{i\mathrm{min}}^{\pm} = \min\left[Q_i^{\pm}(t): t = 0, \dots, J_i\right] \tag{2.9}$$

$$Q_{i\mathrm{max}}^{\pm} = \max\left[Q_i^{\pm}(t): t = 0, \dots, J_i\right] \tag{2.10}$$

$$\dot{Q}_{i\mathrm{min}}^{\pm} = \min\left[\dot{Q}_i^{\pm}(t): t = 0, \dots, J_i\right] \tag{2.11}$$

$$\dot{Q}_{i\mathrm{max}}^{\pm} = \max\left[\dot{Q}_i^{\pm}(t): t = 0, \dots, J_i\right] \tag{2.12}$$

Similarly to the Cov metric, a CR less than one is not a show stopper and the interpretation of the CR is discussed in 2.3.2.

2.3 Guidelines for presenting evaluation results

The evaluation method yields several results. Guidelines for the compilation and interpretation of these results are presented separately.

2.3.1 Results compilation

The evaluation method yields several results and this Section offers suggestions on how to effectively present these results.

There are three sets of results, one per evaluation metric. Each metric has six results per test profile to cover the six LAU inputs. These results can be presented in a compact manner using Table 2.1. The results can be color coded using the suggested scale and the actual value of each value can be indicated as well. This will be demonstrated in Chapter Three.

Table 2.1: Tabulated Results from the test bench evaluation metrics.

Test Bench Capability Summary

	Coverage Error						Capability Ratio											
							Magnitude						Ramp Rate					
Test Profile	Fx	Fy	Fz	Mx	My	Mz or Spd	Fx	Fy	Fz	Mx	My	Mz or Spd	Fx	Fy	Fz	Mx	My	Mz or Spd
#1																		
#2																		
…																		
# N																		

Coverage Error Scale		Capability Ratio Scale		Capability Ratio Scale	
	Zero		> 2		0.8-1
	> Zero		1-2		< 0.8

Table 2.1 gives a visual indication of how well the test bench considered should be able to replicate the loads of interest. The Cov results set the expectations while the CR

results indicate the excess or shortage in test bench capability. Excess capability of the test bench brings confidence in the ability of the test bench to replicate the test profiles simulated loads, but large excess capability indicates that the test bench may be oversized for the test article.

Table 2.1 captures all results but it does not offer any details “behind” the tabulated results. To better understand a coverage value of a particular LAU input, the ramp rate and magnitude of that LAU input can be plotted with an overlay of the test bench capability for that LAU input. Examples of such plots are presented in Fig. 2.2 for two cases of Cov with the corresponding CR coverage for magnitude and ramp rate. Figure 2.2 depicts the excess and deficit in capability of the test bench, which complements the results from Table 2.1. The use of a solid line for the magnitude limits is to reflect a hard limit. In contrast, the use of a dotted lines for the ramp rate limits indicates growth potential. Section 3 describes how plots like those shown in Fig. 2.2 can be useful in evaluating the capabilities of a test bench as well as checking the results from Table 2.1.

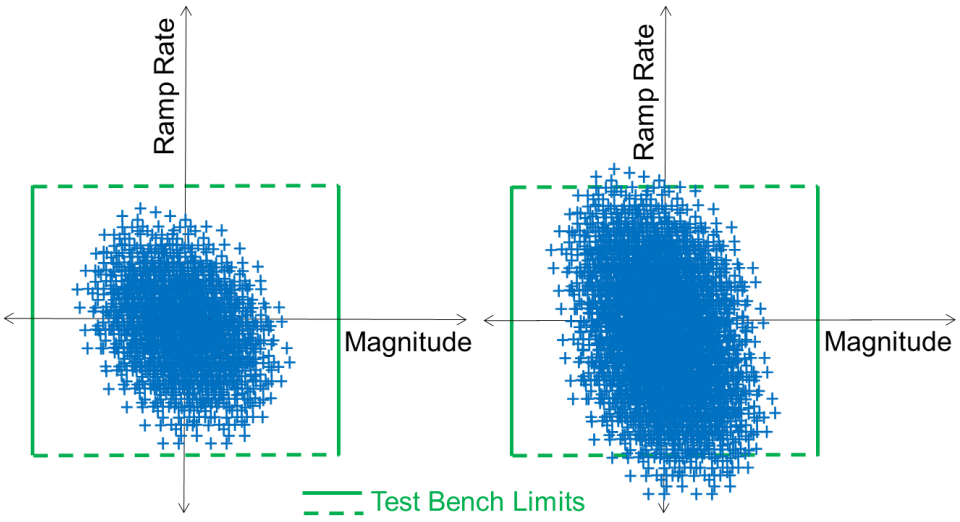

Figure 2.2: Scatter plot of load magnitude and ramp rate for zero Cov error, CRm>1, CRrr>1 (left) and non-zero Cov error, CRm>1, CRrr<1 (right).

As will be explained in the next Section, the evaluation can be limited to the coverage values for the simulated loads, and the capability ratios should be evaluated for both the design and simulated loads.

2.3.2 Results interpretation

The results of the evaluation method provide the basis for answering three main questions:

1. Is the nominal test bench capability encompassing the design and simulated loads of the test article overall?
2. Are the non-zero Cov error values acceptable or is there a way to compensate for the shortcoming(s)?
3. Is the excess capability of the test bench expected to be sufficient to compensate for the stiffness of the test article? This question can also be posed as how stiff can the test article be based on the excess test bench capability?

The test bench capability summary presented in Table 2.1 provides the answer to the first question and the second question as well if applicable. The test bench nominal capability encompass the loads of interest if all Cov errors are greater than zero. Not having this outcome is not a show stopper, however, for several reasons. First and foremost, having non-zero Cov errors for the design loads is not a concern if driven by the ramp rates only, which the CR metrics indicate. The intent of scaling the simulated loads from extreme DLC is to design to higher loads magnitude (static loading), not higher ramp rates (dynamic loading). Furthermore, non-zero Cov errors for the simulated loads that are driven solely by limitations in ramp rates can be potentially addressed by revisiting the ramp rate limits. Specifically, the test bench operator and wind turbine manufacturer can

assess the potential for increasing the ramp rate limits to the extent suggested by the results. Second, it may be possible to compensate for Cov errors greater than zero by filtering of the test profiles or by changing the test article setup on the test bench. The evaluation of the design loads can be limited to the calculation of the capability ratio of each load because this metric gives the capability of the test bench to replicate the design loads statically. Accordingly, the evaluation of the Cov error for the simulated loads is sufficient to understand the capability of the test bench to replicate the dynamic loads of interest.

The third question is relevant only if the results indicate excess capability of the test bench as compared with the design or simulated loads. If that is the case, the minimum capability ratio overall and the expected level of stiffness of the test article provides the answer. The larger the minimum *CR*, the less sensitive the results are to this uncertainty resulting in a greater potential of the test bench to replicate the loads profiles of interest to the test article. The minimum *CR* based on the simulated loads drives the answer specific to testing with dynamic loads whereas the minimum *CR* for the design loads drives the answer for testing under static conditions.

2.4 Summary

A systematic method to evaluate the capability of a wind turbine drivetrain test bench to replicate the design loads of a drivetrain design has been developed. The method can be applied to any test bench and drivetrain design, and at any phase of a test campaign. Furthermore, the method can be used to select a test bench for testing a particular drivetrain design and/or determine the design loads of a drivetrain to be tested on a given test bench. Using the method early in the planning phase of a drivetrain test can provide sufficient time for the test bench operator and wind turbine manufacturer to

address any shortcomings in capability, especially for ramp rate limitations. The input data for the method are known to the test bench owner/operator and the manufacturer of the drivetrain. The method is easy to use and guidelines for presenting and interpreting the results were presented. The complexity comes from the large amount of data to be analyzed. The overall methodology aims to establish guidelines for consideration by the wind industry. The demonstration of the evaluation method is presented in Chapter Three.

.

CHAPTER THREE

CASE STUDY WITH A 2.3-MW DRIVETRAIN

There are now at least ten ground-based test facilities for utility-scale wind turbine drivetrains generally available to the industry [9]. These dedicated laboratory resources are typically referred to as test benches, or test rigs, and they offer the obvious advantage of controlling the loads that are applied to the drivetrain. As such, the use of a test bench that can apply torque and non-torque loads is the only way to validate a wind turbine drivetrain design by replicating design loads. Results of a systematic evaluation of the capability of the Clemson University 7.5-MW test bench to replicate design loads of a multi-MW drivetrain are presented in this Section. The evaluation method presented in Chapter Two of this article will be applied and discussed. The case study is only one example of applying the proposed evaluation method, and thus any wind turbine drivetrain design and test bench may benefit.

The design loads to be replicated are the hub-centered forces and bending moments. Figure 3.1 depicts the hub center location (red circle) on a wind turbine and on the test bench. Depending on the component, the design loads are either extreme values of these forces and bending moments or the accumulation of fatigue damage. The extreme and fatigue loads come from simulations of the overall wind turbine system that are prescribed by design standards such as the IEC 61400-1 [45]. The simulations cover a broad range of wind conditions and operating states of the wind turbine that are defined in several load cases, and their output include several thousands of time series of hub-centered loads. The fatigue loads come from simulating normal operation whereas the

extreme loads typically come from simulating extreme wind conditions and/or operating states.

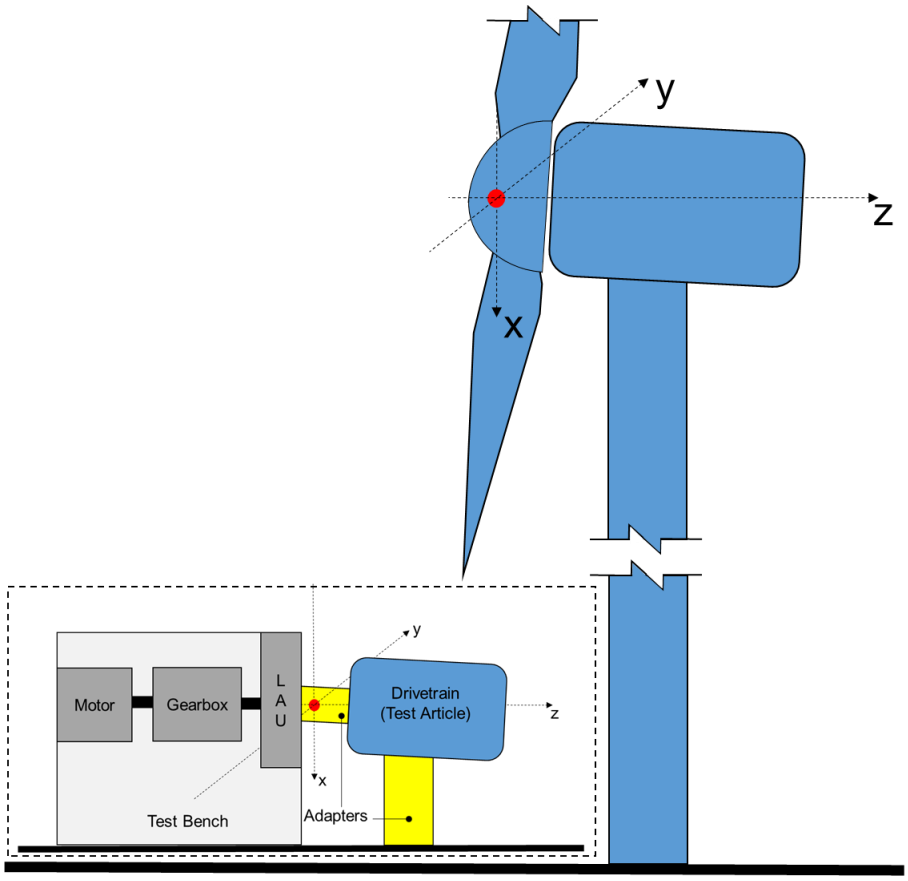

Figure 3.1: Schematic showing the hub center location (red circle) on a wind turbine and also within the context of a test bench.

The load cases yielding the drivetrain design loads depend on the design conditions as well as the wind turbine design and its controller. The design loads can always be defined as time series of Fx, Fy, Fz, Mx, My, and Mz. Time series for extreme loads are captured from 16 load profiles that cover the extreme value of the four forces and four bending moments when including the resultant force and bending moment in each direction. A partial safety factor of 1.1, 1.35, or 1.5 is applied to the simulated

extreme loads depending on the load case [45]. For fatigue loads, the metric of damage equivalent load (DEL) can be used to define the time series of the hub centered loads. A DEL covers the range of wind speeds, the inherent randomness of the wind, and the typical yaw misalignments of the wind turbine rotor with the wind direction. Replicating all time the series of hub-centered loads from normal operation is not practical. However, the use of DEL may introduce new failure modes, which is undesired.

The ability of a test bench to apply design loads hinges on having a capability that matches or exceeds these design loads both in terms of magnitude and the rate at which the loads can be varied. The fluctuations of the loads in the time series define ramp rates, which relates to the dynamic capability of a test bench. The evaluation method introduces various metrics quantifying the capability of a test bench to replicate the magnitude and also the ramp rates corresponding to selected design loads of the drivetrain of interest.

The validation of a drivetrain design calls for replicating the selected design loads, which include the applicable safety factor for extreme loads, and replicating the simulated loads is also relevant for extreme loads. The accuracy of a model to accurately predict the loads on a wind turbine drivetrain and the corresponding dynamic behavior should be based on using the simulated loads as-is (safety factor excluded) as input to the test bench. This distinction is only important for extreme loads given that a safety factor of 1.0 is used for fatigue loads. Although the focus of this research is on replicating design loads, the evaluation methodology is also applicable to any hub-centered loads of interest.

The case study presents results for the metrics introduced with the evaluation method; namely, the test bench coverage error and capability ratios for individual test profiles capturing the load cases. Results are also presented in the context of validating

simulated loads vs. design loads. The literature suggests that this research has been leading the evaluation of wind turbine drivetrain test bench capability to replicate dynamic loads over the last four years.

3.1 Description of test facility and test article

A variety of inputs are required to evaluate a wind turbine drivetrain using the proposed method. These inputs are the test bench system parameters and the selected design loads of the drivetrain design, which is also referred to as the test article. The test bench and the test article used for this case study are described below.

3.1.1 Test bench

The 7.5-MW test bench of Clemson University has been in operation since November 2014. It is part of the Energy Innovation Center of Clemson University, which also includes a 15-MW test bench and a 15-MW grid simulator [4]. The 7.5-MW test bench has a 8.5-MW asynchronous water-cooled motor, an adaptation gearbox having a gearbox ratio of approximatively 100:1, a low-speed coupling, a load application unit (LAU) capable for applying non-torque loads, and adapter to connect the LAU to the drivetrain under test (test article). Figure 3.2 shows a photo of this test bench with the test article attached to the LAU and to the isolated foundation of the test bench.

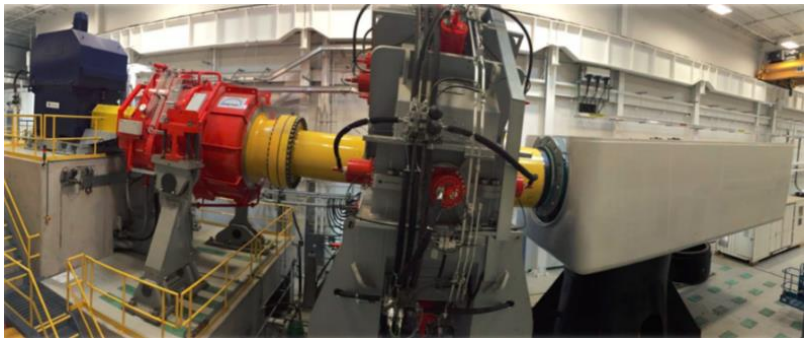

Figure 3.2: Clemson University 7.5-MW test bench with Nacelle enclosing a multi-MW drivetrain (photo credit: Konstantin Bulgakov).

The test bench can be adjusted to apply torque loads along a 4-6 deg. tilt angle to accommodate the typical tilting of wind turbine drivetrains. The maximum torque and speed of the test bench is 6.5 MNm and 20 rpm, respectively.

The LAU is made up of 24 hydraulic actuators (red cylinders in Fig. 3.2) capable of thrust and radial forces of ±2 MN and bending moments of ±10 MNm. The combined hydraulic actuation result in a load on the adapter connecting the LAU to the test article. For a 7.5-MW test bench, this resulting load exceeds 100 kN in force and 1000 kNm in bending moment making the option of direct measurement difficult. The resulting load, which is to be controlled and is critical element to this research, can be estimated applying Newton's second law considering the loads acting on the LAU. This estimation is subject to five sources of uncertainty [47]:

- Uncertainty in actuator pressure measurements
- Changing geometry caused by the displacement of the LAU disk
- Friction losses
- Inertial effect
- Spline effect at the low-speed coupling

This research leveraged a readily available uncertainty analysis that considered the first two sources of uncertainty listed above [47] for static measurements. The uncertainty due to the geometry change from the displacement of the LAU disk depends of course on the displacement of the actuators. This uncertainty is always function of time for dynamic test profiles, which is the focus on this research. In order to have a constant measurement uncertainty for data normalization purposes, only the uncertainty in actuator

pressure measurements was taken into account. This uncertainty was defined using a 99% confidence interval to compensate for neglecting the four other sources of uncertainty. This is admittedly a simplification, which adds to the simplification of using results from an uncertainty analysis for static measurements [47] to measurements made with dynamic test profiles. A complete uncertainty analysis is part of the recommended research directions given in Section 7.2 in order to quantify the impact of both simplifications and include the neglected sources of uncertainty.

Table 3.1 gives the measurement uncertainty for all LAU loads for a 99% confidence interval and also as a percentage of the test bench magnitude limits. For example, the ±23 kN for Fx and Fy represents 1.2% of the maximum force that the test bench LAU can apply to the test article (2000 kN). The measurement uncertainty is mostly epistemic (systematic) [47] and is thus referred to as measurement error.

Table 3.1: Measurement uncertainty of the LAU loads.

LAU Loads	Measurement Error (99% CI)	% of Max Capability
Fx [kN]	±23	1.2%
Fy [kN]	±23	1.2%
Fz [kN]	±63	3.2%
Mx [kNm]	±74	0.74%
My [kNm]	±74	0.74%

The measurement of the rotational speed of the low-speed shaft of the test bench, which is transfer to the drivetrain, are made with Baumer HOG 163 encoders having a resolution of 4096 pulses. The data sheet of this encoder [49] does not state its accuracy, but a representative of Baumer Ltd indicated that the accuracy should be on the order of 2 arc minutes (N. Toleos, commercial engineer, Baumer Ltd., personal communication, March 29, 2019). A measurement error of unity was assumed for the low-speed shaft speed measurements.

The rate at which the forces and moments can be changed with time is another characteristic of a test bench. In the case of Clemson's 7.5-MW test bench, the maximum ramp rate for the forces and moments range from 300-2200 kN/s for the forces and 500-4000 kNm/s for the moments. These ranges represent the nominal magnitude and ramp rate limits of the test bench as of April 2017. More details are given in Table 3.2 including the maximum speed and ramp rate that the test bench can turn the main shaft of the test article.

As suggested in Section 1.3, the nominal capabilities assume an infinitively stiff drivetrain for the magnitude and reflect demonstrated capabilities for the ramp rates based on prior testing. The test bench commands Fx, Fy, Fz, Mx, My, and Spd to the LAU and torque (Mz) to the generator. The test bench limits applied for the case study were those from 2015.

Table 3.2: Nominal magnitude and ramp rate limits for the forces and moments of Clemson University 7.5-MW test bench LAU.

Quantity	Units	Magnitude ; Ramp Rate 2015	Magnitude ; Ramp Rate 2017
Fx	kN ; kN/s	± 2000 ; ± 300	± 2000 ; ± 300
Fy	kN ; kN/s	± 2000 ; ± 500	± 2000 ; ± 500
Fz	kN ; kN/s	± 2000 ; ± 2200	± 2000 ; ± 2200
Mx	kNm ; kNm/s	± 10000 ; ±4000	± 10000 ; ±8000
My	kNm ; kNm/s	± 10000 ; ± 4000	± 10000 ; ± 8000
Mz	kNm ; kNm/s	± 6500 ; ±500	± 6500 ; ±500
Spd	rpm ; rpm/s	20 ; ±3	20 ; ±3

A critical element of a test bench is its controller, especially for replicating dynamic loads. The 7.5-MW test bench of Clemson University was designed to apply quasi-static loads to the test article. As such, this research combined with the demands from commercial testing motivated enhancements to the test bench controller to greatly

improve the dynamic capability of the test bench without changing the hardware. Specifically, the maximum ramp rate limits of the 7.5-MW test bench for the yawing and nodding moments have doubled over the last two years as indicated in Table 3.2. This remarkable achievement was primarily achieved by adding feed-forward to the control loop, which is shown in Fig. 3.3.

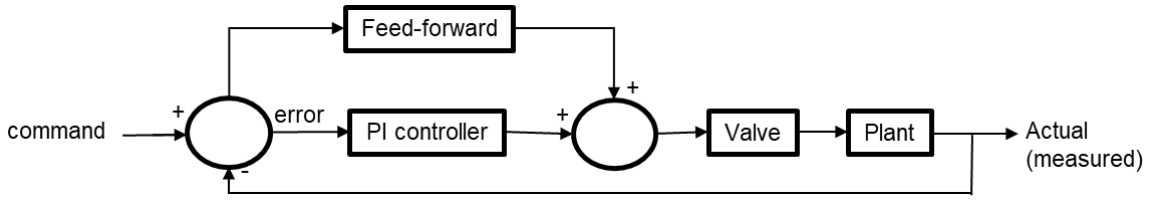

Figure 3.3: Schematic of the test bench controller.

The feed-forward applies proportional gains to the rate of change of the forces and moments that are input to the LAU. Feed-forward is not applied to the speed input. The feed-forward gains T_d are optimized for each force and moment to augment dynamic capability while preserving controller stability. The feed-forward transfer function implemented in the test bench controller is given in Eq. 3.1.

$$H = \frac{2500(T_d \cdot s + 1)}{s^2 + 100 \cdot s + 2500} \tag{3.1}$$

The effect of the feed-forward is presented in Fig. 3.4 for the yawing moment (Mx) time series of an example test profile. The effect of feed-forward (black line) vs. the original test profile (red line) is clearly visible when zooming in the time range of 20-40 seconds, which is shown on the lower plot of Fig. 3.4.

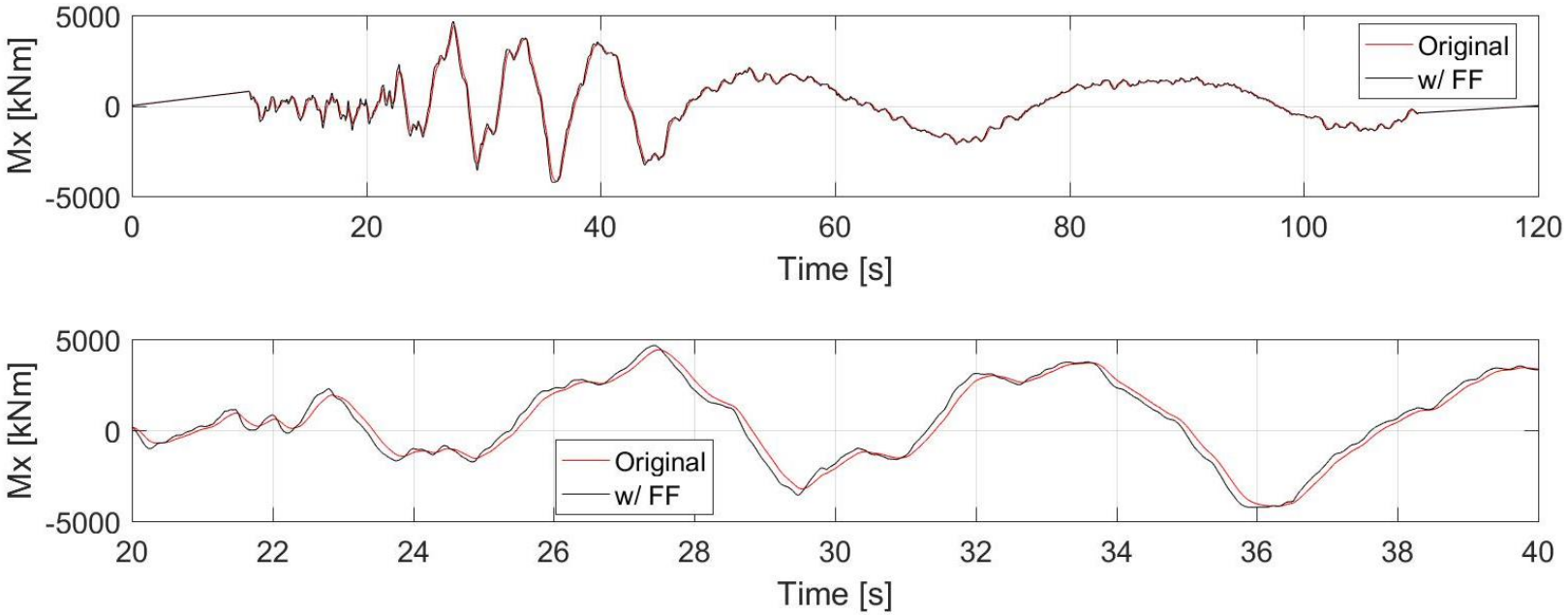

Figure 3.4: Yawing moment (Mx) with (black line) and without (red) the effect of feed-forward. The bottom plot zooms in the time frame of 20-40 seconds from the upper plot.

3.1.2 Drivetrain design and test profiles

The drivetrain considered in this case study is used in several commercial wind turbines since 2015. It has a 2.3-MW rating meaning that it can produce up to that amount of power. This drivetrain uses a single main-bearing, multi-stage planetary/helical gearbox, doubly-fed induction generator, and a high-speed shaft coupling to protect from excessive torque loads. This drivetrain architecture is shown in Fig. 3.5.

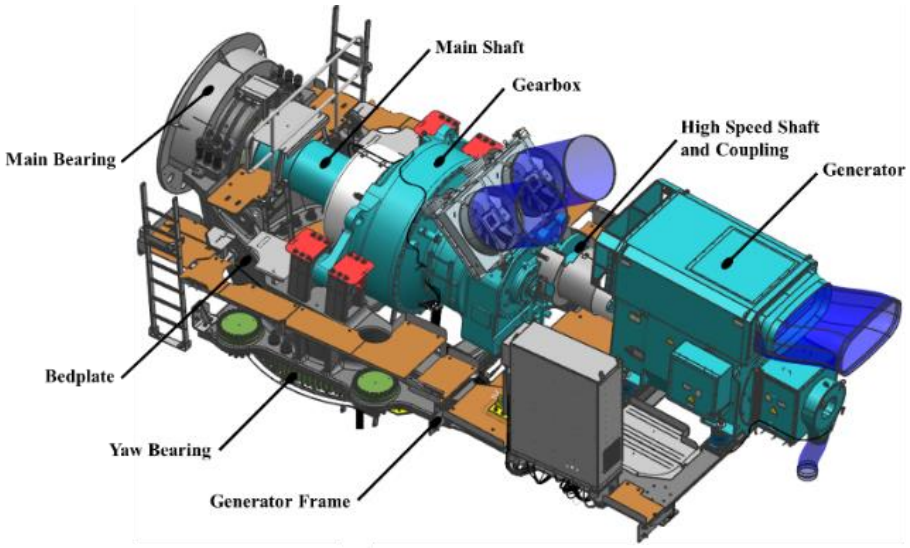

Figure 3.5: 2.3-MW drivetrain architecture schematic.

The demonstration of the method is performed using design and simulated loads from extreme load cases. A total of 14 test profiles are considered in this case study: min/max of Fx, Fy, Fz, Fr, Mx, My, and Mr. The two load cases specific to the extreme values of torque are disregarded. These 14 load profiles resulted from four IEC 61400-1 design load cases (DLCs) [45], namely: DLCs 1.5, 1.6 [48], 2.1, and 6.2 for one, two, six, and five test profiles, respectively. Time series for Fx, Fy, Fy, Mx, My, and Spd define each test profile and Fig. 3.6 gives these time series for the case of the maximum Fx. The forces, bending moments, and speed have been normalized to the peak value (absolute

maximum) of each time series. This normalization allows Fig. 3.6 to represent the load time series for both the selected design loads and the corresponding simulated loads because they only differ by the applicable partial safety factor (1.35 in this case). The time step for the time series shown in Fig. 3.6 is 40 ms.

3.2 Evaluation results

The first step of the method is to calculate the ramp rates for all inputs to the LAU for all test profiles. Figure 3.7 presents the normalized ramp rates that corresponds to the time series shown in Fig. 3.6. The variation in ramp rates is much greater than the variation in loads, which is typical. Similarly to the time series, Fig. 3.7 also represents the ramp rates for the simulated loads because of the normalization.

The second step is to compare the magnitude and ramp rate value of the LAU inputs at each time step with the nominal test bench limits. Continuing with the test profile for max Fx, Fig. 3.8 presents scatter plots for each LAU input showing each 40 ms time step of the time series (blue symbols) in terms of magnitude and ramp rates. Co-plotted are the magnitude and ramp rates limits of Clemson's 7.5-MW test bench shown with green lines, which have been normalized as well. The green lines depict the nominal test bench limits. The use of a solid line for the magnitude limits is to reflect a hard limit. In contrast, the use of a dotted line for the ramp rate limits is to indicate the potential to grow these limits further as previously mentioned. The normalized test bench limits shown in Fig. 3.8 correspond to the simulated loads, which exclude the load safety factor and are most relevant when testing dynamic loads. As explained in Section 2.3.2, the intent of scaling the simulated loads from extreme DLC is to design to higher loads magnitude (static loading), not to design to higher ramp rates (dynamic loading).

The third step is to calculate the three evaluation metrics and the results for the simulated loads and those for the design loads are presented in Table 3.3 and 3.4, respectively. The three metrics are given for each combination of test profile and LAU input. Due to the proprietary nature of the simulated and design loads, the specific values of the capability ratios are not included in Tables 3.3 and 3.4. The same is done with the coverage error for consistency. Also, the results for the design loads are limited to the CR for magnitude because this loading level is intended for static testing, not dynamic. The zero Cov error for Fz and Spd for the max Fx test profile is illustrated in Fig. 3.8 with all blue symbols being within the test bench limits. A *CR* value <1 represents a deficit whereas CR>1 represents excess capability. The CR results for the max Fx test profile are given directly in Fig. 3.8 from having normalized the magnitude, ramp rate, and test bench limits with the maximum value of each LAU input. For example, the normalized magnitude value corresponding to the vertical green line to the positive side of each scatter plot corresponds to CRm, and the ramp rate value corresponding to the upper green dotted line is CRrr.

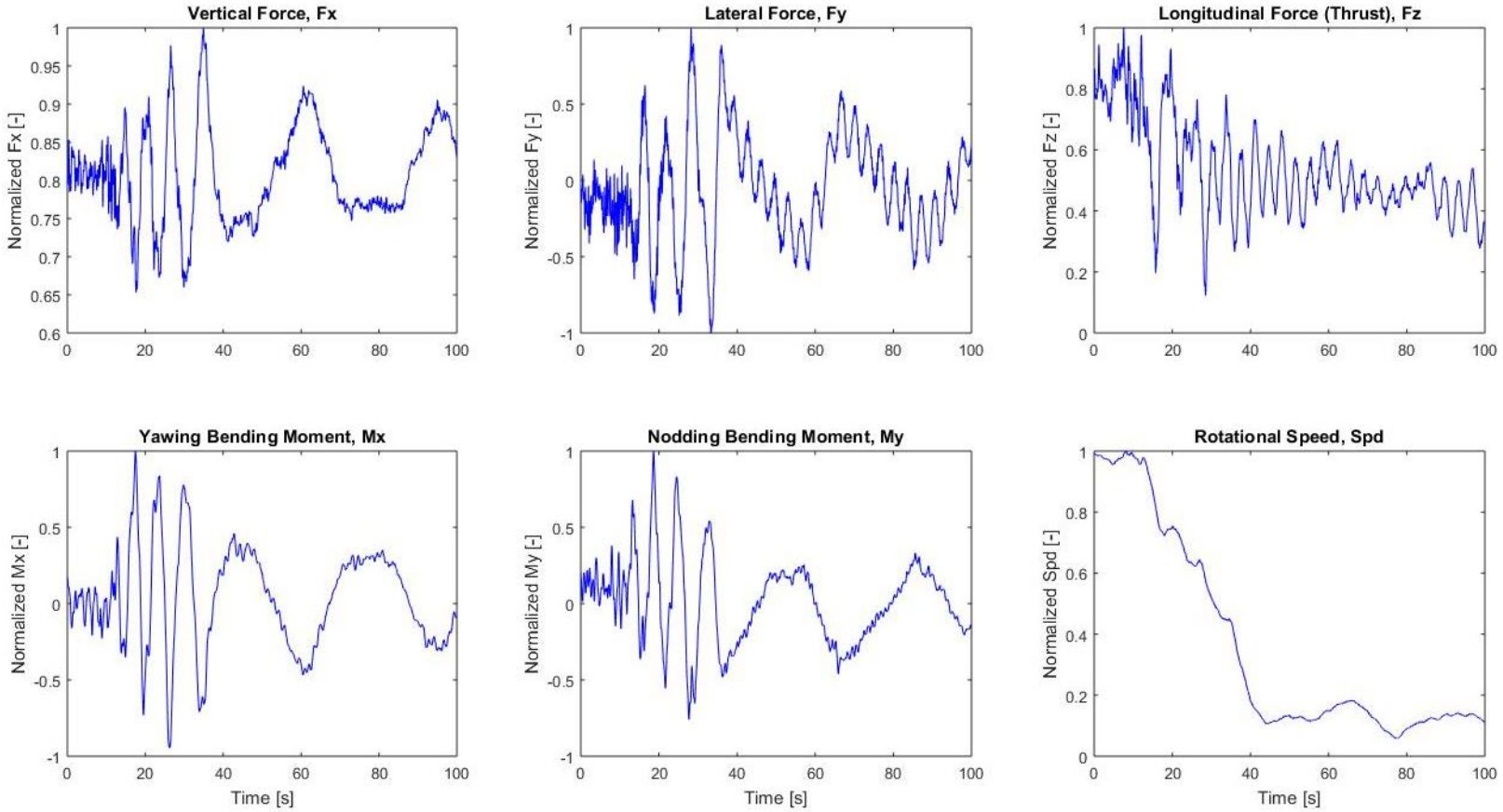

Figure 3.6: Time series of the normalized forces and bending moments defining the test profile for maximum vertical force (Fx).

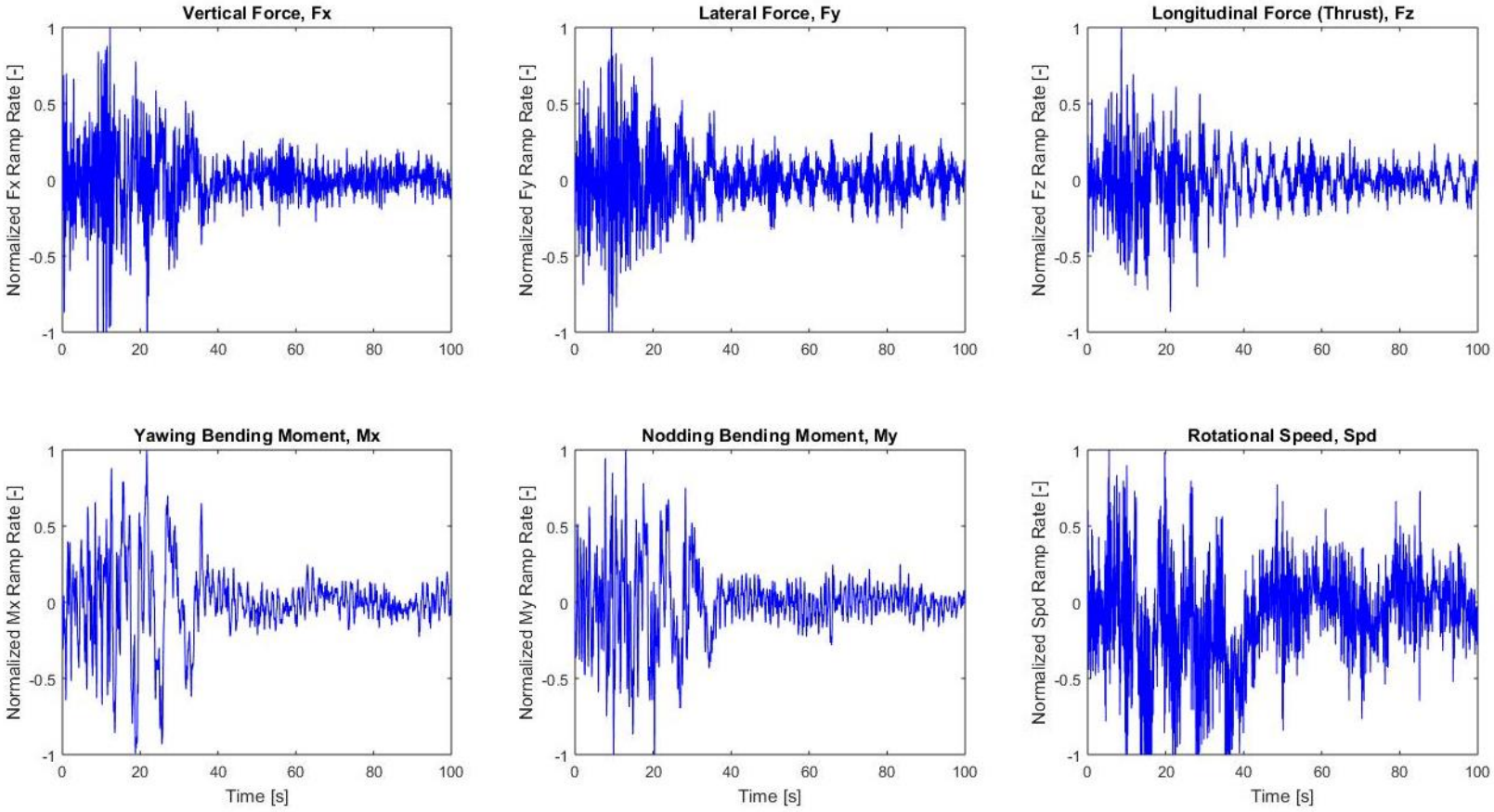

Figure 3.7: Time series of the normalized ramp rates for the forces and bending moments that define the test profile for maximum vertical force (Fx).

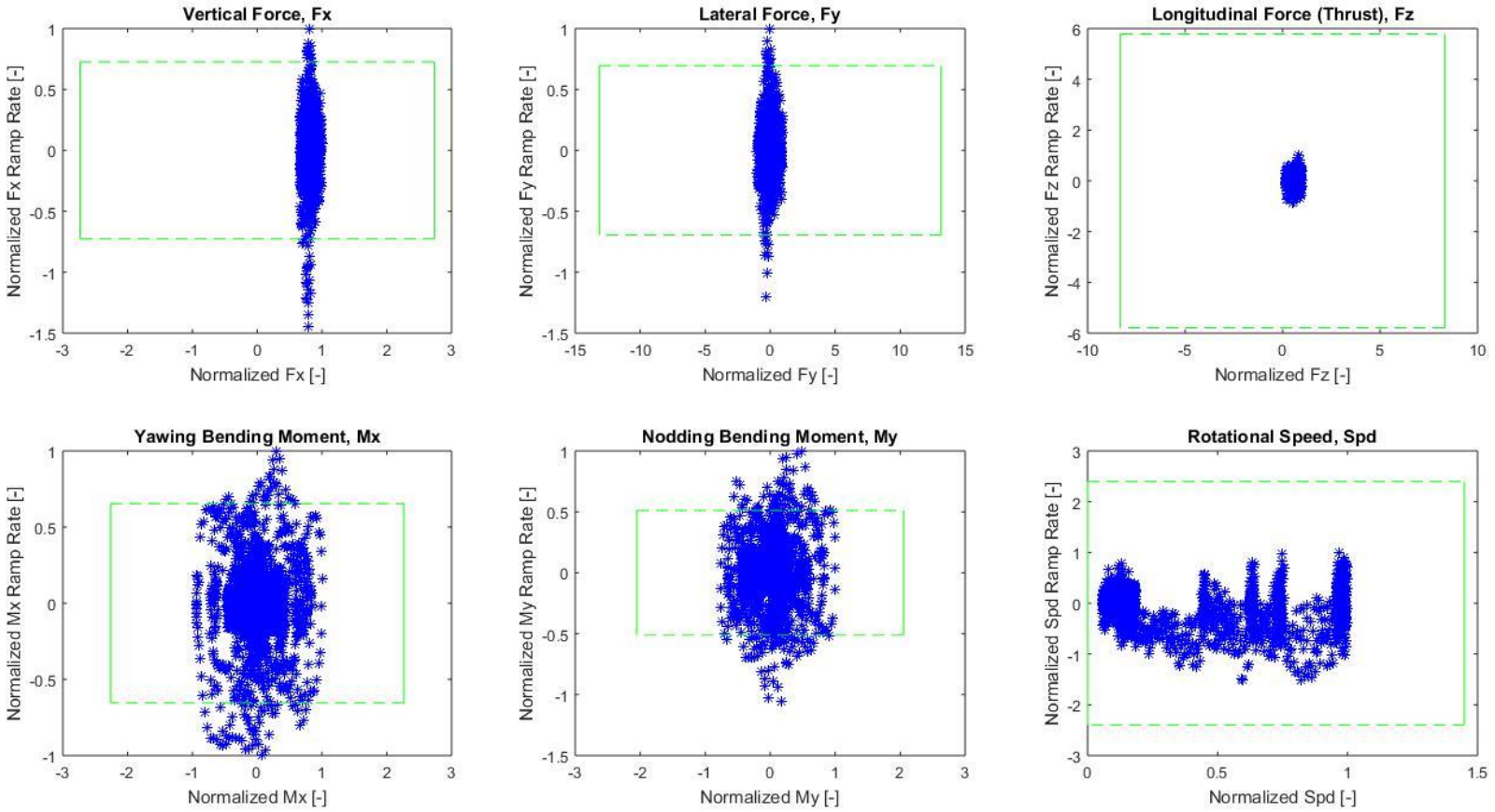

Figure 3.8: Scatter plots of the normalized ramp rates vs. the normalized magnitudes for the forces and bending moments defining the test profile for maximum Fx; the green lines representing the nominal test bench limits from Table 3.2 with the dotted lines indicating growth potential.

Table 3.3: Test bench evaluation summary for the simulated loads.

Test Profile	Coverage Error						Capability Ratio											
							Magnitude						Ramp Rate					
	Fx	Fy	Fz	Mx	My	Spd	Fx	Fy	Fz	Mx	My	Spd	Fx	Fy	Fz	Mx	My	Spd
Fx min																		
Fx max																		
Fy min																		
Fy max																		
Fz min																		
Fz max																		
Fr min																		
Fr max																		
Mx min																		
Mx max																		
My min																		
My max																		
Mr min																		
Mr max																		

Coverage Error Scale		Capability Ratio Scale			
	Zero		> 2		0.8-1
	> Zero		1-2		< 0.8

Table 3.4: Test bench capability ratios for the magnitude from the design loads.

Test Profile	Capability Ratio					
	Magnitude					
	Fx	Fy	Fz	Mx	My	Spd
Fx min						
Fx max						
Fy min						
Fy max						
Fz min						
Fz max						
Fr min						
Fr max						
Mx min						
Mx max						
My min						
My max						
Mr min						
Mr max						

Capability Ratio Scale			
	> 2		0.8-1
	1-2		< 0.8

3.3 Results interpretation

The results presented in Table 3.3 have a CRm value greater than one for all LAU inputs and the test bench has at least 100% excess capability in most cases. Accordingly, the test bench has the capability to statically ramp up to the magnitude of the selected design loads. This excess capability should be more than sufficient to compensate for the finite stiffness of the drivetrain, which can reduce the forces and bending moments that can be replicated on the test article from the available stroke length of the LAU actuators. Therefore, there is no concern with imposing the design loads magnitude of the 2.3-MW drivetrain considered in this case study. This finding is not surprising considering that the drivetrain considered has a rated power that is not even half that of the 7.5-MW capacity of the test bench. What is interesting and requires further attention is the excess capability not being greater for some of the LAU inputs, namely Mx and My. This observation can be explained by a change in wind turbine designs since the specifications for the 7.5-MW test bench were developed. Since then, wind turbines have evolved to have much larger rotors for a given rated power (MW capacity). The use of larger rotors increase the design loads, which demands greater test bench capability. Accordingly, it is important to advertise test bench capability in terms of the maximum forces, bending moments, and speed in addition to MW capacity. The compilation of test center capabilities of IEA Wind Task 35 [9] includes the maximum forces and bending moments that each test bench can generate in addition to its MW capacity. The speed and ramp rate capabilities are not included.

The results for the ramp rates from simulated loads presented in Table 3.2 indicate that tracking error due to a lack of test bench capability is expected for 10 of the 14 test profiles. These results were initially a concern but the significant increase in maximum

ramp rate that the test bench can safely deliver mitigated most shortcomings when time came to test as it will be shown in Chapter Four.

3.4 Summary

A case study was performed to demonstrate the application of a novel methodology for evaluating the capability of a test bench to replicate dynamic loads of a drivetrain design. The case study considered a 2.3-MW drivetrain and the 7.5-MW test bench of Clemson University. The results were presented per the recommendations made in Chapter Two. The findings suggest sufficient capability in terms of magnitude, and some deficit in ramp rate. The excess capability in magnitude was less than one would anticipate when comparing design loads of a 2.3-MW drivetrain with the capability of a 7.5-MW test bench. This finding was traced to the increase in rotor size of wind turbines for a given MW rating over the recent years. Accordingly, MW capacity should not be used alone in determining if a wind turbine test bench should have the capability to replicate design loads of a drivetrain. The maximum magnitude of the forces and bending moments that the test bench can generate must be considered as well and there should be sufficient excess capacity to compensate for the finite stiffness of the drivetrain design of interest. Specific to dynamic loads, the rate at which the test bench can vary the loads as a function of time must be also taken into account, and the evaluation methodology developed with this research offers a simple way to compare the ramp rates of a test profile with the test bench capability. It is important to note that the ramp rate limits of a test bench can be increased from tuning its controller. Accordingly, obtaining results from the proposed evaluation methodology early can provide sufficient time to address any shortcomings in test bench capability identified with the evaluation metrics. This was the case with the drivetrain considered for this case study. The results were available nearly a year before

that drivetrain was tested. Overall, the findings from the case study establish a basis for an experimental verification.

CHAPTER FOUR

EXPERIMENTAL VERIFICATION WITH A 2.3-MW DRIVETRAIN

The first phase of the experimental verification was performed with a GE 2.3-MW drivetrain on Clemson's 7.5-MW test bench during a total of 6 days over the time frame of February 2 to May 16, 2017. These tests were part of a commercial test campaign, which provided the opportunity for an experimental verification of the evaluation method under constraints. The development of test plan specific to this research was a balancing act between maximizing the return from the tests (commercially) while minimizing test time to obtain the data to validate the evaluation method.

The test plan for this research consisted of the same test profiles considered for the case study. These test profiles were of commercial importance for the validation of the design of the drivetrain used as test article and simulation models of that drivetrain. All test profiles were tested with reduced ramp rate limits for the yawing (Mx) and nodding (My) moments in order to obtain data covering a range of Cov and CR values. This approach was necessary given that the metrics of test bench coverage error (Cov) and capability ratio (CR) indicated Cov to be zero and CR > 1 for most test profiles, which is not surprising given the rating of the test article (2.3 MW) in comparison to the rating of the test bench (7.5-MW).

Table 4.1 presents the test date of each combination of test profile and either the nominal or reduced ramp rate limit applied to the yawing (Mx) and nodding (My) moments. These ramp rate limits are presented in Table 4.2. The nominal ramp rate limit for the yawing (Mx) and nodding (My) moments is 8000 kNm/s. The reduced ramp rate limits for the yawing (Mx) and nodding (My) moments were selected for each test profile to sample

a range of Cov values of at least 60%-100%. Most test profiles were tested with four reduced ramp rate limits in addition to the nominal limit. Note that the test profiles representing parked conditions of the wind turbine in a storm were tested with zero speed instead of using LAU speed inputs reflecting the idling motion of the rotor under parked conditions.

Table 4.1: Test dates (2017) for the executed test plan for the 2.3-MW drivetrain for the nominal and reduced ramp rate limits imposed on the yawing (Mx) and nodding (My) moments.

Case		**Nominal**	**Reduced #1**	**Reduced #2**	**Reduced #3**	**Reduced #4**
NO	8 m/s	Feb 2 (3x), 3 (2x) May 9, 15, 17	Feb 3 May 9	Feb 21 May 9	Feb 21 May 9	Feb 21 May 9
NO	12 m/s	Feb 2	Feb 3	Feb 22	Feb 22	Feb 22
NO	16 m/s	Feb 3 May 16	Feb 3	May 16	May 16	May 16
Fx	Min	May 12	May 12	May 12	May 12	None
	Max	May 12	May 12	May 12	May 12	May 12
Fy	Min	May 15	May 15	May 15	May 15	May 15
	Max	May 15	May 15	May 15	May 15	May 15
Fz	Min	May 12	May 12	May 12	May 12	None
	Max	May 12	May 12	May 12	May 12	May 12
Fr	Max	May 12	May 12	May 12	May 12	May 12
Mx	Min	May 12	May 12	May 12	May 12	May 12
	Max	May 16	May 16	May 16	May 16	May 16
My	Min	May 15	May 15	May 15	May 15	May 15
	Max	May 12	May 12	May 12	May 12	May 12
Mr	Min	May 16	May 16	May 16	May 16	None
	Max	May 15	May 15	May 15	May 15	May 15

Table 4.2: Ramp rate limits for the yawing and nodding moments for the executed test plan for the 2.3-MW drivetrain.

Case		Ramp Rate Limit for Yawing and Nodding Moments [kNm/s]										
		8000	4000	3500	3000	2500	2000	1500	1250	1000	750	<1000
NO	8 m/s	☑	☑				☑			☑	☑	750
NO	12 m/s	☑	☑				☑			☑	☑	750
NO	16 m/s	☑	☑		☑		☑			☑		
Fx	Min	☑						☑		☑		500
	Max	☑			☑			☑			☑	500
Fy	Min	☑										500 300 200
	Max	☑										500 350 250 200
Fz	Min	☑						☑				500 200
	Max	☑										500 250 150 100
Fr	Max	☑		☑			☑			☑		500
Mx	Min	☑				☑			☑		☑	500
	Max	☑			☑		☑			☑	☑	
My	Min	☑		☑			☑			☑		500
	Max	☑	☑					☑		☑		500
Mr	Min	☑										350 250 150
	Max	☑		☑			☑			☑		500

Per the dates indicated in Table 4.1, the tests for a given test profile were mainly conducted on the same day. The multiple dates indicated for test profile for the NO 8 m/s case reflects its use for quantifying the repeatability of the measurement system over the days testing was conducted. Overall, a total of 89 tests were performed covering 16 test profiles over 6 days spanning a 3.5-month time frame. The testing was done within the context of a larger commercial test campaign and the practice of randomizing the tests was not done for the sake of testing efficiency.

4.1 Data normalization approach

The commercial nature of the testing done as part of this research requires the normalization of all data to preserve confidentiality. The measurements made with the test bench and other metrics are normalized using the approaches listed in Table 4.3, which also includes examples for their use. Normalizations E and P are demonstrated in Fig. 4.1 with a sinusoidal function and using an assumed measurement error of 2. The OP normalization is not shown in Fig. 4.1 because it is a special case of normalization P that is applicable only when comparing multiple data sets.

Table 4.3: Data normalization approaches.

Label	Description	Use Example
E	Data normalized with the measurement error.	Normalization of tracking (RMS) error results from multiple test profiles.
P	Data normalized with the maximum absolute value of a given metric metrics when considering a single data set (peak).	Normalization of LAU inputs for a given test profile.
OP	Data normalized with the maximum absolute value of a given metric when considering multiple data sets (overall peak).	Normalization of peak tracking errors from multiple test profiles

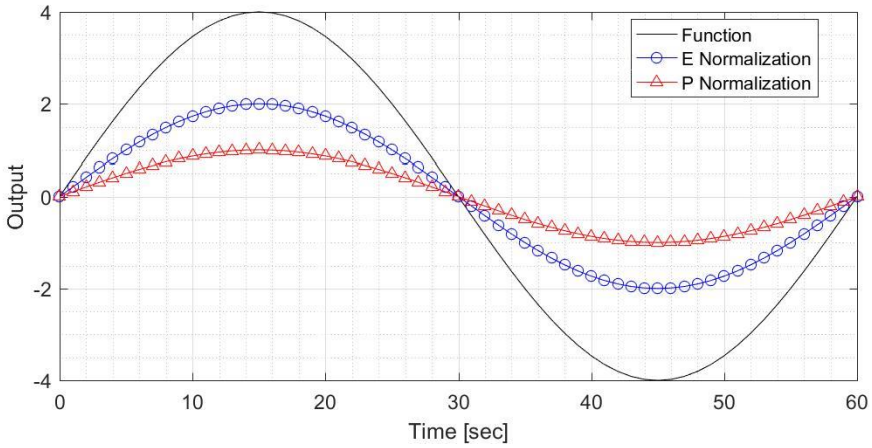

Figure 4.1: Sinusoidal time series with and without normalizations E and P.

4.2 Experimental results

The experimental results presented in this Section consist of measurements of the loads and rotational speed at the low-speed shaft that were applied to the test article during the tests. The measurements are of the LAU cylinder pressures are used to estimate the loads applied to the test article. For simplicity and brevity, the load estimates from the LAU cylinder pressures are referred to as measurements of the LAU loads.

The first results presented are an aggregated view of the measured LAU loads both in terms of magnitude and ramp rates from all test profiles. These results indicate the demonstrated test bench capability with the 2.3-MW drivetrain, which can be compared with the commanded LAU inputs and the test bench limits used to calculate the evaluation metrics.

The second results presented are those specific to quantifying the repeatability of the measurements. The scale of the hardware involved for the test and its cost did not allow testing to quantify the reproducibility of the measurements.

The third results presented are illustrating the tracking performance of the test bench under various conditions. Results are presented in both time and frequency domain. The tracking performance is first presented when the test bench operates within the limits of the test bench in terms of the magnitude and ramp rate of the loads that it can apply to the test article. These results are referred to the nominal tracking performance of the test bench. The tracking performance is also presented for the tests in which the limits on ramp rates were limited to different levels to span a range of Cov values for each test profile.

4.2.1 Demonstrated test bench capability

The 16 test profiles tested with the nominal test bench capability represent a total of 532,749 measurements of the LAU loads and speed. The first representation of the capability of the 7.5-MW test bench with the 2.3-MW drivetrain is from plotting the measured LAU loads and speed in terms of magnitude vs. ramp rate when grouping the data from all test profiles together. Figure 4.2 provides this representation for the normalized LAU loads and speed (OP normalization) for the tests done with the nominal test bench limits. The commanded values of the LAU loads and speed are co-plotted and note that repeats of test profile NO 8 are excluded from the data presented in Fig. 4.2. The same scale is used to facilitate the comparison between the different LAU loads and the speed. There are three important observations from Fig. 4.2.

- The test bench is able to deliver magnitude and ramp rate of the loads and speed that are commanded.
- The measured magnitudes of the forces are larger than the commanded forces.
- The measured ramp rates of the LAU loads are larger than that of the commanded values, especially for the forces.

It is important to note that the first observation does not demonstrate that the test bench is tracking the commanded test profiles accurately, but it is a necessary condition for tracking the peak magnitudes and ramp rates of the test profiles. In that regard, the results presented in Fig. 4.2 are encouraging.

Specific to the second observation, a cross-coupling effect between the bending moments and forces applied by the LAU result in reaction forces in the LAU cylinders from the application of bending loads. The reaction forces from the cross-coupling effect also impact the ramp rates of the forces, which partly explains the third observation. Other

contributors to the large measured ramp rate values are the use of feed-forward in the test bench controller strategy and data acquisition quantization error.

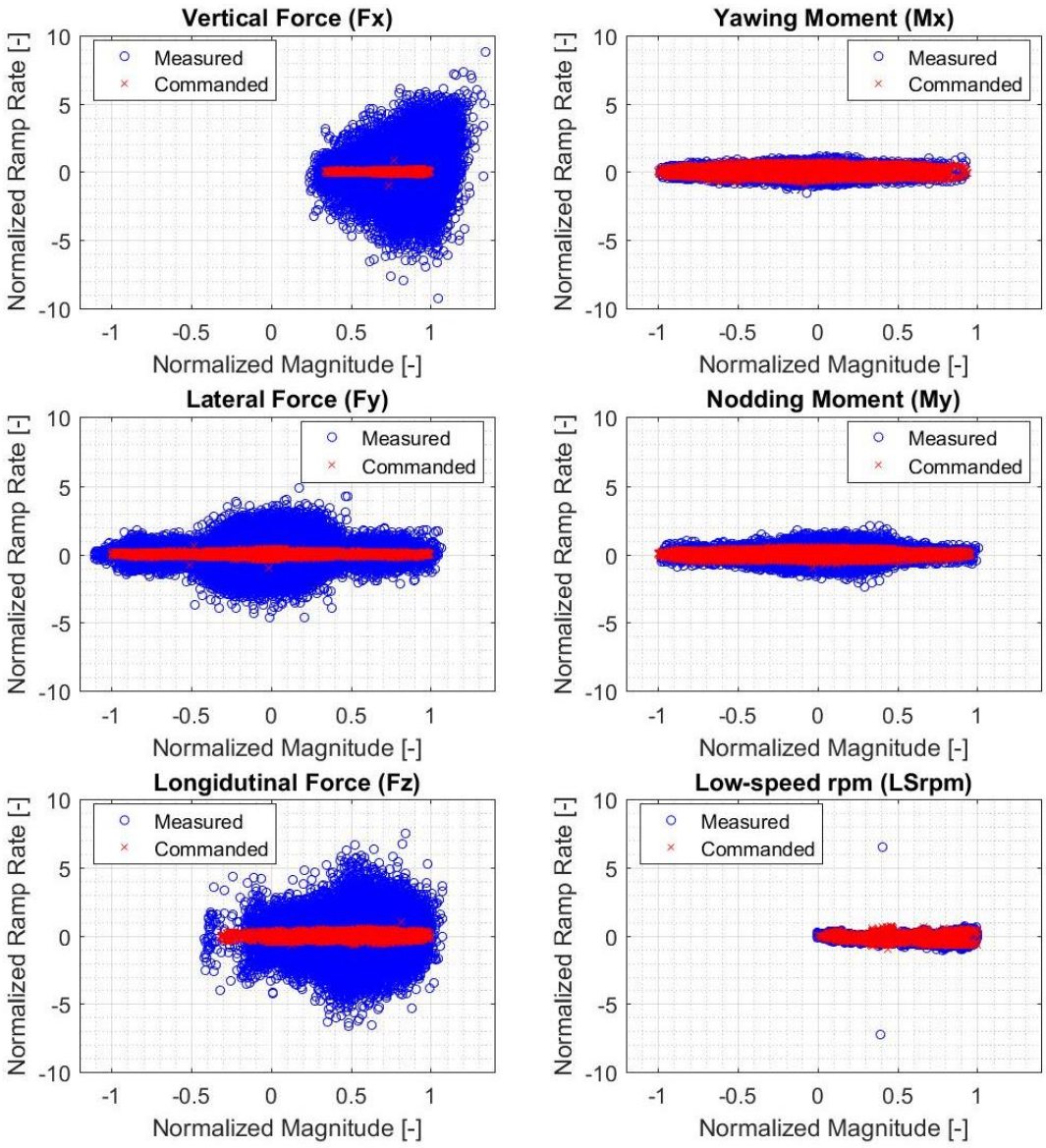

Figure 4.2: Magnitude vs. ramp rate of the measured and commanded LAU loads and speed for all test profiles tested with the nominal test bench limits.

Figure 4.2 does not indicate the frequency of occurrence of the demonstrated capability of the test bench with the 2.3-MW drivetrain. To add this important perspective, the data shown in Fig. 4.2 is presented in the form of histograms in Figs. 4.3-4.8. These

six figures cover the six LAU inputs and each figure presents histograms for the magnitude on the left and ramp rate on the right. The plots in the first row are for the commanded LAU loads and speed whereas those in the second row are for the measurements. Note that consistent ranges for the x and y axes are used for the magnitude of a given load or speed to facilitate comparisons. The same is done for the ramp rate. The red dotted lines in these plots indicate the limits set in the test bench controller for the LAU loads and speed. Limits are set for the magnitude and ramp rate of the loads and speed. The limits on magnitude were set from the maximum value of the magnitude from the test profiles. Note that these magnitude limits are not shown for the forces because they are outside of the range of the x-axis in Figs. 4.3-4.5. The limits on the ramp rate were determined during the tuning of the test bench controller with the 2.3-MW drivetrain installed on the test bench. The observations from Figs. 4.3-4.8 are summarized below Fig. 4.8.

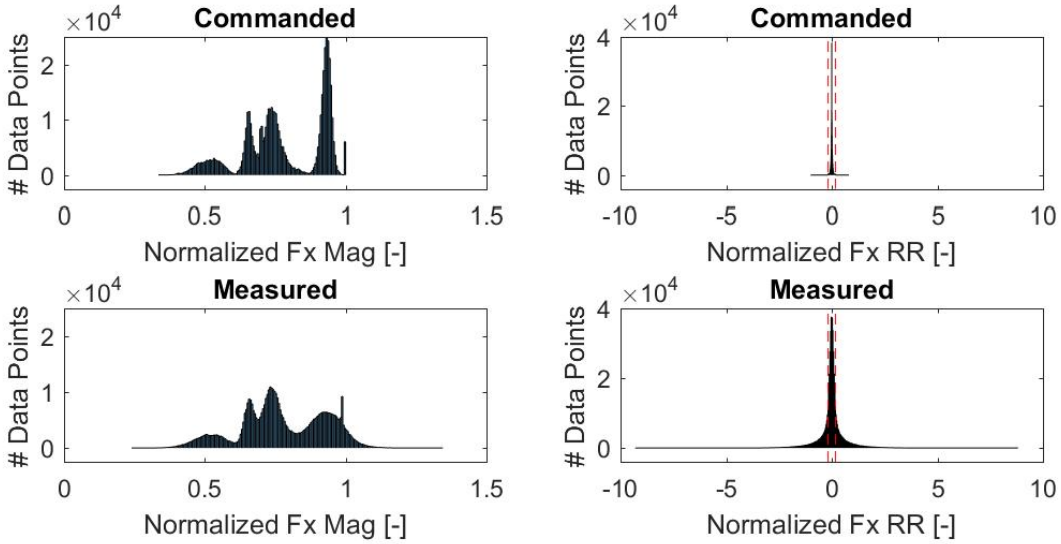

Figure 4.3: Histogram of the magnitude (Mag, left) and ramp rate (RR, right) of the vertical force (Fx) for the commanded values (1st row) and measurements (2nd row) for all test profiles tested with the nominal test bench limits (red dotted lines). The OP normalization is applied to the data and the test bench limits are not shown for the magnitude histograms because outside the x-axis range.

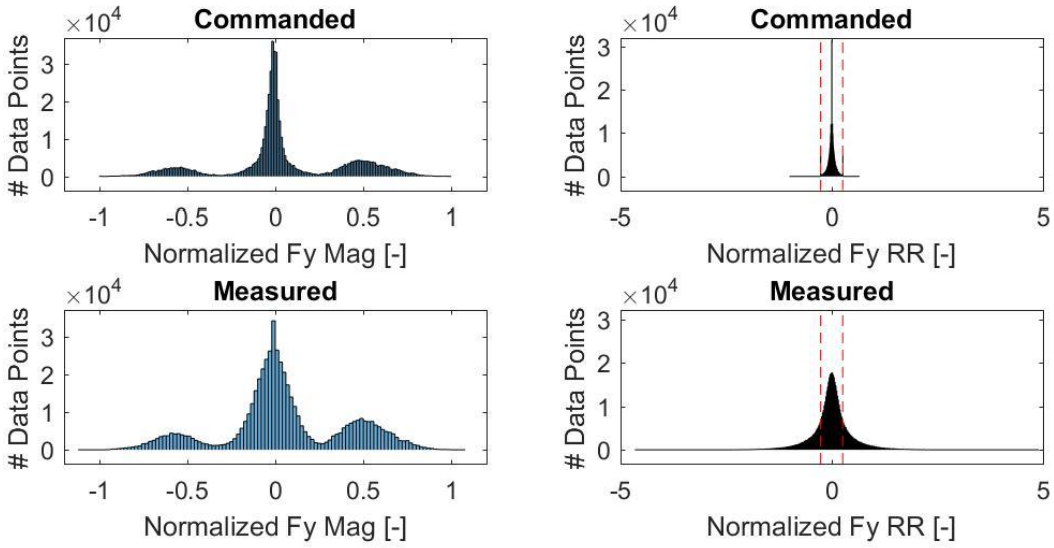

Figure 4.4: Histogram of the magnitude (Mag, left) and ramp rate (RR, right) of the lateral force (Fy) for the commanded values (1st row) and measurements (2nd row) for all test profiles tested with the nominal test bench limits (red dotted lines). The OP normalization is applied to the data and the test bench limits are not shown for the magnitude histograms because outside the x-axis range.

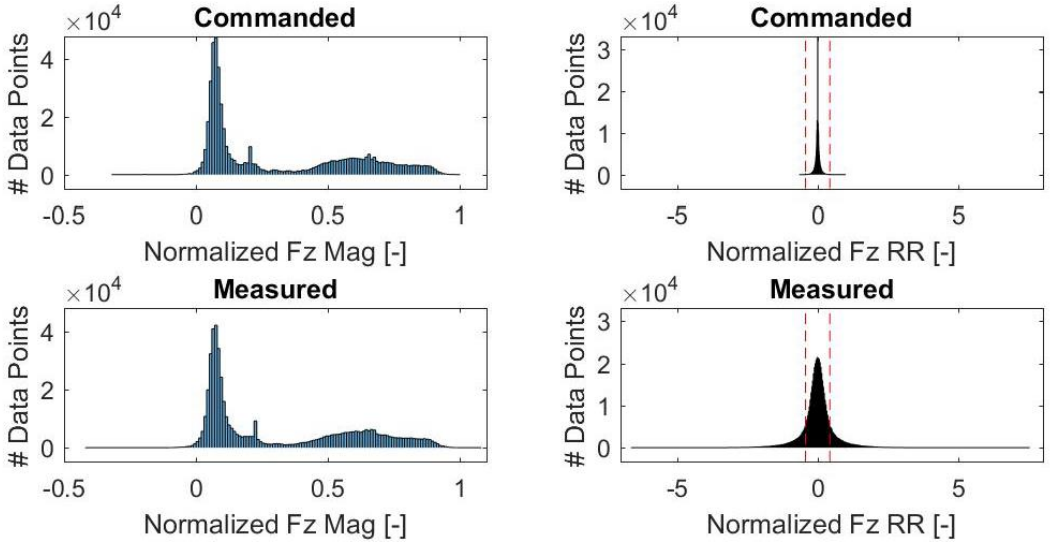

Figure 4.5: Histogram of the magnitude (Mag, left) and ramp rate (RR, right) of the longitudinal force (Fz) for the commanded values (1st row) and measurements (2nd row) for all test profiles tested with the nominal test bench limits (red dotted lines). The OP normalization is applied to the data and the test bench limits are not shown for the magnitude histograms because outside the x-axis range.

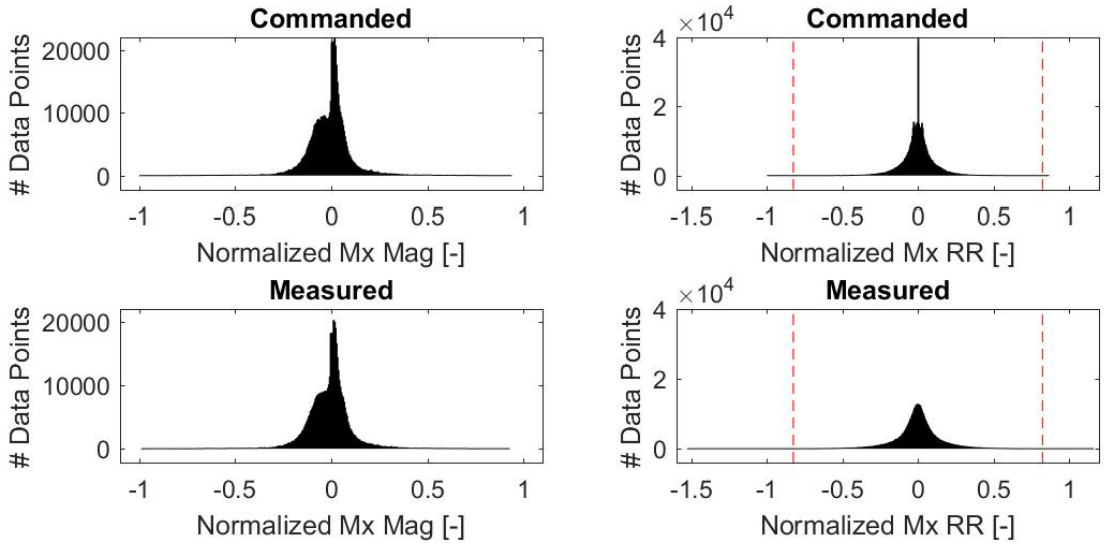

Figure 4.6: Histogram of the magnitude (Mag, left) and ramp rate (RR, right) of the yawing moment (Mx) for the commanded values (1st row) and measurements (2nd row) for all test profiles tested with the nominal test bench limits (red dotted lines). The OP norm. is applied to the data and the test bench limits are not shown for the magnitude histograms because outside the x-axis range.

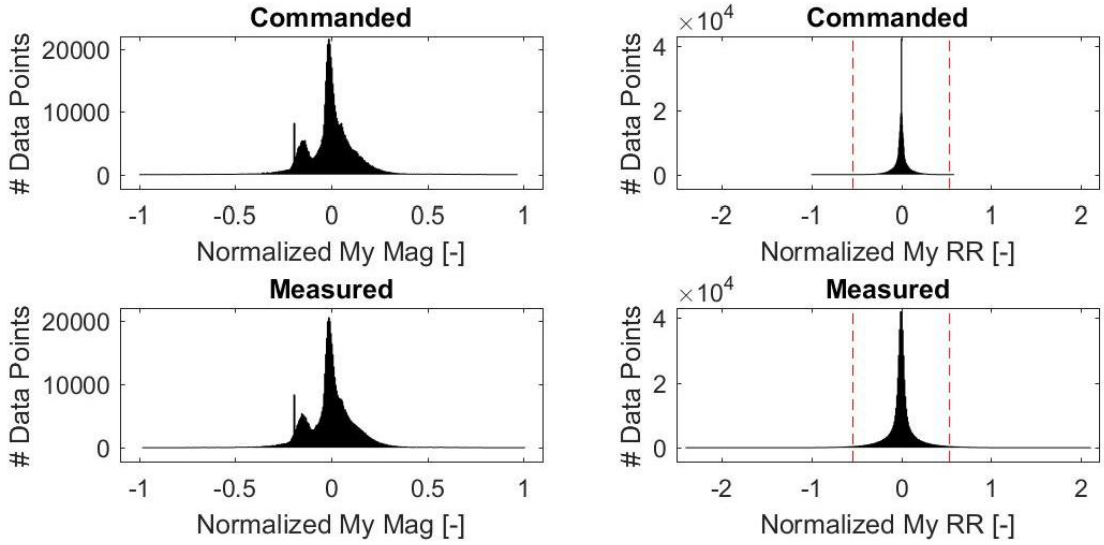

Figure 4.7: Histogram of the magnitude (Mag, left) and ramp rate (RR, right) of the nodding moment (My) for the commanded values (1st row) and measurements (2nd row) for all test profiles tested with the nominal test bench limits (red dotted lines). The OP norm. is applied to the data and the test bench limits are not shown for the magnitude histograms because outside the x-axis range.

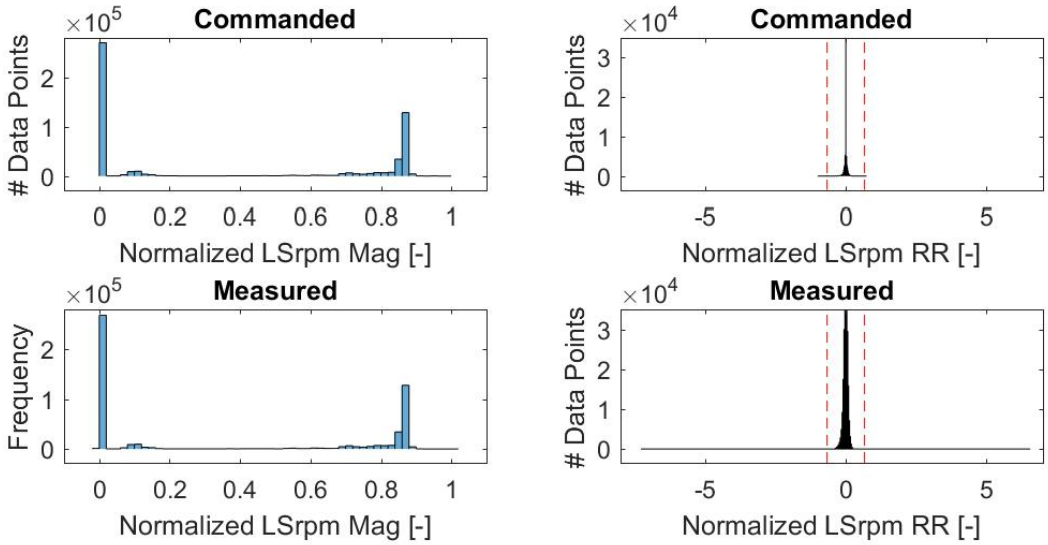

Figure 4.8: Histogram of the magnitude (Mag, left) and ramp rate (RR, right) of the LAU speed (LSrpm) for the commanded values (1st row) and measurements (2nd row) for all test profiles tested with the nominal test bench limits (red dotted lines). The OP normalization is applied to the data and the test bench limits are not shown for the magnitude histograms because outside the x-axis range.

The following observations can be made from Figs. 4.3-4.8.

- All commanded loads and speed are well within the limits set in the test bench controller.
- The peaks in the distributions of the measured forces are broader.
- The distributions of the moments and speed magnitude between the commanded values and measurements are nearly identical.
- The distributions of the measured ramp rates of all LAU inputs are elongated with much broader tails.
- A significant number of data points for the forces have ramp rates in excess of the set limits in the test bench controller.

The first two observations suggest that the tracking error of the test bench should not be driven by the peak magnitudes of the forces.

The third observation indicates that the tracking error of the test bench should not be driven by the magnitude of the moments and speed.

The fourth observation implies that the ramp rate values at the tails of the distributions should not drive the tracking error in terms of RMS value due to their low occurrence.

The fifth observation is driven by the cross-coupling effect. To quantify this observation, the percentage of the data points outside of the test bench limits set in the test bench controller are given in Table 4.4 for both the commanded and measured values. The commanded LAU inputs resulted in ramp rates exceeding the nominal test bench limits 0.18% (959 of 532749 data points) of the time at most. This is for the lateral force and the other LAU inputs have 1-2 order of magnitude less data points outside the test bench limits. In contrast, 27%-46% of the ramp rates from the measurements exceed the test bench limits for the forces. That percentage for the moments is 1-3 order of magnitude less. The larger percentage of the nodding moment as compared with that of the yawing moment illustrates the effect of gravity and how feed-forward has to compensate more in nodding than in yaw.

Table 4.4: Percentage of commanded and measured ramp rates larger than the nominal test bench limits.

LAU Input	Ramp Rate	
	Commanded	Measured
Fx	0.017%	46%
Fy	0.18%	39%
Fz	0.013%	27%
Mx	<0.01%	0.037%
My	0.013%	2.7%
LSrpm	<0.01%	0.015%

Overall, Figs. 4.2-4.8 as well as Table 4.4 point to a test bench having the capability to replicate the test profiles of the 2.3-MW drivetrain for at least the bending moments and speed. The cross-coupling effect makes tracking of the forces challenging.

4.2.2 Repeatability

The test profile (TP) representing normal operation for a wind speed of 8 m/s (NO8) was used as the reference TP during the test period. Per Table 4.1, this TP was tested eight times with the nominal capability of the test bench. These eight tests were performed over a total of five days, with three tests on the first day, two tests on the second day, and one test on three different days. The first test was done on the first day of the testing period and the last test was done on the last day. The test profiles for the 2.3-MW drivetrain were tested over 6 days and the NO8 TP was tested on all but one of the test days.

The RMS error from these 8 tests and all LAU inputs are presented in Fig. 4.9. The results from Fig. 4.9 are presented for each LAU input individually in Fig. 4.10 with the y axis scaled to capture a range of 10% (±5%) of the mean value (dotted line). Overall, there is no significant pattern in the data in terms of clustering, mixture, trends, and oscillations with one exception. There is a significant pattern of clustering for the normalized RMS error of the yawing moment, which indicate a shift in the measurements. The shift is quite small, however, with the mean normalized error for the first four tests being 0.8% greater than that for the last four tests. The shift is within 1% of the measurement error of the yawing moment. The larger than unity normalized RMS error for the vertical and lateral forces is due to the previously mentioned cross-coupling effect between the bending moments and forces applied by the LAU.

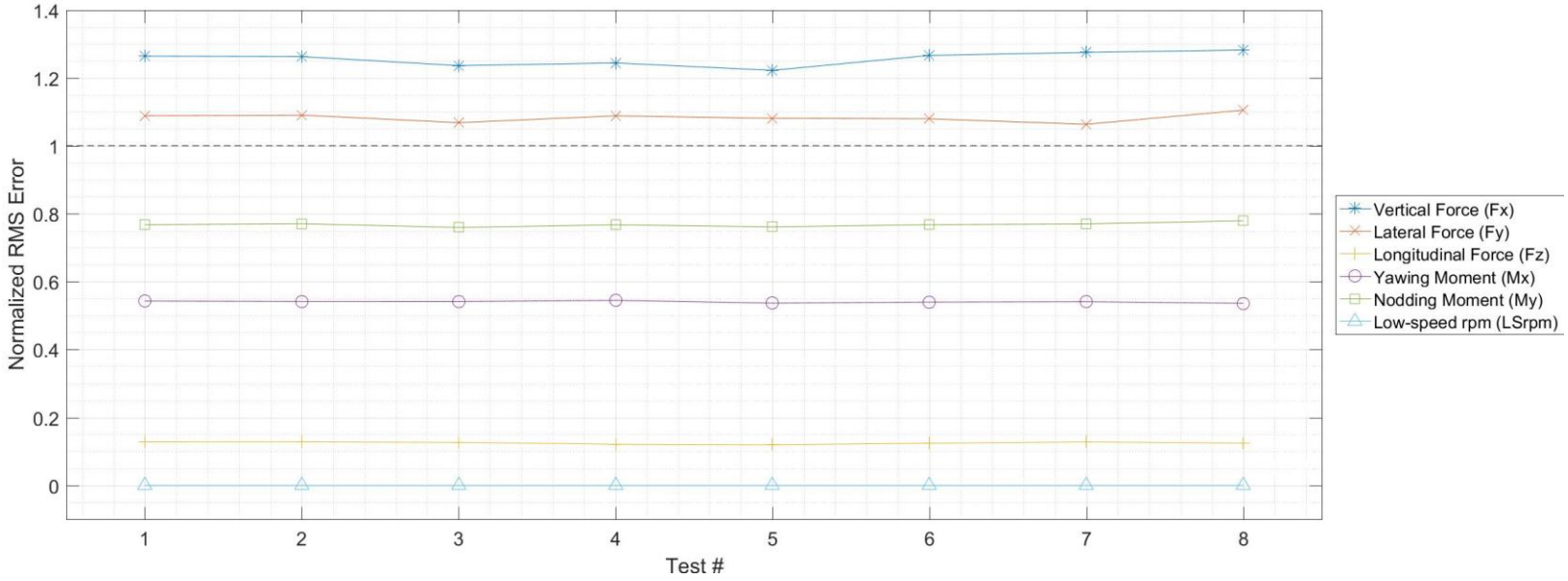

Figure 4.9: Repeatability of the normalized RMS error (E norm.) between the measured and commanded LAU loads for the reference test profile (TP NO8). The larger than unity normalized RMS error for the vertical and lateral forces is due to a cross-coupling effect from the simultaneous LAU application of bending moments and forces dynamically.

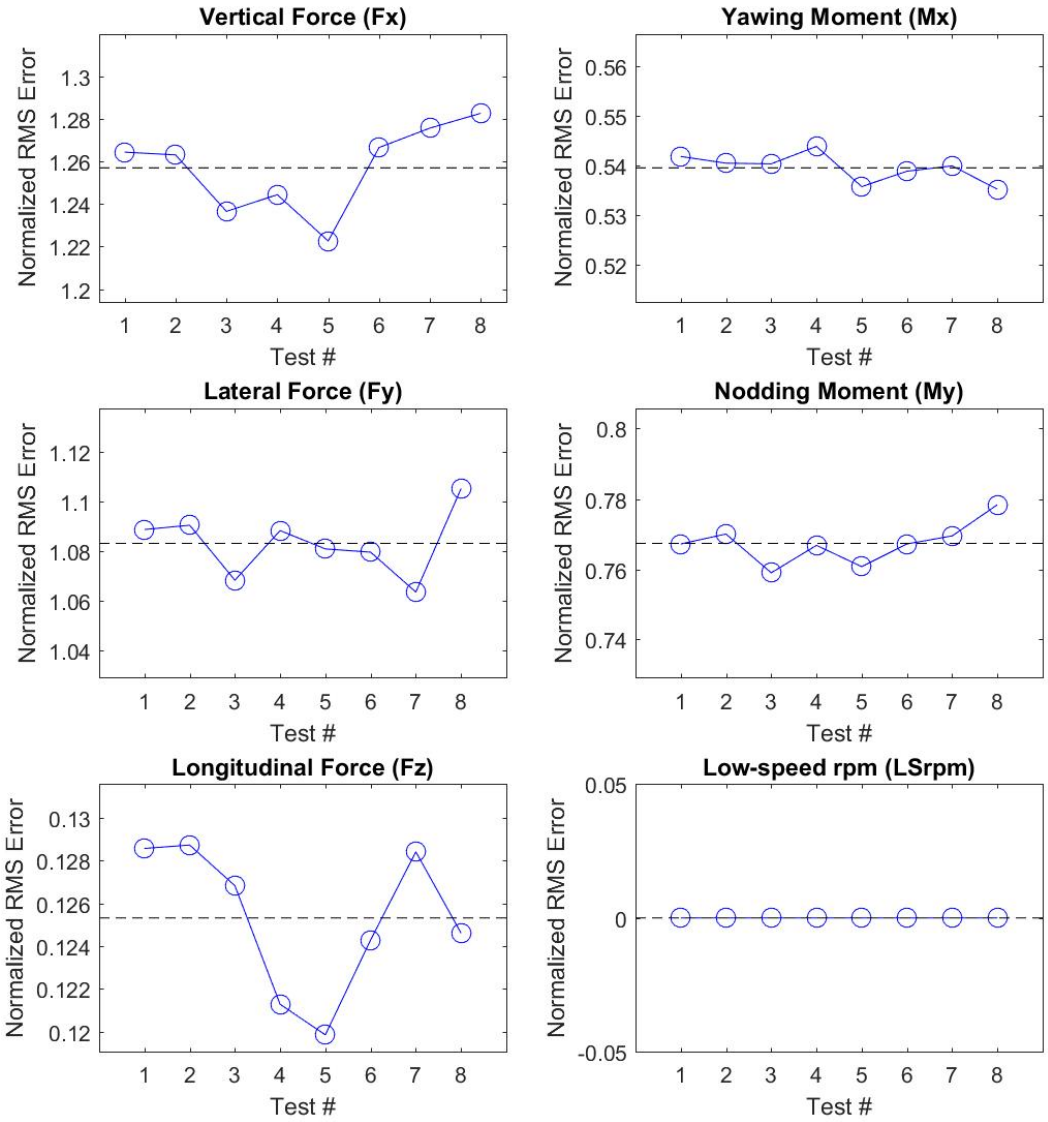

Figure 4.10: Repeatability of the normalized RMS error between the measured and commanded LAU loads for the reference test profile (TP NO8) presented individually.

The histograms of the RMS error for each LAU input are presented in Fig. 4.11 with an overlay of a normal distribution with the p-value from the Anderson-Darling test using 95% confidence. The p-values given in Fig. 4.11 indicate that the distribution of the normalized RMS error is normal for all LAU loads inputs (the null hypothesis cannot be rejected). There is no variation in the low-speed rpm.

The 95% confidence interval for each LAU loads input can be determined using a student-t distribution using seven degrees of freedom (8 measurements) for a two-tail distribution. The corresponding factor on the standard deviation is 2.365 for 95% confidence and the confidence intervals are given in Table 4.5 for both normalizations. The results presented in Table 4.5 indicate that the repeatability of the measurements is excellent with worst-case variation of 2.2% of the peak loads of the reference test profile in the case of the lateral force and 4% of the measurement error in the case of the vertical force. The repeatability of the longitudinal force and bending moments are within 1% of the normalized RMS errors.

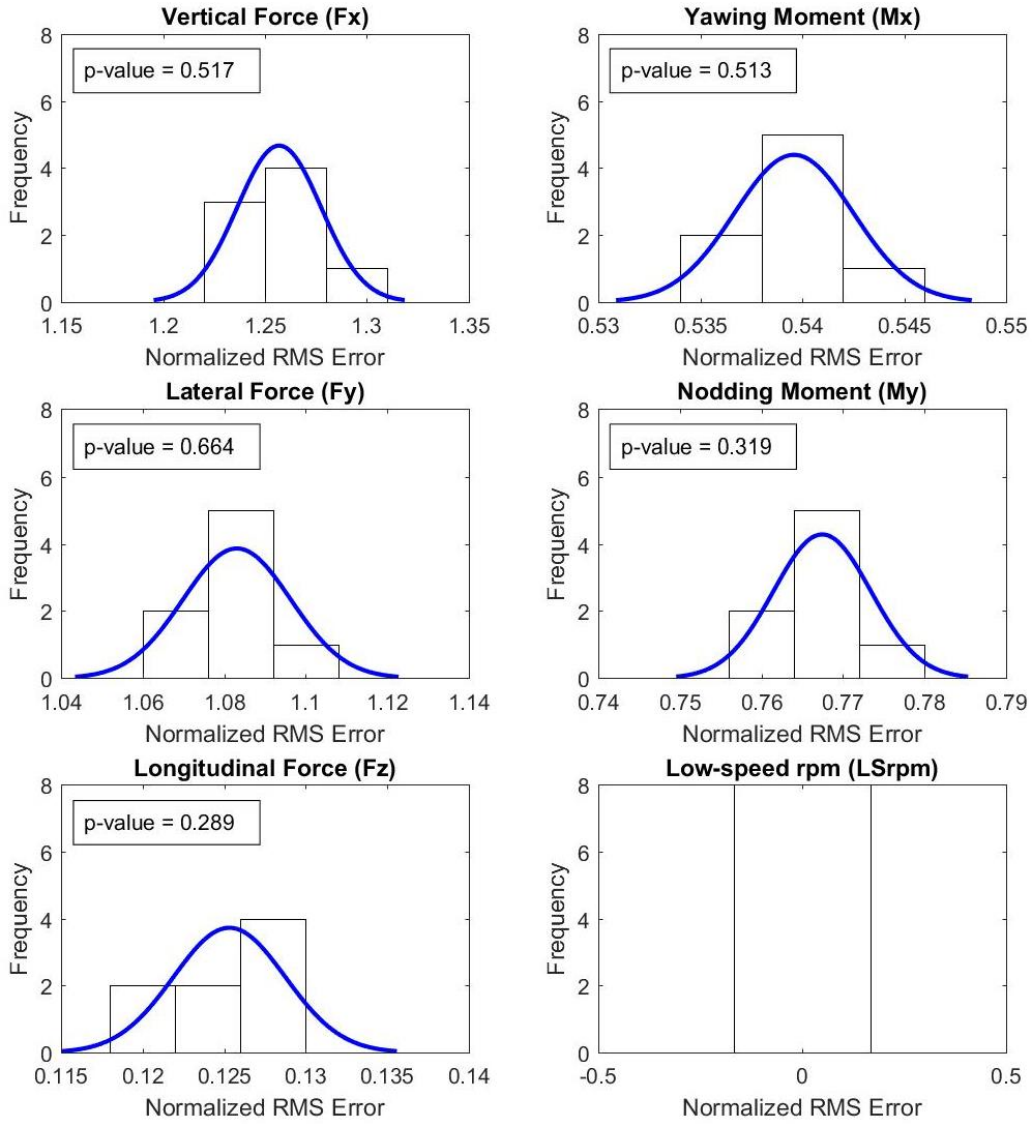

Figure 4.11: Histogram of the RMS error between the measured and commanded LAU loads for the reference test profile (TP NO8) for all LAU inputs.

Table 4.5: 95% confidence interval (CI) for the normalized RMS error between the measured and commanded LAU loads. The confidence intervals are normalized with the measurement error and peak value of each LAU load.

95% CI [%] Normalized RMS Error	Vertical Force, Fx	Lateral Force, Fy	Longitudinal Force, Fz	Yawing Moment, Mx	Nodding Moment, My
Peak (P)	±0.19	±2.2	±0.12	±0.03	±0.08
Meas. Error (E)	±4.9	±3.1	±0.81	±0.69	±1.4

The repeatability of the measurements was also quantified in the case of reducing the ramp rate limit for the yawing and nodding moments. Specifically, the tests with a reduced ramp rate limit for the moments were done twice on different days. The variation in RMS error due to the reduced ramp rate limits and the nominal limit of 8000 kNm/s is presented in Fig. 4.12. In the case of reducing the test bench ramp rate limits, the commanded test profile is truncated to the reduced level. Accordingly, the commanded test profile is not the reference of interested when the ramp rate is reduced. Instead, the commanded test profile subject to the nominal test bench limits is used as reference. All RMS errors presented in Fig. 12 are based on that common reference. The two test used for the nominal test limits results (out of the eight tests in total) were the successive tests having the largest difference in RMS error for a given LAU input. These two test can be selected using the run charts presented in Fig. 4.10. For example, the 5^{th} and 6^{th} tests are the successive tests with the largest difference in RMS error for the vertical force (Fx) whereas the 4^{th} and 5^{th} tests have the largest difference for the yawing moment (Mx). This approach establish an acceptable level of variation given that the repeatability of the test results with the nominal test bench limit was found to be excellent. Note that the y axis of each plot shown in Fig. 4.12 captures a different range of normalized RMS error between the different LAU loads and results should be compared within a given LAU input.

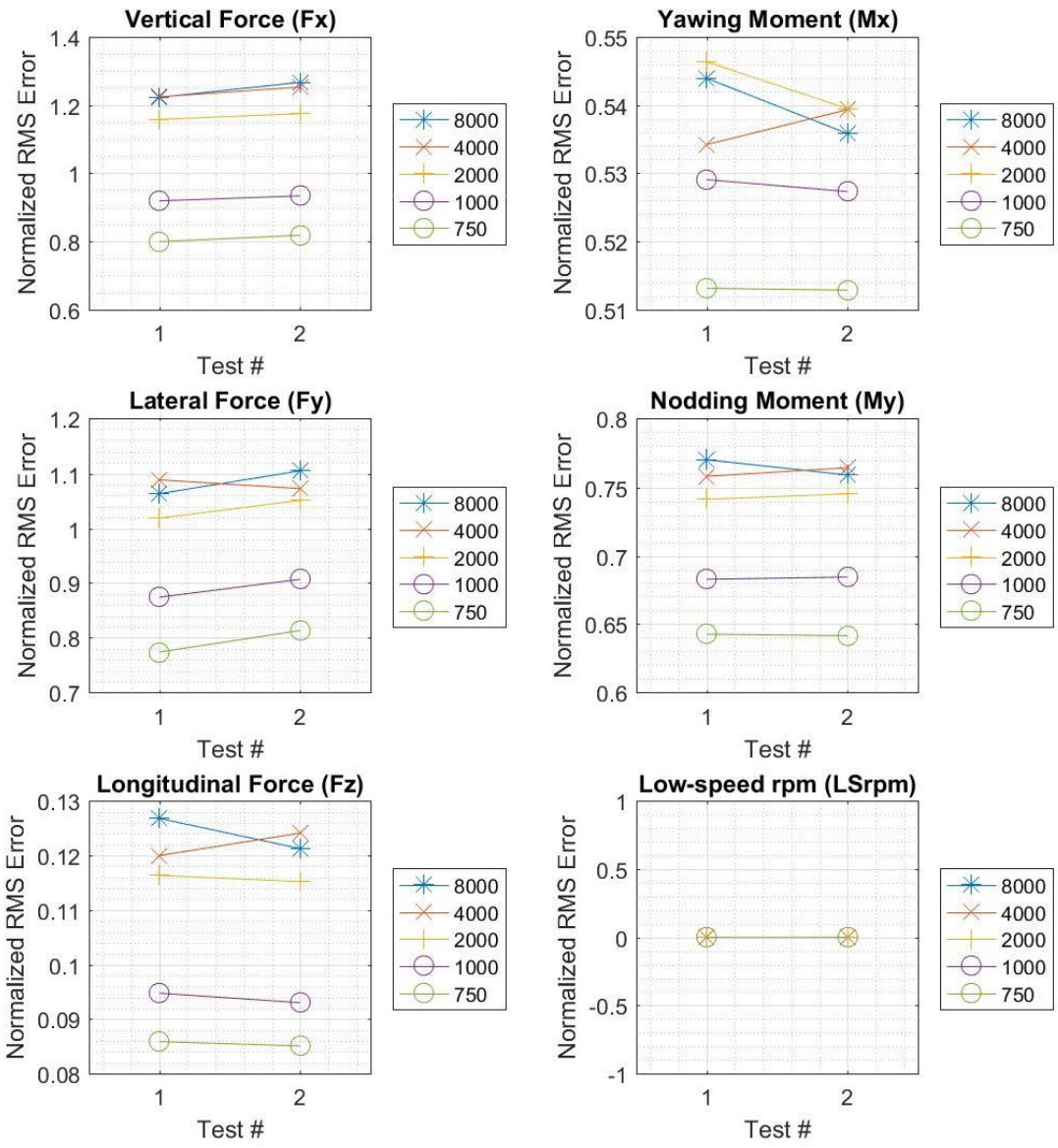

Figure 4.12: Repeatability of the normalized RMS error between the measured and commanded loads for the all ramp rate limits tested with the reference test profile (TP NO8).

Overall, the level of variation of the RMS error with reduced ramp rate limits is either similar or smaller than that with the nominal ramp rate limit. This is indicated by the

slope of the curves connecting the results from both tests taking the slopes in absolute term. This demonstrates that the excellent repeatability of the results is maintained when reducing the ramp rate limit applied to the yawing and nodding moments.

The repeatability of the peak error for all LAU inputs from the eight tests done with the reference test profile are presented in Fig. 4.13 using the P normalization. The peak errors for the lateral force are plotted separately due to the difference in scale, which is due to the combined effect of cross coupling with the relatively small peak value of the lateral force as compared with the other LAU loads for the reference test profile (NO8).

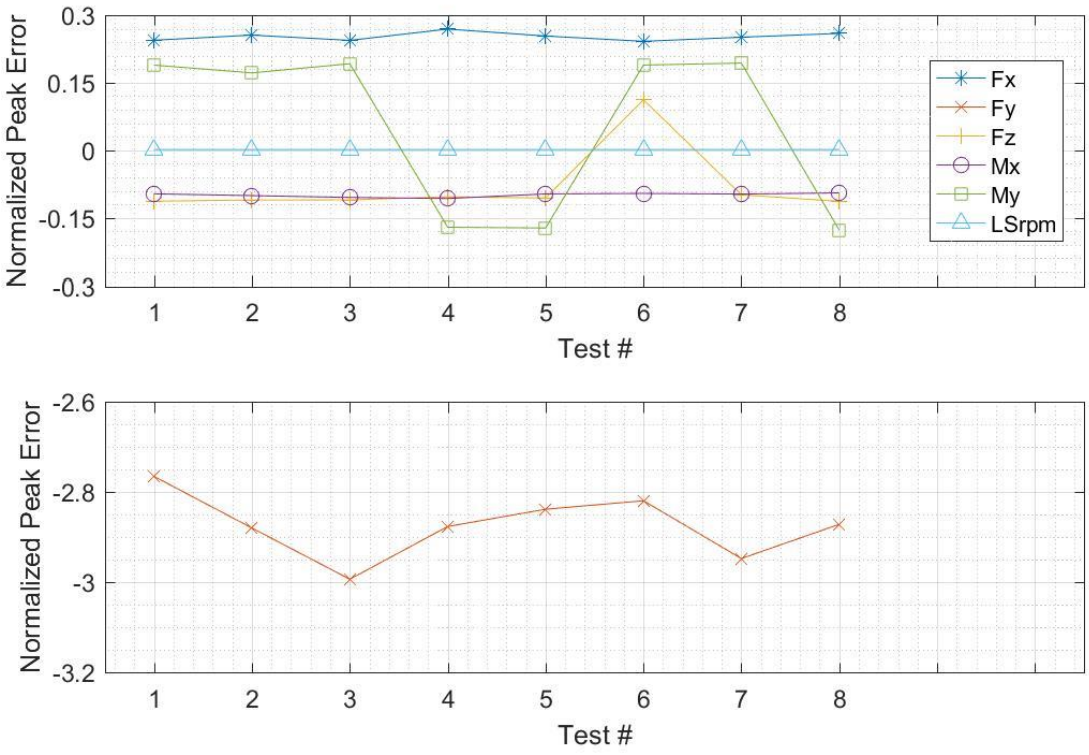

Figure 4.13: Repeatability of the normalized peak error (P normalization) between the measured and commanded LAU loads for the reference test profile (NO8). The larger than unity normalized peak errors for the lateral force are due to the combined effect of cross coupling with relatively small peak value of the lateral force as compared with the other LAU loads for the reference test profile (NO8).

The peak errors for the nodding moment (My) in Fig. 4.13 show a change in sign for the 4th and 5th tests, which can be explained by the min and max errors for this LAU load being comparable as shown in Fig. 4.14. Overall, the peak errors have good repeatability.

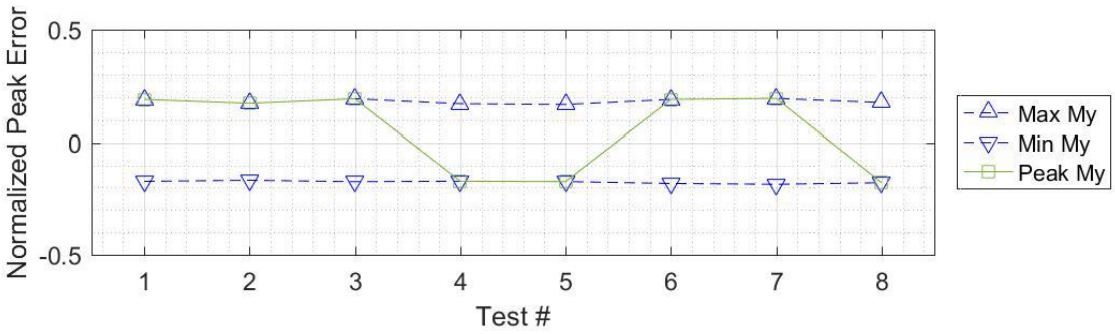

Figure 4.14: Normalized minimum, maximum, and peak errors (P normalization) for the nodding moment (My) for all tests done with the reference test profile (NO8) for the nominal test bench limits. The larger than unity normalized Peak errors are from the normalization with the measurement error.

4.2.3 Tracking performance

The performance of the test bench at tracking the test profiles are presented first for the tests done with the nominal test bench limits. These tracking results represent the capability of the test bench with the 2.3-MW drivetrain and were of most importance to validate the design and simulation models of this drivetrain.

The tracking performance with a reduced ramp rate limit for the yawing and nodding moments is presented separately. These tracking results are of most importance for this research.

4.2.3.1 Nominal test bench ramp rate limits

The tracking performance of the reference TP (NO8) for all LAU inputs is depicted in Fig. 4.14. The measured LAU loads and speed (blue) and commanded LAU inputs (red) are co-plotted. The measurements presented in Fig. 4.14 show the test bench is applying loads that are tracking the commanded values for the moments, longitudinal force and the test bench shaft speed. The tracking is best for the speed input, which comes from using high-precision encoders. The measurements show significant differences with the commanded values for the vertical and lateral forces. These forces are subject to cross coupling with the yawing and nodding moments resulting in large induced forces. This cross-coupling effect was considered in the design of the test bench with the implementation of a compensation scheme in the test bench controller, which was active during all tests. This compensation scheme was clearly not sufficient to track the vertical and lateral forces in the case of the NO8 TP and cross-coupling was measured for all test profiles to a varying degree. As an example of reduced cross-coupling, Fig. 4.15 depicts the tracking performance for the test profile having the smallest resulting moment from the yawing and nodding moments. The cross-coupling effect remains visible but to a much lesser extent as compared with the cross-coupling effect from Fig. 4.14. The good agreement between the measured and commanded loads remains for the other LAU loads and the speed as well.

The tracking performance of all test profiles is presented in Appendix X and the RMS errors corresponding to all LAU inputs and test profiles are summarized in Fig. 4.16. Overall, the tracking is excellent for all LAU inputs except for the vertical and lateral forces (Fx and Fy) due to the previously mentioned cross-coupling effect. The normalized RMS error is within the measurement error (normalized RMS error of 1) for the longitudinal force

(Fz), yawing moment (Mx), and input shaft speed (LSrpm). The nodding moment is within the measurement error for all but one test profile.

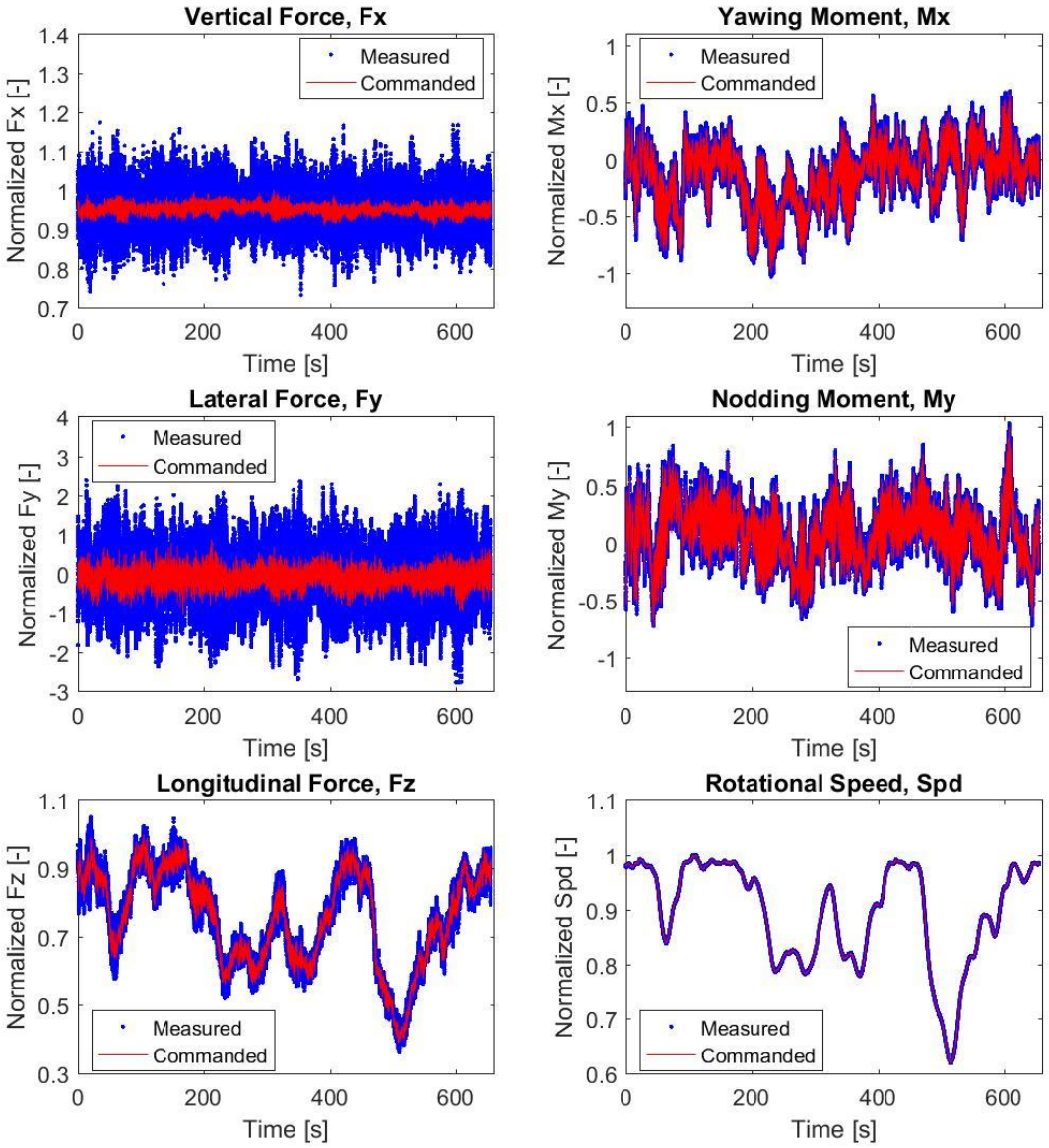

Figure 4.15: Time series of the normalized LAU inputs (P normalization) for the NO8 TP.

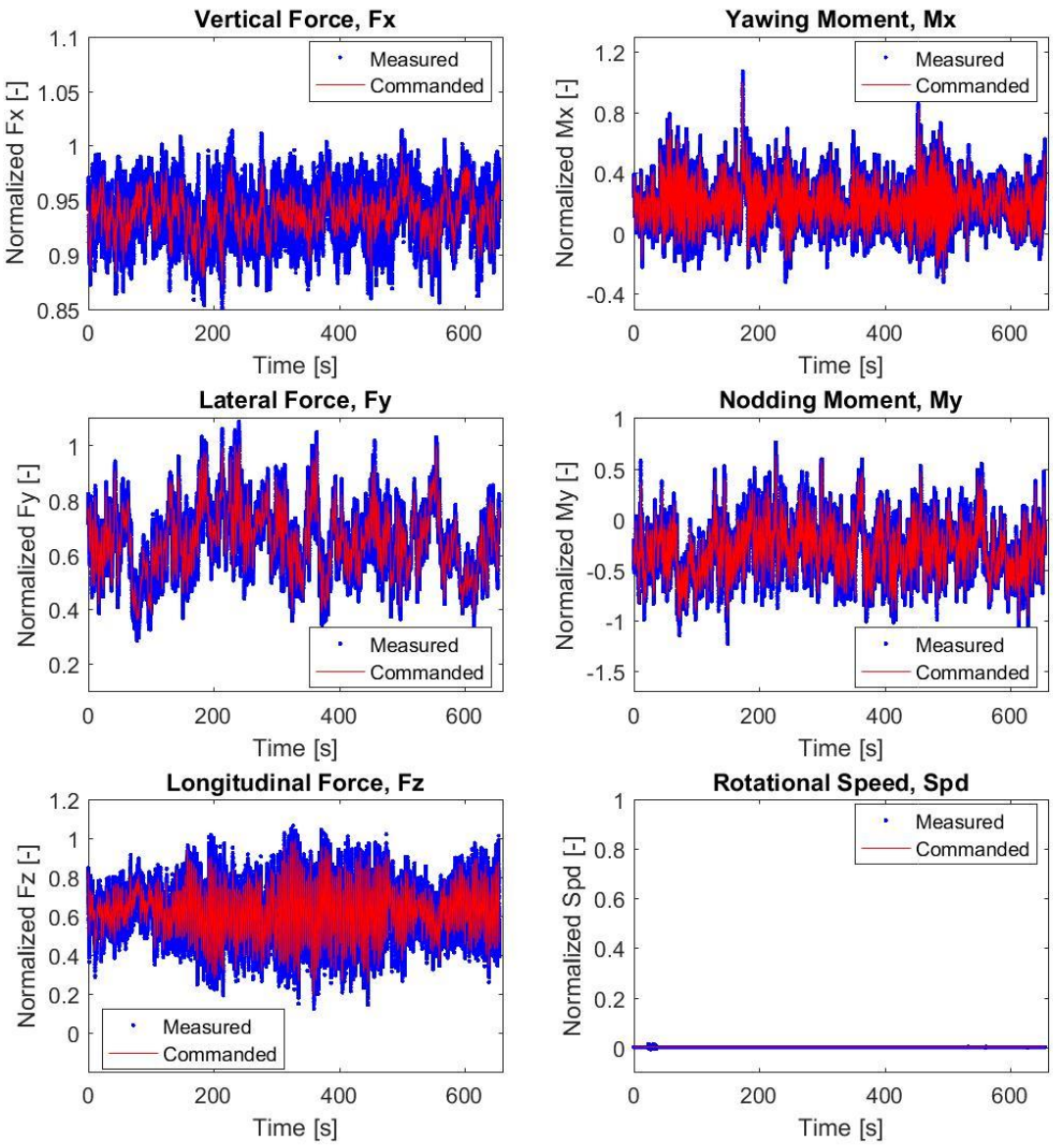

Figure 4.16: Time series of the normalized LAU inputs (P norm.) for the Min Mr TP.

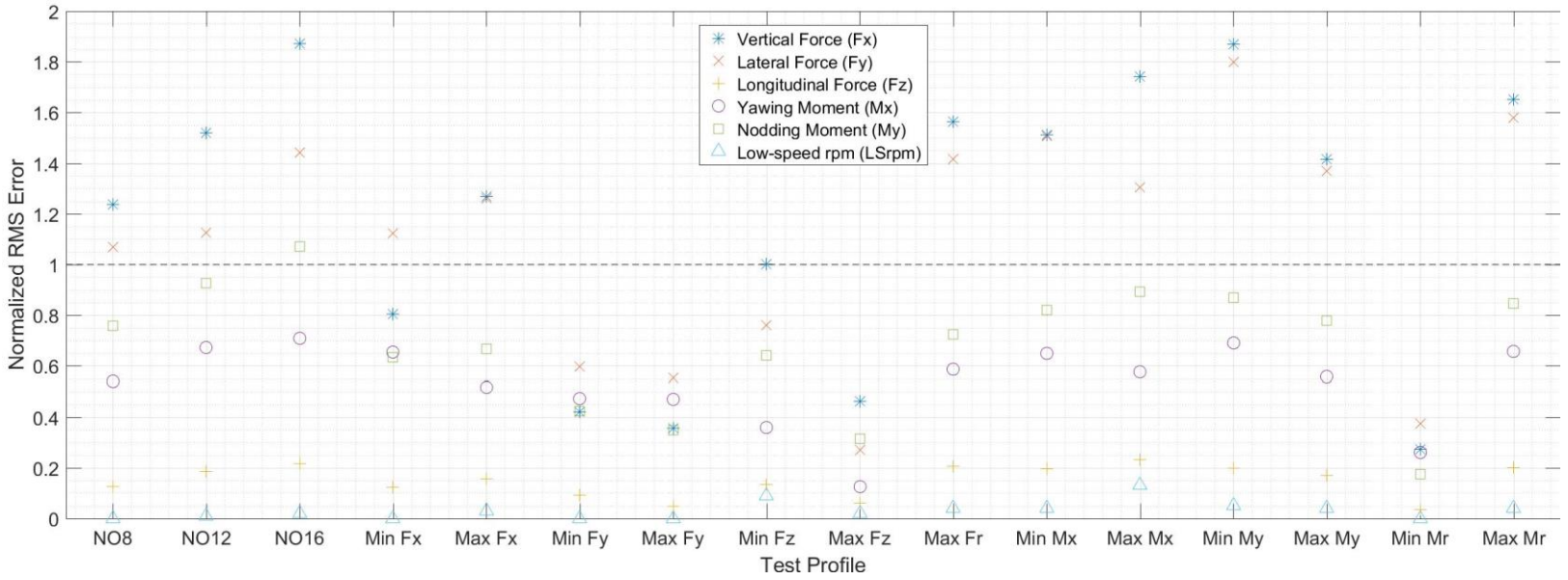

Figure 4.17: Normalized RMS error between the measured and commanded loads and speed for all test profiles for the nominal test bench capability (E normalization).

The RMS error is the primary metric to evaluate the tracking performance of the test bench, but the maximum difference between the measurement and the commanded value over a complete test profile or peak error is also relevant. The peak error for all LAU loads and speed and all test profiles are presented in Fig. 4.17. The peak errors shown in this figure are normalized with the measurement error (E normalization). There are six peak errors per test profile for the six LAU inputs. Positive normalized peak errors indicate measurements larger than the commanded value and the opposite for negative normalized peak errors. The largest peak errors are for the two forces most impacted by the previously mentioned cross-coupling effect between the bending moments applied by the LAU and the forces. The peak errors in the LAU loads are relatively evenly spread from the zero error line with most peak errors falling outside a normalized RMS error of ± 1 representing errors larger than the measurement error. This is not surprising for peak errors normalized with the measurement error because the peak loads from all test profiles are approximately up to 5x and 9x of the measurement error for the bending moments and forces, respectively.

The peak errors normalized with the peak value of each load for a given test profile (P normalization) are presented in Fig. 4.18. Except for the lateral force, the peak errors are less than 50% of the peak load/speed value of each test profile (normalized peak errors within ± 0.5). As previously stated, the large peak errors for the lateral forces reflect the combined effect of cross coupling with relatively small peak value of the lateral force as compared with the other LAU loads for the reference test profile (NO8).

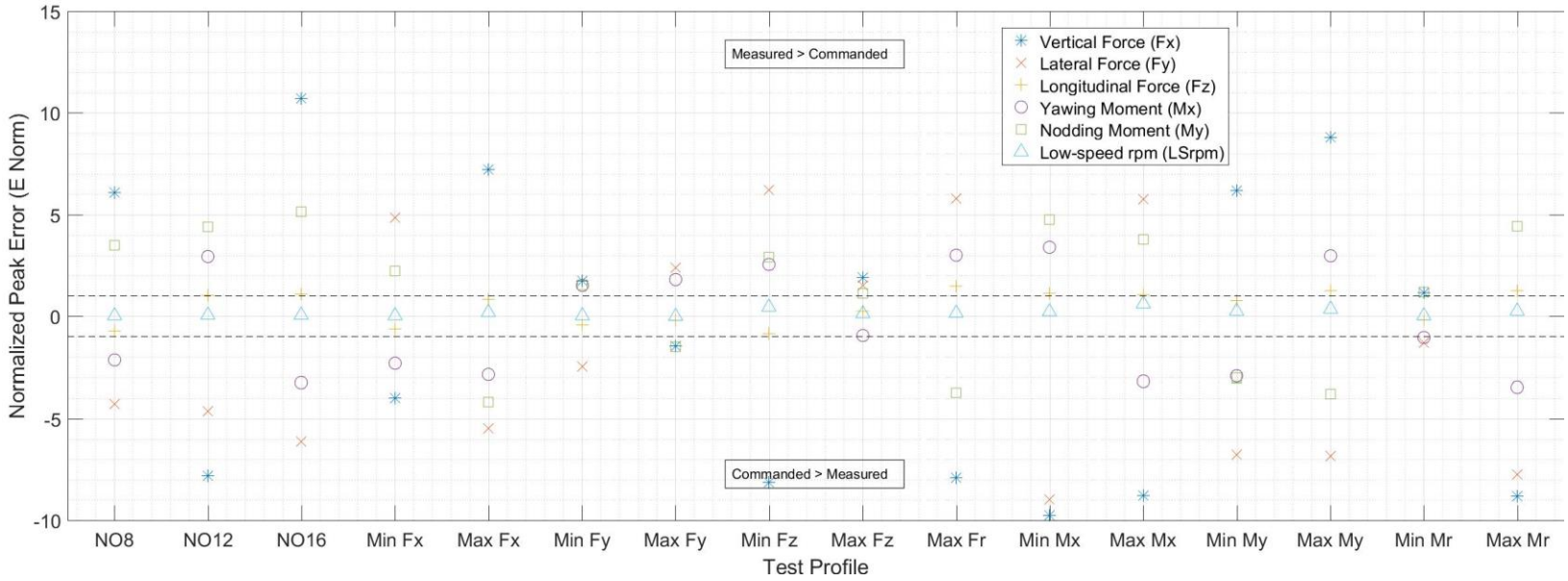

Figure 4.18: Normalized peak error between the measured and commanded loads and speed for all test profiles for the nominal test bench capability (E normalization).

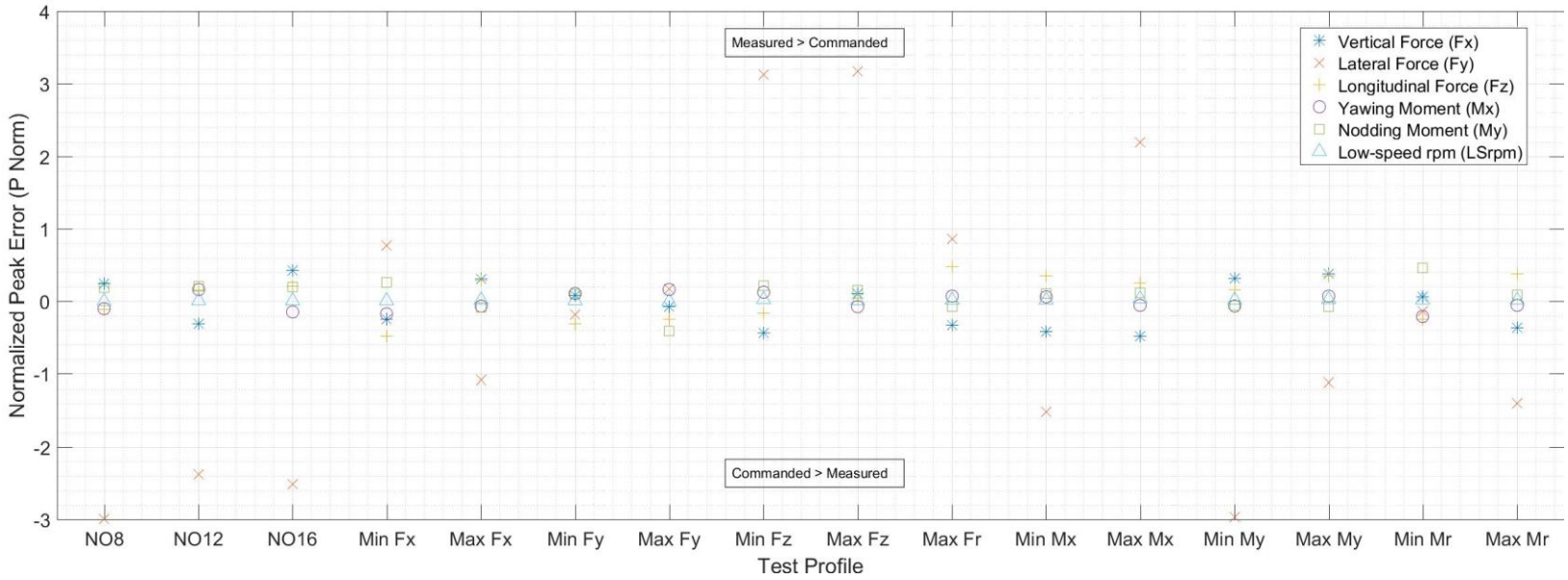

Figure 4.19: Normalized peak error between the measured and commanded loads and speed for all test profiles for the nominal test bench capability (P normalization).

The dynamic nature of the test profiles that were tested combined with the tracking performance summarized in Fig. 4.16 suggest that the test bench can match the commanded test profile in the frequency domain at least for the longitudinal force, both moments and the speed. This is shown in Fig. 4.20 for the reference TP (NO8) for all LAU inputs in the frequency domain. This figure corresponds to the time series presented in Fig. 4.14 with the amplitude normalized with the peak commanded values of the LAU loads and speed. The frequency range of 5 Hz captures over 99% of the total spectral energy in the signal. The cross-coupling effect causes the peak amplitudes for the vertical and lateral forces to be greater than the commanded peak amplitudes by a factor of 2.1 and 4.2, respectively, as indicated with the scale for the amplitude in Fig. 4.20. The frequency for the peak amplitude is also altered from the cross-coupling effect. Specifically, the frequency for the peak amplitude for the vertical and lateral forces corresponds to the second peak in amplitude (0.7 Hz, 3P) for the yawing and nodding moments. To further demonstrate that the differences in the measured vertical and lateral forces are driven by the cross coupling effect, Fig. 4.21 presents the Fast Fourier Transform (FFT) for all LAU loads and speed for the test profile commanding the smallest resultant bending moment between the yawing and nodding moments. The cross-coupling effect is present, but the peak amplitude for the vertical and lateral force is remain within the commanded value with an additional peak in amplitude that corresponds to the amplitude peak of the moments near a frequency of one Hz. The FFT plots for the lateral force and yawing moment in Fig. 4.20 demonstrate that the cross-coupling effect on the lateral force comes primarily from the yawing moment. The additional peak amplitude for the lateral force is at the frequency of the peak amplitude of the yawing moment. A similar relationship is present between the vertical force and the nodding moment. Note that there is no FFT for

the low-speed in the case of the min Mr test profile because the speed signal was set to zero due to the test bench not able to apply rotation is both directions, which is what the parked or idling load case have has speed input.

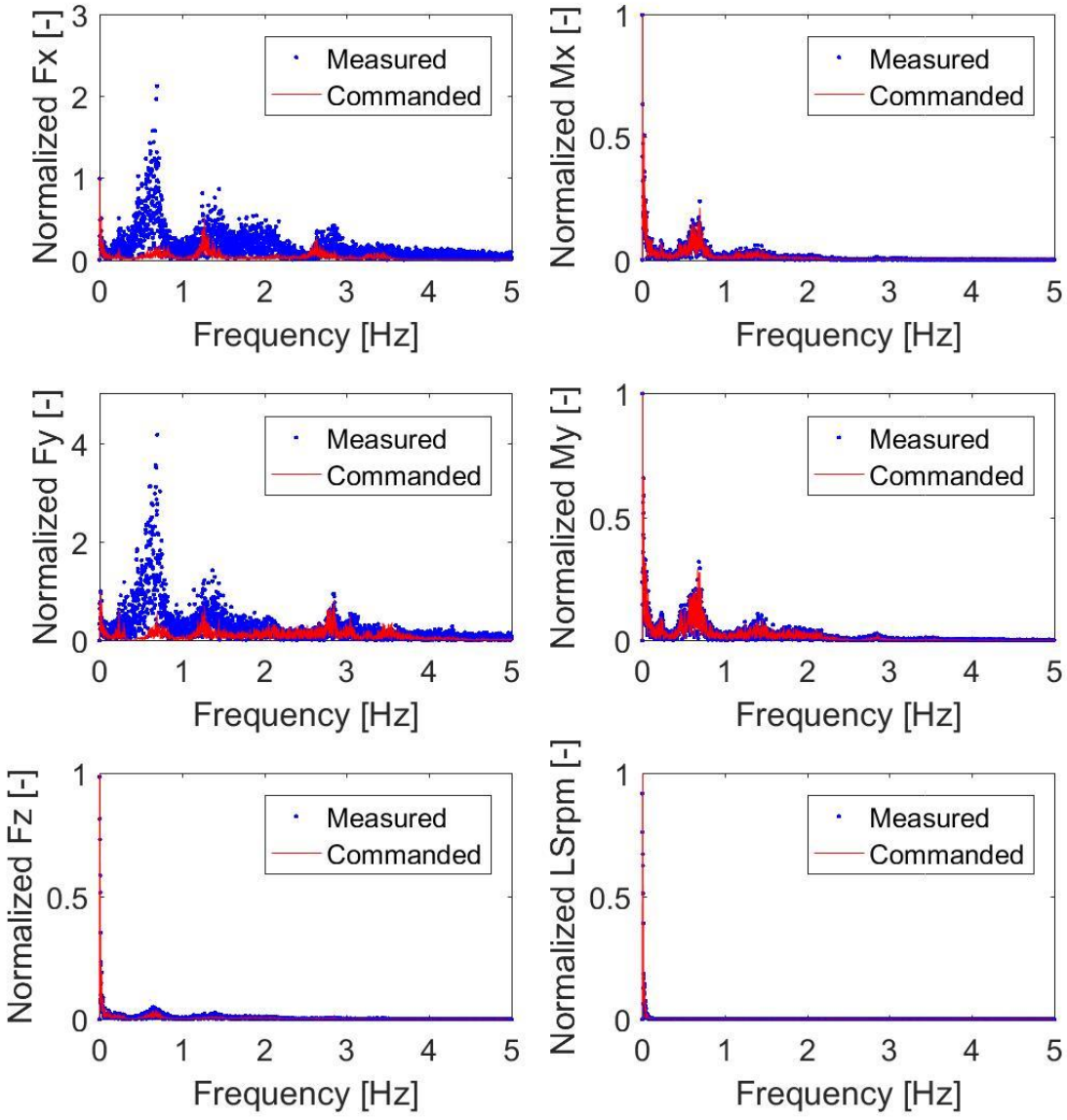

Figure 4.20: Frequency domain representation of the normalized LAU loads and speed (P normalization) for the NO8 test profile.

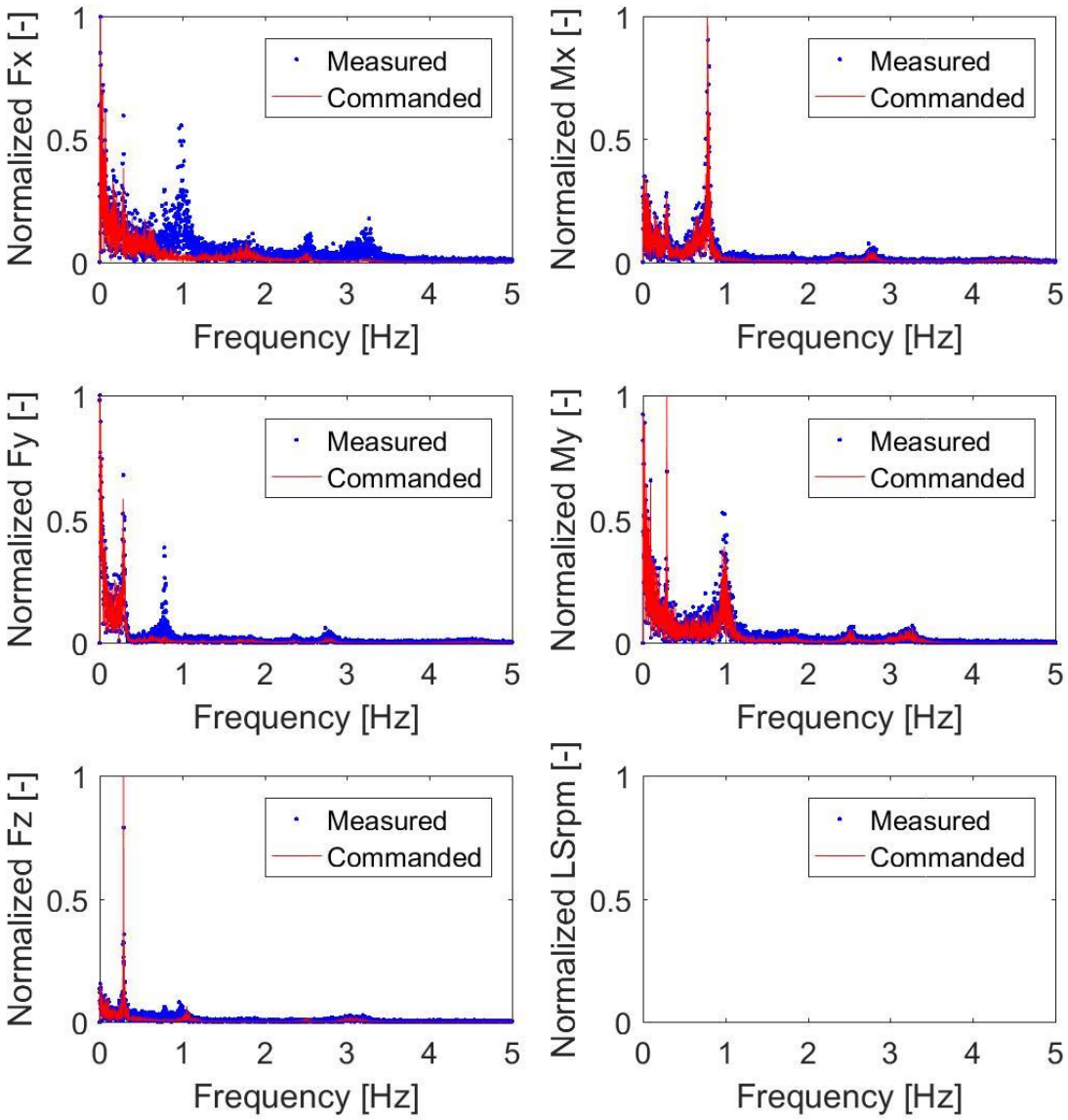

Figure 4.21: Frequency domain representation of the normalized LAU loads and speed (P normalization) for the min Mr test profile.

4.2.3.2 Reduced ramp rate limits

As stated in the introduction of this Chapter and summarized in Table 4.1, tests were conducted with reduced ramp rate limits in order to expand the range of test bench coverage error and capability ratio covered by the measurements. Given the cross-coupling effect and the excellent tracking of the commanded speed, the reduction of the ramp rate limits was imposed only on the yawing and nodding moments. At least three and up to six ramp rate limits were tested per test profile including the nominal limit of 8000 kNm/s for the yawing and nodding moments. Figures 4.22 and 4.23 present the RMS error normalized with the measurement error as a function of the ramp rate limit for the yawing and nodding moments, respectively. In these figures, all results are shown in the upper left plot with the other three plots focusing on a subgroup of the test data. Table 4.6 describes the data subgroups and gives the number of samples (data points) for the overall data set and for the three subgroups. Repeats of the same test profile were excluded in the sample count and only one result was used per combination of test profile and ramp rate limit. Note that the range of the y axis vary between the plots in Figs. 4.22 and 4.23, and the RMS errors are from comparing the measured LAU loads and speed with the commanded values for the nominal test bench limits.

Table 4.6: Description and number of samples for the data subgroups.

Subgroup (TP Type)	Description	# Data Points
All	All test profiles	76
NO	Test profiles representing the normal operation of the wind turbine	15
NR	Test profiles reflecting a parked and non-rotating wind turbine in a storm	17
SD	Test profiles in which the wind turbine controller triggers a shutdown due to a particular fault	25

The results presented in Figs. 4.22 and 4.23 show an increase in RMS error with decreasing ramp rate limit, as expected, with the increase being non-linear and highly dependent on the test profile. The results for the yawing moment of the min Mr test profile does not show this trend, but the normalized RMS errors for this TP are less than 20% of the measurement error. The measurement accuracy masks the impact of the reduction in ramp rate limit on the RMS error for test profiles having load magnitude and ramp rate levels similar to the measurement accuracy. Accordingly, trending of the RMS error with reduced ramp rate limit is best done when the RMS error exceeds the measurement error, which is indicated with the dotted horizontal line at unity in Figs. 4.22 and 4.23.

The RMS error clearly depends on the level of magnitude and ramp rates of a given test profile. The larger values of RMS error for the test profiles causing the wind turbine to shutdown (SD subgroups) indicate that the test profiles from that subgroup are most demanding.

The ramp rate limit reflects different values of the evaluation metrics, which are used to infer and predict the actual tracking (RMS) error. This is discussed in Section 4.3.

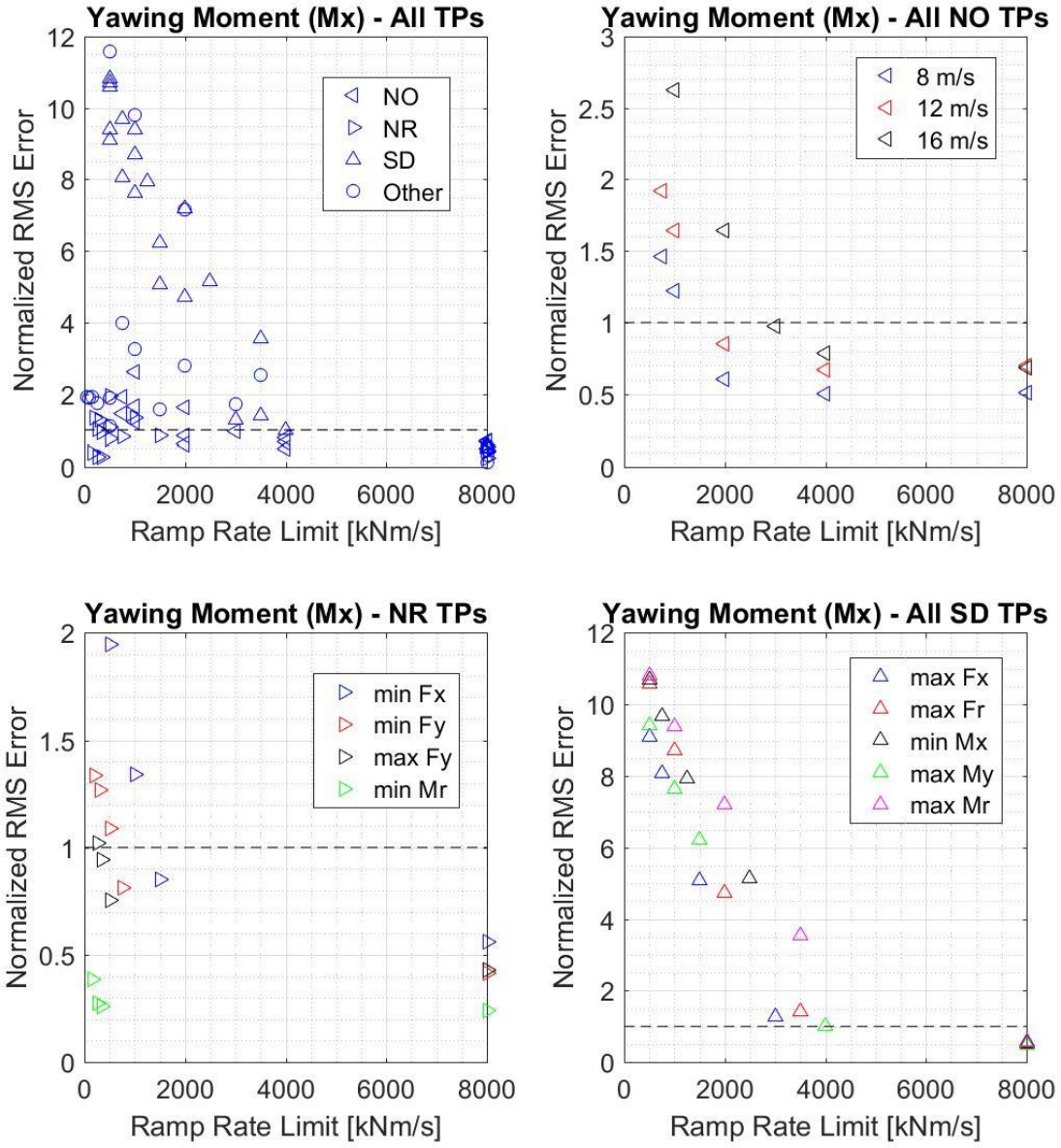

Figure 4.22: Normalized RMS error (E normalization) as a function of the ramp rate limit for the yawing moment for all tests (upper left plot) and three different subsets (NO: TPs reflecting normal operation conditions, NR: TPs reflecting non-rotating operating conditions, SD: TPs reflecting a turbine shut down).

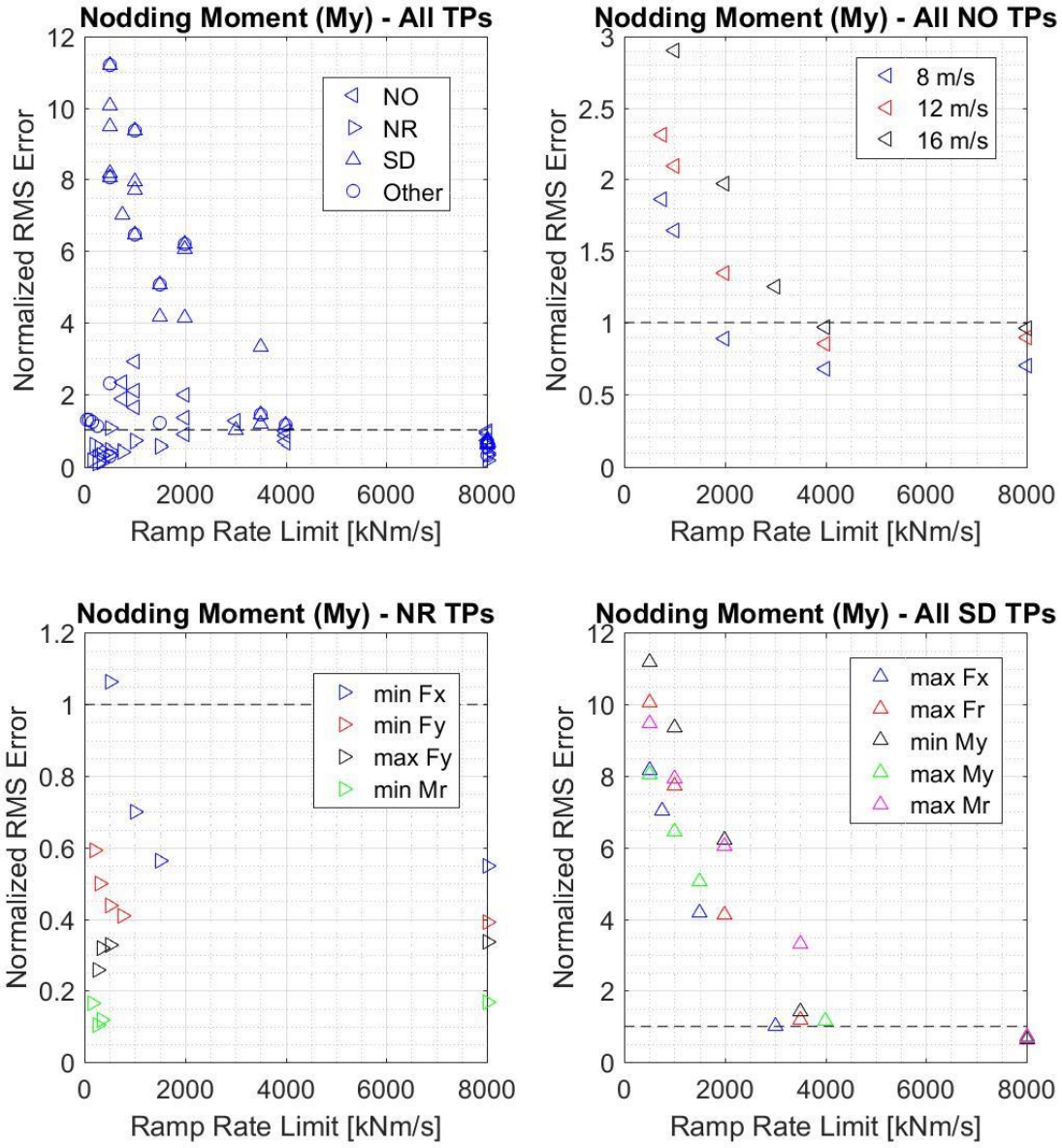

Figure 4.23: Normalized RMS error (E normalization) as a function of the ramp rate limit for nodding moment for all tests (upper left plot) and three different subsets (NO: TPs reflecting normal operation conditions, NR: TPs reflecting non-rotating operating conditions, SD: TPs reflecting a turbine shut down).

The RMS error is a useful metric to quantify the tracking of the LAU loads and speed over the test profiles. It is also useful to visualize the tracking in the time and frequency domain to determine if the RMS error is driven by a few large misses or from the accumulation of a fairly consistent error. Figures 4.24 and 4.25 present the time series of the reference test profile (NO8) for all tested ramp rate limits for the yawing and nodding moments, respectively. There are 10 plots in each of these figures with the time series of the measured moments on the left and the histogram of the ramp rate from the commanded moments on the right. The reference is the commanded moment for the nominal ramp rate limit of 8000 kNm/s. The time series and histograms are presented in decreasing order of the imposed ramp rate limit starting with the nominal value at the top. Note that the scale of all of the time series plots and histograms are the same to facilitate comparison and that scale does not capture the nominal ramp rate limit. The red vertical dotted lines in the histograms indicate the ramp rate limit and the reduction in ramp rate limit is clearly seen. In contrast, the differences (errors) between the measurements and the reference in Figs. 4.24 and 4.25 are not as obvious. These errors are presented in Figs. 4.26 and 4.27 as time series on the left and histograms on the right. The normalization of the error with the peak value of the moments of the NO8 test profile puts the error in perspective with the largest error being approximately 50% and 65% of the peak value of the yawing and nodding moments, respectively. The growth in the error is clearly seen from the histograms in Fig. 4.26 and 4.27, and the tracking error is an accumulation of smoothly distributed (but non-normal) errors having a mean of nearly zero with growing tails with decreasing ramp rate limits. The time series shown in Figs. 4.24 and 4.25 are presented in the frequency domain in Figs. 4.28 and 4.29. The frequency range is limited to 2 Hz, which captures the overall frequency content in the signal. Figures

4.28 and 4.29 show that the differences in amplitude spectrum mainly occur at the largest frequencies with non-zero amplitudes as one would expect.

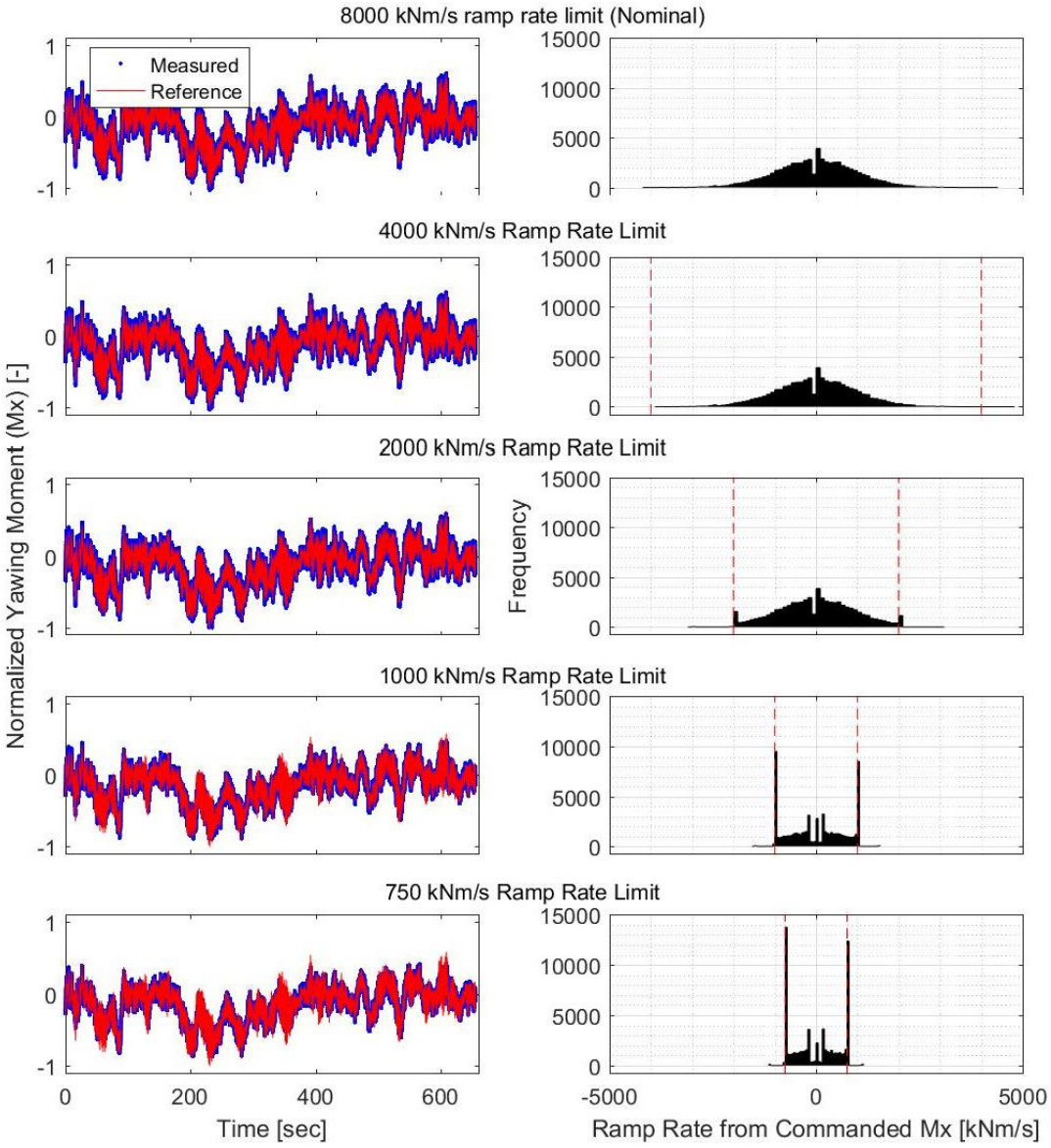

Figure 4.24: Time series of the measured yawing moment (Mx) of the reference (NO8) test profile for all test bench ramp rates tested and histograms of the commanded ramp rate of Mx of each test. The P normalization was applied to Mx and the reference is the commanded test profile for the case of the nominal test bench limit. The vertical red lines in the histograms indicate the ramp rate limit imposed at each test.

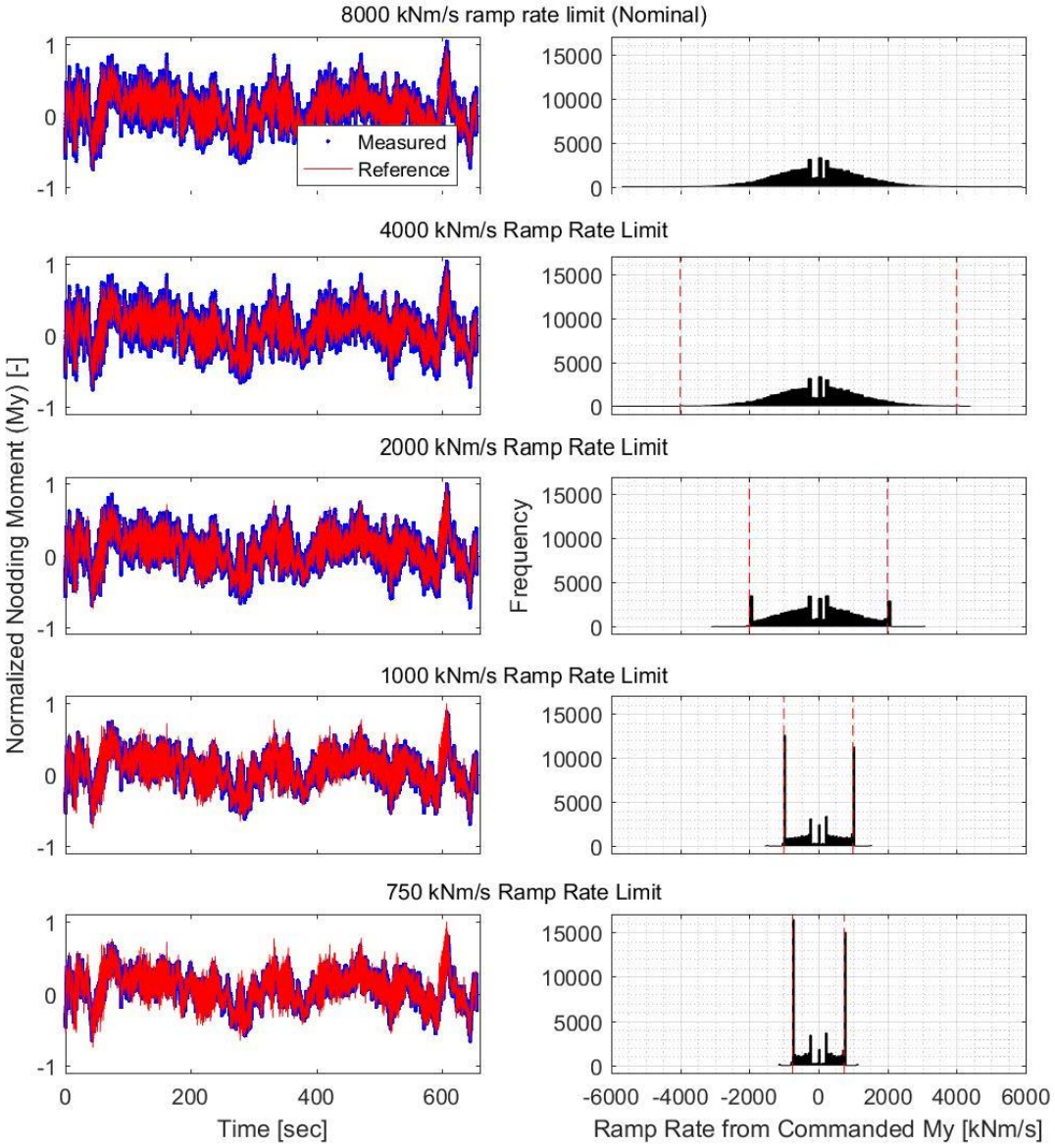

Figure 4.25: Time series of the measured nodding moment (My) of the reference (NO8) test profile for all test bench ramp rates tested and histograms of the commanded ramp rate of My of each test. The P normalization is applied to Mx and the reference is the commanded test profile for the case of the nominal test bench limit. The vertical red lines in the histograms indicate the ramp rate limit imposed at each test.

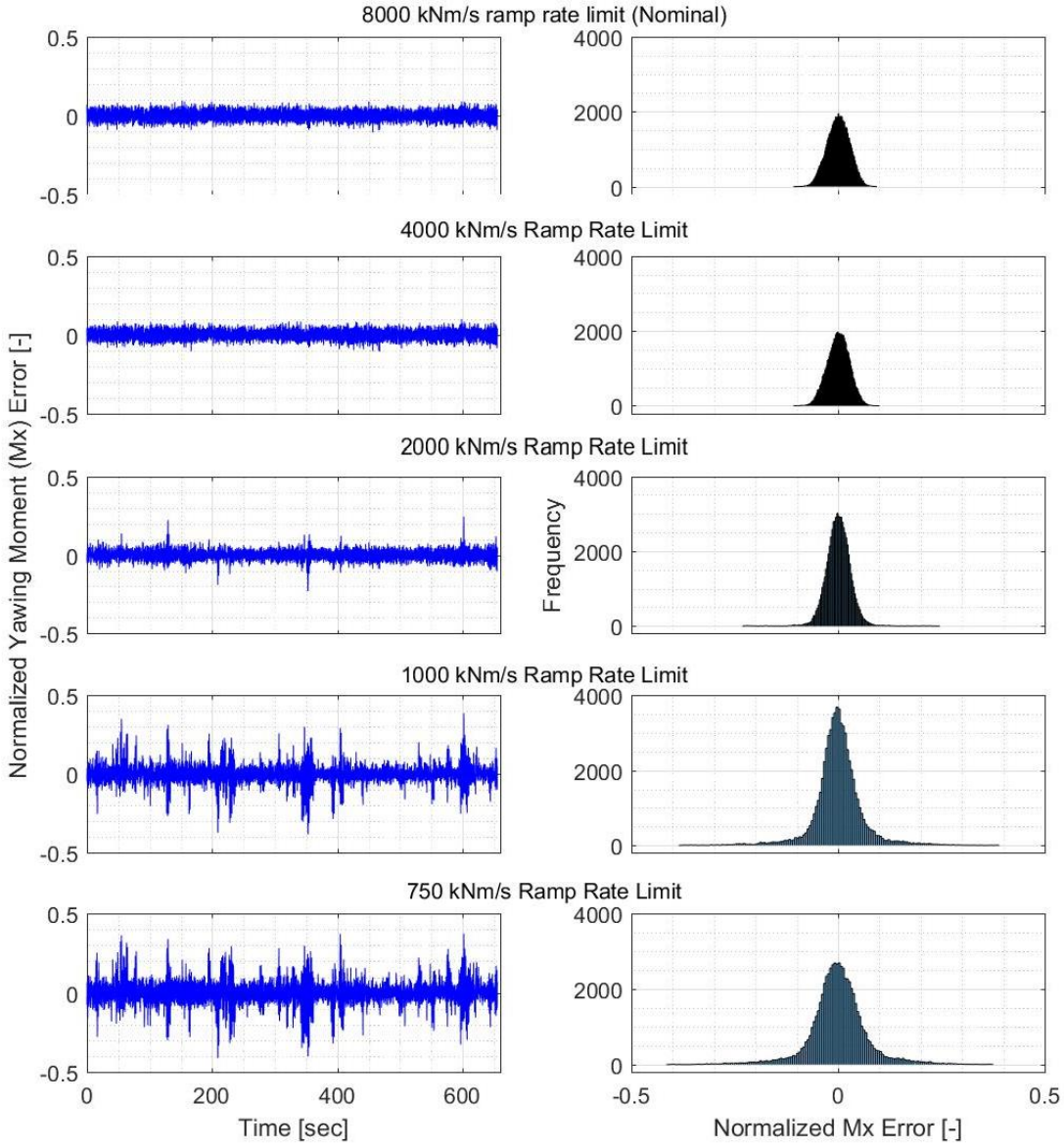

Figure 4.26: Time series and histograms of the error in yawing moment (Mx) between the measurements and reference from Fig. 4.24. The P normalization is applied to the Mx error.

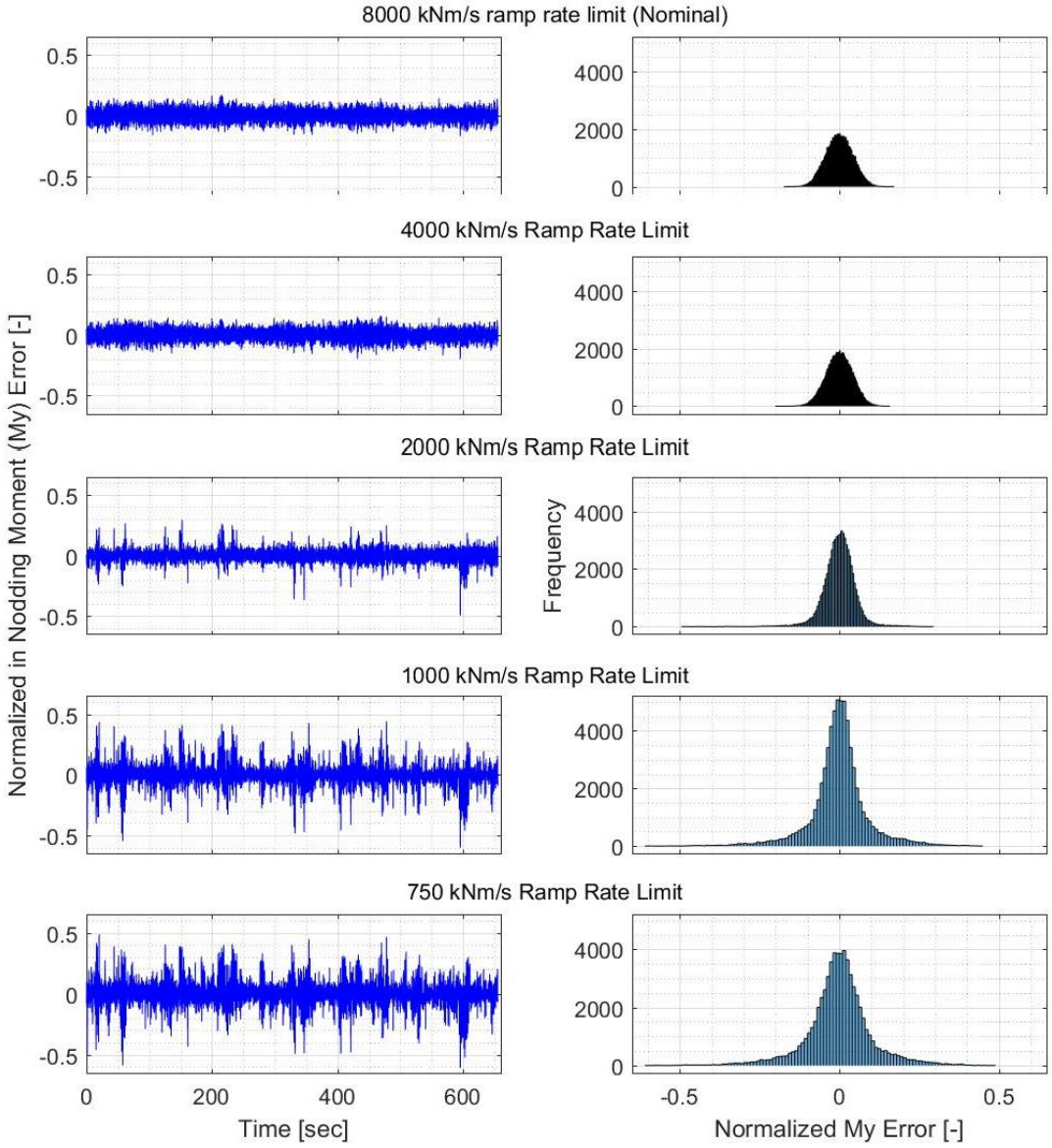

Figure 4.27: Time series and histograms of the error in nodding moment (My) between the measurements and reference from Fig. 4.25. The P normalization is applied to the My error.

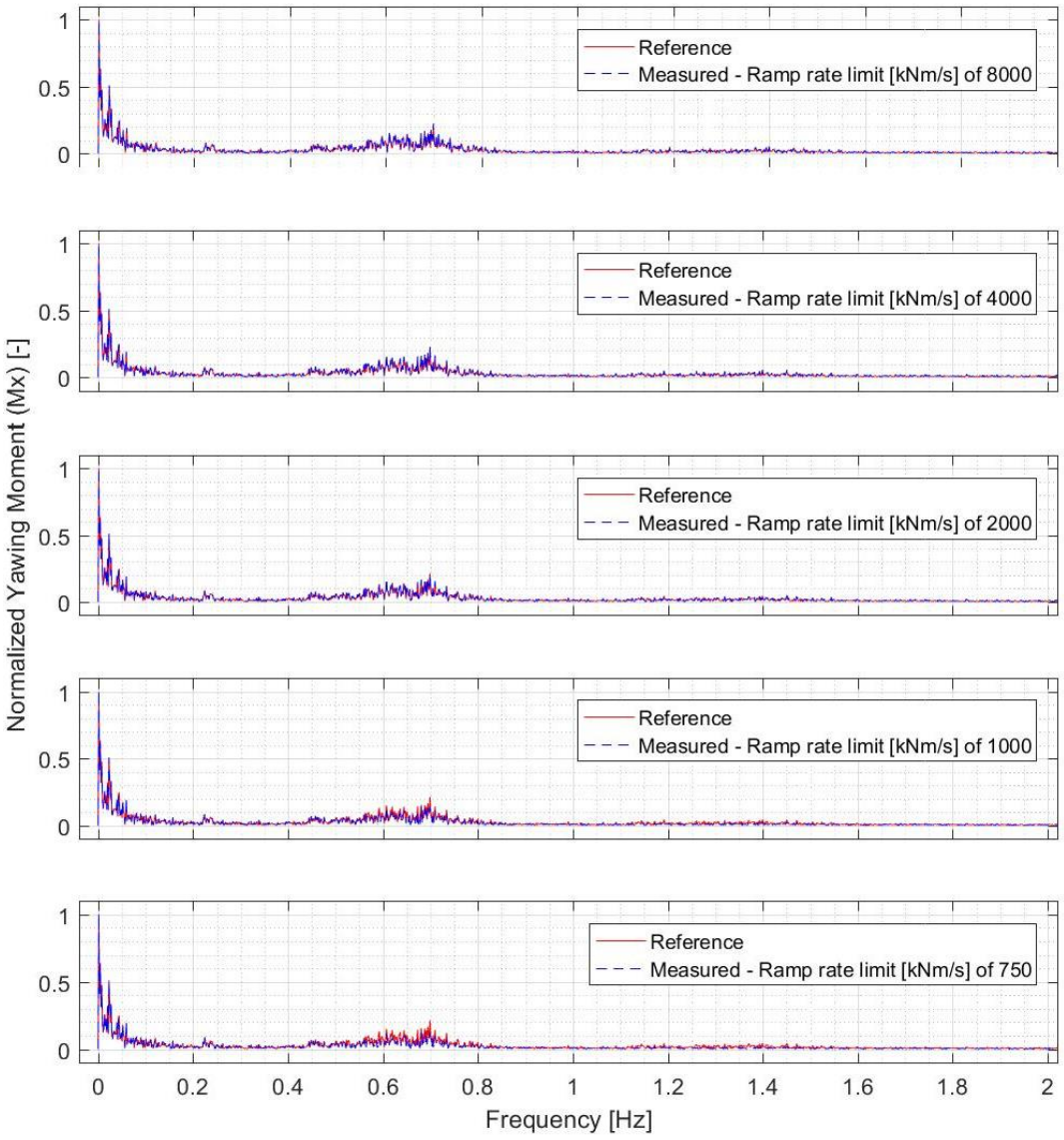

Figure 4.28: Frequency domain representation of the normalized yawing moment (Mx) of the NO8 test profile measured for the test bench ramp rate limits considered. The P normalization was applied to Mx and the reference is the commanded test profile for the case of the nominal test bench limit.

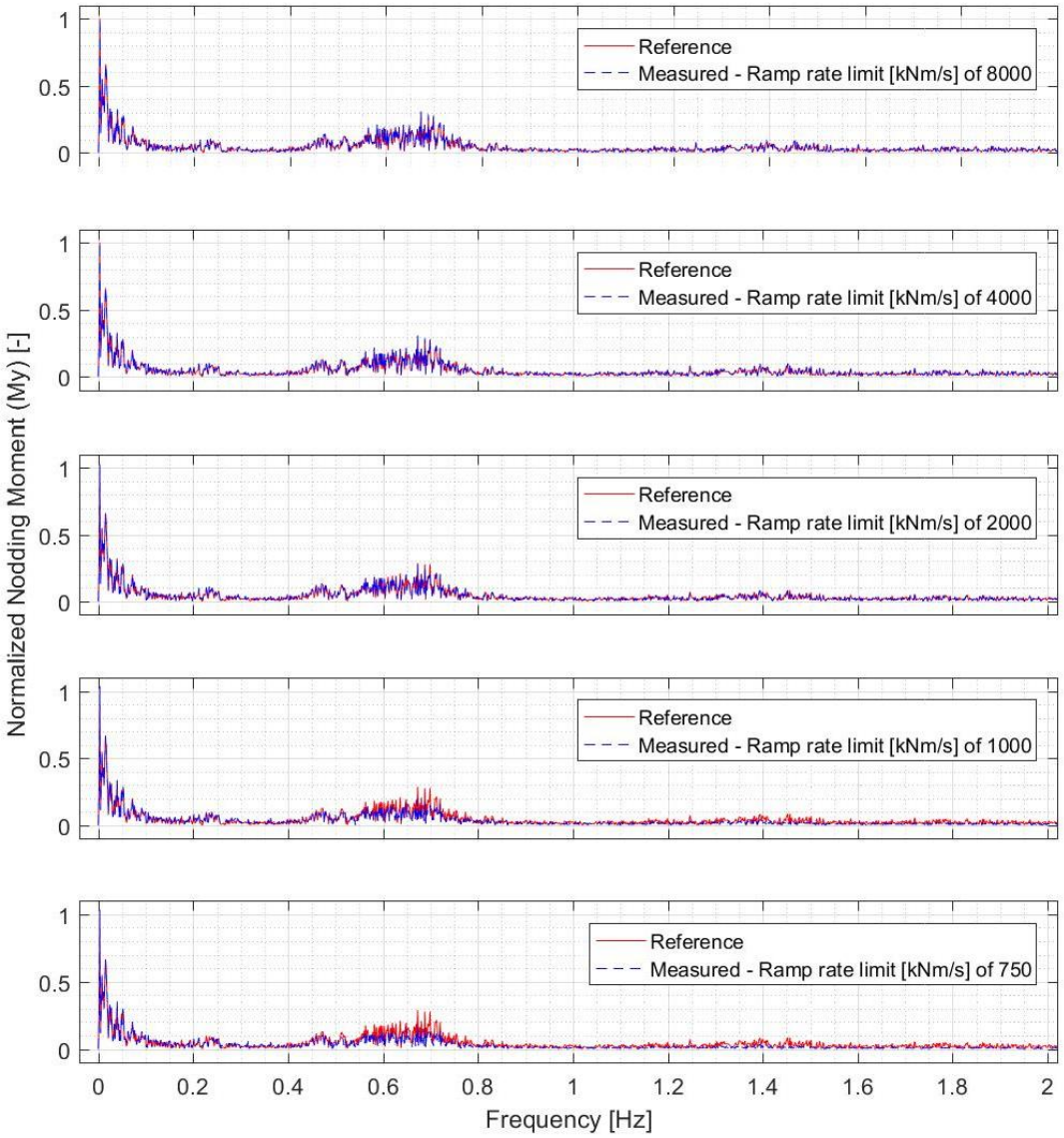

Figure 4.29: Frequency domain representation of the normalized nodding moment (My) of the NO8 test profile measured for the test bench ramp rate limits considered. The P normalization was applied to My and the reference is the commanded test profile for the case of the nominal test bench limit.

4.3 Comparison with predictions

The measurements presented in Section 4.2 are compared with the evaluation metrics of test bench coverage error and capability ratio. The predictions presented in Section 3.2 suggest that the 7.5-MW test bench should be able to replicate the test profiles with acceptable tracking error when considering the doubling of the ramp rate limit on the moments since the predictions were made. The results from Fig. 4.17 indicated this to be the case for the longitudinal force, yawing and nodding moments, and speed when using the measurement error as threshold. The cross-coupling effect induced forces that made the tracking error of the vertical and lateral forces exceed the measurement error for most of the test profiles. Given the cross-coupling effect and the bending moments from the test profiles being significantly larger in magnitude than the forces, the comparison with predictions focuses on the yawing and nodding moments.

Figure 4.30 presents the RMS error for the yawing and nodding moments with the coverage RMS error for the nominal test bench limits. The coverage RMS error is zero for the yawing moment for all test profiles and zero or nearly zero for the yawing moment. The variation in the RMS error from the measurements is not captured by the coverage RMS error. This finding is not surprising when considering that the RMS errors from measurements (actual RMS error) reflect a combined error covering the following:

- Test-bench hardware limitation error, which reflects the ability of the LAU hardware to apply the desired magnitude and ramp rate of the commanded LAU inputs onto the test article.
- Test-bench controller error, which reflects the ability of the test bench controller to track the commanded test profile.

For test profiles having commanded LAU inputs within the test bench capability, which is the case for all test profiles tested with the 2.3-MW drivetrain and the nominal test bench limits, the test-bench hardware limitation error is not contributing to the total error. Accordingly, the RMS errors presented in Fig. 4.30 reflect test-bench controller error.

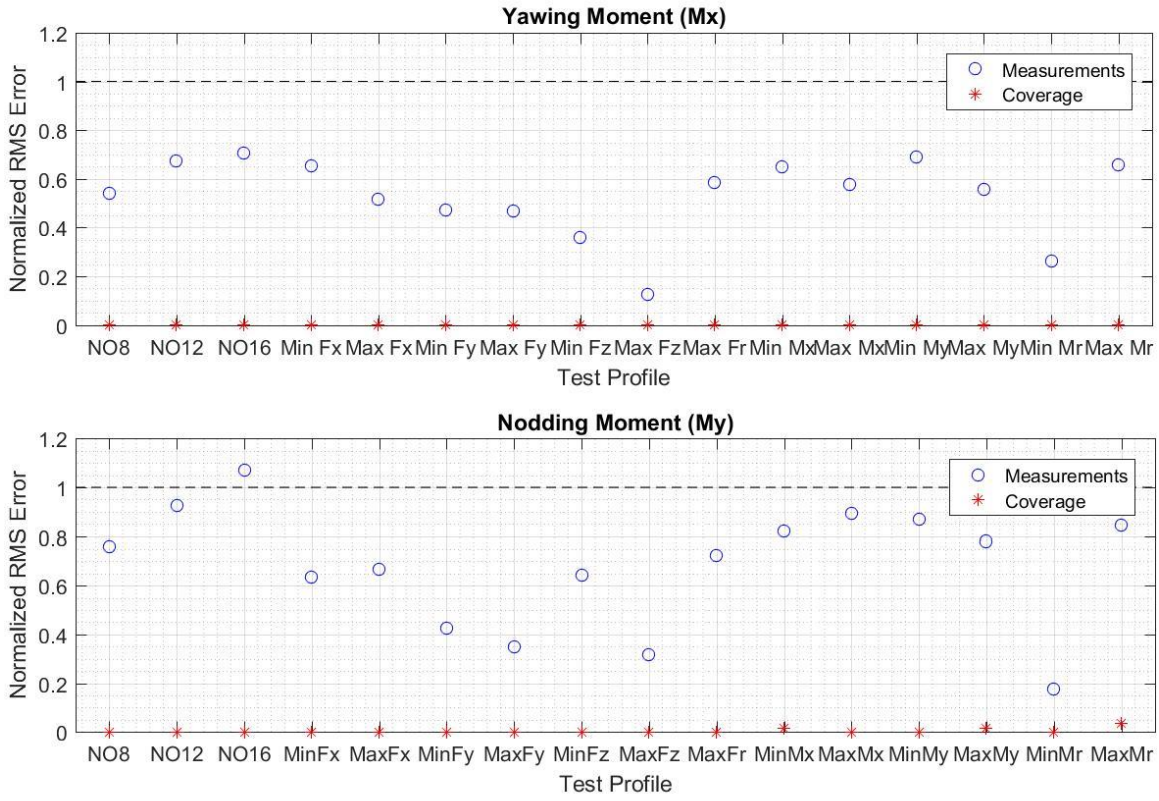

Figure 4.30: Normalized RMS error (E normalization) for the yawing (Mx) and nodding (My) moments from measurements and coverage values for all test profiles.

Such controller error is unavoidable, especially with dynamic input test profiles, and the test bench operator aims to minimize the controller error. The metrics of test bench coverage RMS error and capability ratio consider only the test-bench hardware limitation error. Furthermore, these metrics aim to predict if a test bench can replicate a test profile with an acceptable level of tracking error. Predicting the actual RMS error goes

beyond that target and the measurements made with reduced ramp rate limits allows the evaluation of the method towards that end.

Figures 4.31 and 4.32 present the RMS error for all test profiles as a function of the four evaluation metrics: test bench coverage RMS error, magnitude capability ratio, and ramp rate capability ratio. Several observations can be made from these figures and they can be summarized as follows.

- The test bench coverage RMS error is the best predictor of the actual RMS error with a linear relationship.
- The test bench coverage RMS error exceeds the actual RMS error for the highest RMS error levels.
- The test bench capability ratio for magnitude does not capture the actual RMS error due to the values of this metric being much greater than one. Accordingly, conclusions on the ability of the predictive capability of the capability ratio are to be drawn from the ramp rate.
- The test bench capability ratio for ramp rate and the actual RMS error shows two main populations and there is no clear value of capability ratio corresponding to an acceptable level of tracking error.

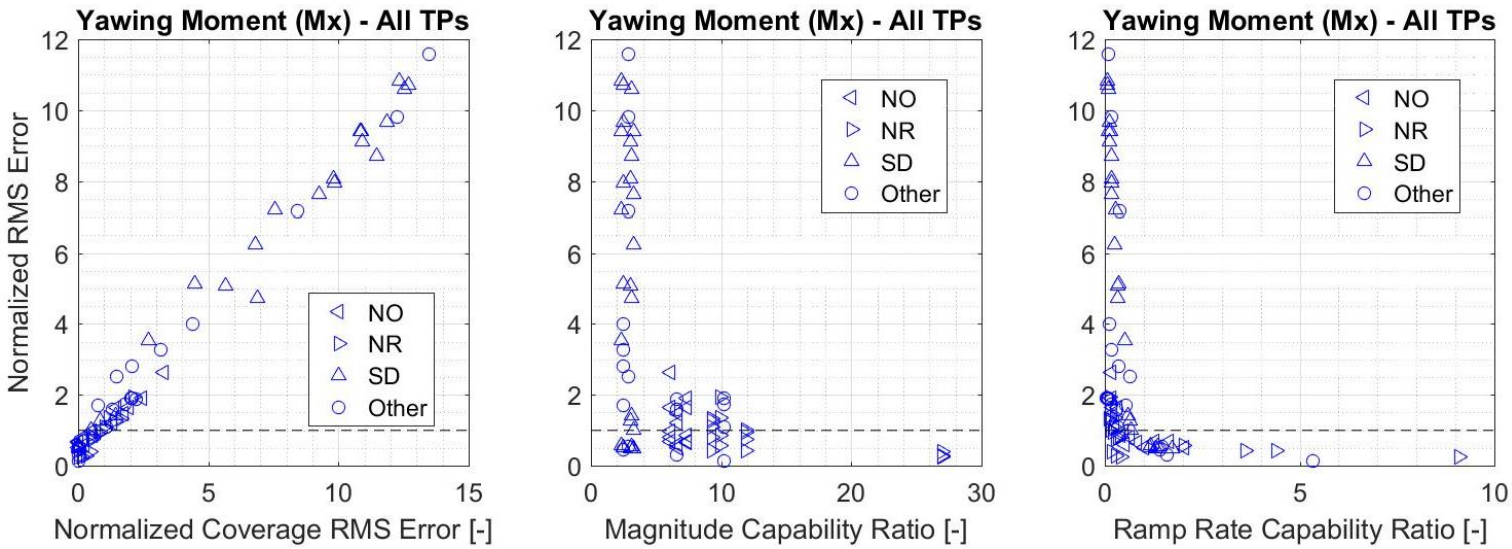

Figure 4.31: Normalized RMS error (E normalization) as a function of the evaluation metrics of test bench coverage error (RMS value), magnitude capability ratio, ramp capability ratio for the yawing moment for all tests and three different subgroups: NO (normal operation), NR (parked turbine under extreme winds), SD (extreme event causing turbine to shut down).

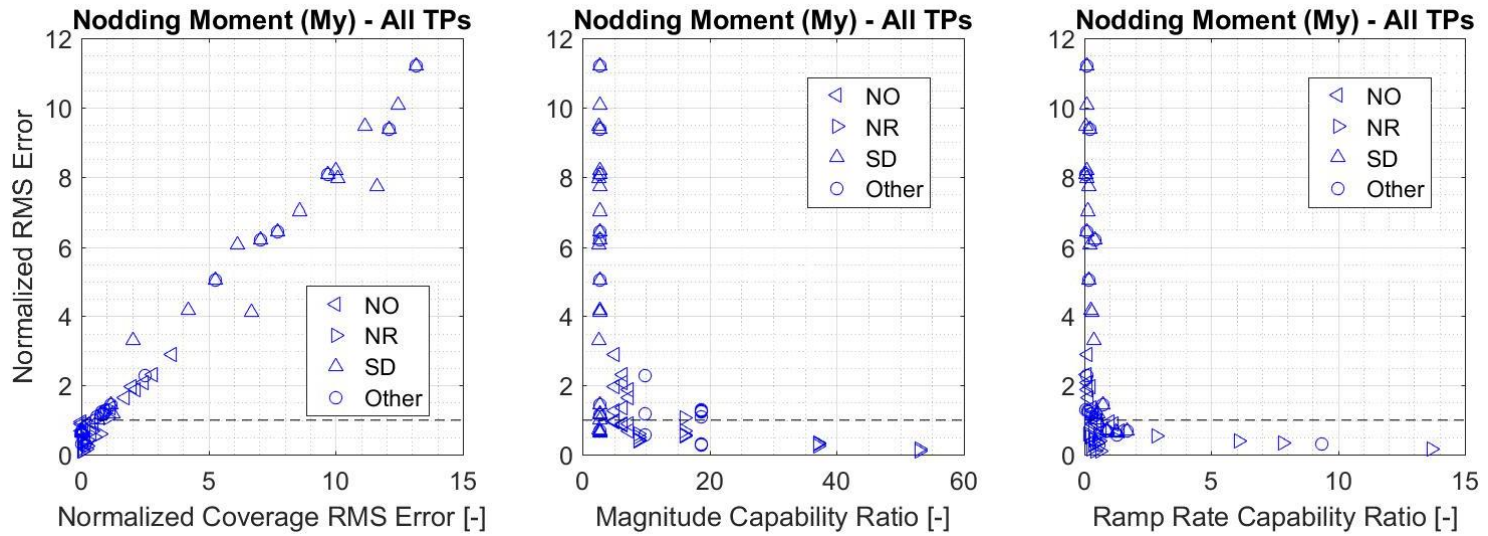

Figure 4.32: Normalized RMS error (E normalization) as a function of the evaluation metrics of test bench coverage error (RMS value), magnitude capability ratio, ramp rate capability ratio for the nodding moment for all tests (upper left plot) and three different subgroups: NO (normal operation), NR (parked turbine under extreme winds), SD (extreme event causing turbine to shut down).

The above observations can be furthered developed by subdividing results by test profile type. Figures 4.33 and 4.34 presents the RMS error of all test profiles as a function of the test bench coverage metric. These figures are repeats of Figs. 4.22 and 4.23 replacing the ramp rate limits with the corresponding coverage values. The same is done for the test bench coverage RMS error and capability ratio in Figs. 4.35-4.38. The capability ratio for magnitude is excluded because the test bench capability exceeds the commanded magnitude of the yawing and nodding moments by at least a factor of 2.4. As a result, the capability ratio for magnitude does not contribute to the predictive capability of the tracking error. Figures 4.35 and 4.36 are for coverage RMS error and Figs. 4.37 and 4.28 are for the capability ratio for ramp rate. Additional observations emerge from the subgrouping of the data by test profile type as summarized below.

- The linear relationship between the test bench coverage RMS error and the actual RMS error is even stronger for test profiles having RMS errors greater than unity (data outside the measurement error). For these test profiles, the actual RMS error corresponding to a coverage RMS error of zero, which corresponds to the test bench controller error, vary within a subgroup.
- The trend between the test bench coverage and the RMS error from measurements is clearer when the results from a given test profiles include RMS errors greater than unity. This is the case for the NO and SD subgroups with a fairly linear trend for NO and a leveling off of the RMS error for SD. The trend is not as strong when the RMS error is less than unity. Using the measurement error as acceptance threshold, coverage above 80%-90% yields acceptable levels of RMS errors.
- The subgrouping for the ramp rate capability ratio results in trends for test profiles having RMS errors greater than unity. For these test profiles, there is clearly a large

increase in the normalized RMS error after the ramp rate capability ratio reaches 0.4-0.6 for the nodding moment for both the yawing and nodding moment. This cross-over point being below a capability ratio of unity suggests that the test bench limit used to calculate the capability ratio is an underestimate of the test bench capability. This can be seen in Figs. 4.2, 4.6, and 4.7 with measured ramp rates for the yawing and nodding moments exceeding the nominal limit of 8000 kNm/s used to calculate the capability ratio.

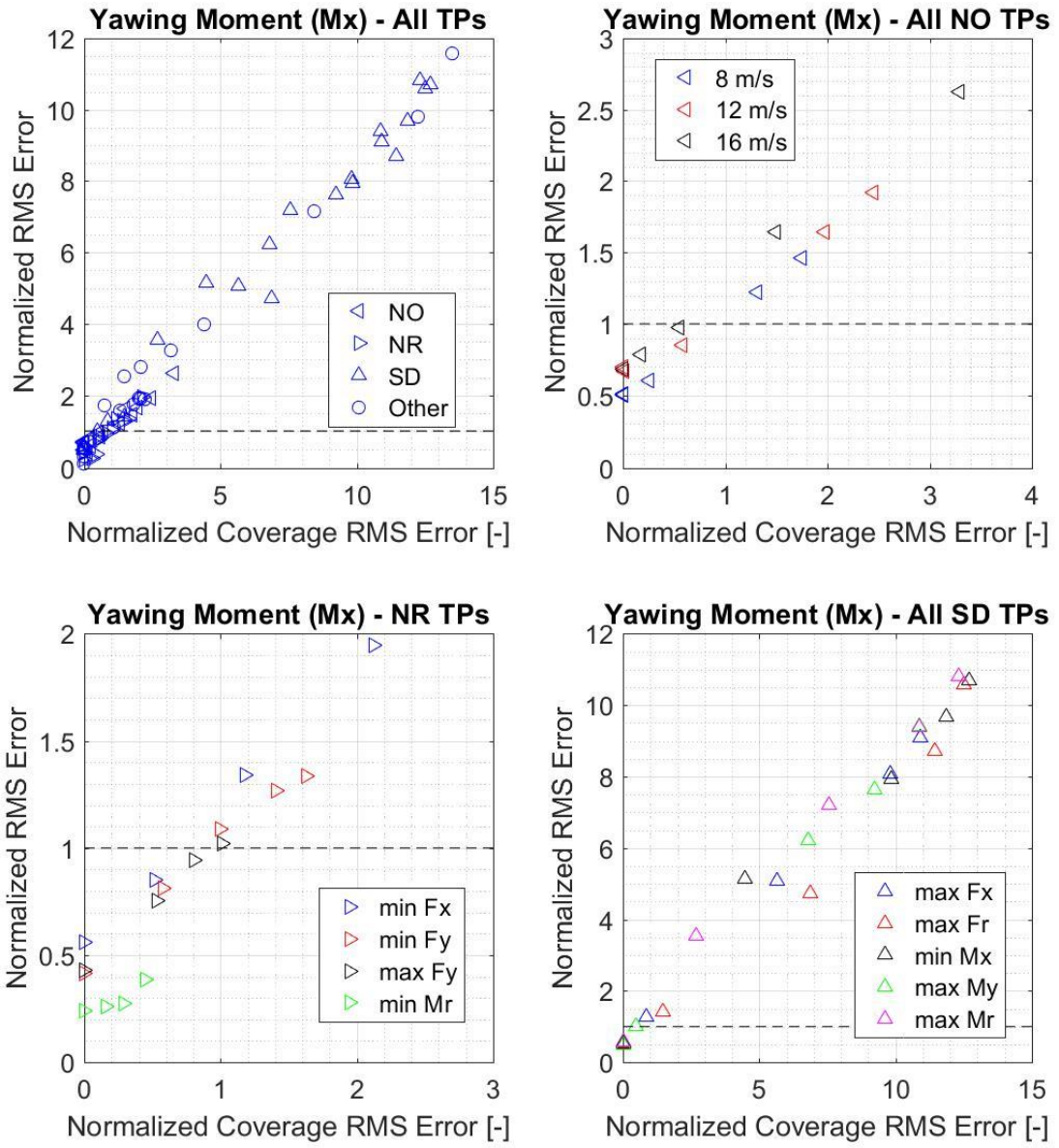

Figure 4.33: Normalized RMS error (E normalization) as a function of the coverage RMS error for the yawing moment for all tests (upper left plot) and three different subgroups: NO (normal operation), NR (parked turbine under extreme winds), SD (extreme event causing turbine to shut down).

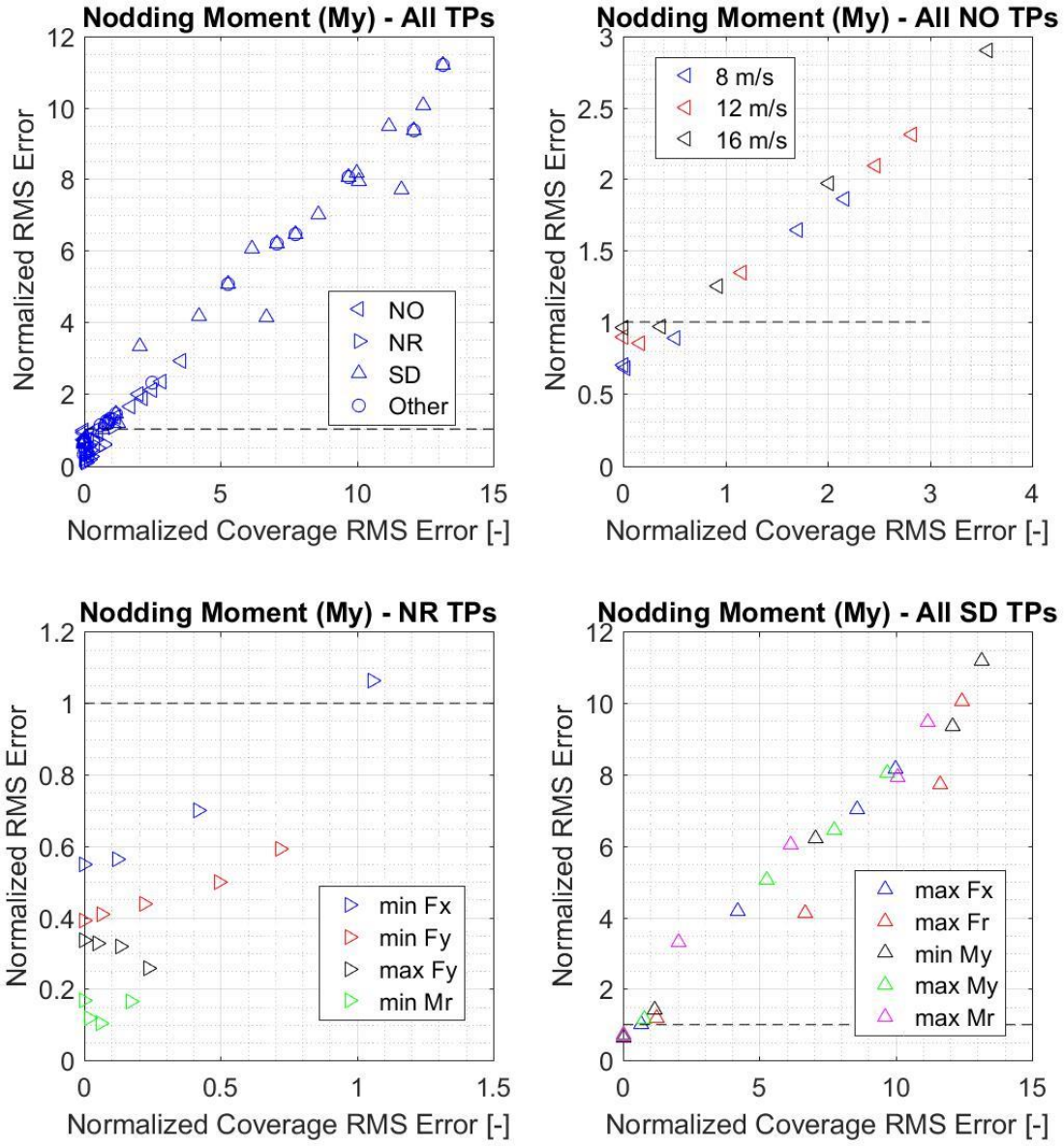

Figure 4.34: Normalized RMS error (E normalization) as a function of the coverage RMS error for the nodding moment for all tests (upper left plot) and three different subgroups: NO (normal operation), NR (parked turbine under extreme winds), SD (extreme event causing turbine to shut down).

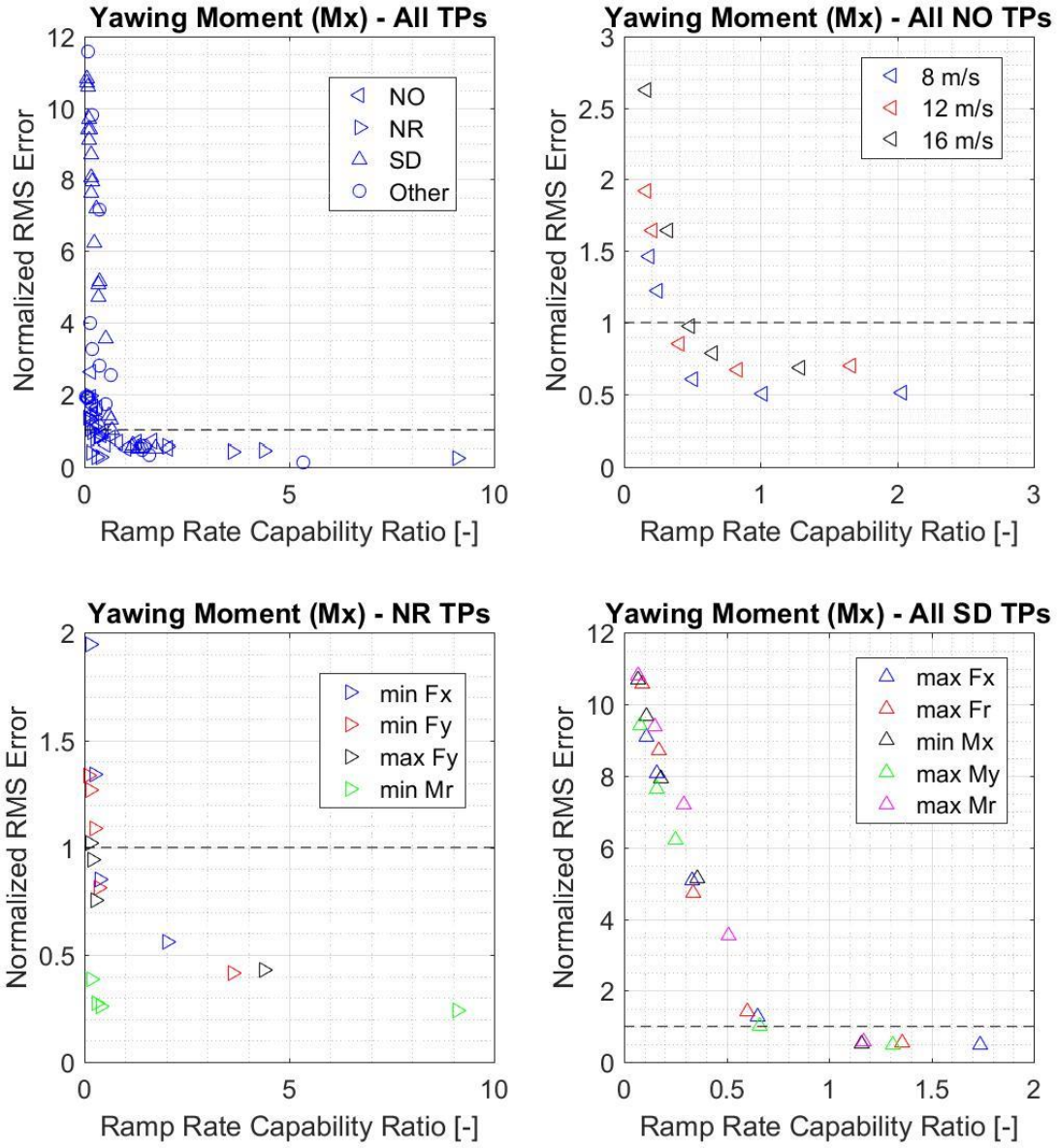

Figure 4.35: Normalized RMS error (E normalization) as a function of the test bench ramp rate capability ratio for the yawing moment for all tests (upper left plot) and three different subgroups: NO (normal operation), NR (parked turbine under extreme winds), SD (extreme event causing turbine to shut down).

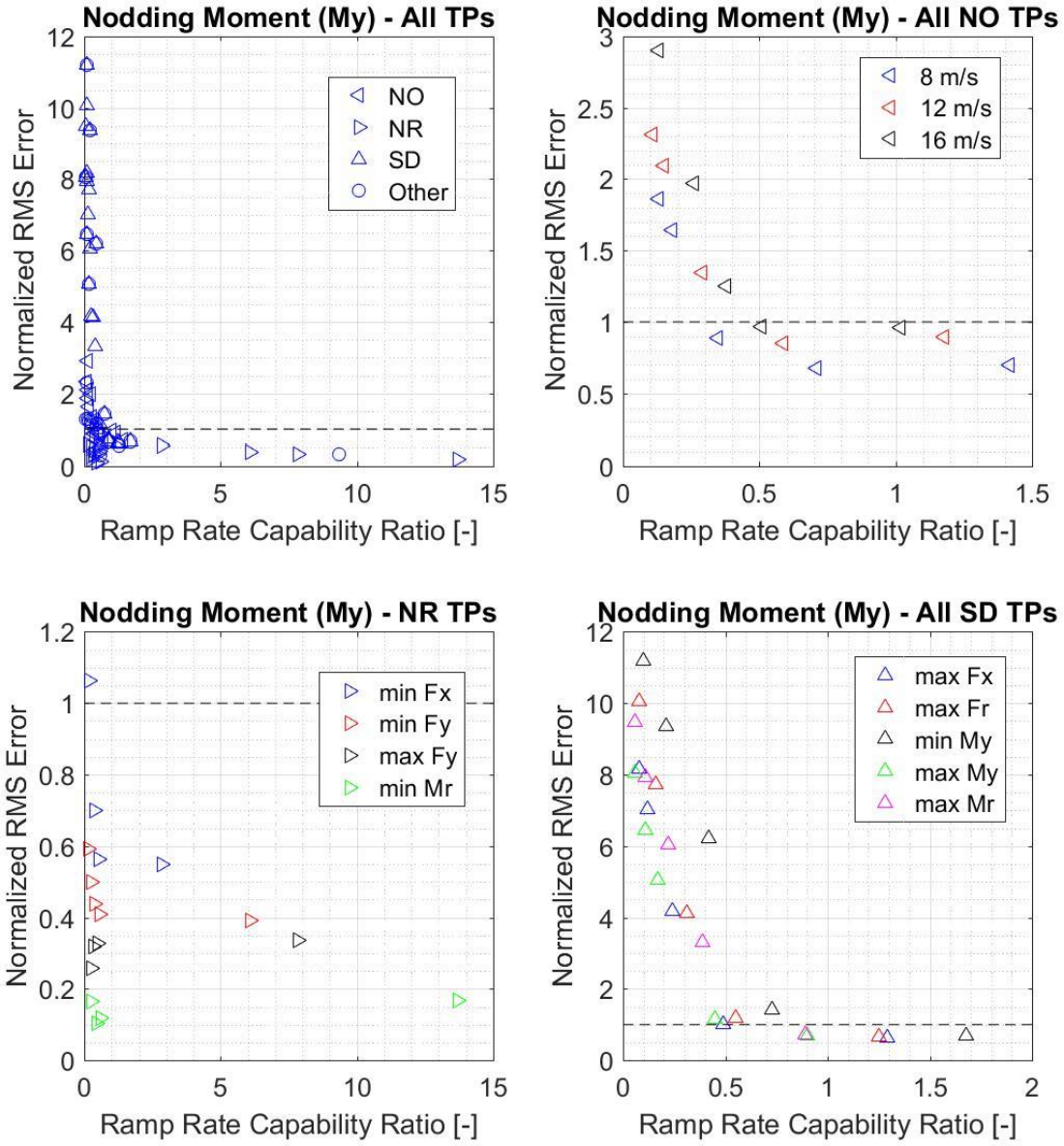

Figure 4.36: Normalized RMS error (E normalization) as a function of the test bench ramp rate capability ratio for the nodding moment for all tests (upper left plot) and three different subgroups: NO (normal operation), NR (parked turbine under extreme winds), SD (extreme event causing turbine to shut down).

To further demonstrate that large values of capability ratio for magnitude do not improve the predictive capability of the RMS error, Figs. 4.37 and 4.38 present scatter plots of the RMS error as a function of both magnitude and ramp rate capability ratios with the size of the symbols reflecting the magnitude of the RMS error. These figures use the same subgroupings of the test profiles used in Figs. 4.33-4.38. The results from both figures indicate that the RMS error increases with decreasing capability ratio for the ramp rate until a certain value of that metric at which point the RMS error remains relatively constant. The level of increase depends on the type of test profiles with those from the NR subgroup showing essentially no variation in RMS error with decreasing capability ratio for ramp rate.

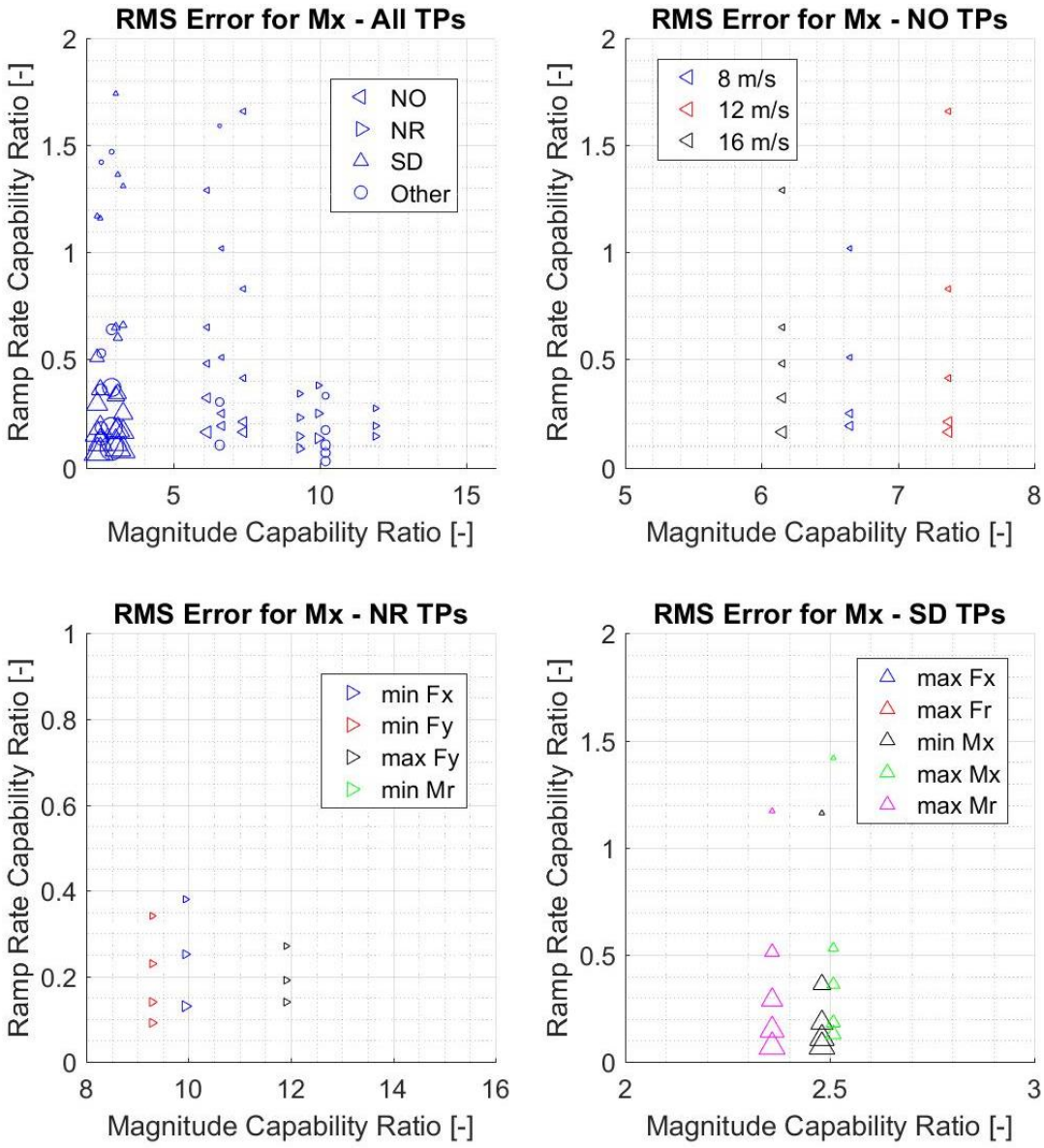

Figure 4.37: Normalized RMS error (E normalization) as a function of the test bench capability ratio for magnitude and ramp rate for the yawing moment for all tests (upper left plot) and three different subgroups: NO (normal operation), NR (parked turbine under extreme winds), SD (extreme event causing turbine to shut down).

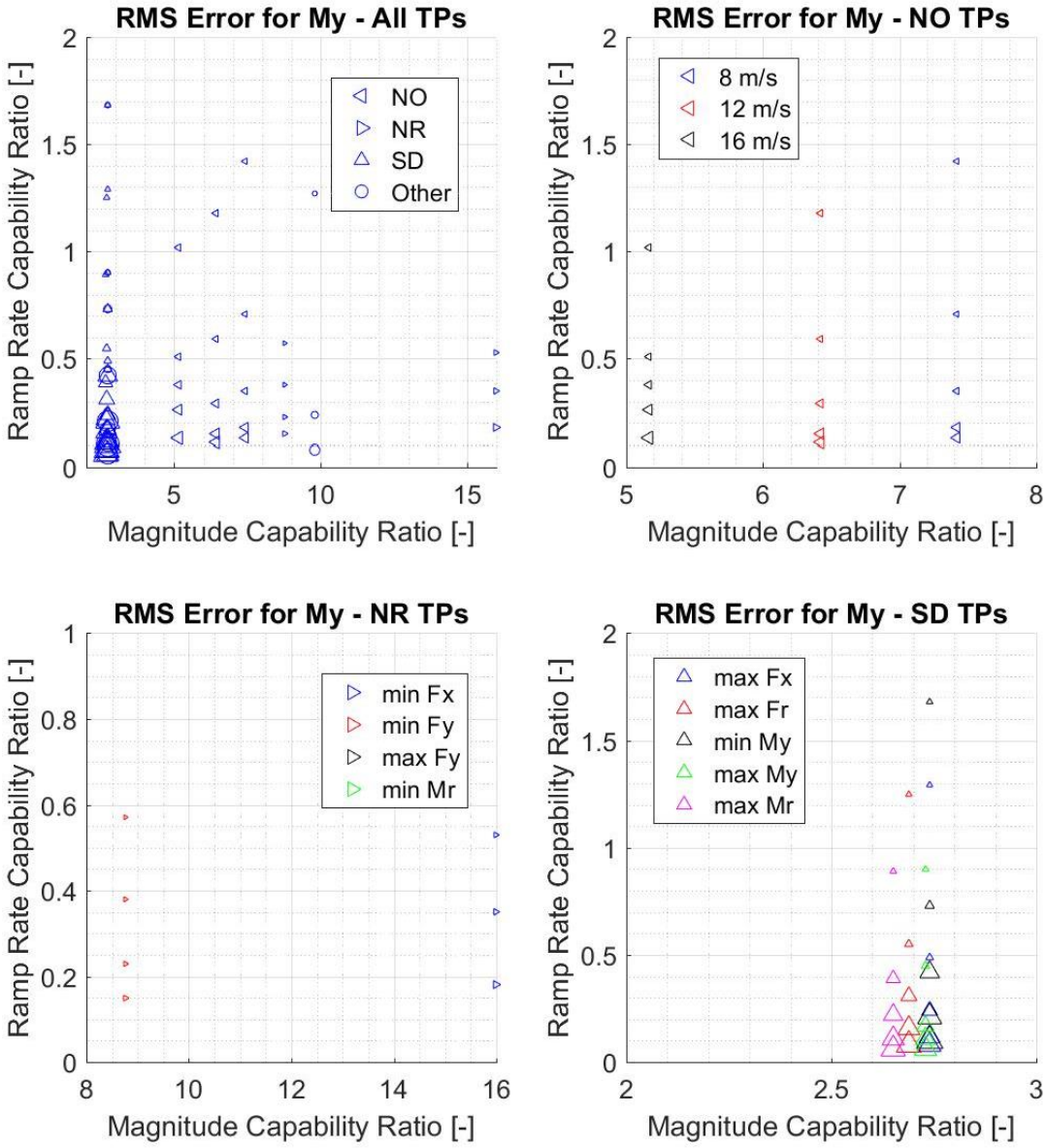

Figure 4.38: Normalized RMS error (E normalization) as a function of the test bench capability ratio for magnitude and ramp rate for the nodding moment for all tests (upper left plot) and three different subgroups: NO (normal operation), NR (parked turbine under extreme winds), SD (extreme event causing turbine to shut down).

4.4 Data Analysis

The results presented in Section 4.3 indicate different level of correlation between the RMS error from the measurements and the four evaluation metrics used to predict the capability of a test bench to replicate design loads. This Section focuses on quantifying those correlations and performing regressions analyses.

The correlation coefficients between the actual RMS errors for the four evaluation metrics are presented in Fig. 4.39. Results are co-plotted for the yawing and nodding moments and these results are presented for the same data subgroups used in Section 4.3. The negative correlation coefficients between the actual RMS error and the test bench coverage and capability ratios reflect the increase in RMS error with decreasing values of these three evaluation metrics. The green and red dotted lines reflect very high and negligible levels of correlation. Specifically, results above/below the green dotted line at correlation coefficients of -0.9/+0.9 indicate strong correlation. In contrast, results within the red dotted lines indicate a lack of correlation.

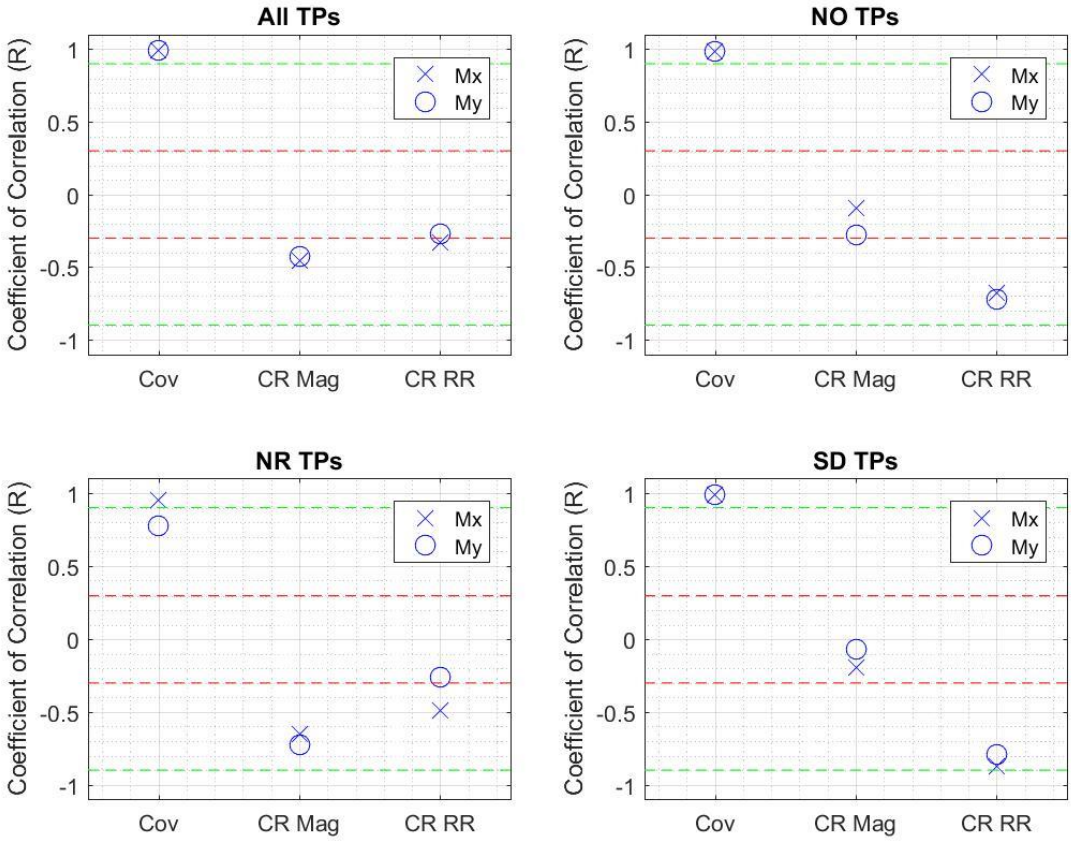

Figure 4.39: Correlation coefficient of the three evaluation metrics and four data subgroups for the yawing moment (Mx) and nodding moment (My). The green and red dotted lines represent the threshold for very high and negligible correlation. The metrics are coverage error (Cov), capability ratio (CR) for magnitude (Mag) and ramp rate (RR). The four subgroups are: All test profiles (All), normal operation TPs (NO), non-rotating TPs (NR), and shutdown TPs (SD).

Several observations can be made from Fig. 4.39.

- The coverage RMS error provides the best correlation and this very high level of correlation holds irrespective of the data subgroup.
- The coverage RMS error is the only evaluation metric with a strong correlation when considering all test profiles and the correlation coefficients for the coverage RMS

error do not benefit from subgrouping the data as it does for the Coverage. This points to the coverage RMS error being a robust evaluation metric.

- Overall, all evaluation metrics except the capability ratio for magnitude show at least a moderate level of correlation.
- The lower levels of correlation of the capability ratio for magnitude reflects the relatively low level of loadings from the test profiles. As such, this result is not surprising and one should not conclude that the capability ratio for ramp rate is not adding predictive capability in general. It did not in the case of the measurements with the 2.3-MW drivetrain, but measurements for more demanding test profiles are needed to draw a conclusion on the merit of this evaluation metric.

The correlation results were used as a starting point for the regression analyses. The regression results are first presented for individual metrics (single regressions) to identify the best fit of the RMS error from the measurements with the individual metrics. Results for single and multiple regressions are presented in separate Sections.

4.4.1 Single regressions

The correlation coefficients presented in Fig. 4.39 are sufficiently high to investigate non-linear regression for the combinations of data subgroup and evaluation metric having at least a moderate level of correlation with the actual RMS error. The single regressions were done with the JMP software using non-linear models to fit the data. Several non-linear functions are available in JMP and the following were considered based on the results presented in Figs. 4.33-4.38: quadratic polynomial, 2-point and 3-point exponential functions, 3-point logistic function, and a 3-point Gompertz function. Table 4.7 presents the results from the single regressions. The selection of the non-linear function was based on the adjusted R^2 in order to reflect the varying number of parameters

of the non-liner functions considered and the different number of samples per data subgroup. Table 4.7 presents the best fit to the data for the different combinations of data subgroup and evaluation metric. A threshold of an adjusted R^2 of 0.5 was used to accept a regression and "none" is indicated in Table 4.7 when this threshold was not achieved. For completeness, Table 4.7 includes the combinations of data subgroup and evaluation metrics for which a linear regression was found to have a strong correlation. For those combinations, the analyses performed with JMP confirmed that a non-linear regression did not provide significant improvement over a linear regression.

Table 4.7: Summary of single regression results for each evaluation metric and data subgroup. The background color reflects the R^2 value with green and yellow used to reflect the range above and below 0.9, respectively.

Subgroup	Yawing Moment (Mx)						Nodding Moment (My)					
	Cov. RMS Err		CR Mag		CR RR		Cov. RMS Err		CR Mag		CR RR	
	Fit	Adj R^2	Fit	Adj R^2	Fit	Adj R^2	Fit	Adj R^2	Fit	Adj R^2	Fit	Adj R^2
All	Linear	0.988	None	NA	None	NA	Linear	0.981	None	NA	None	NA
NO	Linear	0.964	None	NA	Exp 3P	0.798	Linear	0.975	None	NA	Exp 3P	0.788
NR	Linear	0.898	None	NA	None	NA	Exp 2P	0.607	None	NA	None	NA
SD	Linear	0.984	None	NA	Exp 3P	0.972	Linear	0.966	None	NA	Exp 3P	0.947

The following observations can be made from the results presented in Table 4.7.

- The coverage RMS error provides the best regressions without the need of a non-linear regression.
- Non-linear regression is insufficient to capture the actual RMS error for the coverage and capability ratio metrics when considered the data from all test profiles.
- Non-linear regression can capture the relationship between the actual RMS error and the Coverage fairly well when the data are subdivided per test profile type (subgroup). This observation also applies to the capability ratio for ramp rate.

- A non-linear regression do not capture the relationship between the actual RMS error with the capability ratio for magnitude.

4.4.2 Multiple regressions

The JMP software was also used to perform the multiple regression analyses. A total of eight multiple regressions were done to cover the four subgroups and both moments (Mx and My). In each case, the multiple regression used the least-square fit approach considering the three main effects (the three evaluation metrics) and their interactions. Only the main effects and interactions that were found to be significant were kept using a p-value of 0.05 as acceptance threshold. Table 4.8 and Fig. 4.40 present the outcome of the multiple regressions. The significant terms of the eight multiple regressions are indicated in Table 4.8. The interactions are identified using a number given to each main effect. For example, the interaction 1 & 2 is the interactions between the coverage RMS error and the capability ratio for magnitude. Figure 4.40 also includes the adjusted R^2 for the single (linear) regression for the coverage RMS error to indicate the improvement in the regression from including the effect of the other three evaluation metrics.

Table 4.8: Summary of the significant (S) and non-significant (NS) main effects and two-way interactions from the multiple regressions.

	Yawing Moment (Mx)						
Subgroup	**Main Effects**			**Interactions**			
	Cov (1)	CR Mag (2)	CR RR (3)	1&2	1&3	2&3	1&2&3
All	S	S	NS	S	NS	NS	NS
NO	S	NS	S	NS	S	NS	NS
NR	S	S	S	NS	S	NS	NS
SD	S	S	S	S	S	S	NS
	Nodding Moment (My)						
Subgroup	**Main Effects**			**Interactions**			
	Cov (1)	CR Mag (2)	CR RR (3)	1&2	1&3	2&3	1&2&3
All	S	S	NS	NS	NS	NS	NS
NO	S	S	S	S	NS	S	NS
NR	S	S	NS	NS	NS	NS	NS
SD	S	NS	S	NS	S	NS	NS

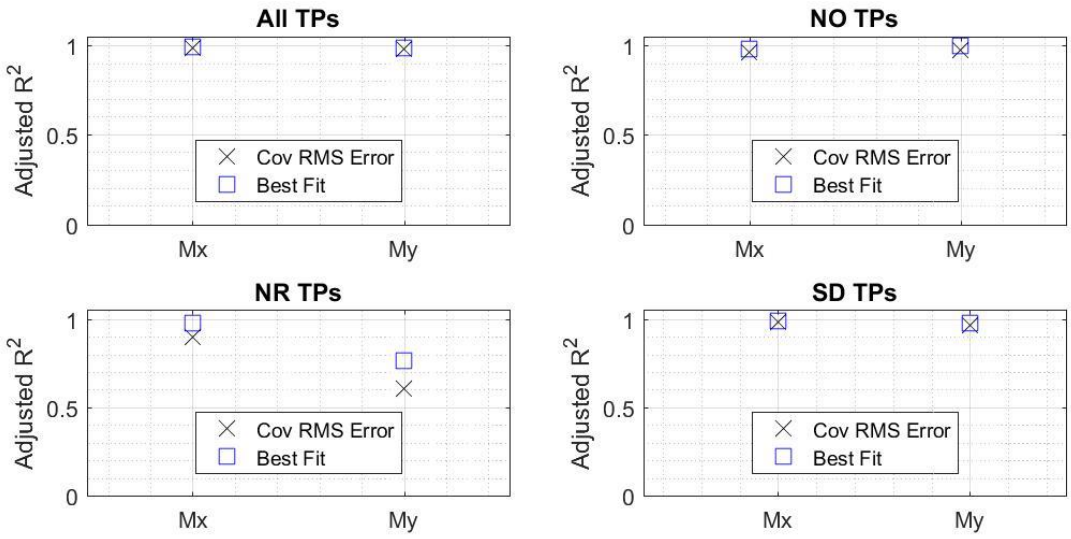

Figure 4.40: Comparison of the adjusted R^2 of the single regression model based on the coverage RMS error and the multiple regression models for the four data subgroups and the yawing moment (Mx) and nodding moment (My). The four subgroups are: All test profiles (All), normal operation TPs (NO), non-rotating TPs (NR), and shutdown TPs (SD).

The following observations can be made from Table 4.8 and Fig. 4.40.

- Multiple regression provides a marginal improvement in the adjusted R^2 for all but one subgroup and the improvement is smallest when considering the data from all test profiles.
- Most of the main effects were found to be significant.
- Most of the interactions were found to be insignificant.
- The significant main effects are fairly consistent between the yawing and the nodding moments.
- The significant interactions are not consistent between the yawing and the nodding moments and they are significant only when considering a subset of the data.

The multiple (and single) regression results were obtained using all available data except for the repeats of test profiles. Accordingly, the regression models developed with

the 2.3-MW drivetrain test data are not validated. The validation of such models will be more meaningful when also considering the test data from the second drivetrain. As such, the validation of the regression models is presented in Chapter Five.

The regression models are used to predict the RMS error of the test profiles of the 3.2-MW drivetrain and these predictions are presented after presenting revisions to the evaluation methodology based on the first experimental validation.

4.5 Revised evaluation methodology

The evaluation method presented in Chapter Three was defined without empirical correlation and the analysis results presented in Section 4.4 can be used to revisit the methodology. The goal of the evaluation method was to determine if a given test profile should be expected to be replicated by a test bench with acceptable tracking error. This goal does not require to predict the exact level of tracking error that is expected, which is why the original formulation of the coverage metric [42] was not formulated in terms of RMS error. The evaluation method aims to quantify the capability of a test bench to replicate dynamic loads at a macro level, but the experimental results indicate potential to extend the evaluation method to predicting the actual RMS error (micro level). Table 4.9 summarizes the goals for the evaluation metrics at macro level and the stretch goal of predicting the actual level of RMS level (micro level) vs. measurements.

Table 4.9: Summary of the goal for each evaluation metric and outcome from the experimental verification with the 2.3-MW drivetrain.

Metric	Goal	Actual vs Goal	Predicting Actual RMS Error
Coverage Error	Determine test profiles that should be replicated with acceptable RMS error	Goal met for Fz, Mx, My, and Spd based on results for tests with nominal test bench limits and using measurement error as acceptance threshold	Excellent correlation even without subgrouping the test profiles
Capability Ratio	Determine buffer between the test bench capability and the loading levels from the test profiles to identify if sufficient to compensate for the finite stiffness of the test article (drivetrain)	Although results for at least two drivetrains and higher loading levels are needed to determine if this goal is met, the results suggest that no buffer may be required given that the tracking error corresponding to capability ratios less than unity were found to be acceptable.	Moderate correlation when test profiles are subdivided per type. Leave the prediction of RMS error to the theoritical RMS error.

The results from Sections 4.3 and 4.4 clearly support the coverage RMS error as a metric for evaluating the capability of a test bench to replicate design loads. The coverage RMS error was found to have strong correlation with the actual RMS error and it does equally well at the macro level for identifying test profiles that should be replicated with an acceptable tracking error.

The prediction of the RMS error should preferably include the error due to the test bench controller. The four evaluation metrics are purely focused, however, on predicting the error due to the limitations of the test bench hardware. As a result, the current evaluation method will capture the test bench controller error with the intercepts of the regression models, which represent the tracking error that is not explained by the evaluation metrics. The magnitude and ramp rates of the loads from a test profile influence the tracking error even when these load magnitudes and ramp rates are within the test bench limits. As such, other characteristics of the test profiles should have some level of correlation with the tracking error due to the test bench controller. The following

characteristics are easily quantified for a test profile: the minimum, maximum, average, and standard deviation of the loads magnitude and ramp rate over the time series (8 characteristics in total per LAU input).

The actual RMS error for all 2.3-MW test profiles is presented as a function of the above characteristics in Figs 4.41-4.44. The correlation between the test profile characteristics and the actual RMS error vary significantly and Fig. 4.48 presents the correlation coefficient for the 8 test profile characteristics considered for both the yawing (Mx) and nodding (My) moments.

The results presented in Figs. 4.41-4.44 and summarized in Fig. 4.45 indicate that there is a moderate to very high level of correlation for the minimum, maximum, and standard deviation of the loads in both magnitude and ramp rate. The correlation is negligible for the average loads, which is not surprising as the average tends to be zero.

The very high level of correlation between some of the test profile characteristics and the RMS error reported in Fig. 4.45 is promising for quantifying the test bench controller error. These correlations are for the test profiles tested with the nominal test bench limits. Accordingly, the RMS errors presented in Figs. 4.41-4.44 mostly correspond to the test bench controller error. It is important to acknowledge that the tracking error due to the test bench controller also depends on the controller design and the tuning of its gains. The tuning of the controller gains has an influence on the tracking error and this research did not investigate the impact of controller tuning on the tracking error. The tuning of the controller gains in the context of this research was done with the constraint of using the same gains for all tests. Therefore, the prediction of the test best controller error is applicable to the controller gain tuning approach and constraint imposed during the measurement campaigns in which the testing for this research was conducted.

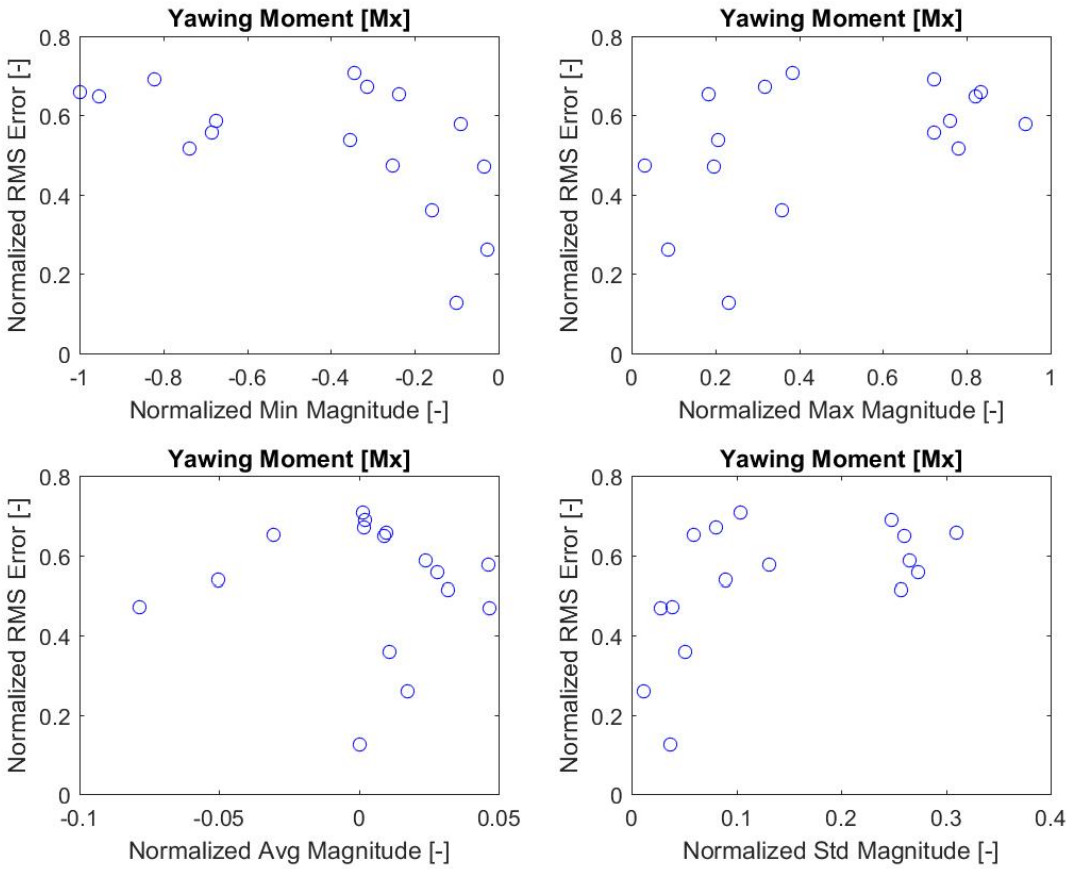

Figure 4.41: Actual RMS error (E normalization) as a function of the normalized minimum (Min), maximum (Max), average (Avg), and standard deviation (Std) of the magnitude of the yawing moment (Mx). The normalization of the RMS error is with the measurement error (E normalization) and Mx is normalized with the maximum peak value from all test profiles.

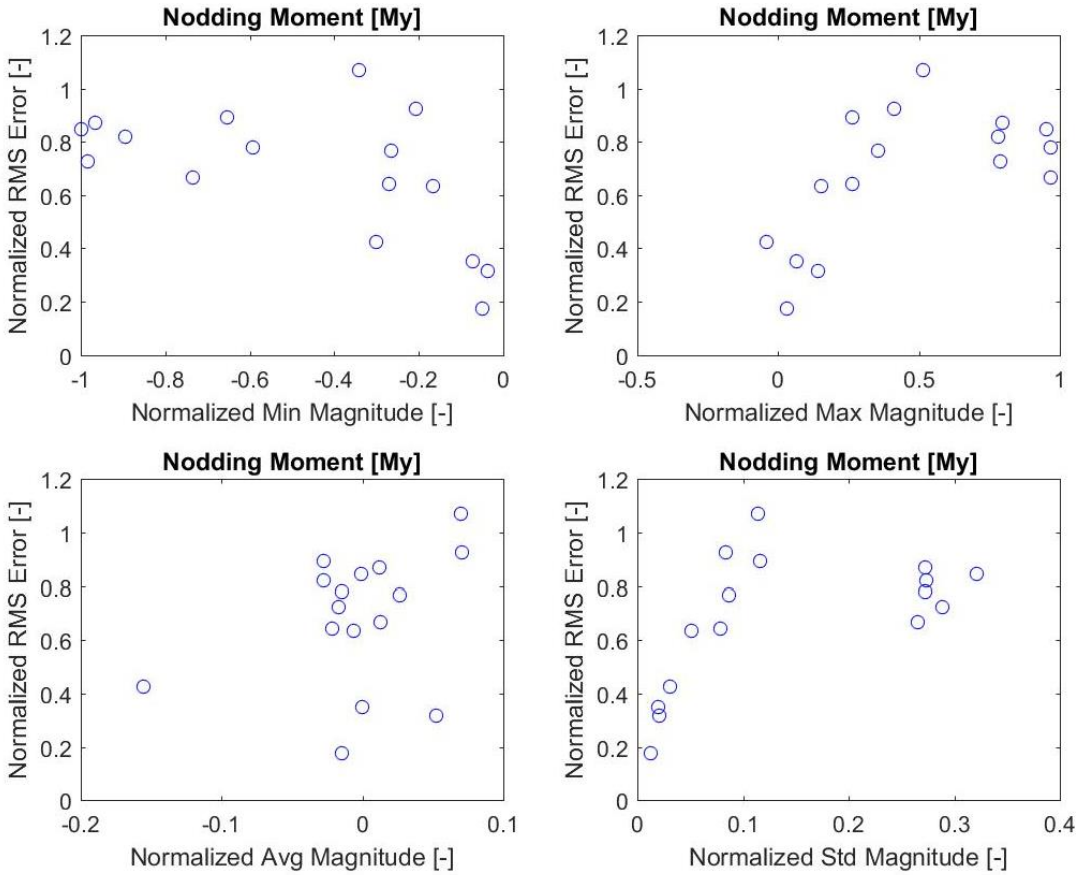

Figure 4.42: Actual RMS error (E normalization) as a function of the normalized minimum (Min), maximum (Max), average (Avg), and standard deviation (Std) of the magnitude of the nodding moment (My). The normalization of the RMS error is with the measurement error (E normalization) and My is normalized with the maximum peak value from all test profiles.

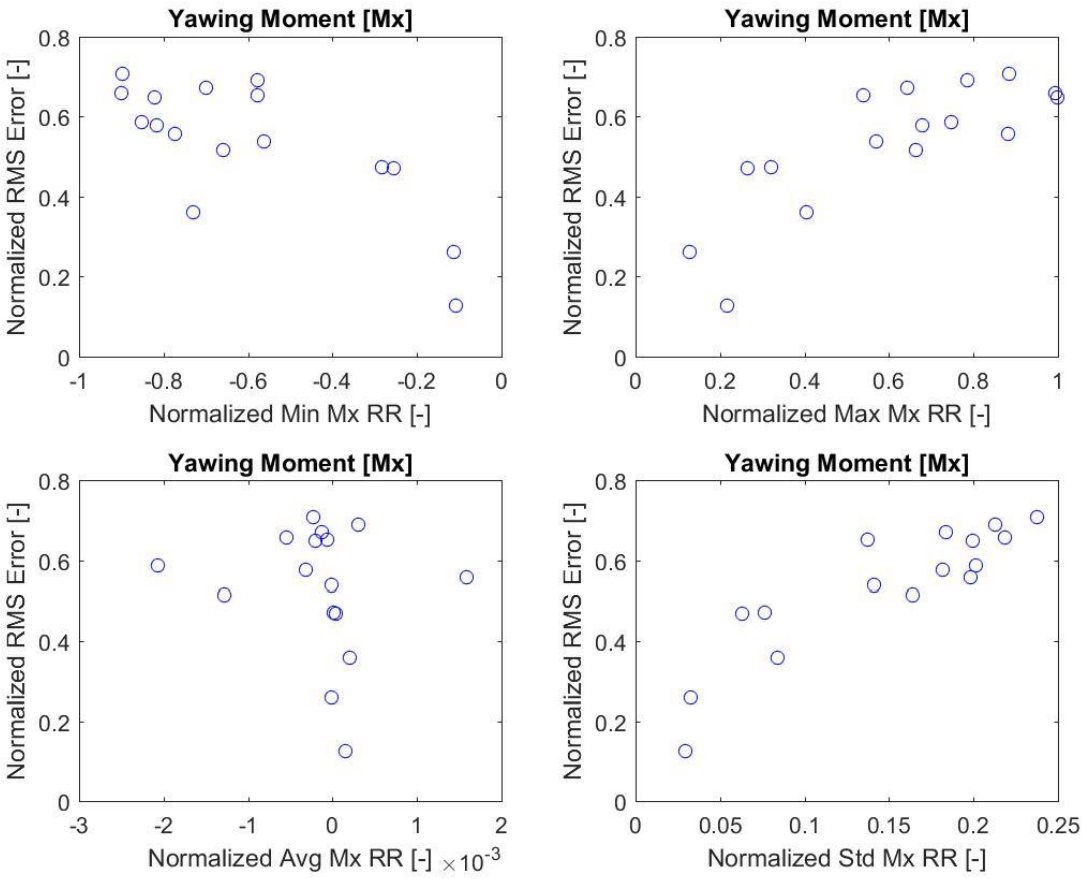

Figure 4.43: Actual RMS error (E normalization) as a function of the normalized minimum (Min), maximum (Max), average (Avg), and standard deviation (Std) of the ramp rate of the yawing moment (Mx). The normalization of the RMS error is with the measurement error (E normalization) and Mx is normalized with the maximum peak value from all test profiles.

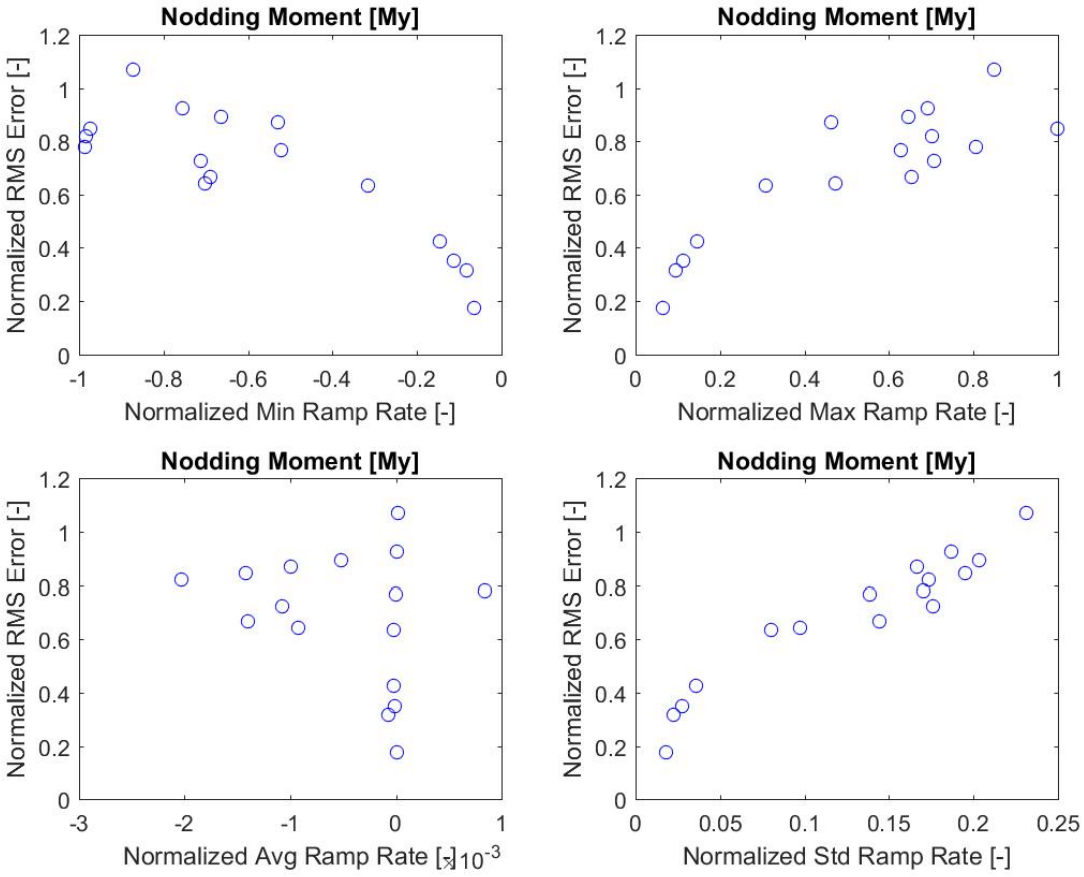

Figure 4.44: Actual RMS error (E normalization) as a function of the normalized minimum (Min), maximum (Max), average (Avg), and standard deviation (Std) of the ramp rate of the nodding moment (My). The normalization of the RMS error is with the measurement error (E normalization) and My is normalized with the maximum peak value from all test profiles.

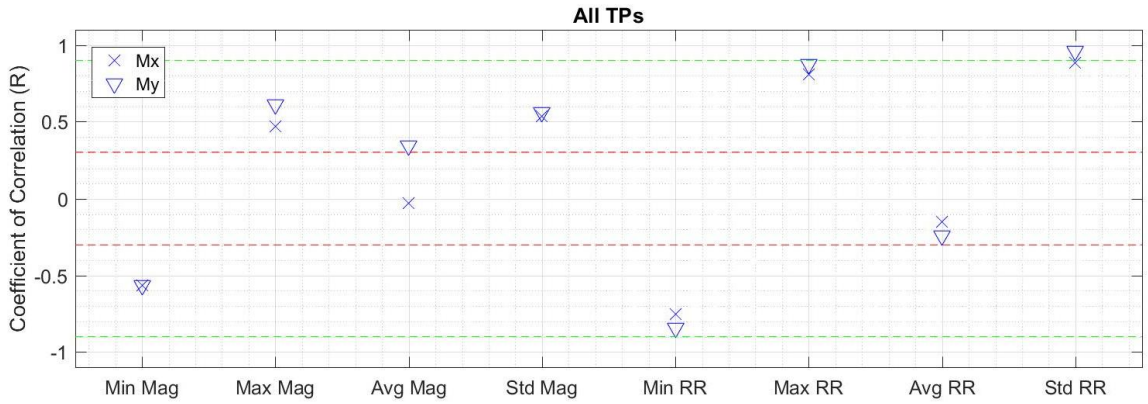

Figure 4.45: Correlation coefficient of test profile characteristics for the yawing moment (Mx) and nodding moment (My) considering the tests done with the nominal test bench limits. The green and red dotted lines represent the threshold for very high and negligible correlation.

4.6 Tracking performance predictions for the 3.2-MW drivetrain

The results from the regression analyses offer multiple options for predicting the tracking performance of the 7.5-MW test bench at replicating the dynamic test profile of the 3.2-MW drivetrain. Predictions for the tracking error (TE) were done for the yawing moment (Mx) and nodding moment (My) for the linear regression model with the Cov error and the multiple regression model. These equations of these models are given with Eqs. 4.1 and 4.2 for the linear regressions and Eqs. 4.3 and 4.4 for the multiple regressions. These equations are based on using the entire data set from the experiments with the 2.3-MW drivetrain. Even though the multiple regression model for the yawing moment did not contain any interaction, the interaction between the Cov error and the CR for magnitude was included to be consistent with the model for the yawing moment.

$$TE_{Mx} = 0.799 \cdot Cov + 0.433 \tag{4.1}$$

$$TE_{My} = 0.763 \cdot Cov + 0.487 \tag{4.2}$$

$$TE_{Mx} = 0.659 \cdot Cov - 0.113 \cdot CRm - 0.030 \cdot [(Cov - 3.201) \cdot (CRm - 6.861)] + 1.359 \tag{4.3}$$

$$TE_{My} = 0.641 \cdot Cov - 0.049 \cdot CRm - 0.013 \cdot [(Cov - 2.854) \cdot (CRm - 10.62)] + 1.359 \tag{4.4}$$

The predictions of the tracking (RMS) error from the four models are presented in Fig. 4.46. The x-axis captures 41 tests planned with the 3.2-MW drivetrain with different ramp rate limits. The x-axis is non descriptive because it does not affect the interpretation. The main observations to take away from Fig. 4.46 are that several of the test profiles are expected to have a small error and the multiple regression model only deviates from the single regression models to capture the largest errors. For most of the test profiles, there is essentially no difference in the predictions between the models. These predictions are compared with measurements in Chapter Six.

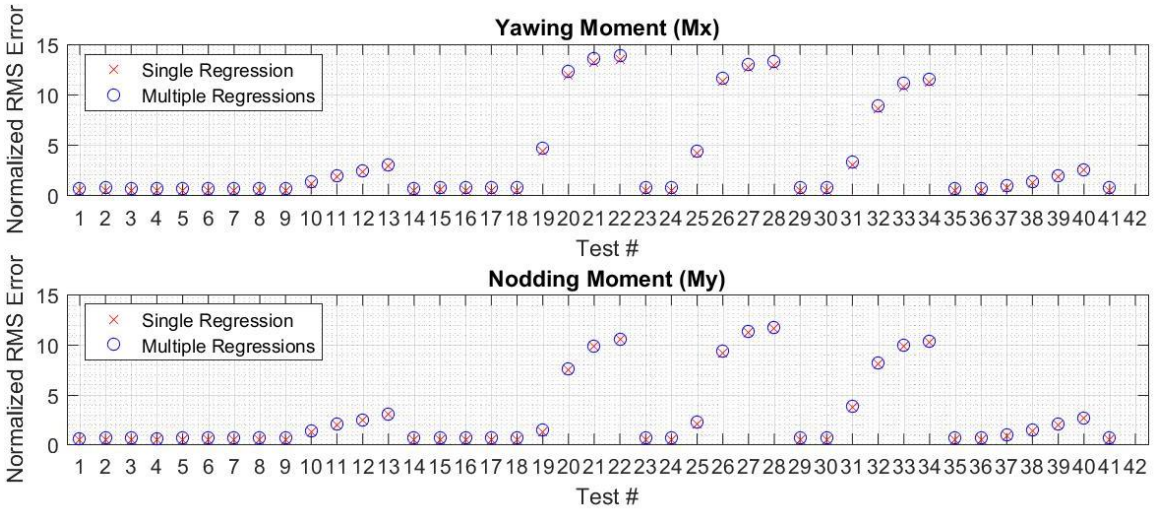

Figure 4.46: Tracking (RMS) error predictions using the prediction models for the single and multiple regressions (E norm).

4.7 Main findings and open questions

There are several findings from the extensive measurements made with the 2.3-MW drivetrain and the comparison of the RMS error with the evaluation metrics.

- The evaluation method correctly identified all but one of the test profiles that can have their bending moments replicated with an acceptable tracking error when using the measurement error as acceptance threshold.
- There is significant cross-coupling that is inducing incremental vertical and lateral forces from the application of bending moments. This cross-coupling results in tracking error beyond the measurement error for these two forces that are not captured by the evaluation method.
- The repeatability of the measurements is excellent.
- The test bench coverage RMS error has excellent correlation to the RMS error with linear regression irrespective of the subgrouping of the data by test profile types making this metric robust as well.
- The test bench capability ratio for ramp rate correlates to the actual RMS error when the data is subdivided in subgroups per test profile type.
- Characteristics of test profiles, such as the standard deviation of the loads magnitude and ramp rate, show correlation with the actual RMS error and thus the evaluation methodology has been extended to include test bench controller error.
- The results from the test bench capability ratio for ramp rates suggest there is no need for a buffer in capability ratio above unity to compensate for finite stiffness of the test article (drivetrain). The actual RMS error for test profile having a test bench capability ratio for ramp rates below unity were found to be within the measurement error.
- The peak errors for the LAU loads are less than 50% of the peak loads except for the lateral force due to cross coupling.
- The test bench load ramp rate limits were exceeded.

The first finding listed above refers to acceptable tracking error on the basis of the RMS error being with the measurement error of the LAU loads. Although this is a reasonable conclusion, it begs the question if the level of measurement error is acceptable. This question is tied to the second critical question this research aims to answer, which is the accuracy level needed when replicating loads on a wind turbine drivetrain test bench. This question is answered using simulations, which is the focus of the tracking performance study presented in Chapter Five.

The second finding in the list can also be investigated with simulations. Specifically, the effect of cross-coupling can be isolated by simulating input loads and speed time series to a drivetrain model with and without including the reaction forces resulting from the cross-coupling. This investigation was added to the scope of the tracking performance study.

CHAPTER FIVE

TRACKING PERFORMANCE STUDY USING MULTI-BODY SIMULATION

The multibody simulation software Simpack was used to study the sensitivity of the dynamic response of the wind turbine due to the following:

- Tracking error between the LAU inputs commanded by the test bench controller and the LAU loads and speed that the LAU applies to the test article.
- Cross-coupling between the bending moments and forces applied by the LAU.

The primary goal of the study is to determine the level of tracking accuracy needed when replicating dynamic test profiles. In light of the results from the tests conducted with the 2.3-MW drivetrain, quantifying the contribution of the cross-coupling effect to the overall tracking error was added as a secondary goal. Perhaps as important then the results that this study aims to provide is the approach used to arrive at these results. The approach is general and can be applied to any dynamic response of the wind turbine whereas the results are tied to the specific dynamic response(s) considered.

As stated, the aim of the study is quite open ended and suggest that simulations will be performed until the tracking error level resulting in an unacceptable change in dynamic response is found. This is too open ended and is surely going to lead to debatable results because the level of change in dynamic response deemed acceptable requires engineering judgement based on knowledge of the drivetrain design of interest. In order to provide an answer that is more practical than debatable, the question was reformulated as follows: are the tracking errors from the tests conducted with the nominal test bench limits (refer to Fig. 4.30) resulting in changes in dynamic response that are

significant or not? From the context of a test bench operator, this is an important question because tracking errors, within the measurement error of the test bench, that are causing changes in the dynamic response of the test article that are not acceptable would be a concern. The reported tracking errors for the yawing and nodding moments (refer to Fig. 4.30) are within the measurement error for all test profiles with a single exception: the RMS error for the nodding moment of the NO 16 test profile is 7% greater than the measurement error. The measurements of the LAU loads and speeds from the tests with the nominal test bench limits were used as reference for the study.

Simpack [50] is one of several general purpose multi-body simulation (MBS) software packages to analyze the dynamics of mechanical or mechatronics systems. The MBS method uses rigid and/or elastic bodies connected with kinematic constraints and force elements. The selection of Simpack was one of convenience as it is available at Clemson University and one of choice as it is widely used in the wind industry, especially for modeling drivetrains.

5.1 2.3-MW drivetrain Simpack model description

The model was developed by researchers at the Energy Innovation Center of Clemson University with input from engineers at GE Renewable Energy. The physical representation of the main model components and the validation of the overall model are presented.

5.1.1 Description

The Simpack model used for the study is based on the 2.3-MW drivetrain design that was tested on Clemson University 7.5-MW test bench. The main components modeled are the main (low-speed) shaft, the main bearing, the gearbox, the bedplate, the high-speed shaft and its coupling, the generator, the generator frame and the support

tower connecting the drivetrain to the ground of the test bench. The test bench LAU disk was modeled, but other parts of the test bench were not modeled for this study.

Figure 5.1 shows top and side views of this drivetrain model. The main shaft is shown in cyan. The point of application of the loading and speed inputs to the drivetrain is indicated with a red circle. The two dotted purple lines circle the main bearing to the left of both views and the high-speed shaft and its coupling on the right. The bedplate, generator frame and the support tower are shown in grey. The generator frame is to the right of each view. The first stage of the gearbox is shown in blue and the rest of the gearbox is shown in orange. The generator is in a darker shade of purple to the right of both views. The opening at the base of the support tower is for access to the drivetrain.

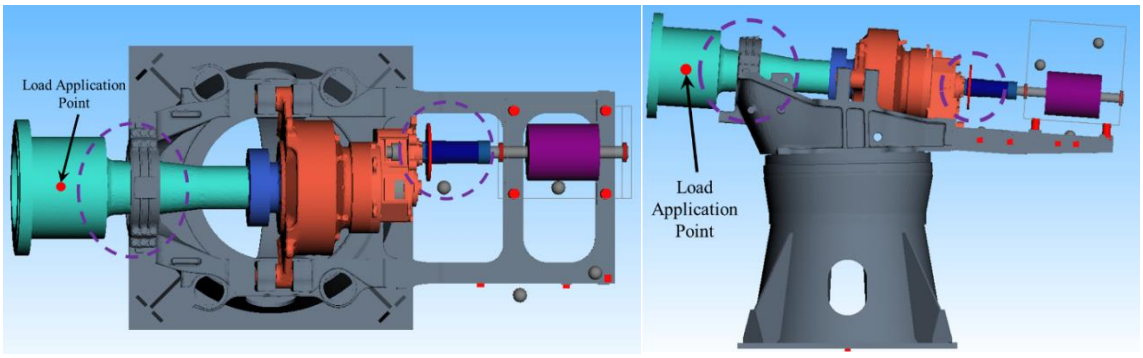

Figure 5.1: Top and side views of the 2.3-MW drivetrain Simpack model.

Table 5.1 summarizes the physical representation of these components and their connections in Simpack. The bushing elements define the stiffness and damping of the six-degree of freedom connections.

Table 5.1: Physics representation of the 2.3-MW drivetrain components and their connection in Simpack.

Component	Simpack Element	Connection
Main shaft	Flexible body	Revolute joint connection to the 1st stage of the gearbox and connected to the main bearing with a bushing element
Main bearing	Bushing element	Rigid connection to the bedplate and 6 degrees of freedom spring-damper connection with the main shaft
Gearbox	Flexible body for the gearbox housing, gears as gearbox ratio	Revolute joint connection to the main shaft and high-speed shaft, and connection to the bedplate with bushing elements representing the gearbox mounts
Gearbox mounts	Bushing elements	Rigid connection to the bedplate and 6 degrees of freedom spring-damper connection with the gearbox
Bedplate	Flexible body	Rigid connection to the tower and connected to gearbox with bushing elements representing the gearbox mounts
High-speed shaft and coupling	Rigid body	Revolute joint connection to the gearbox and generator
Generator	Rigid body	Revolute joint connection to the high-speed shaft and connection to the generator frame using bushing elements
Generator frame	Flexible body	Rigid connection to the bedplate and connection to the generator using bushing elements
Tower	Flexible body	Rigid connection to the bedplate and ground

5.1.2 Validation

The 3.2-MW drivetrain tested on the 7.5-MW test bench was fully instrumented and the test data included displacement and acceleration measurements for most drivetrain components. As such, there are multiple options for validating the model and using all of the measurements was not deemed necessary to demonstrate the level of validation needed to pursue the goals of the study. Measurements made at the “entrance” and “exit” of the drivetrain were deemed sufficient (M. Panyam, Research Associate,

Clemson Energy Innovation Center, personal communication, Jan. 2019). Specifically, displacements of the main shaft with respect to the main bearing and the relative displacements of the high-speed shaft at the end of the gearbox were selected for validating the model. The main shaft displacements were measured at four azimuthal positions as shown in Fig. 5.2. The measurement of the high-speed shaft displacement consisted of axial, lateral, and vertical displacements.

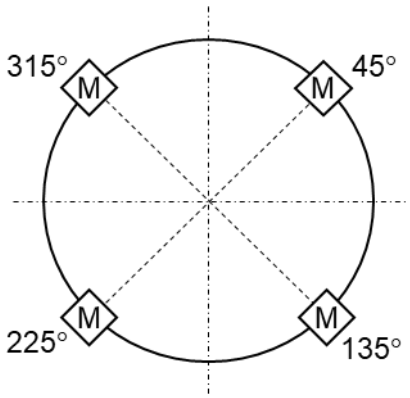

Figure 5.2: Main shaft displacement measurement locations (M).

The displacements were measured using laser sensors [51]. These sensors are mounted on a rigid frame isolated from the drivetrain and connected to the ground.

The validation of the model was done with static and dynamic loads. The dynamic test profile considered for this validation was the reference test profile of the 2.3-MW drivetrain. The results of this validation were presented at the 2019 Wind Power Drive Conference but they are not part of the published paper in the proceedings of this conference [44]. In brief, the simulation results for the main shaft yaw and nodding (tilt) angular displacements with respect to the main bearing were in good agreement with measurements. The agreement with the displacement measurements of the high-speed

shaft at the gearbox end were mixed between the axial, horizontal (lateral), and vertical directions.

5.2 Simulations

The simulation plan and process used to execute each simulation and extract the results are described before presenting the results.

5.2.1 Plan

As summarized in Table 5.2, all test profiles of the 2.3-MW drivetrain were simulated under three sets of inputs.

A. LAU loads and speed per the commanded profiles.

B. Measured LAU loads and speed from the tests conducted with the nominal test bench limits.

C. Measured LAU moments and speed, and commanded forces.

Table 5.2: Simulation plan for the 2.3-MW drivetrain.

Case		**LAU Input Set**		
		A	B	C
NO	8 m/s	☑	☑	☑
NO	12 m/s	☑	☑	☑
NO	16 m/s	☑	☑	☑
Fx	Min	☑	☑	☑
	Max	☑	☑	☑
Fy	Min	☑	☑	☑
	Max	☑	☑	☑
Fz	Min	☑	☑	☑
	Max	☑	☑	☑
Fr	Max	☑	☑	☑
Mx	Min	☑	☑	☑
	Max	☑	☑	☑
My	Min	☑	☑	☑
	Max	☑	☑	☑
Mr	Min	☑	☑	☑
	Max	☑	☑	☑

The comparison of the results from input sets A and B target the primary goal of the study whereas the comparison between the results from input sets B and C target the cross-coupling effect. The LAU input set B is used as the baseline being common to both comparisons and the test data for the nominal test bench limits were specifically used.

5.2.2 Process

The simulation were done using Simpack 2017.2 [50]. A systematic process was used to run the simulations and process the results. This process consist of the following steps.

1. Put the system in static-equilibrium.
2. Obtain a state set of the system reflecting the starting speed of the test profile of interest and apply to the system.
3. Run the simulation for the desired test profile.

The system was put in static equilibrium using the specific solver Simpack offers for this purpose. The force elements prescribing the loads and speed to be imposed at the point of application were disabled. The static equilibrium solver was executed until static equilibrium was achieved saving the states each time. The resulting state of static equilibrium was used as the starting point for all simulations.

As the starting speed varied for most test profiles, a time integration of the system was performed such that each simulation would start with a state set reflecting the starting speed of the test profile of interest. The force element prescribing the loads to be imposed onto the drivetrain remained disabled and the speed was enabled. A 30-second ramp up was simulated with an end speed corresponding to the starting speed of the test profile of interest. The resulting state set from this ramp up was applied to the system.

Prior to executing the simulation with a dynamic test profile, the solver time was set to the total time of the test profile. The default solver and tolerance level prescribed in Simpack were used for all simulations.

The displacements mentioned in Section 5.1.2 were extracted from the simulation results. The first step of this data extraction process was to remove the DC offset of each displacement. The axial displacements (z) of the main bearing at the four azimuthal positions shown in Fig. 5.2 were used to calculate the angular displacements of the main shaft in yaw (α) and nodding (β) using Eqs. 5.1 and 5.2. The calculation was done at every time step of the simulation.

$$\alpha = \left(\frac{z_{135}+z_{225}}{2}\right) - \left(\frac{z_{45}+z_{315}}{2}\right) \tag{5.1}$$

$$\beta = \left(\frac{z_{45}+z_{135}}{2}\right) - \left(\frac{z_{225}+z_{315}}{2}\right) \tag{5.2}$$

The differences in the angular displacements of the main shaft as well as the lateral and vertical displacements of the high-speed shaft between the LAU input sets are aggregated as a RMS value. Therefore, the results are presented as percentage difference in RMS values of the displacements considered between the three LAU input data sets.

5.2.3 Results

The effects of the tracking error on the displacements considered are presented in Fig. 5.3 for all test profiles. The RMS values were normalized using the peak value of each displacement from the simulations done using the measured LAU inputs (LAU input set A). Therefore, the percentage values are a direct measure of the peak displacements from the measured LAU loads and speed of each test profile.

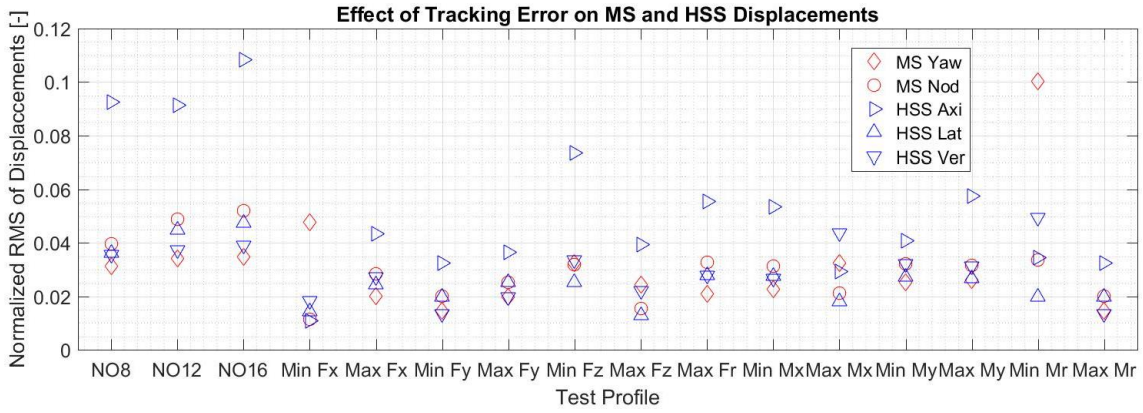

Figure 5.3: Normalized RMS value of the differences in the five displacements considered due to the tracking error. The P normalization has been applied using the simulations results for the measured LAU input (LAU input set B) as reference. The five displacements are the main shaft (MS) yaw and nodding angles and the high-speed shaft (HSS) axial, lateral, and vertical displacements.

Per Fig. 5.3, the RMS value of the differences in displacements of the main shaft and high-speed shaft due to the tracking error are within 11% of the peak value of each displacement with most RMS values falling into the range of 1%-3%. On average, the RMS values for a given displacement are between 2.6%-3.1% of the peak value of all but one displacement. The exception is the axial displacement of the high-speed shaft, which has an RMS value that is 5.2% of the peak value. This larger RMS value on average is attributed to the peak axial displacements of the high-speed shaft being 2.7-5.2 times smaller than the lateral and vertical displacements on average over the 16 test profiles. Overall, the effect of the tracking error on the displacements is not significant.

The level of tracking error modeled with Simpack corresponds to the test results with the nominal test bench limits. Referring to Fig. 4.30, the tracking error for the yawing and nodding moments were within the measurement error for all test profiles with a single exception. Accordingly, it can be concluded that a tracking accuracy within the measurement error of the 7.5-MW test bench of Clemson University is sufficient when

replicating dynamic loads. A larger tracking error could actually be acceptable and thus the measurement error is not necessarily an upper acceptance threshold. As explained in the introduction of this Chapter, the level of tracking error that is acceptable was not investigated further but the outlined method can be used for that purpose.

Figure 5.4 presents the cross-coupling effect on the displacements considered for all test profiles. These results present the RMS value of the differences in displacement from the simulations performance with LAU input sets B and C.

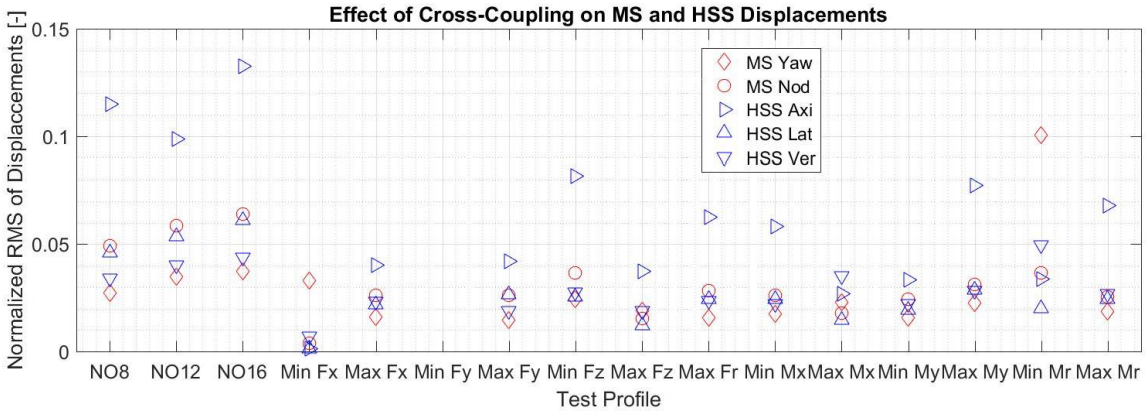

Figure 5.4: Normalized RMS value of the differences in the five displacements considered due to the cross-coupling. The P normalization has been applied using the simulations results for the measured LAU input (LAU input set B) as reference. The five displacements are the main shaft (MS) yaw and nodding angles and the high-speed shaft (HSS) axial, lateral, and vertical displacements.

The results from Fig. 5.4 suggest that the cross-coupling effect does not significantly change the displacements. There is no result for the case of the minimum lateral force (min Fy) because the simulations done with the LAU input data set C were found to have large oscillations in the displacements over the first 25 seconds. The results for the same test profile for the two other LAU input data sets did not have these oscillations and their cause could not be determined. Given that these oscillations only

manifested themselves for this test profile and specific LAU input data set and this part of the study was secondary, this was not investigated further.

The relationship between the effect of the tracking error on the main shaft and high-speed shaft displacements and the cross-coupling effect is presented in Fig. 5.5. There is no result for the min Fy test profile for the same reason mentioned previously.

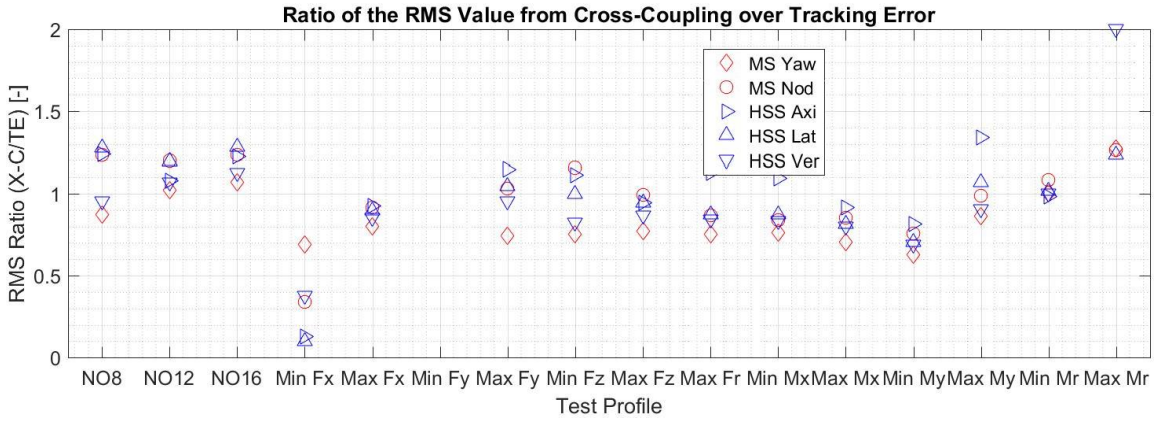

Figure 5.5: Ratio of the RMS value of the differences in the five displacements considered due to the cross-coupling over that from the tracking error. The five displacements are the main shaft (MS) yaw and nodding angles and the high-speed shaft (HSS) axial, lateral, and vertical displacements.

The RMS values of the differences in the displacements due to the cross-coupling effect are mostly less than that from the tracking error, but not always. Some test profiles, such as those for normal operation (OP), have mostly larger changes in displacements from the cross-coupling than the tracking error. This observation may be explained by the approach, which is not fully isolating the effect of the cross-coupling. The effect of the moments onto the forces is removed, but the effect of the forces on the moments is not. For most test profiles, the magnitude of the moments is significantly larger than the forces, and thus the induced moments from the forces are small. Ultimately, it depends on the difference in magnitude of the forces and moments. Noteworthy is that the test profiles

representing normal operation (NO) show a cross-coupling effect that is mostly larger than that from the tracking error. These test profiles have the largest average vertical force over all test profiles (top 3). Interestingly, the test profile having the smallest average vertical force, which is of course min Fx, has the smallest effect from cross-coupling. The results presented in Fig. 5.5 suggest that the vertical force is contributing to the cross-coupling effect.

5.3 Main findings

There are three main findings from the Simpack simulation results.

- The changes in dynamic response from a tracking error within the measurement error of the 7.5-MW test bench are not significant.
- Although the cross-coupling effect significantly alter the forces applied to the drivetrain, this effect has a small impact on the dynamic response of the drivetrain. That effect can be larger than the effect from the tracking error.
- The vertical force appears to be a contributor to the cross-coupling effect.

The first finding is not an upper acceptance threshold, however, but a necessary requirement for using a test bench to replicate dynamic test profiles. Also, the first finding is expected to be applicable to other drivetrains of similar designs when using inputs to the model from measurements made with the same test bench. This is the case for the 3.2-MW drivetrain and the study was no repeated.

The second finding could be revisited for test profile for which the forces are on the same order of magnitude than the moments, but most of the test profiles driving the design of wind turbine drivetrains come from test profiles in which the moments are substantially greater than the forces.

CHAPTER 6

EXPERIMENTAL VERIFICATION WITH A 3.2-MW DRIVETRAIN

The second phase of the experimental verification was performed during a commercial test campaign with a GE 3.2-MW drivetrain on Clemson's 7.5-MW test bench during a total of 3 consecutive days (Aug. 28-30, 2018). A schematic of this drivetrain is shown in Fig. 6.1. The test plan was similar to that of the 2.3-MW drivetrain with tests conducted with nominal and reduced ramp rate limits for the yawing (Mx) and nodding (My) moments. One difference was test profiles representing normal operation and the min Fz case were not tested. Another was to include test profiles tested with the 2.3-MW drivetrain in order to investigate the effect of the drivetrain on tracking performance.

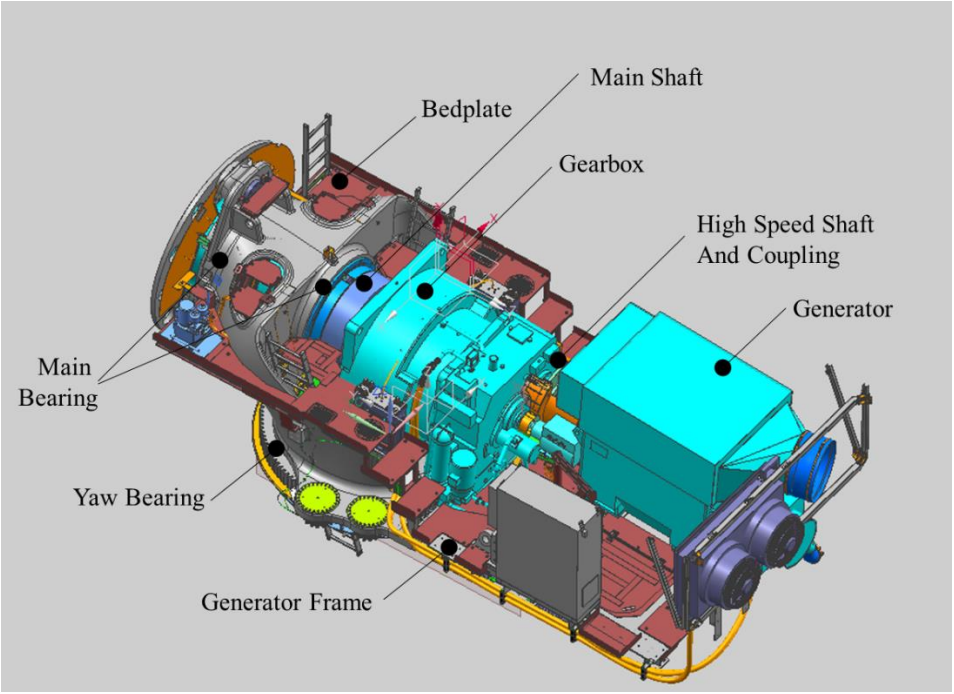

Figure 6.1: 3.2-MW drivetrain architecture schematic.

Table 6.1 presents the test date of each combination of test profile and either the nominal or reduced ramp rate limit applied to the yawing (Mx) and nodding (My) moments. These ramp rate limits are presented in Table 6.2. The same nominal ramp rate limit of 8000 kNm/s for the yawing (Mx) and nodding (My) moments was used with the 3.2-MW drivetrain for consistency. The reduced ramp rate limits for the yawing (Mx) and nodding (My) moments were selected for each test profile to sample a range of Cov values of at least 60%-100%. Only five of the test profiles were tested with reduced ramp rate limits in addition to the nominal limit due to reduced time for testing. Overall, 49% of the test profile and ramp rate limit combinations were tested. The test profiles that were also tested on the 2.3-MW drivetrain are identified with "2.3" in Tables 6.1 and 6.2.

Table 6.1: Test dates (2018) for the executed test plan for the 3.2-MW drivetrain for the nominal and reduced ramp rate limits imposed on the yawing (Mx) and nodding (My) moments.

Case		Nominal	Reduced #1	Reduced #2	Reduced #3	Reduced #4
Fx	Min	Aug 30	Not tested	Not tested	Not tested	Not tested
	Max	Aug 29	Not tested	Not tested	Not tested	Not tested
Fy	Min	Aug 28	Not tested	Not tested	Not tested	Not tested
	Max	Aug 28	Not tested	Not tested	Not tested	Not tested
	Max 2.3	Aug 30	Not tested	Not tested	Not tested	Not tested
Fz	Min	Not tested	Not tested	Not tested	Not tested	Not tested
	Max	Aug 28 (2x), 29 (2x), 30 (2x)	Aug 30	Aug 30	Aug 30	Aug 30
Fr	Max	Aug 29	Not tested	Not tested	Not tested	Not tested
Mx	Min	Aug 29	Not tested	Not tested	Not tested	Not tested
	Max	Aug 29, 30	Aug 30	Aug 30	Aug 30	Aug 30
My	Min	Aug 29, 30	Aug 30	Aug 30	Aug 30	Aug 30
	Max C1	Aug 29, 30	Aug 30	Aug 30	Aug 30	Aug 30
	Max C2	Aug 28, 30	Aug 30	Aug 30	Aug 30	Aug 30
Mr	Max	Aug 29	Not tested	Not tested	Not tested	Not tested
	Max 2.3	Aug 30	Not tested	Not tested	Not tested	Not tested

Table 6.2: Ramp rate limits for the yawing and nodding moments for the executed test plan for the 3.2 MW drivetrain.

Case		Ramp Rate Limit for Yawing and Nodding Moments [kNm/s]										
		8000	4000	3500	3000	2250	1750	1500	1250	1000	750	<750
Fx	Min	☑										
	Max	☑										
Fy	Min	☑										
	Max	☑										
	Max 2.3	☑										
Fz	Min											
	Max	☑						☑		☑	☑	500
Fr	Max	☑										
Mx	Min	☑										
	Max	☑		☑					☑			500 250
My	Min	☑	☑					☑				500 250
	Max C1	☑			☑			☑			☑	500
	Max C2	☑	☑		☑	☑	☑					
Mr	Max	☑										
	Max 2.3	☑										

Per the dates indicated in Table 4.1, the tests with reduced ramp rates were done on the same day including a repeat of a test with the nominal test bench limits. The test profile for the max Fz case was used to quantify the repeatability of the measurement system over the three days of testing. This reference test profile was also used for tests with reduced ramp rates. The four other test profiles tested with reduced ramp rates were tested twice with the nominal ramp rate limit in order to have all tests done on the same day. Overall, a total of 43 tests were performed covering 14 test profiles over three consecutive days in Aug. 2018, which is 15 months after the completion of the tests conducted with the 2.3-MW drivetrain. Each test day started and ended with testing the reference test profile (max Fz) and the test sequence in between was organized to maximize test efficiency.

The emphasis in the presentation of the experimental results obtained with the 3.2-MW drivetrain is to first highlight similarities and differences with the 2.3-MW drivetrain results. Additionally, the predictive capability of single and multiple regression models based on the 2.3-MW drivetrain data is evaluated.

6.1 Experimental results

The experimental results are presented in the same way they were for the 2.3-MW drivetrain starting with the demonstrated test bench capability followed by the measurements repeatability and tracking performance. Refer to Section 4.1 for a description of the normalization of the test data.

6.1.1 Demonstrated test bench capability

The 12 test profiles of the 3.2-MW drivetrain that were tested with the nominal test bench capability represent a total of 347,414 measurements of the LAU loads and speed. The demonstrated capability of the 7.5-MW test bench with the 3.2-MW drivetrain is presented in Fig. 6.2. All measured LAU loads and speed in terms of magnitude vs. ramp rate (OP normalization) are co-plotted together excluding measurement repeats. The same scale is used except for the speed to facilitate the comparison between the different LAU loads.

The demonstrated capability of the 7.5-MW test bench with the 3.2-MW drivetrain is qualitatively the same as that with the smaller drivetrain. There are differences quantitatively of course from the difference in scale of the drivetrains but the observations from Table 4.4 applies to the demonstrated capability of the test bench with the 3.2-MW drivetrain as well. The differences in scale are illustrated in Figs. 6.3-6.5 for the forces, moments, and speed, respectively. The normalization is done using the peak value from the commanded loads and speed of both drivetrains. The peak loads come from the 3.2-

MW drivetrain, indicated with the normalized loads for that drivetrain reaching 1 or -1, and the peak speed is from the 2.3-MW drivetrain. The following observations can be made from comparing the demonstrated capability of the test bench for both drivetrain.

- The commanded LAU loads magnitude of the 3.2-MW drivetrain are 30%-50% larger than that of the 2.3-MW drivetrain.
- The range in commanded and measured ramp rates of the LAU loads is comparable for both drivetrains and the 2.3-MW drivetrain even has larger measured ramp rates for the nodding moment (My) than the 3.2-MW drivetrain.
- The 3.2-MW drivetrain has nearly twice the range of ramp rates at high speed (rpm) as compared with the 2.3-MW drivetrain

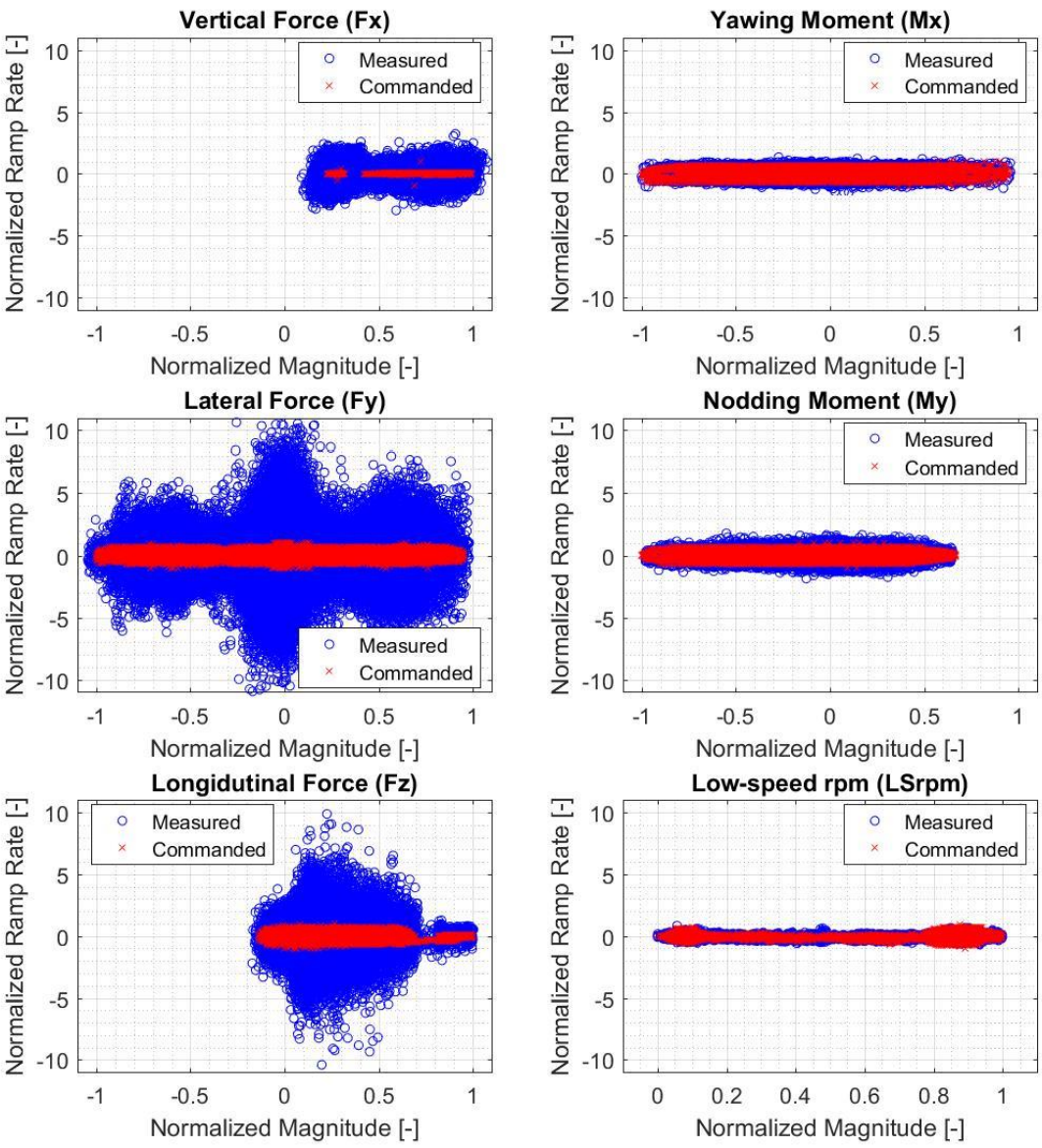

Figure 6.2: Magnitude vs. ramp rate of the measured and commanded LAU loads and speed for all (3.2-MW) test profiles tested with the nominal test bench limits.

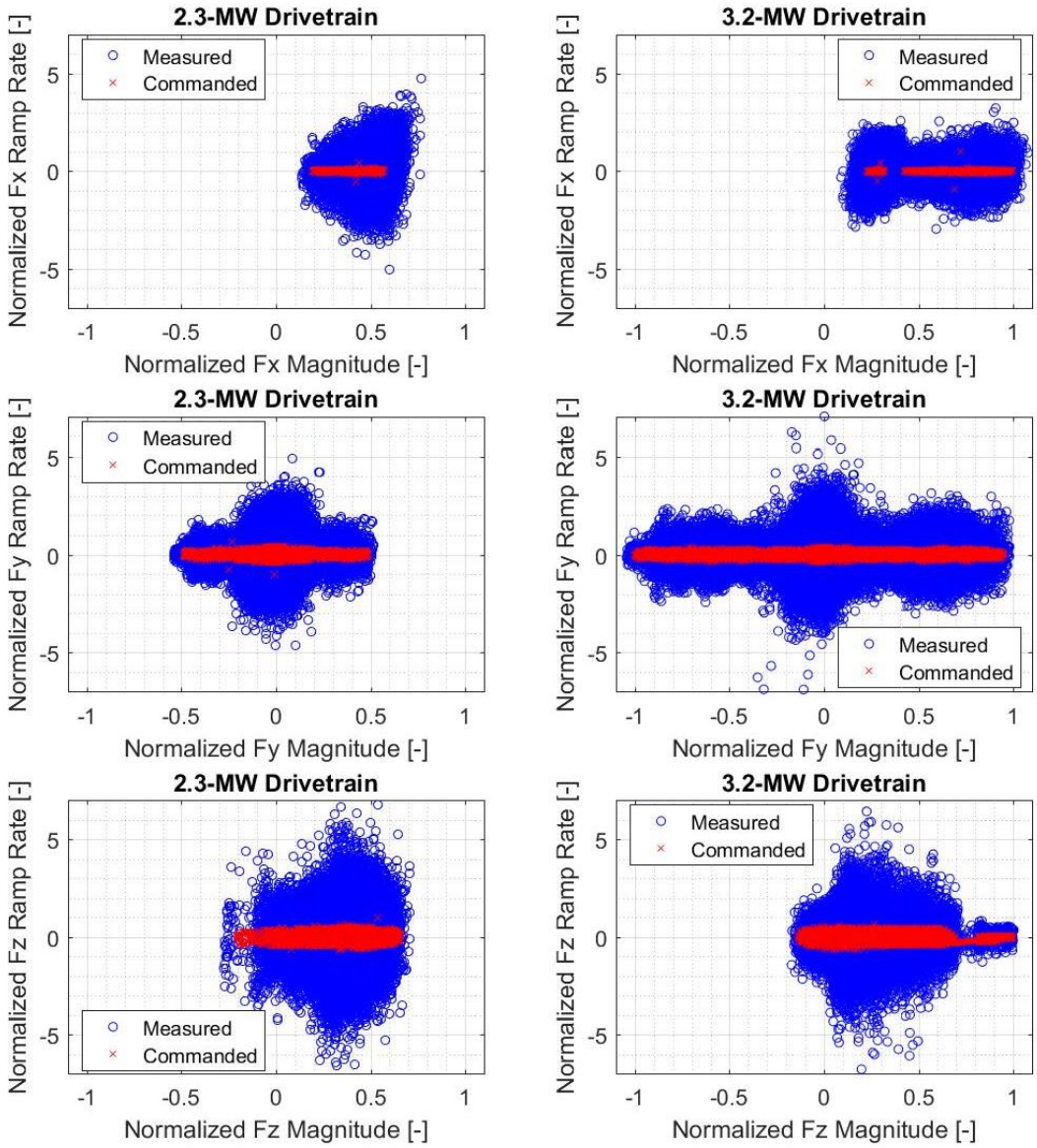

Figure 6.3: Magnitude vs. ramp rate of the measured and commanded LAU forces for all 2.3-MW (left) and 3.2-MW (right) test profiles.

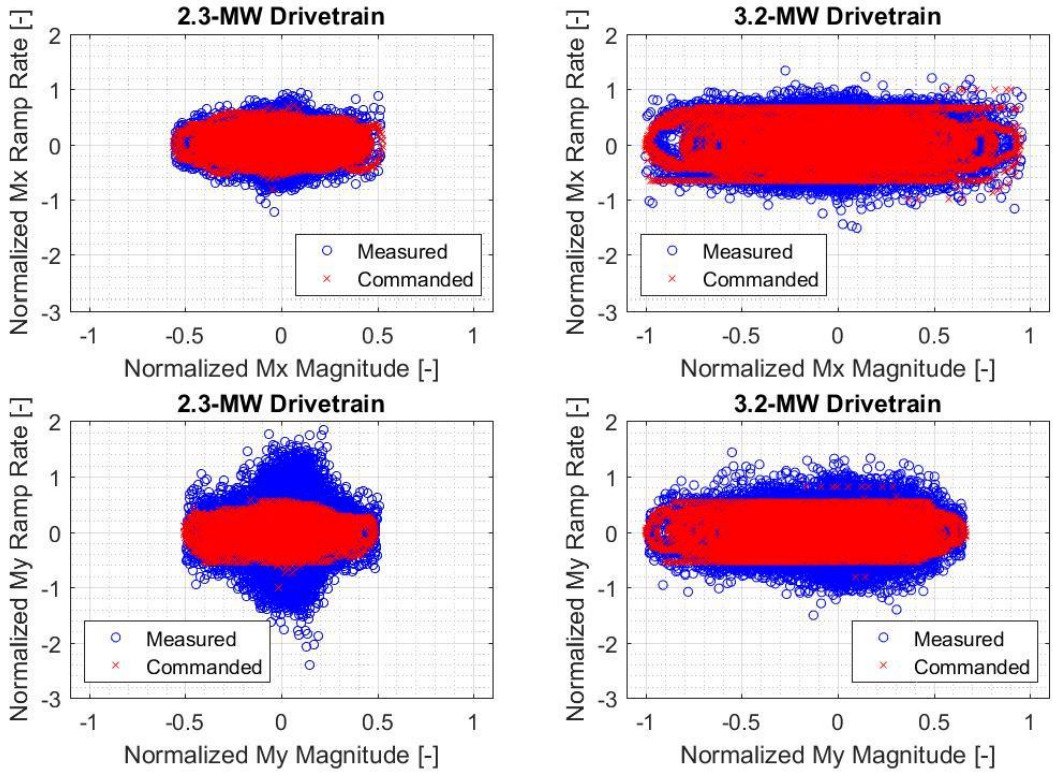

Figure 6.4: Magnitude vs. ramp rate of the measured and commanded LAU moments for all 2.3-MW (left) and 3.2-MW (right) test profiles.

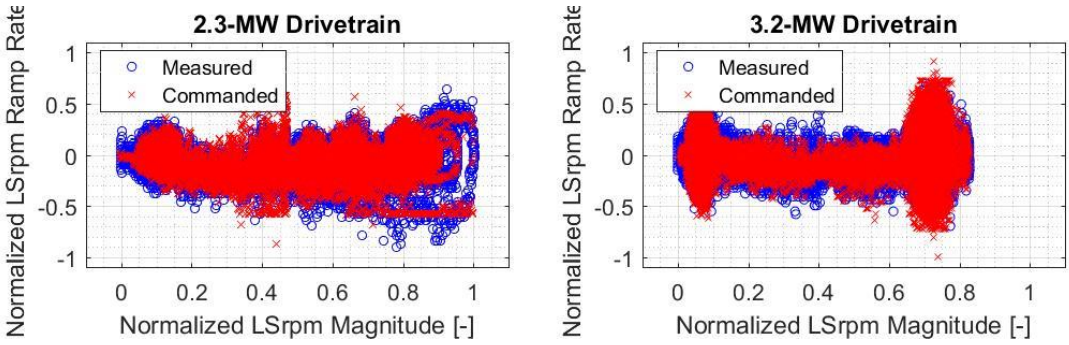

Figure 6.5: Magnitude vs. ramp rate of the measured and commanded LAU speed for all 2.3-MW (left) and 3.2-MW (right) test profiles.

The histograms corresponding to Fig. 6.2 are shown in Figs. 6.6-6.11. These six figures cover the six LAU inputs and each figure presents histograms for the magnitude on the left and ramp rate on the right. The plots in the first row are for the commanded LAU loads and speed whereas those in the second row are for the measurements. Note that consistent ranges for the x and y axes are used for the magnitude of a given load or speed to facilitate comparisons. The same is done for the ramp rate. The red dotted lines in these plots indicate the limits set in the test bench controller for the LAU loads and speed. Limits are set for the magnitude and ramp rate of the loads and speed. Note that these magnitude limits are not shown for the forces because they are outside of the range of the x-axis in Figs. 6.6-6.8. Overall, most observations from the same results for the 2.3-MW drivetrain applies to the 3.2-MW drivetrain with one exception that is listed under Fig. Table 6.3.

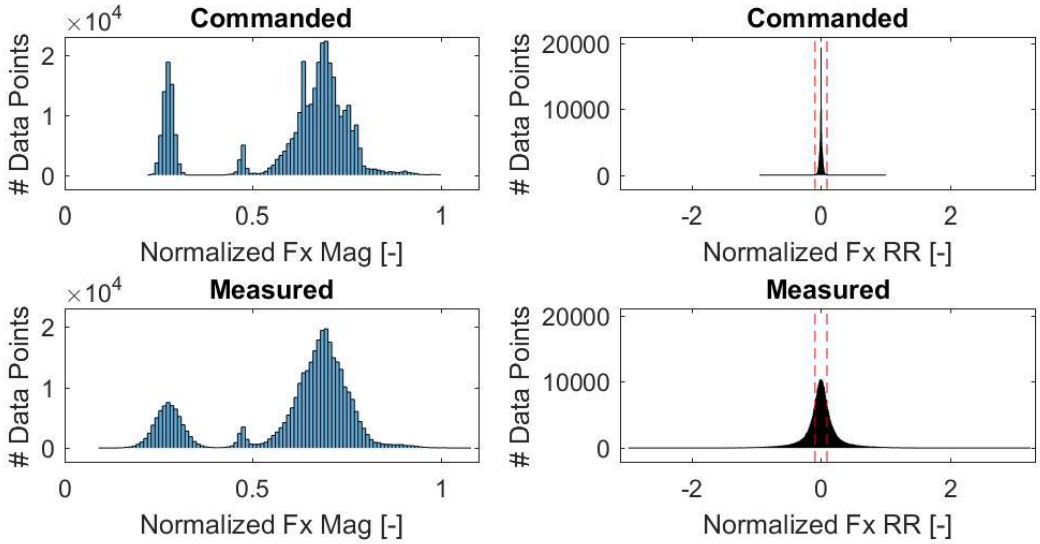

Figure 6.6: Histogram of the magnitude (Mag, left) and ramp rate (RR, right) of the vertical force (Fx) for the commanded values (1st row) and measurements (2nd row) for all (3.2-MW) test profiles tested with the nominal test bench limits (red dotted lines). The OP normalization is applied to the data and the test bench limits not shown for the magnitude histograms because outside the x-axis range.

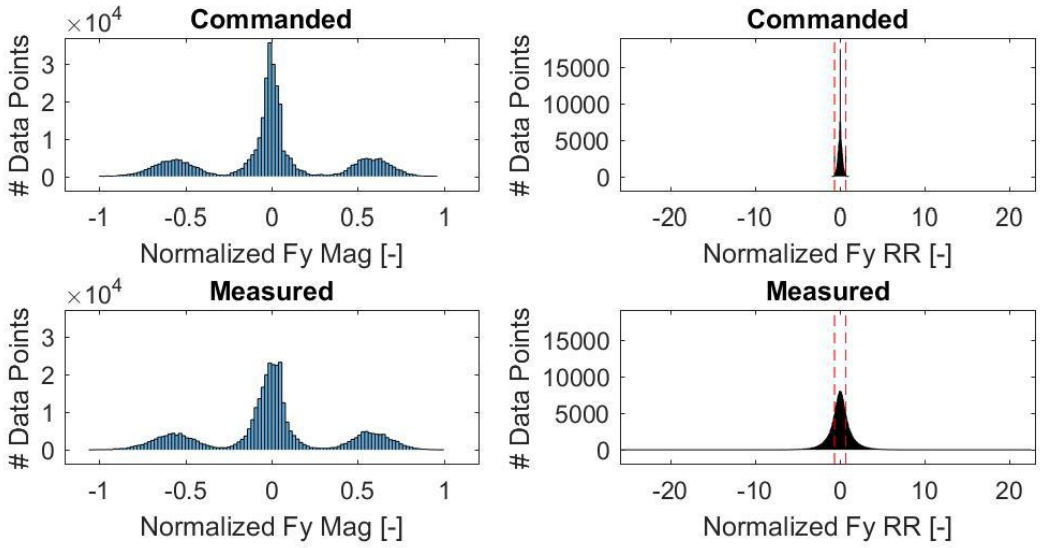

Figure 6.7: Histogram of the magnitude (Mag, left) and ramp rate (RR, right) of the lateral force (Fy) for the commanded values (1st row) and measurements (2nd row) for all (3.2-MW) test profiles tested with the nominal test bench limits (red dotted lines). The OP normalization is applied to the data and the test bench limits not shown for the magnitude histograms because outside the x-axis range.

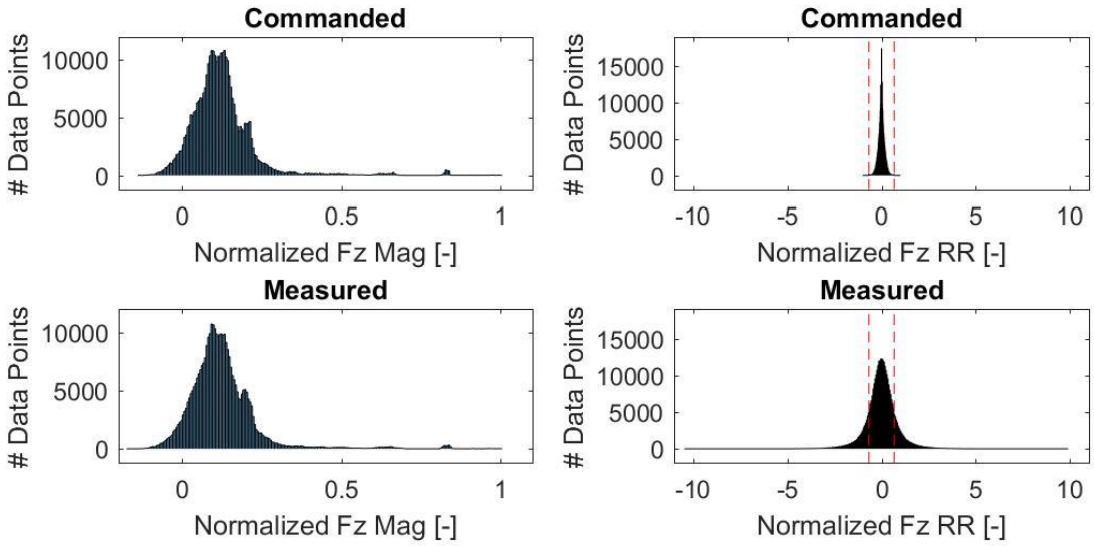

Figure 6.8: Histogram of the magnitude (Mag, left) and ramp rate (RR, right) of the longitudinal force (Fz) for the commanded values (1st row) and measurements (2nd row) for all (3.2-MW) test profiles tested with the nominal test bench limits (red dotted lines). The OP normalization is applied to the data and the test bench limits not shown for the magnitude histograms because outside the x-axis range.

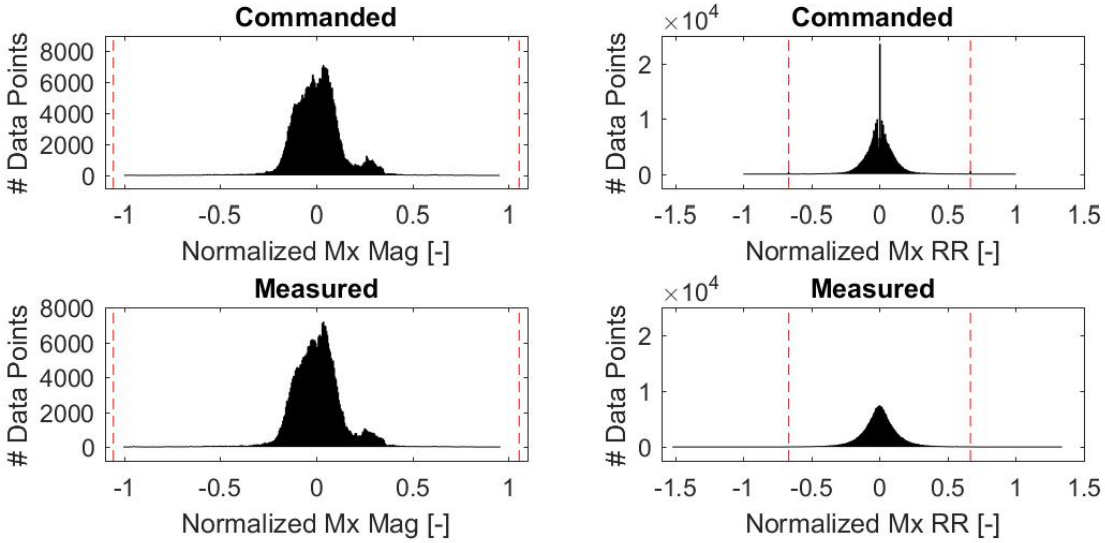

Figure 6.9: Histogram of the magnitude (Mag, left) and ramp rate (RR, right) of the yawing moment (Mx) for the commanded values (1st row) and measurements (2nd row) for all (3.2-MW) test profiles tested with the nominal test bench limits (red dotted lines). The OP normalization is applied to the data and the test bench limits not shown for the magnitude histograms because.

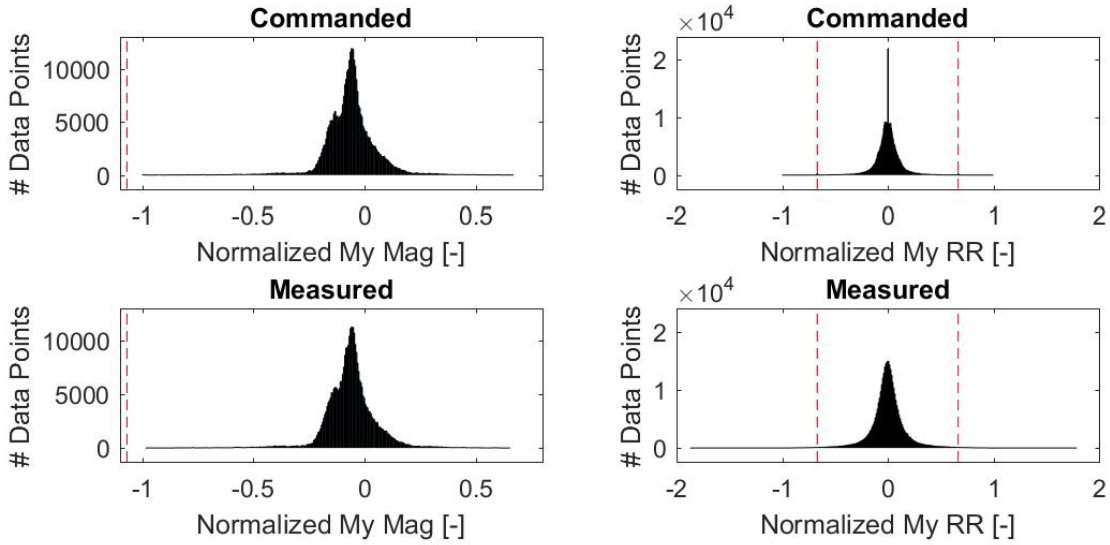

Figure 6.10: Histogram of the magnitude (Mag, left) and ramp rate (RR, right) of the nodding moment (My) for the commanded values (1st row) and measurements (2nd row) for all (3.2-MW) test profiles tested with the nominal test bench limits (red dotted lines). The OP normalization is applied to the data.

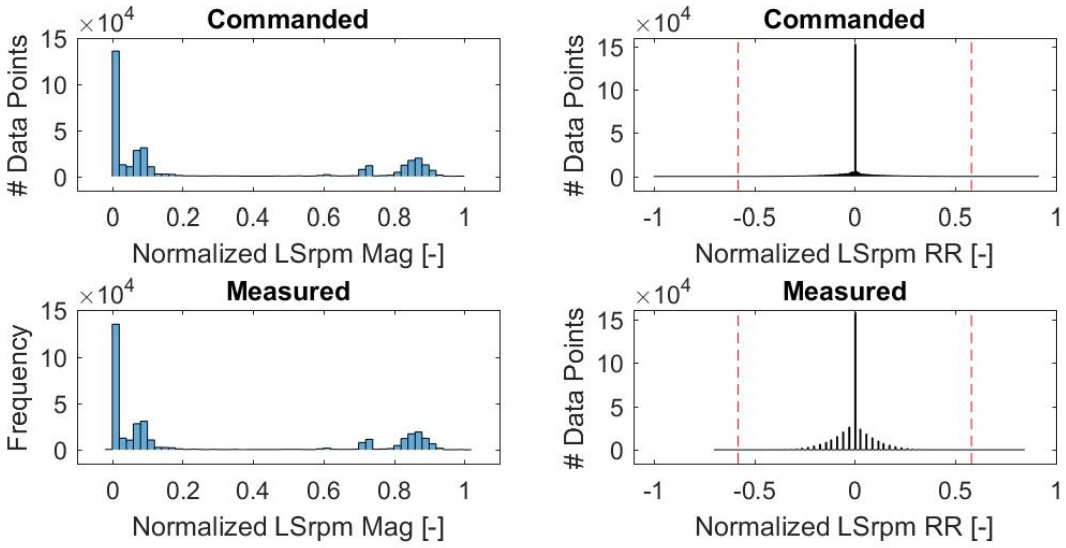

Figure 6.11: Histogram of the magnitude (Mag, left) and ramp rate (RR, right) of the LAU speed (LSrpm) for the commanded values (1st row) and measurements (2nd row) for all (3.2-MW) test profiles tested with the nominal test bench limits (red dotted lines). The OP normalization is applied to the data and the test bench limits not shown for the magnitude histograms because outside the x-axis range.

The similarities in observations from Figs. 6.6-6.11 with those made for the same results for the 2.3-MW drivetrain are:

- All commanded forces and speed are within the limits set in the test bench controller
- The distributions of the moments and speed magnitude are nearly identical.
- The distributions of the measured ramp rates of all LAU inputs and speed are elongated with much broader tails although to a lesser extent for the 3.2-MW drivetrain in the case of the moments.
- A significant number of data points have force ramp rates in excess of the set limits in the test bench controller. This observation is quantified in Table 6.3. The percentage of the data points outside of the test bench limits set in the test bench controller are given for the commanded and measured ramp rate. These

percentages are similar to those for the 2.3-MW drivetrain albeit higher for the 3.2-MW drivetrain specific to the measured ramp rates for the forces.

Table 6.3: Percentage of commanded and measured ramp rates larger than the nominal test bench limits.

LAU Input	Ramp Rate	
	Commanded	Measured
Fx	0.014%	53%
Fy	0.19%	49%
Fz	0.020%	30%
Mx	0.014%	0.32%
My	0.0086%	1.1%
LSrpm	0.13%	0.0055%

The difference between the results for the 3.2-MW drivetrain and those for the 2.3-MW drivetrain is that the distributions of the measured forces are in good agreement with that from the commanded forces. This is not the case for the 2.3-MW drivetrain (refer to Figs. 4.6-4.5). This observation suggests a reduced effect from cross-coupling.

Overall, Figs. 6.2-6.11 as well as Table 6.3 indicate that the test bench will be challenged more to replicate the test profiles of the 3.2-MW drivetrain as compared with the 2.3-MW but the capability is there.

6.1.2 Repeatability

The test profile for max longitudinal force (max Fz) was used as the reference TP during the test period. Per Table 6.1, this TP was tested six times with the nominal capability of the test bench, twice on each test day.

The RMS error from these six tests and all LAU inputs are presented together in Fig. 6.12 and individually in Fig. 6.13. The y-axis from all plots in Fig. 6.13 are scaled to capture a range of 12% ($\pm$6%) of the mean value (dotted line) except for the lateral force, which has a y-axis spanning 38% of the mean value. Overall, there are no pattern in the

data in terms of clustering, mixture, and oscillations, but the vertical and longitudinal forces show significant trends, especially for the longitudinal force. These trends are within 6% of the measurement error, however, and the smaller magnitude of the forces as compared with the bending moments mitigate the impact of these trends.

The histograms of the RMS error for each LAU input are presented in Fig. 6.14 with an overlay of a normal distribution with the p-value from an Anderson-Darling test using 95% confidence. The p-values given in Fig. 6.14 indicate that the distribution of the normalized RMS error is normal for all LAU loads inputs except for the lateral force due to the 5th test. There is no variation in the low-speed rpm.

Except for the lateral force, the 95% confidence interval for each LAU loads input can be determined using a student-t distribution using five degree of freedoms for a two-tail distribution. The corresponding factor on the standard deviation is 2.571 for 95% confidence. For the lateral force, a non-parametric analysis using a 1-sample sign test was used. The confidence intervals are given in Table 6.4 for both normalizations. The results presented in Table 6.4 indicate that the repeatability of the measurements is excellent and also puts in perspective the repeatability results for the lateral force. The 95% confidence interval of the RMS error of the lateral force is approximately one third of the peak lateral force that the reference test profile is commanding, which is 1.8 times the measurement error. Therefore, the relatively poor repeatability of the lateral force measurements as compared to the other LAU loads can be explained by the test bench applying lateral forces to the test article that are at most 1.8x the measurement error. In fact, the average lateral force over the reference test profile is exactly the same as the measurement error.

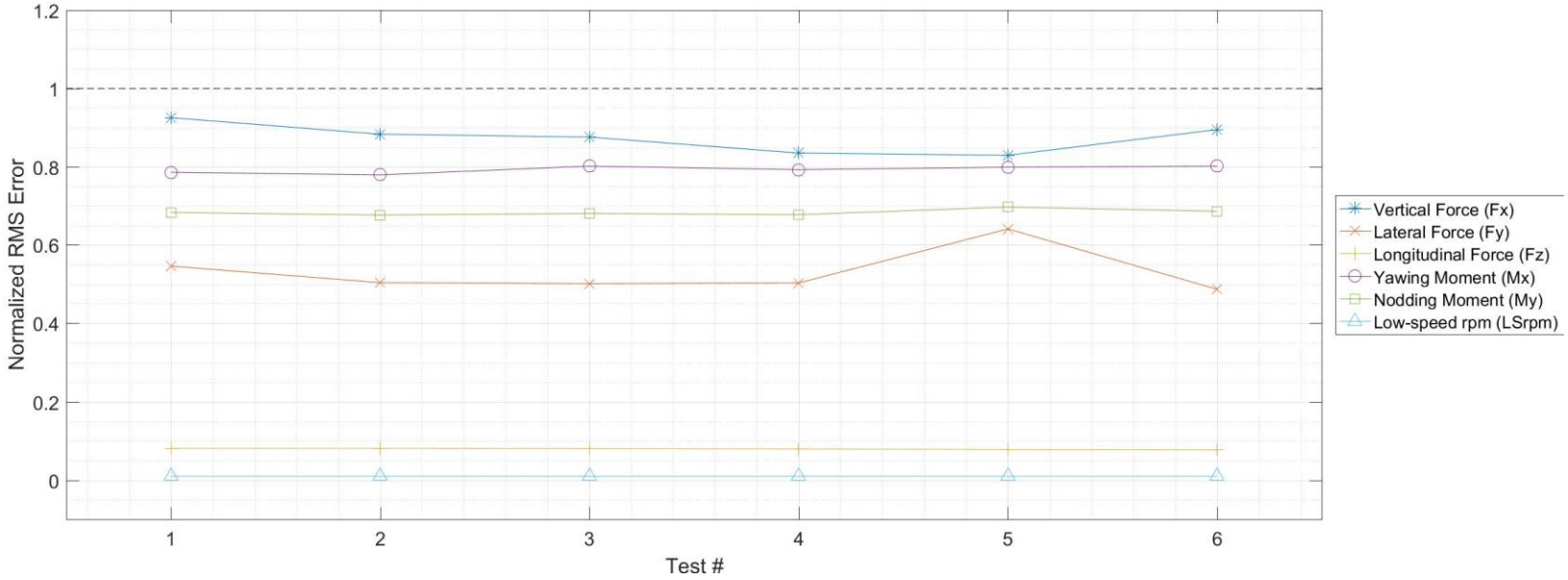

Figure 6.12: Repeatability of the normalized RMS error (E normalization) between the measured and commanded LAU loads for the reference test profile of the 3.2-MW drivetrain (TP max Fz). The larger than unity normalized RMS error for the vertical and lateral forces is due to a cross-coupling effect from the simultaneous LAU application of bending moments and forces dynamically.

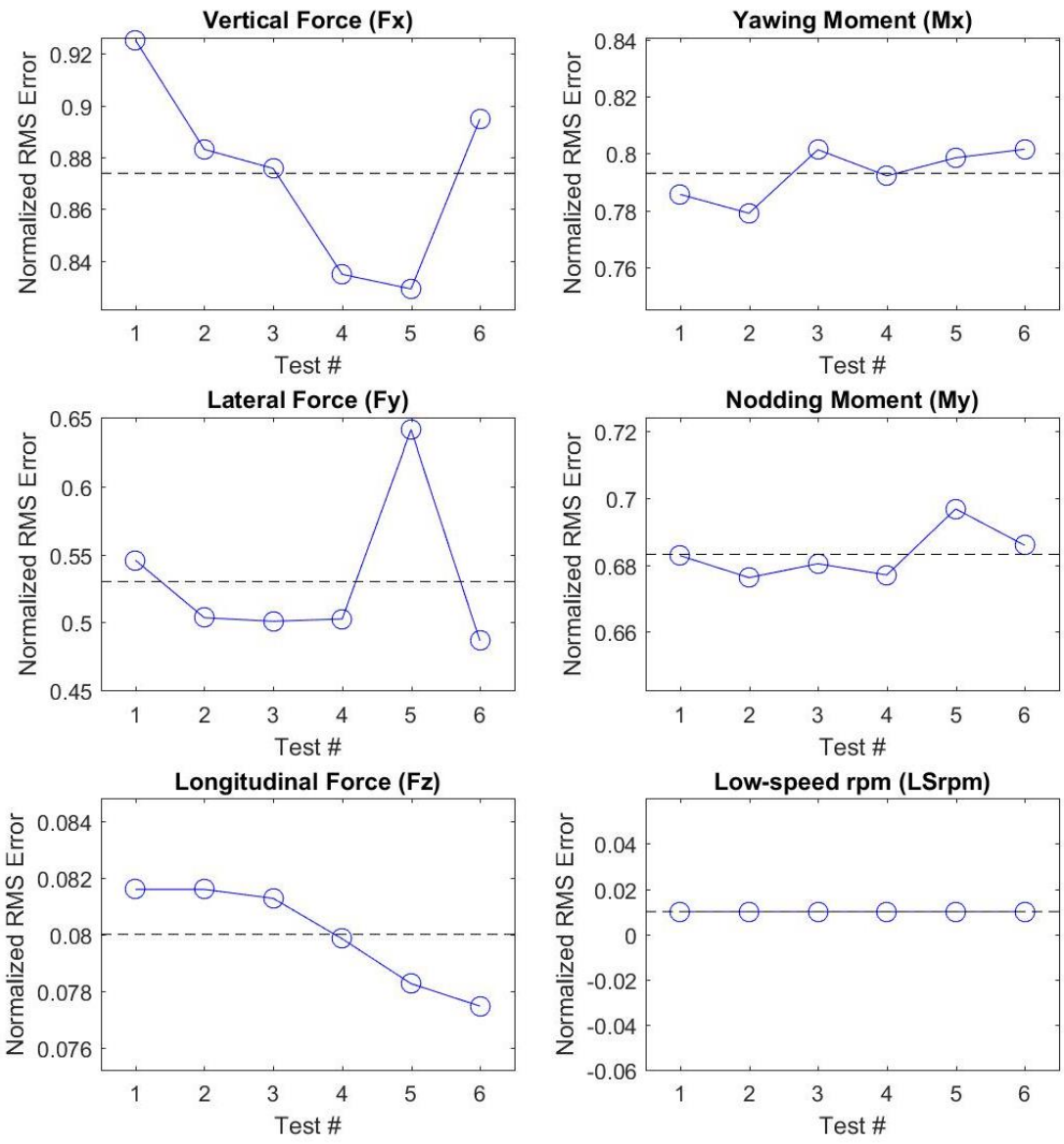

Figure 6.13: Repeatability of the normalized RMS error between the measured and commanded LAU loads for the reference test profile of the 3.2-MW drivetrain (TP max Fz) presented individually.

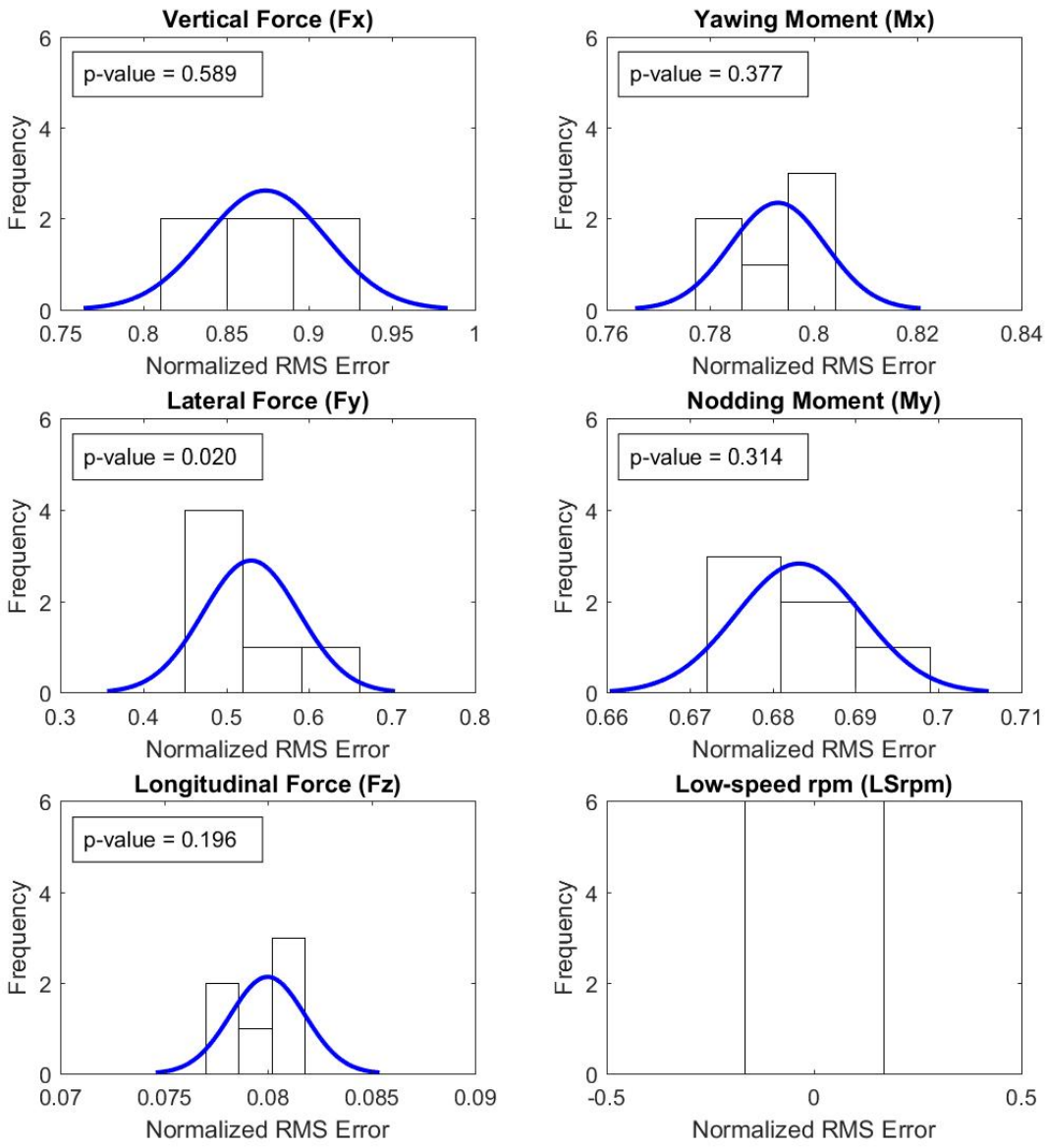

Figure 6.14: Histogram of the RMS error between the measured and commanded LAU loads for the reference test profile of the 3.2-MW drivetrain (TP max Fz) for all LAU inputs.

Table 6.4: 95% confidence interval (CI) for the normalized RMS error between the measured and commanded LAU loads. The confidence intervals are normalized with the measurement error and peak value of each LAU load.

95% CI [%] Normalized RMS Error	Vertical Force, Fx	Lateral Force, Fy	Longitudinal Force, Fz	Yawing Moment, Mx	Nodding Moment, My
Peak (P)	±0.27	-27 / +33	±0.04	±0.07	±0.07
Meas. Error (E)	±9.4	-49 / +61	±0.46	±2.4	±2.0

A comparison of the 95% confidence intervals for the RMS error normalized by the measurement error for both drivetrains and all LAU loads is presented in Fig. 6.15. With the exception of the CI for the lateral force of the 3.2-MW drivetrain, the results are similar and all confidence intervals are well within the measurement error.

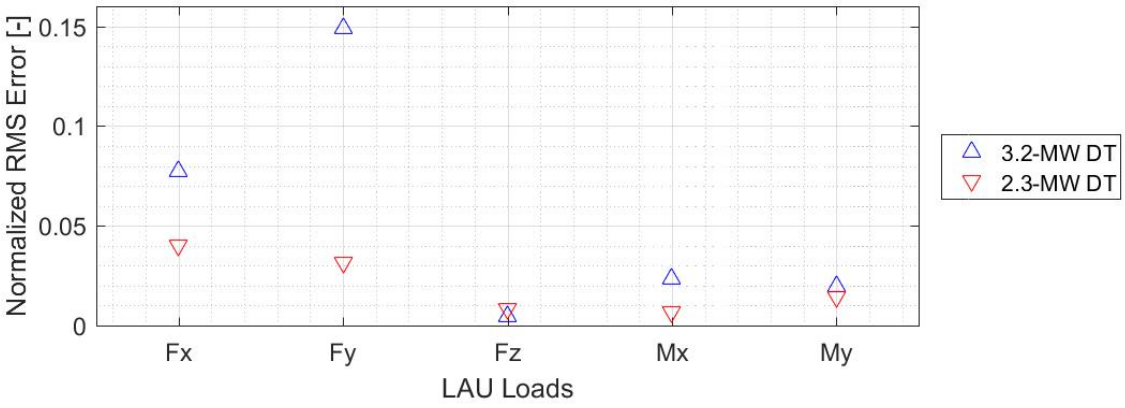

Figure 6.15: Comparison of the 95% confidence interval for the repeatability of the RMS error (E Normalization) for both drivetrains.

The repeatability of the measurements was also quantified with four other test profiles that were tested twice in order to understand consistency across the test profiles of most interest. Figure 6.16 presents the RMS error for the LAU loads and speed for the two measurements of the four test profiles in question. The first and last measurements for reference test profile (max Fz) are also included to guide the comparison. The slopes

of the lines connected the RMS error for both test indicate that the level of variation from the test profiles of most interest are similar to that of the reference test profile. Accordingly, the excellent repeatability of the measurements is consistent. The approach of testing multiple test profiles twice was selected to be complementary to the tests done with the 2.3-MW drivetrain in which repeatability was investigated for reduced ramp rates.

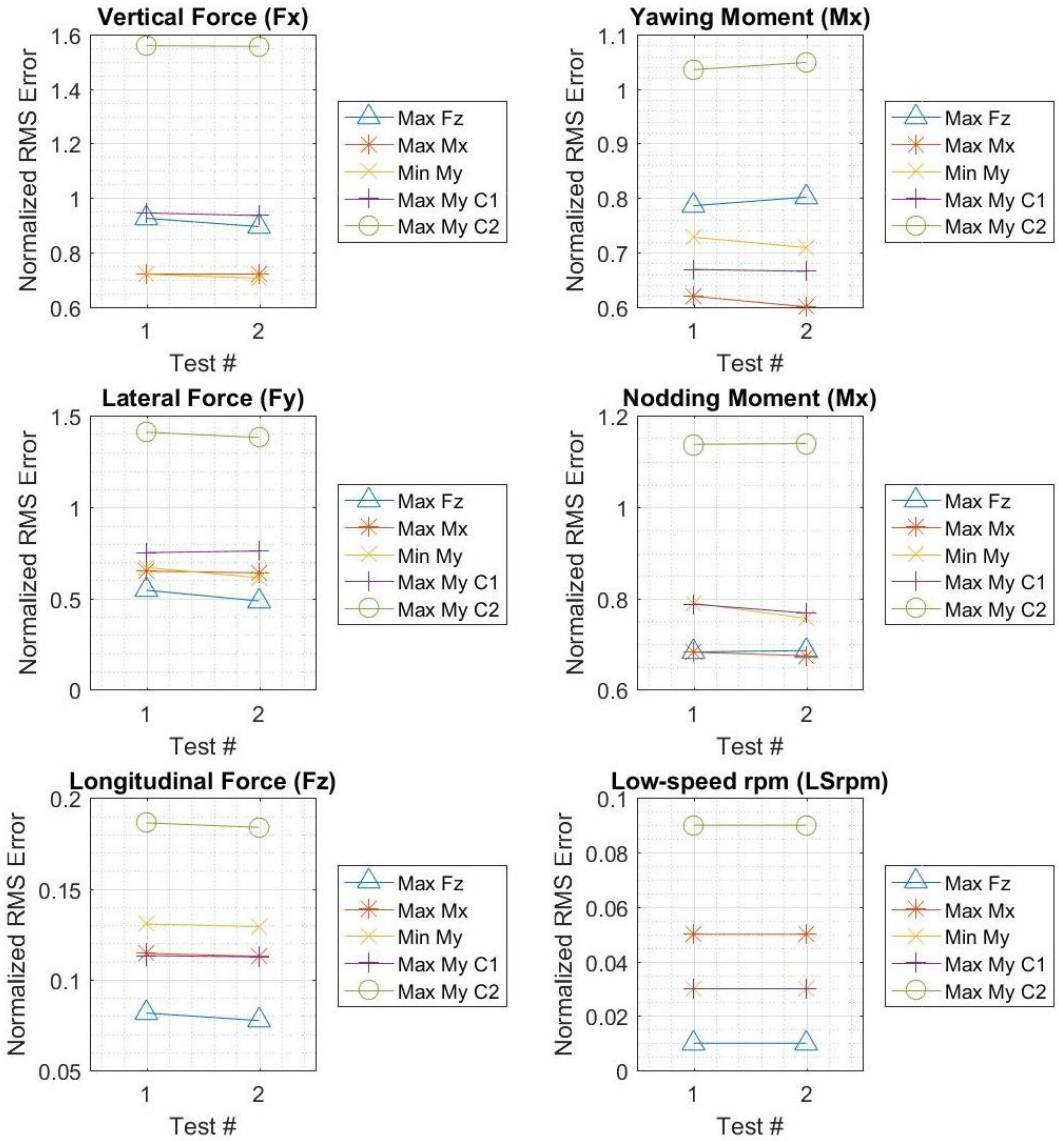

Figure 6.16: Repeatability of the normalized RMS error between the measured and commanded loads for the test profiles of the 3.2-MW drivetrain that were tested twice.

The repeatability of the peak error for all LAU inputs from the six tests done with the reference test profile is presented in Fig. 6.17 using the P normalization. The peak errors for the lateral force are plotted separately due to the difference in scale, which is due to the combined effect of cross coupling with the relatively small peak value of the lateral force as compared with the other LAU loads for the reference test profile (max Fz). Overall, the peak errors have good repeatability. The repeatability is comparable to that of the 2.3-MW drivetrain when considering that the peak loads of the 3.2-MW drivetrain are approximatively 1.4x to 2x that of the 2.3-MW drivetrain.

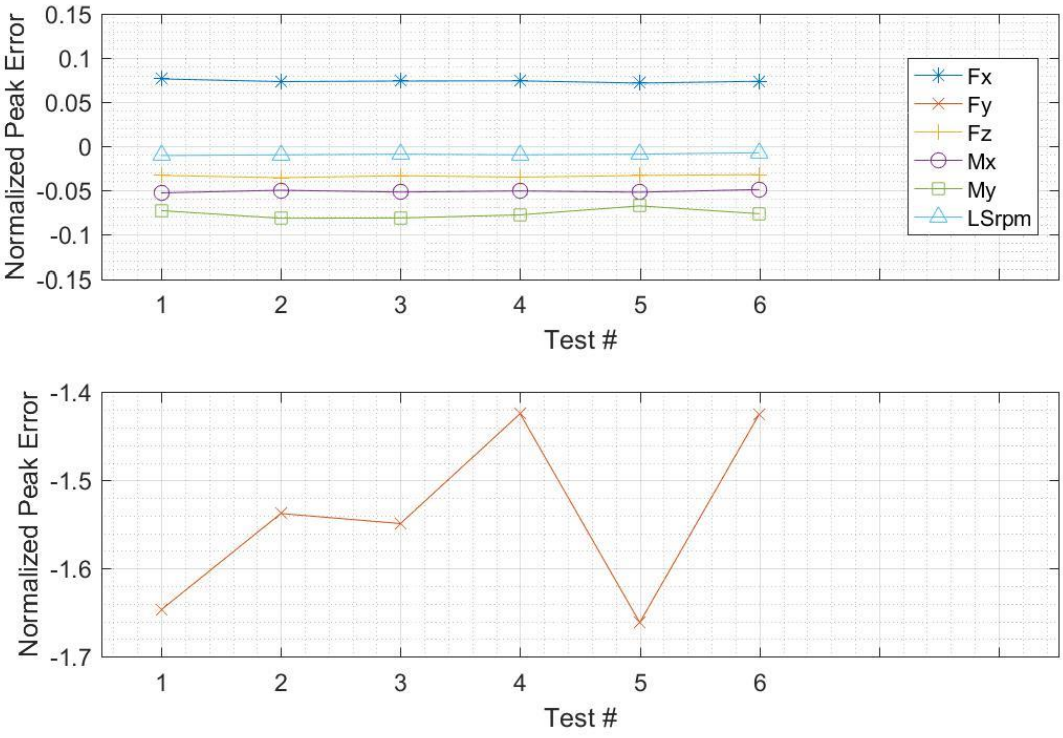

Figure 6.17: Repeatability of the normalized peak error (P normalization) between the measured and commanded LAU loads for the reference test profile of the 3.2-MW drivetrain (max Fz). The larger than unity normalized peak errors for the lateral force are due to the combined effect of cross coupling with relatively small peak value of the lateral force as compared with the other LAU loads for the reference test profile.

6.1.3 Tracking performance

The performance of the test bench at tracking the test profiles are presented separately for the nominal and reduced ramp rate limits.

6.1.3.1 Nominal test bench ramp rate limits

The tracking performance for the reference test profile of the 3.2-MW drivetrain (max Fz) and all LAU inputs is depicted in Fig. 6.18.

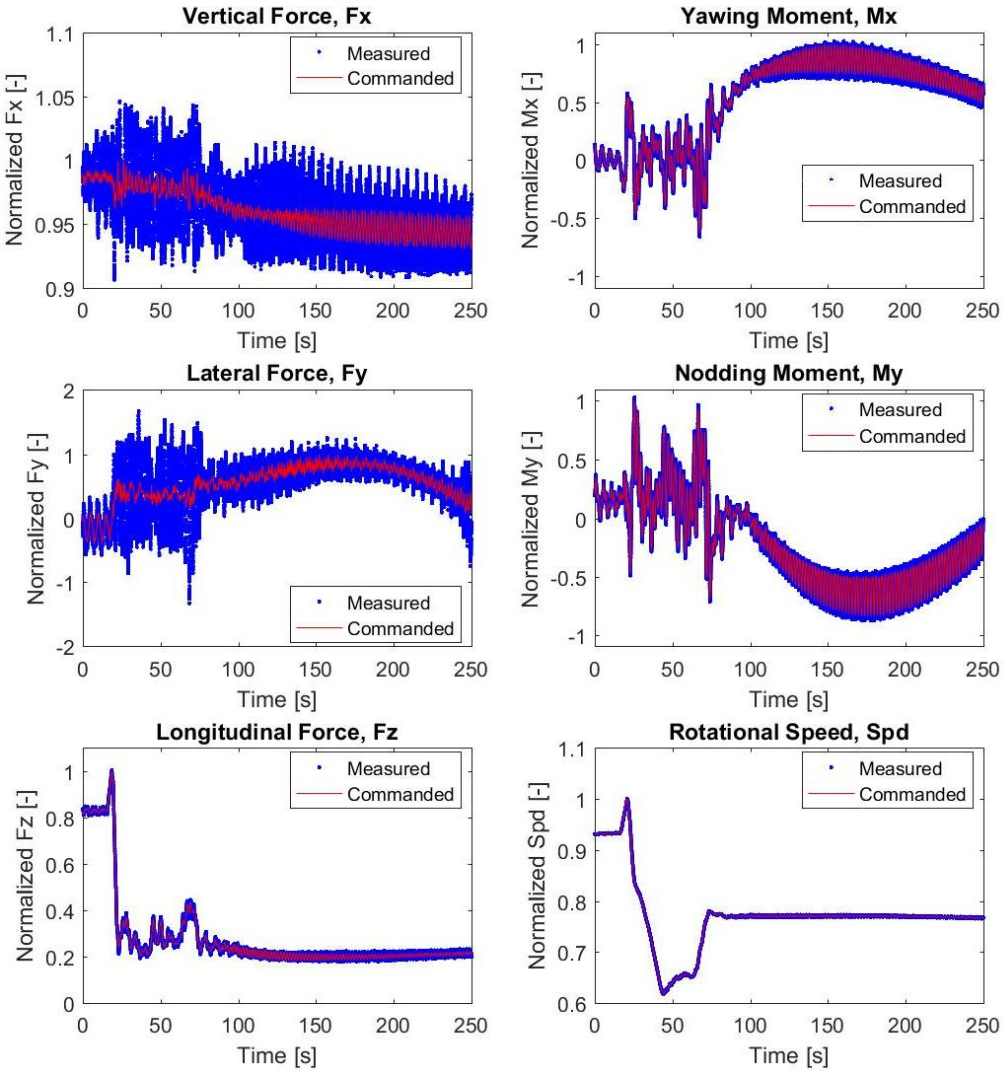

Figure 6.18: Time series of the normalized LAU inputs (P normalization) for the reference test profile of the 2.3-MW drivetrain (max Fz).

The measured LAU loads and speed (blue) and commanded LAU inputs (red) are co-plotted. Figure 6.18 presents the results for the test having RMS errors for the LAU loads and speed that are closest to the average over the six tests with the reference test profile. There is good tracking of the longitudinal force, bending moments, and speed. The tracking is poor for the vertical and lateral forces due to the cross coupling effect.

The tracking performance of all test profiles is presented in Appendix C and the RMS errors corresponding to all LAU inputs and test profiles are summarized in Fig. 6.19. Note that results for the two test profiles of the 2.3-MW drivetrain that were also tested with the 3.2-MW drivetrain are excluded from Fig. 6.19. These results are presented in Section 6.1.3.1.2.

The tracking error is mostly within the measurement error and in the same range than the tracking error for the 2.3-MW drivetrain (refer to Fig. 4.17). The normalized RMS errors above unity for the moments are indications of tracking error likely due to test bench hardware limitations.

The peak errors for all LAU loads and speed for all test profiles of the 3.2-MW drivetrain are presented in Figs. 6.20 and 6.21 for the E and P normalization, respectively. Overall, the ratio of the peak errors to the measurement error is in the range of 2-9 for the forces impacted by cross-coupling and 4-6 for the moments. The peak errors for the longitudinal force are mostly within the measurement error. All peak errors are within the peak value of the LAU loads except for the lateral force. This observation applies to the 2.3-MW drivetrain as well.

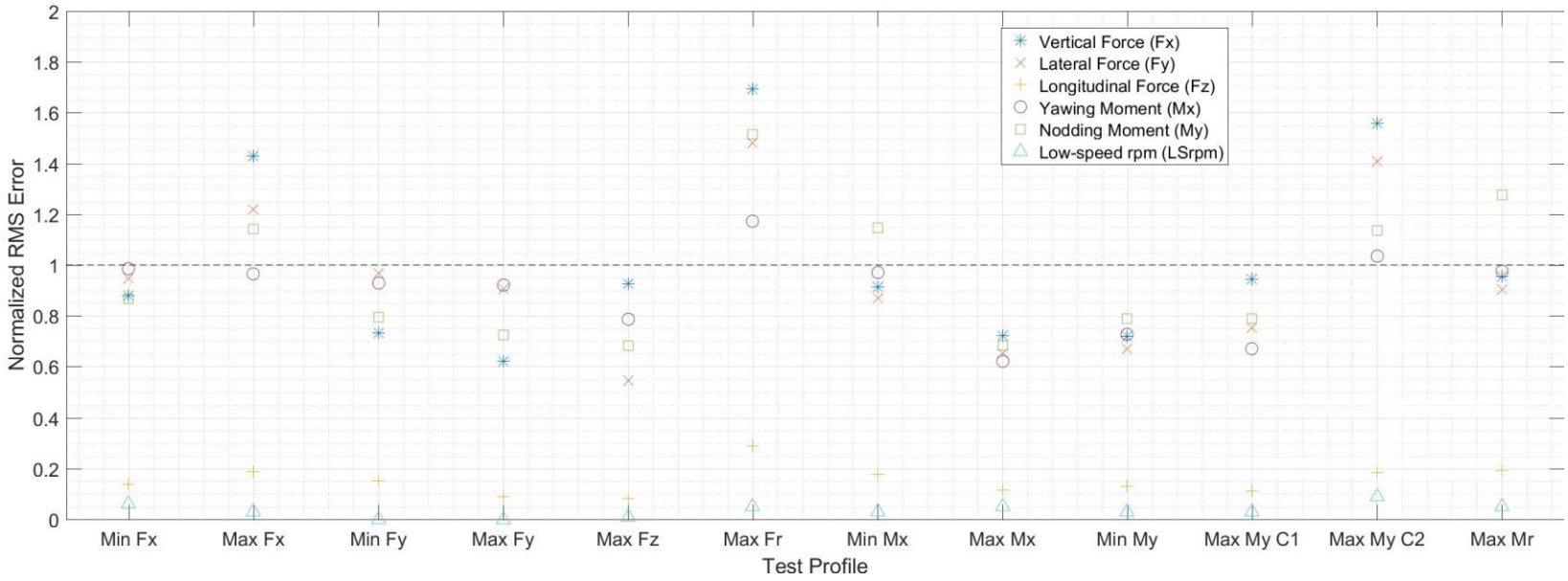

Figure 6.19: Normalized RMS error between the measured and commanded loads and speed for all test profiles of the 3.2-MW drivetrain for the nominal test bench capability (E normalization).

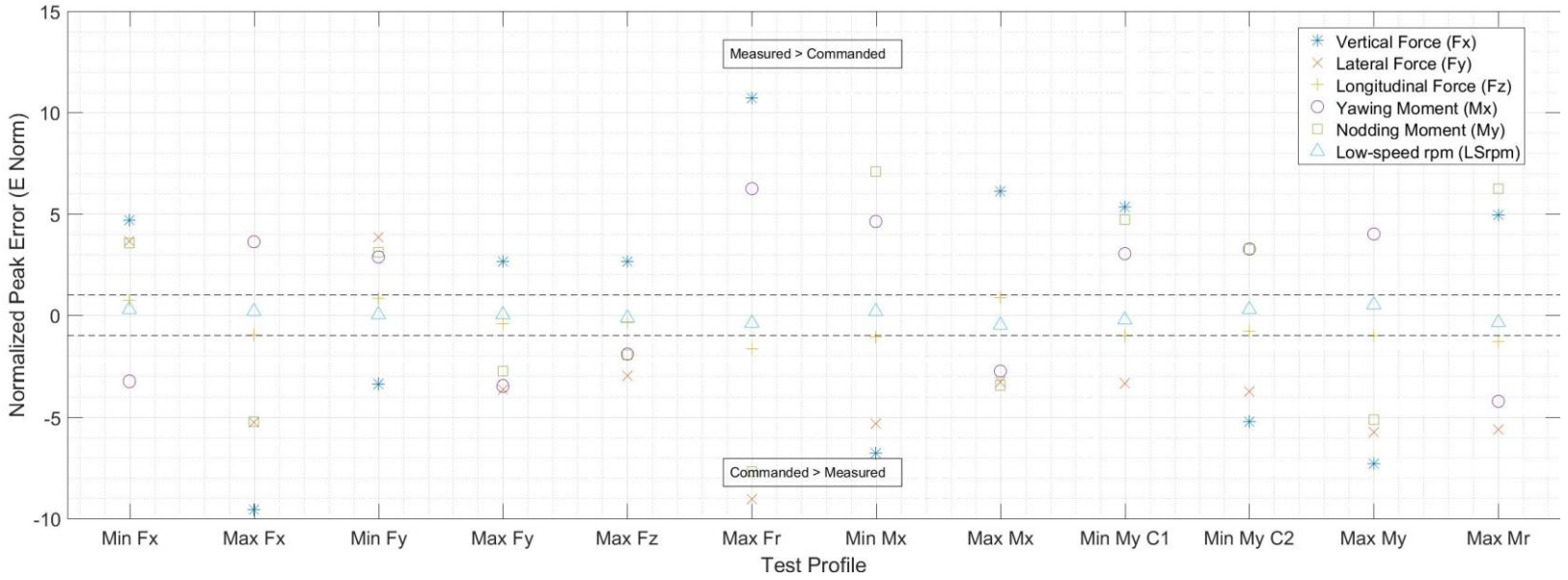

Figure 6.20: Normalized peak error between the measured and commanded loads and speed for all test profiles of the 3.2-MW drivetrain for the nominal test bench capability (E normalization).

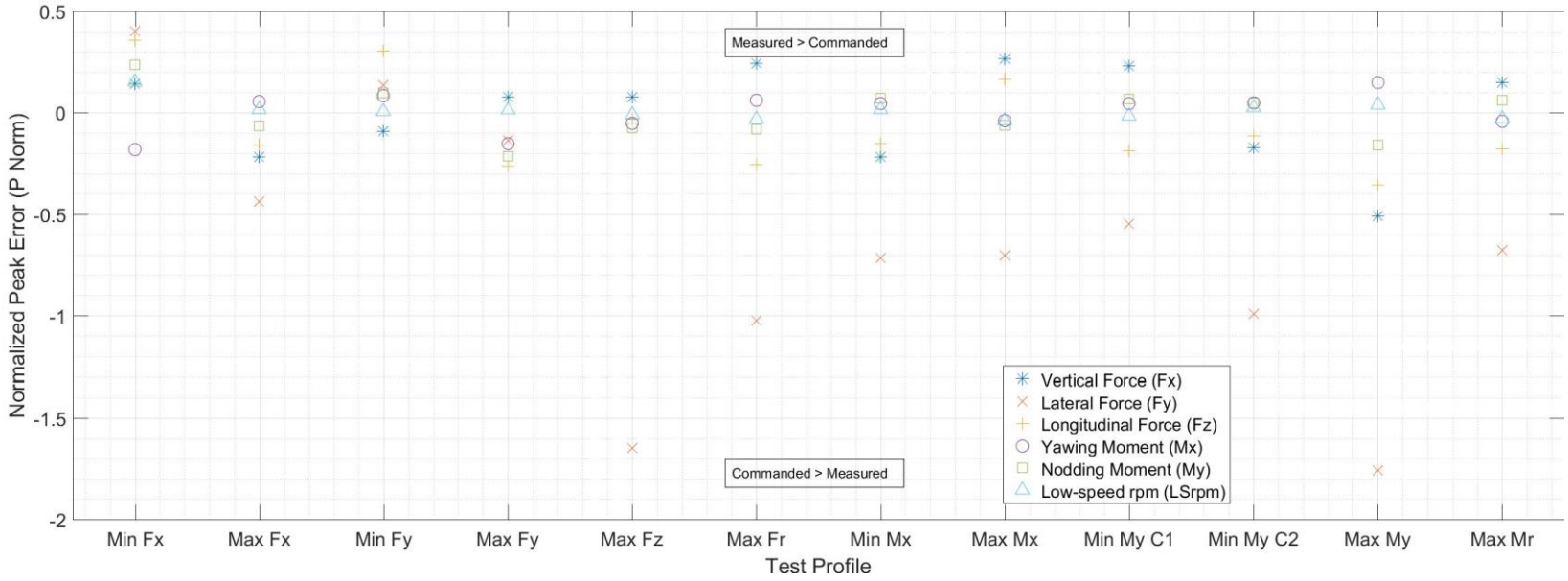

Figure 6.21: Normalized peak error between the measured and commanded loads and speed for all test profiles for the nominal test bench capability (P normalization).

The tracking performance of the reference test profile in the frequency domain is presented in Fig. 6.22. The frequency range of 2 Hz captures over 99% of the total spectral energy in the signal. The cross-coupling effect causes the peak amplitudes for the vertical and lateral forces to be greater than the commanded peak amplitudes. The frequency for the peak amplitude is also altered from the cross-coupling effect. Specifically, the peak amplitude for moments at 0.5 Hz increases the peak amplitude of the vertical and lateral forces at that frequency.

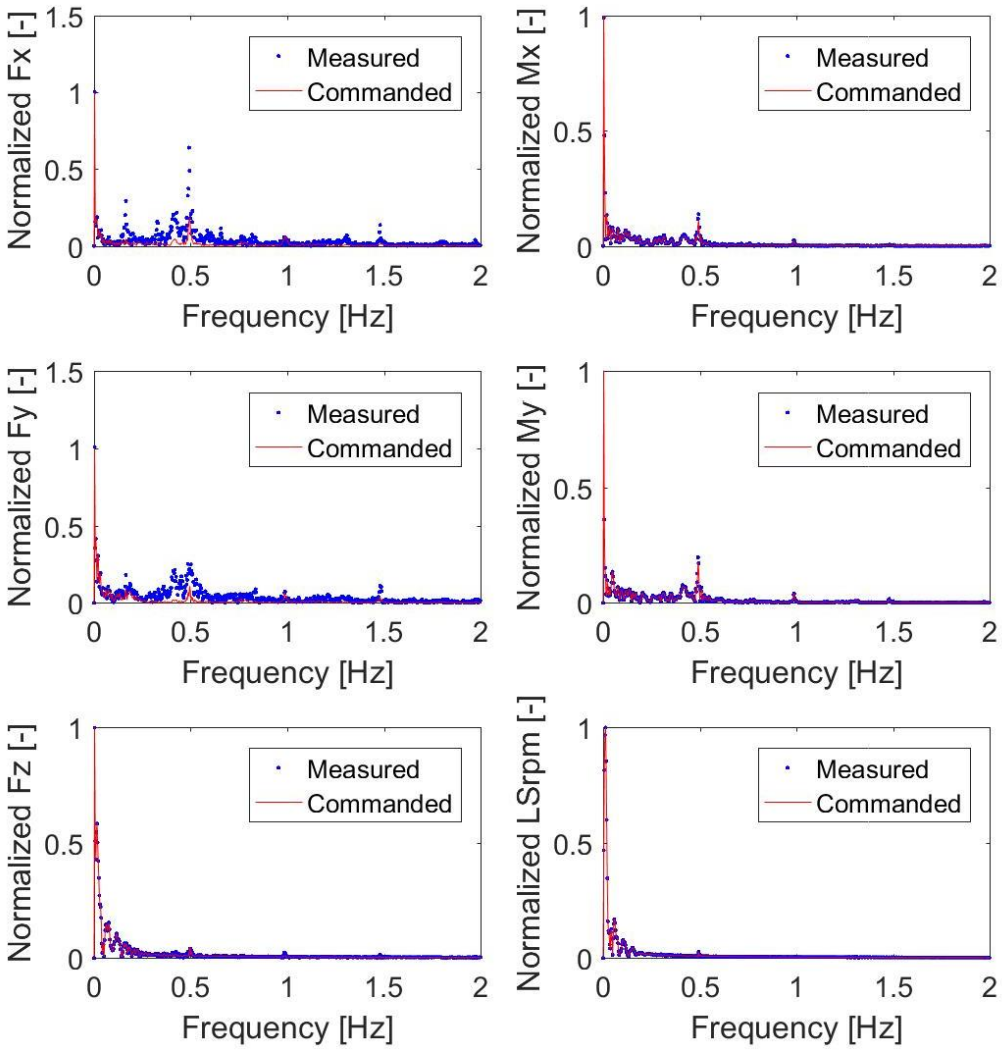

Figure 6.22: Frequency domain representation of the normalized LAU loads and speed (P normalization) for the ref. test profile of the 3.2-MW drivetrain (max Fz).

6.1.3.2 Drivetrain effect

Two test profiles from the 2.3-MW drivetrain were also tested with the 3.2-MW drivetrain. These test profiles are for case max Fy and max Mr. These two test profiles were selected to test both drivetrain with a test profile representing shutdown conditions (zero speed) and with the highest combination of yawing and nodding moments. Figure 6.23 presents the tracking performance of the test bench in replicating these two test profiles with both drivetrains. Results for the peak error are given in Fig. 6.24 for the OP normalization to have a common peak load reference for all LAU loads and speed. In both Figs. 6.23 and 6.24, the results for the Max My test profile are on the left and those for the Max Mr test profile are on the right. A consistent scale for the errors is used for both test profiles to facilitate comparison of the results. Results for the LAU speed are not included for the max Fy test profile due to commanding zero speed.

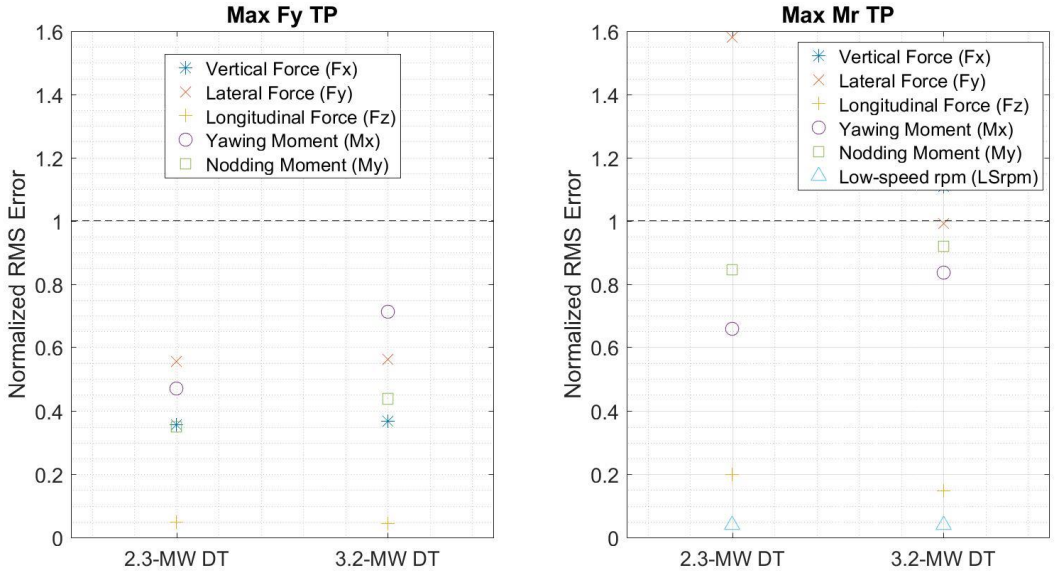

Figure 6.23: RMS error from both drivetrains (DT) for all LAU loads and speed for the two test profiles (TP) tested with both drivetrains (E normalization for the RMS error).

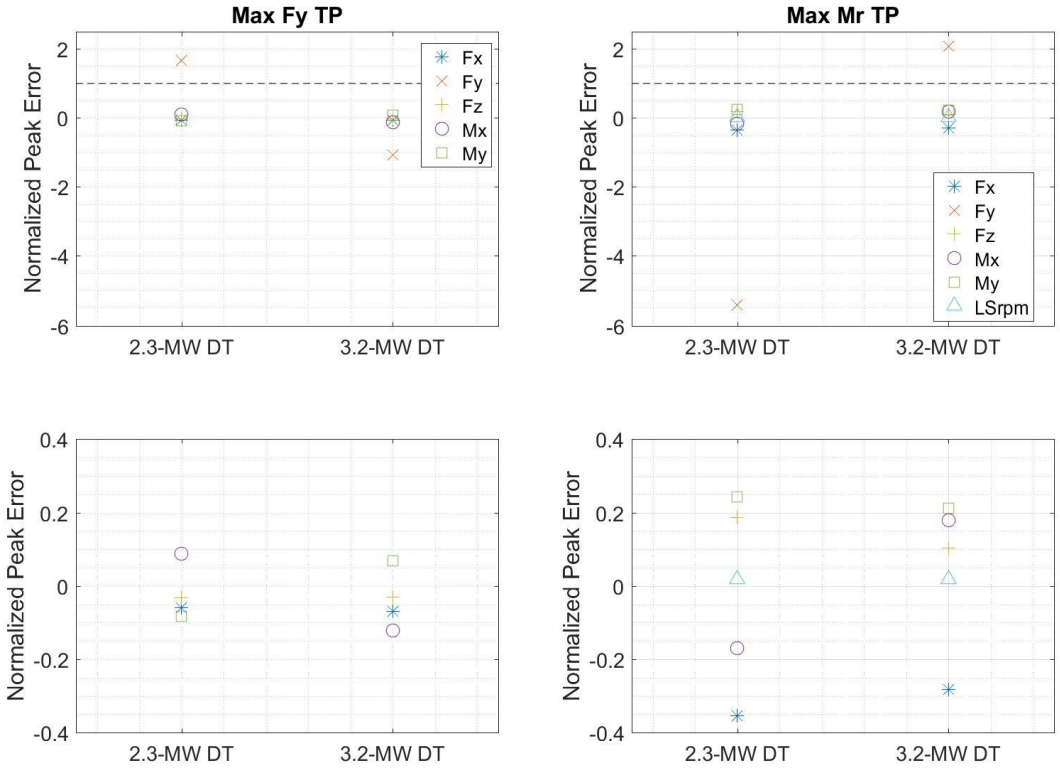

Figure 6.24: Peak error from both drivetrains (DT) for all LAU loads and speed for the two test profiles tested (TP) with both drivetrains (OP normalization for the peak error). Plots on the lower row are for a reduced range of peak error.

The results from Figs. 6.23 and 6.24 show that the effect of the drivetrain on the tracking performance is mostly within the measurement error or peak value of the loads, respectively, with the exception of the RMS error for the three forces for the max Fy test profile. Beside this exception, the drivetrain effect is small but it is larger than the 95% confidence intervals from the uncertainty range for repeatability. Table 6.5 summarizes the effect of the drivetrain on the LAU loads and speed. The relatively consistent RMS error of the vertical and lateral forces for both drivetrains for the max Fy test profile and

the significantly different RMS error for the other test profile points to the drivetrain impacting the cross-coupling effect differently.

Table 6.5: Summary of the effect of the drivetrain on tracking performance.

LAU Input	Effect of DT on RMS Error	Effect of DT on Peak Error
Vertical Force (Fx)	Greatly varies between TPs. Insignificant for max Fy TP, significant for max Mr TP	Change within 10% of peak Fx value
Lateral Force (Fx)		Greatly varies between TPs
Longitudinal Force (Fz)	Insignificant for max Fy TP, small for max Mr TP	Change within 10% of peak Fz value
Yawing moment (Mx)	Relatively consistent change in error with larger error with larger DT.	Inconsistent change within 25% of peak Mx value
Nodding moment (My)		Inconsistent change within 20% of peak value
Speed (LSrpm)	No change	No change

The effect of the drivetrain on the RMS and peak errors of the moments are presented as a function of the stiffness and total mass of the drivetrains in Figs. 6.25 and 6.26, respectively. The use of the mass is a proxy for the moment of inertia due to uncertainty about the mass distribution over the drivetrains and their respective center of gravity location. The scale of all plots in Figs. 6.25 and 6.26 is identical allowing direct comparison of the slopes of the lines connecting the data. The slopes of the lines connecting the RMS data between the drivetrain stiffness and mass are relatively consistent for each moment, which suggest potential in using either or both of these drivetrain characteristics in a predictive model. The drivetrain stiffness and mass do not provide a consistent a consistent trend for the peak error, but the trends between these two drivetrain characteristics within a test profile is similar.

The increasing RMS error with increased stiffness shown in Fig. 6.25 is counter intuitive as one would expect that the stiffer 3.2-MW drivetrain in both yaw and nodding would result in better tracking for a given set of LAU inputs. This finding suggests that the

change in mass (inertial effects) has a greater impact on the tracking performance than the change in stiffness, but it is likely more a reflection of differences in test bench controller tuning. The gains of the test bench controller were tuned for both drivetrains for their respective set of test profiles with the constraint of using the same gains for all test profiles of a given drivetrain. The magnitude and ramp rate of the loads from the test profiles of the 3.2-MW drivetrain are higher than those of the 2.3-MW drivetrain (refer to Appendix A for the comparison). Accordingly, the test bench used controller gains tuned for higher loads when it tracked the 2.3-MW drivetrain test profiles with the 3.2-MW drivetrain. In contrast, the tracking performance with the 2.3-MW drivetrain was done with controller gains tuned for the loads from the test profiles of that drivetrain.

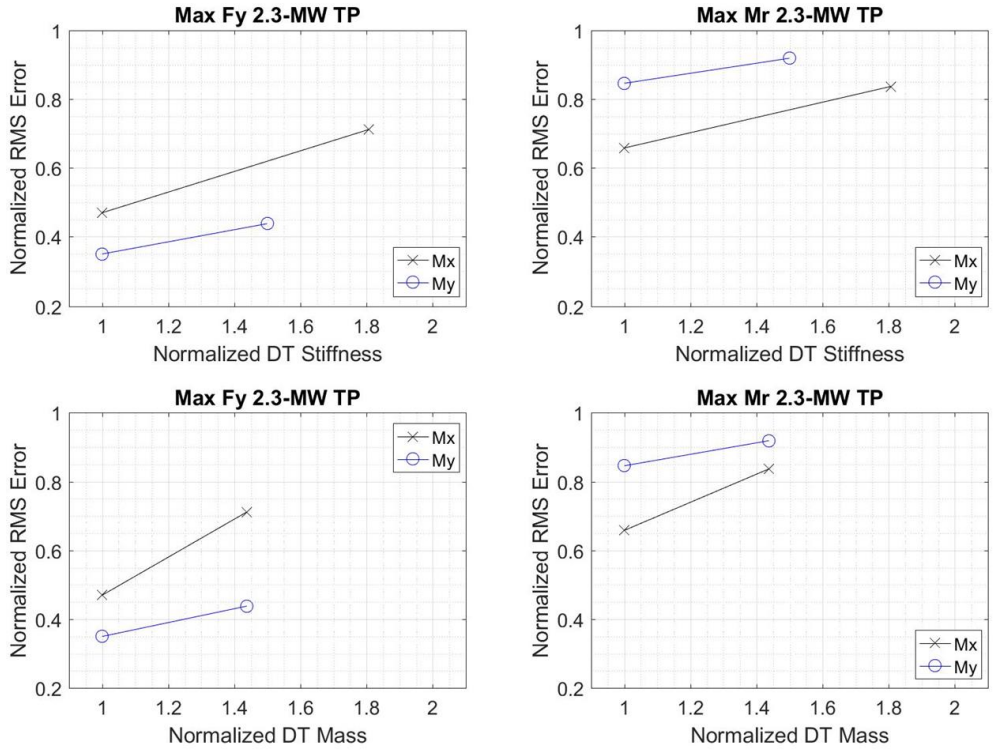

Figure 6.25: RMS error as a function of drivetrain (DT) stiffness (top row) and DT mass (lower row) for the yawing (Mx) and nodding (My) moments for the two test profiles (TP) tested with both drivetrains (E normalization for the RMS error).

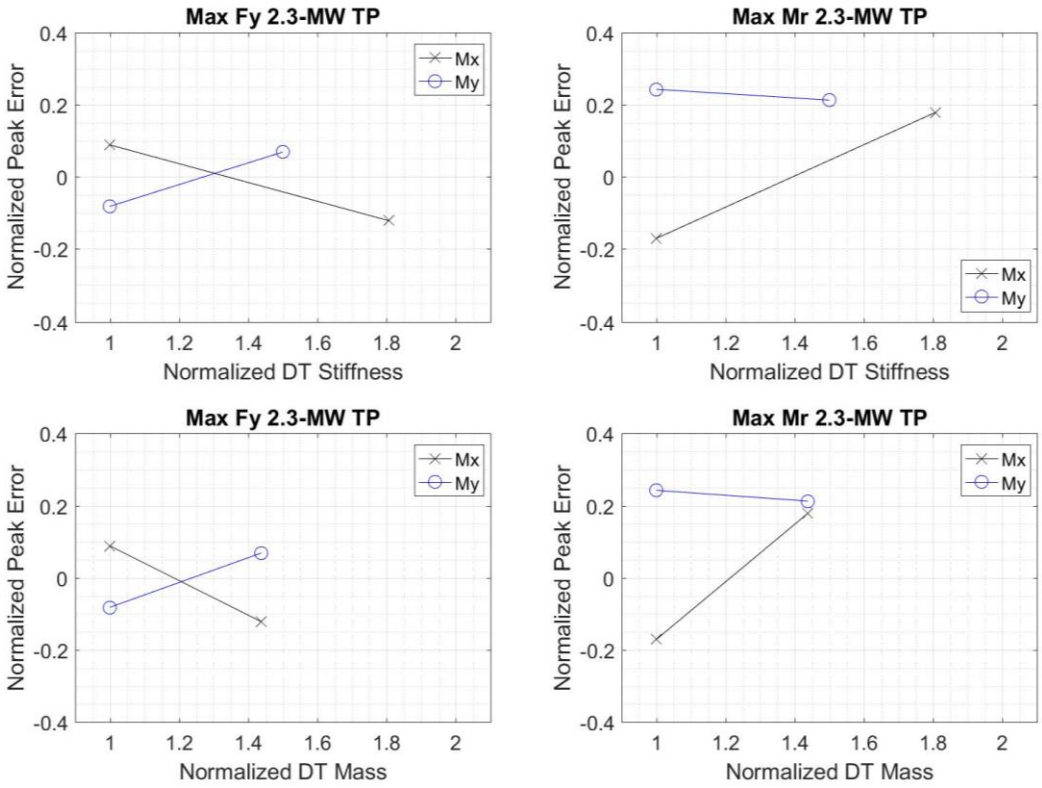

Figure 6.26: Peak error as a function of drivetrain (DT) stiffness (top row) and DT mass (lower row) for the yawing (Mx) and nodding (My) moments for the two test profiles (TP) tested with both drivetrains (OP normalization for the peak error).

The difference in controller gains tuning between the 2.3-MW and 3.2-MW drivetrains is a lurking variable in the results presented in Figs. 6.23-6.26 that prevents precise conclusions from being formulated. Nevertheless, the results presented in these Figures are the first quantification of the drivetrain effect on the tracking error of a test bench, and the effect is mostly small. Future investigation of the effect of the drivetrain on the tracking performance should be tied to the tuning of the test bench controller gains. Specifically, the tests performance with both drivetrains and the same test profiles should

have included the tuning of the test bench controller gains for each drivetrain for each test profile.

6.1.3.3 Reduced ramp rate limits

Figures 6.27 and 6.28 present the RMS error normalized with the measurement error as a function of the ramp rate limit for the yawing and nodding moments, respectively. There are 25 results in total corresponding to the five test profiles tested with five test bench ramp rate limits. These five test profiles span four types of test profiles giving a single opportunity for a subgroup. This subgroup and the corresponding number of data points are indicated in Table 6.6. The results for the subgroup are on the right of Figs. 6.27 and 6.28. Repeats of the same test profile were excluded in the sample count and only one result was used per combination of test profile and ramp rate limit. The measurement results presented in Figs. 6.27 and 6.28 are from tests conducted on the same day (Aug. 30). Note that the range of the y axis vary between the plots in Figs. 6.27 and 6.28, and the RMS errors are from comparing the measured LAU loads and speed with the targeted values (not the commanded values) as explained in Section 4.2.3.2.

Table 6.6: Description and number of samples for the data subgroups.

Subgroup (TP Type)	Description	# Data Points
All	All test profiles	25
SD	Test profiles in which the wind turbine controller triggers a shutdown due to a particular fault	15

Overall, the results presented in Figs 6.27 and 6.28 show similar trends than those from the 2.3-MW drivetrain test data.

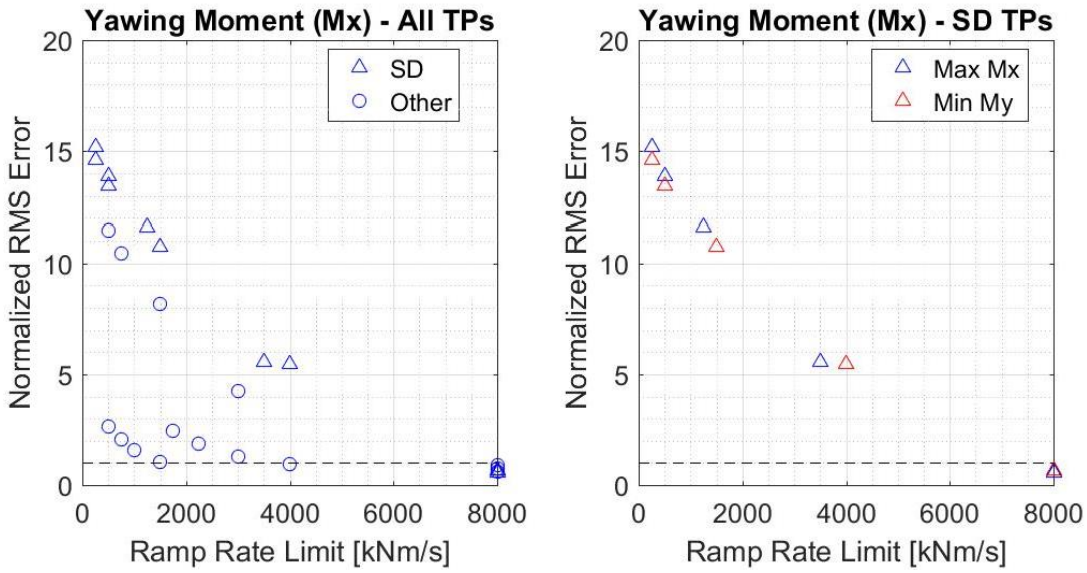

Figure 6.27: Normalized RMS error (E normalization) as a function of the ramp rate limit for the yawing moment for all tests and turbine shutdown (SD) subset.

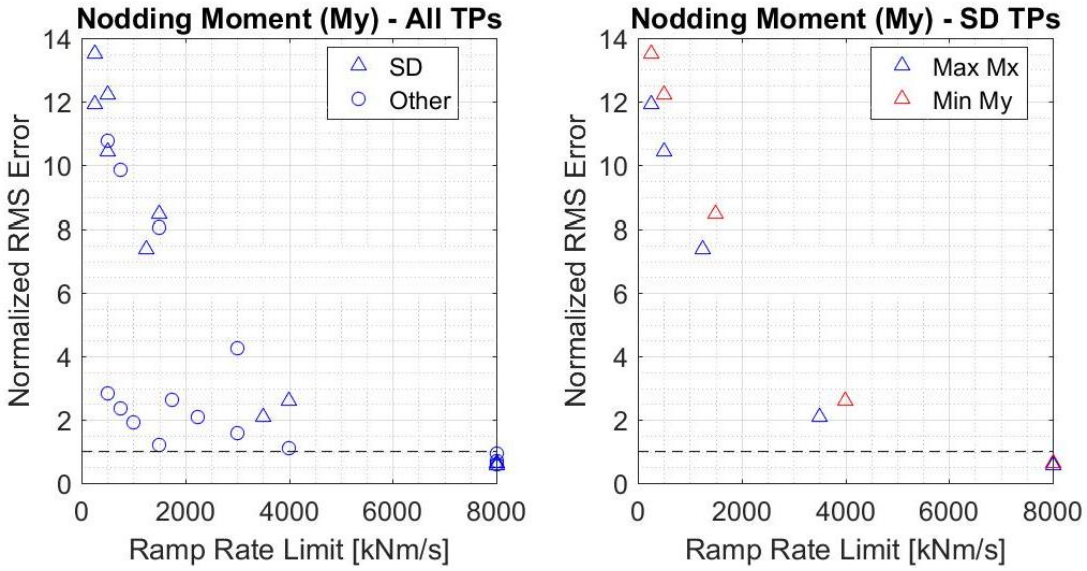

Figure 6.28: Normalized RMS error (E normalization) as a function of the ramp rate limit for the nodding moment for all tests and turbine shutdown (SD) subset.

Figures 6.29 and 6.30 present the time series of the reference test profile (max Fz) for all tested ramp rate limits for the yawing and nodding moments, respectively. The reference is the commanded moment for the nominal ramp rate limit of 8000 kNm/s. The time series and histograms are presented in decreasing order of the imposed ramp rate limit starting with the nominal value at the top. Note that the scale of all of the time series plots and histograms are the same to facilitate comparison and that scale does not capture the nominal ramp rate limit. The red vertical dotted lines in the histograms indicate the ramp rate limit and the reduction in ramp rate limit is clearly seen. The differences (errors) between the measurements and the reference in Figs. 6.29 and 6.30 are presented in Figs. 6.31 and 6.32 as time series on the left and histograms on the right. The largest error is approximately 55% and 80% of the peak value of the yawing and nodding moments, respectively. The growth in the error is clearly seen from the histograms in Figs. 6.31 and 6.32, and the tracking error is an accumulation of smoothly distributed (but non-normal) errors having a mean of nearly zero with growing tails with decreasing ramp rate limits.

The time series shown in Figs. 6.29 and 6.30 are presented in the frequency domain in Figs. 6.33 and 6.34. The frequency range is limited to 1 Hz, which captures more than 99% of the spectral energy in the signal. Figures 6.33 and 6.34 show that the differences in amplitude spectrum mainly occur at the largest frequencies with non-zero amplitudes as one would expect.

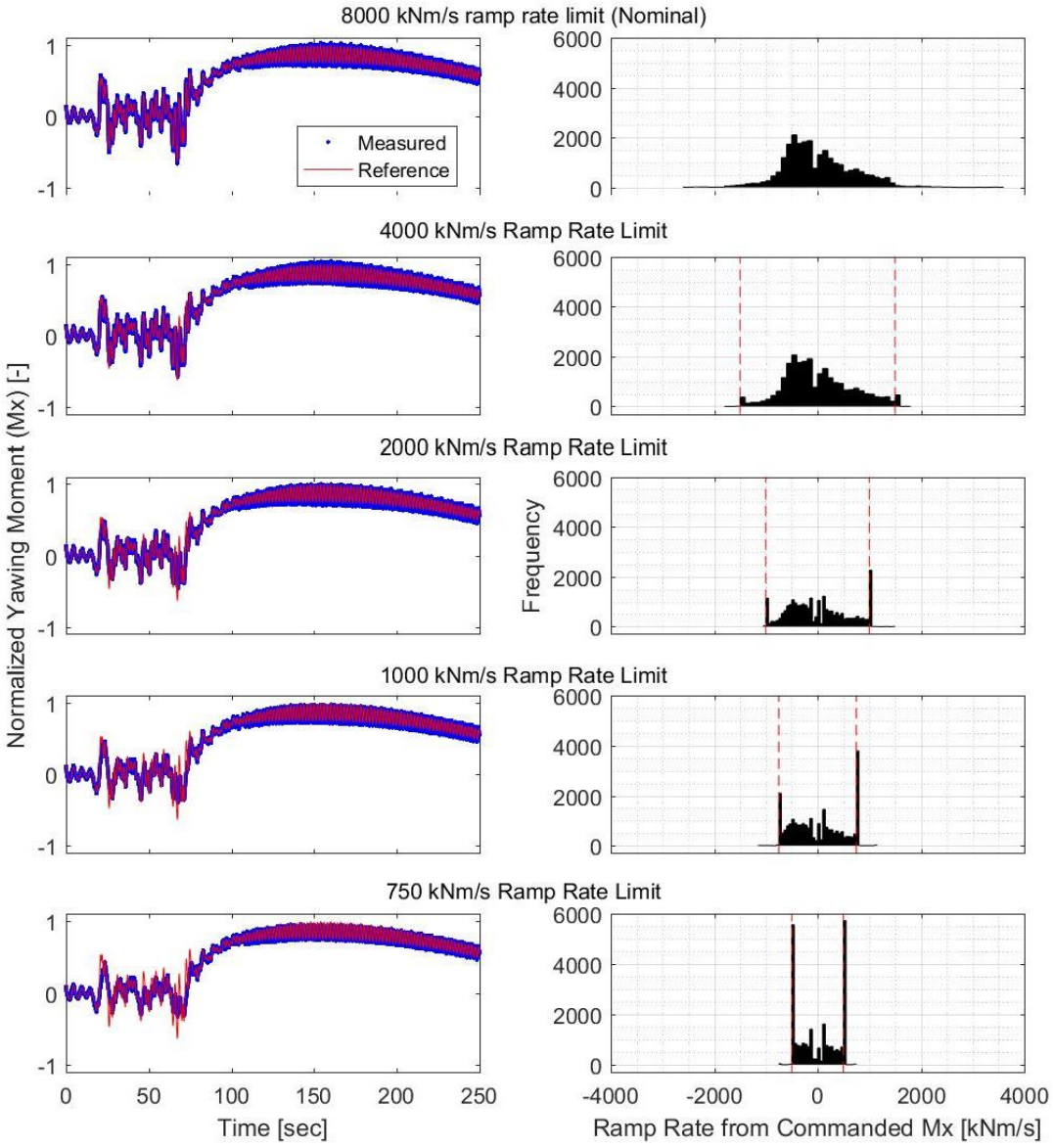

Figure 6.29: Time series of the measured yawing moment (Mx) of the reference (max Fz) test profile of the 3.2-MW drivetrain for all test bench ramp rate tested and histograms of the commanded ramp rate of Mx of each test. The P normalization was applied to Mx and the reference is the commanded test profile for the case of the nominal test bench limit. The vertical red lines in the histograms indicate the ramp rate limit imposed at each test.

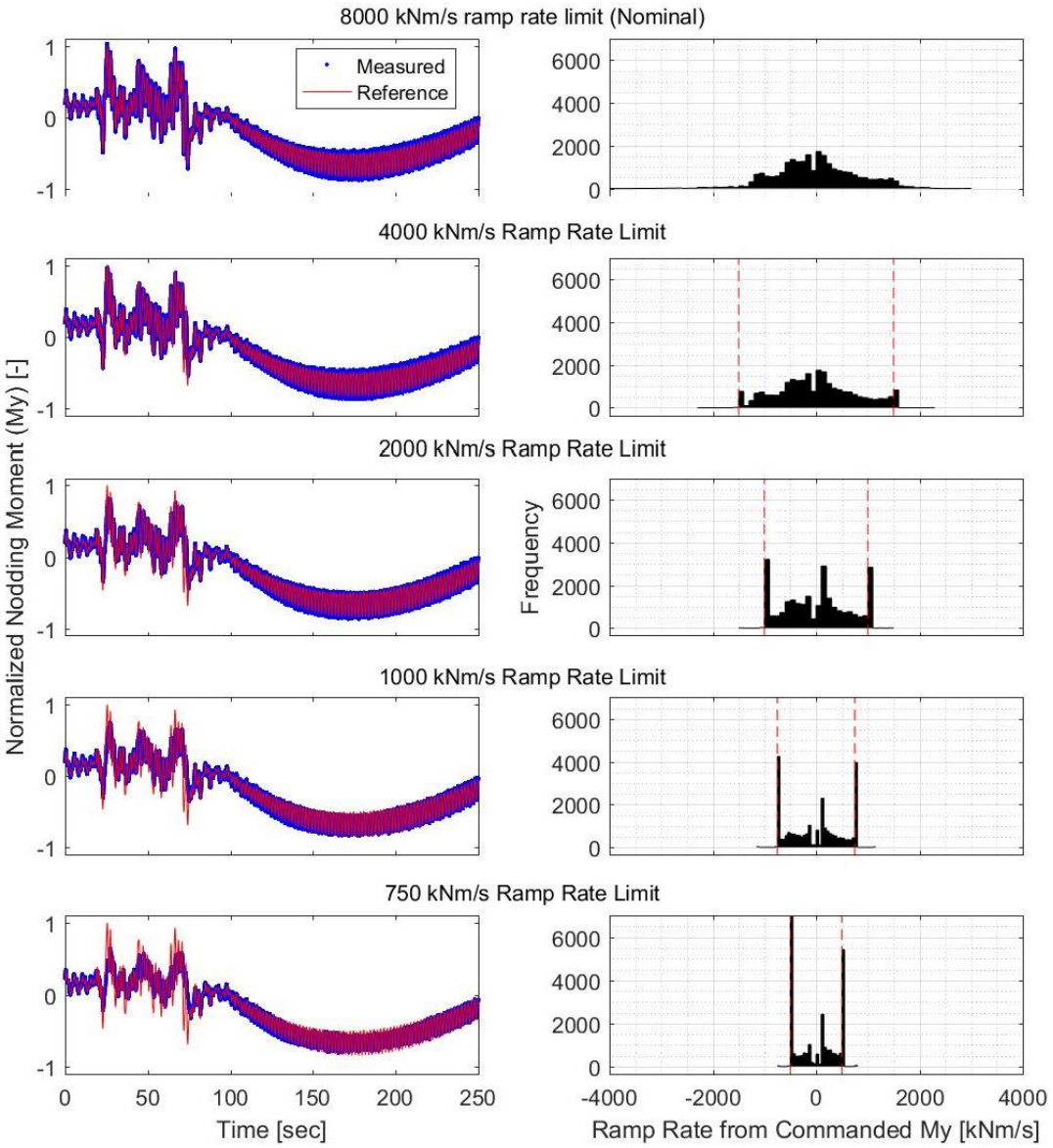

Figure 6.30: Time series of the measured nodding moment (My) of the reference (max Fz) test profile for all test bench ramp rate tested and histograms of the commanded ramp rate of My of each test. The P normalization is applied to Mx and the reference is the commanded test profile for the case of the nominal test bench limit. The vertical red lines in the histograms indicate the ramp rate limit imposed at each test.

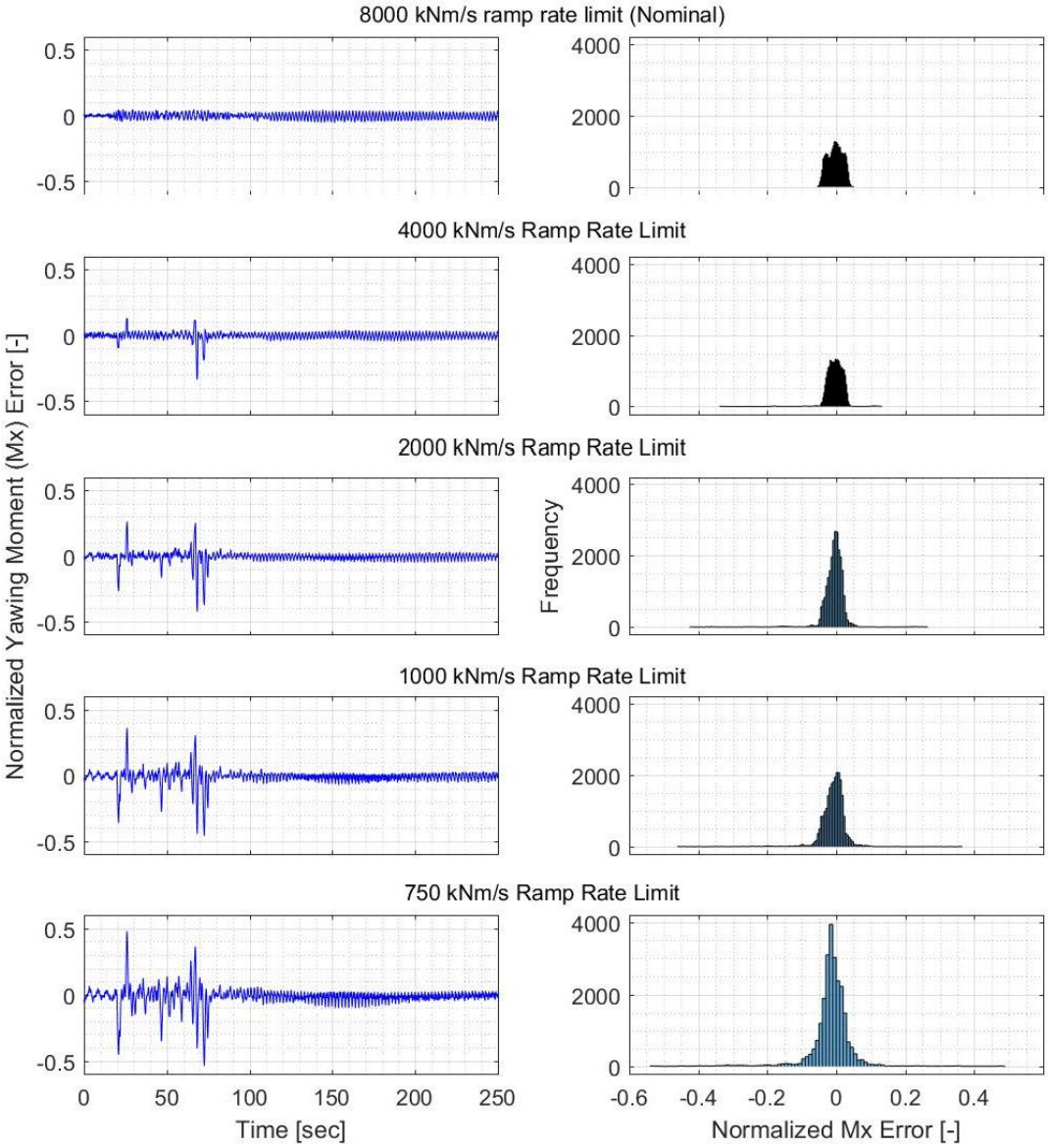

Figure 6.31: Time series and histograms of the error in yawing moment (Mx) between the measurements and reference from Fig. 6.29. The P normalization is applied to the Mx error.

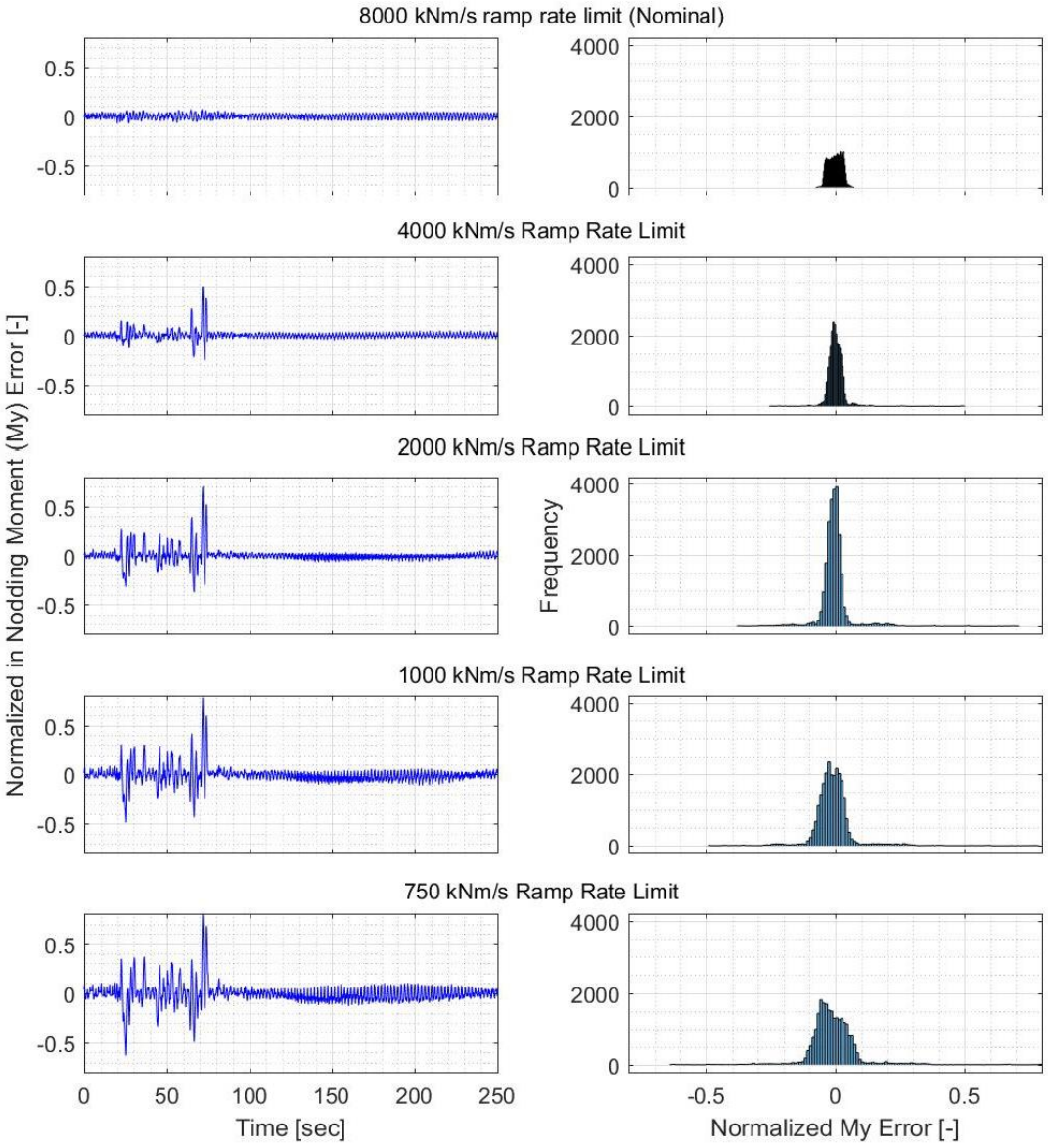

Figure 6.32: Time series and histograms of the error in nodding moment (My) between the measurements and reference from Fig. 6.30. The P normalization is applied to the My error.

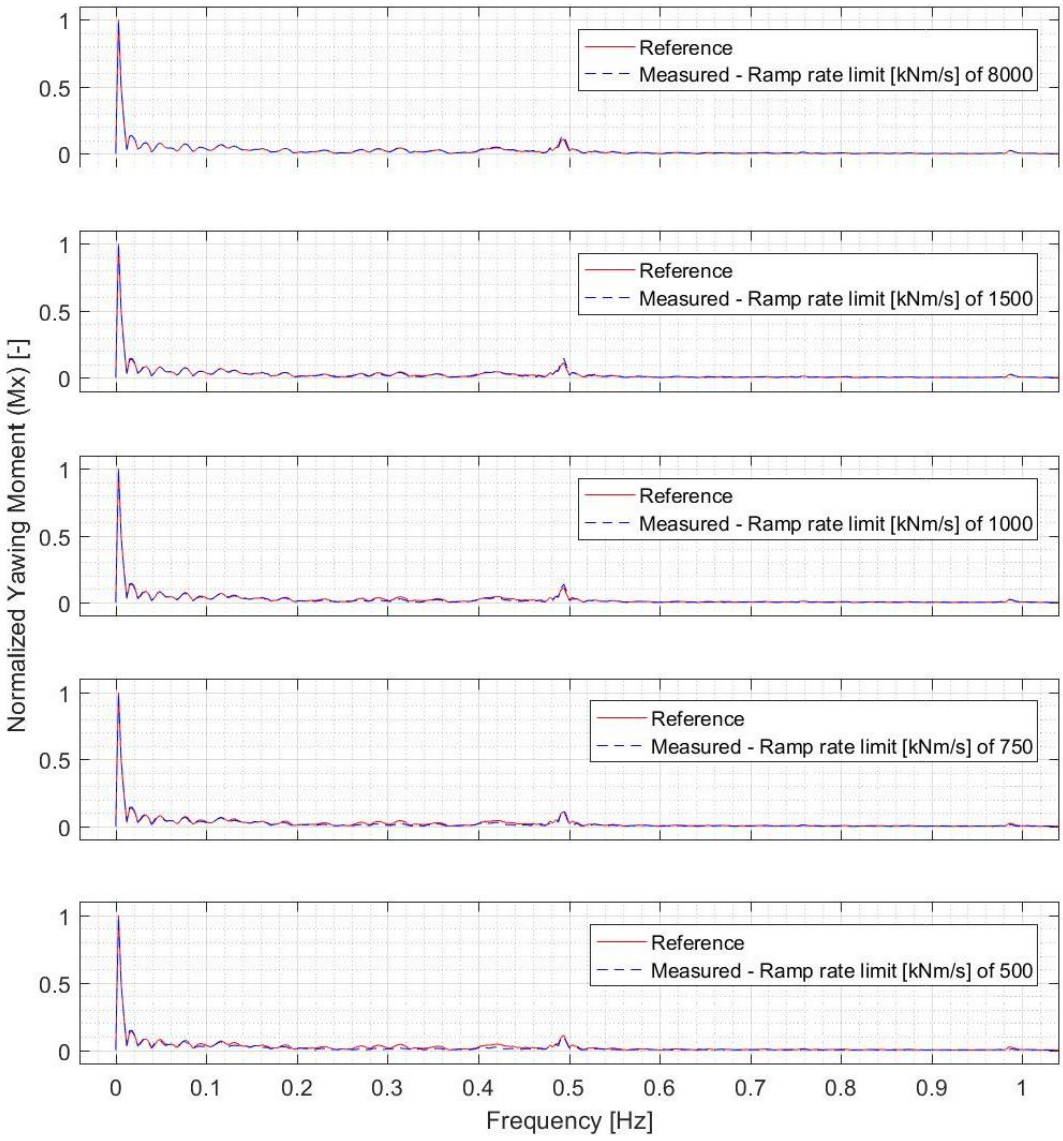

Figure 6.33: Frequency domain representation of the normalized yawing moment (Mx) of the reference test profile of the 3.2-MW drivetrain (max Fz) measured for the test bench ramp rate limits considered. The P normalization was applied to Mx and the reference is the commanded test profile for the case of the nominal test bench limit.

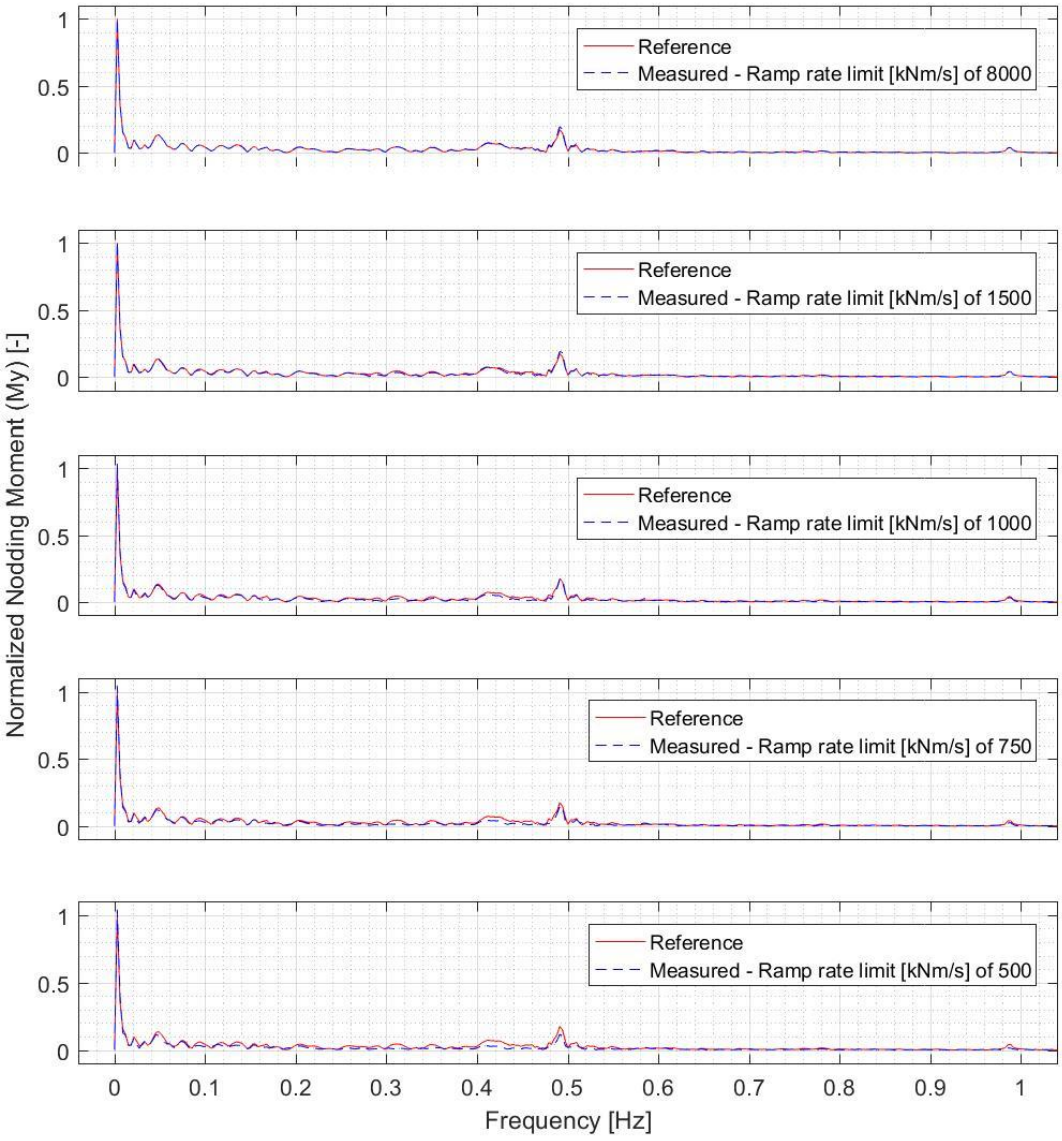

Figure 6.34: Frequency domain representation of the normalized nodding moment (My) of the reference test profile of the 3.2-MW drivetrain (max Fz) measured for the test bench ramp rate limits considered. The P normalization was applied to My and the reference is the commanded test profile for the case of the nominal test bench limit.

6.2 Comparison with predictions

Three sets of predictions are compared. First, the predictions from the evaluation metric to identify test profiles that should be replicated with an acceptable tracking error are compared with the measurements. Second, the predictive capability of single and multiple regression models based on the 2.3-MW drivetrain data are evaluated. Third, predictions from single and multiple regression models based on a data set combining the tests done with both drivetrains are compared with the test results.

6.2.1 Evaluation metrics

Figure 6.35 presents the measured and coverage RMS error for the 12 test profiles of the 3.2-MW drivetrain when tested with the nominal test bench limits. Results are only presented for the yawing and nodding moments due to the cross-coupling effect and the moments being much larger than the forces. The coverage RMS error is zero or essentially zero for all but one test profile (max Fr) and the measured RMS error is largest for this test profile. The other test profiles have an actual RMS error that is mostly within the measurement error but there are exceptions. Within the exceptions, the largest actual RMS error is 30% greater than the measurement error (max Mr). Overall, the test profiles having an RMS error of zero have an actual RMS error in the range of 60% to just over 100% of the measurement error for the yawing moment (Mx) and the range is 70% to 130% for the nodding moment (My). Using the measurement error as threshold of acceptance, the coverage RMS error correctly identified that all but one test profile would be subject only to tracking error due to the test bench controller for the yawing moment and 8 out of 12 test profiles for the nodding moment.

The measurements presented in Section 6.1.3.2 are compared with the evaluation metrics of test bench coverage, coverage RMS error, and capability ratio. The comparison is limited to the yawing and nodding moments.

Figure 6.36 presents the RMS error for the yawing and nodding moments with the coverage RMS error for the nominal test bench limits. The coverage RMS error is zero for the yawing moment for all test profiles and zero or nearly zero for the yawing moment. The variation in the RMS error from the measurements is not captured by the coverage RMS error.

For test profiles having commanded LAU inputs within the test bench capability, which is the case for all test profiles tested with the 2.3-MW drivetrain and the nominal test bench limits, the test-bench hardware limitation error is not contributing to the total error. Accordingly, the RMS errors presented in Fig. 4.30 reflect test-bench controller error. Such controller error is unavoidable, especially with dynamic input test profiles, and the test bench operator aims to minimize the controller error. The metrics of test bench coverage, coverage RMS error, and capability ratio consider only the test-bench hardware limitation error. Furthermore, these metrics aim to predict if a test bench can replicate a test profile with an acceptable level of tracking error. Predicting the actual RMS error goes beyond that target and the measurements made with reduced ramp rate limits allows the evaluation of the method towards that end.

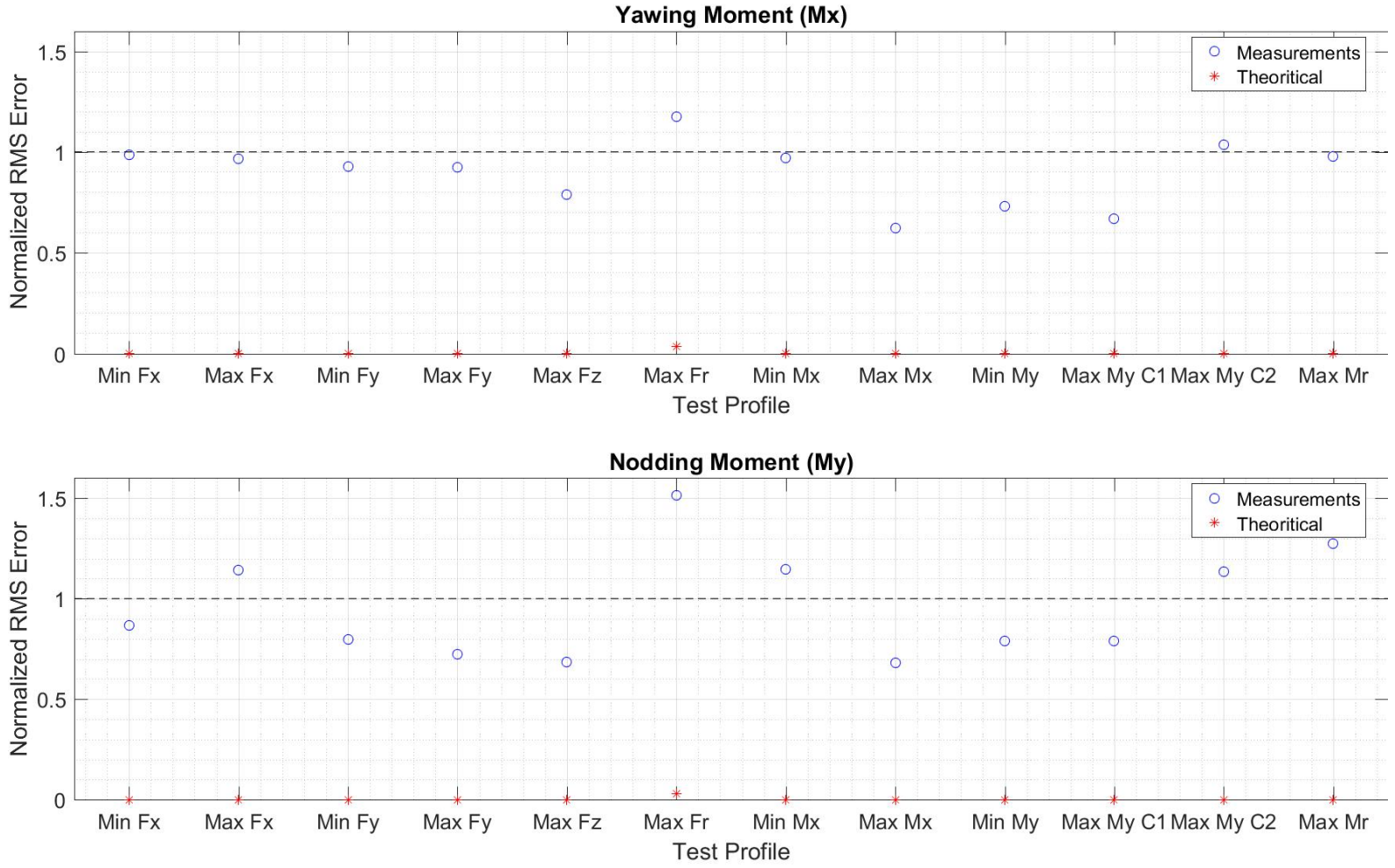

Figure 6.35: Normalized RMS error (E normalization) for the yawing (Mx) and nodding (My) moments from measurements and coverage values for all test profiles.

Figures 6.36 and 6.37 present the RMS error for all test profiles as a function of the four evaluation metrics: test bench coverage, coverage RMS error, magnitude capability ratio, and ramp rate capability ratio. The observations made from the results with the 2.3-MW drivetrain apply to the results of the 3.2-MW drivetrain as well.

- The test bench theoretical RMS is the best predictor of the actual RMS error with a linear relationship.
- The test bench coverage RMS error exceeds the actual RMS error for the highest RMS error levels.
- The trend between the test bench coverage and the actual RMS error subdivides the data into two main populations, and there is no clear value of coverage corresponding to an acceptable level of tracking error.
- The test bench capability ratio for magnitude does not capture the actual RMS error due to the values of this metric being much greater than one. Accordingly, conclusions on the ability of the predictive capability of the capability ratio are to be drawn from the ramp rate.
- Similarly to the test bench coverage, the trend of test bench capability ratio for ramp rate and the actual RMS error shows two main populations and there is no clear value of capability ratio corresponding to an acceptable level of tracking error.

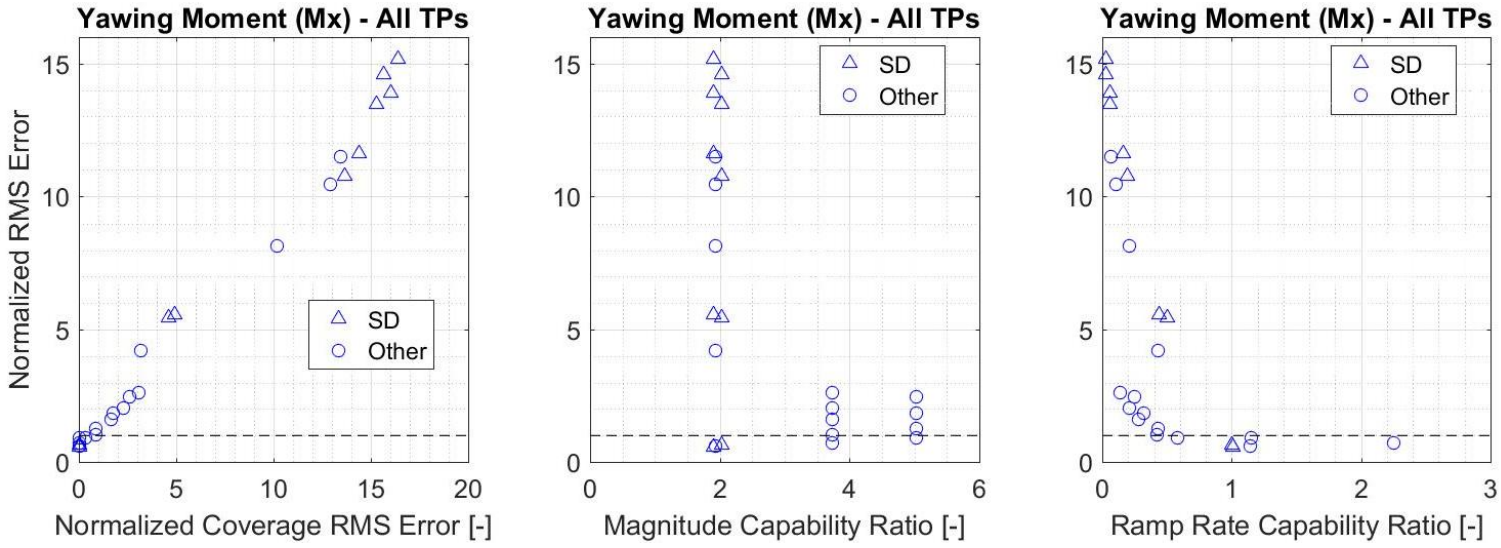

Figure 6.36: Normalized RMS error (E normalization) as a function of the evaluation metrics of test bench coverage, coverage RMS error, magnitude capability ratio, ramp rate capability ratio for the yawing moment for all tests (upper left plot) and the subgroup for extreme events causing the turbine to shut down (SD, right).

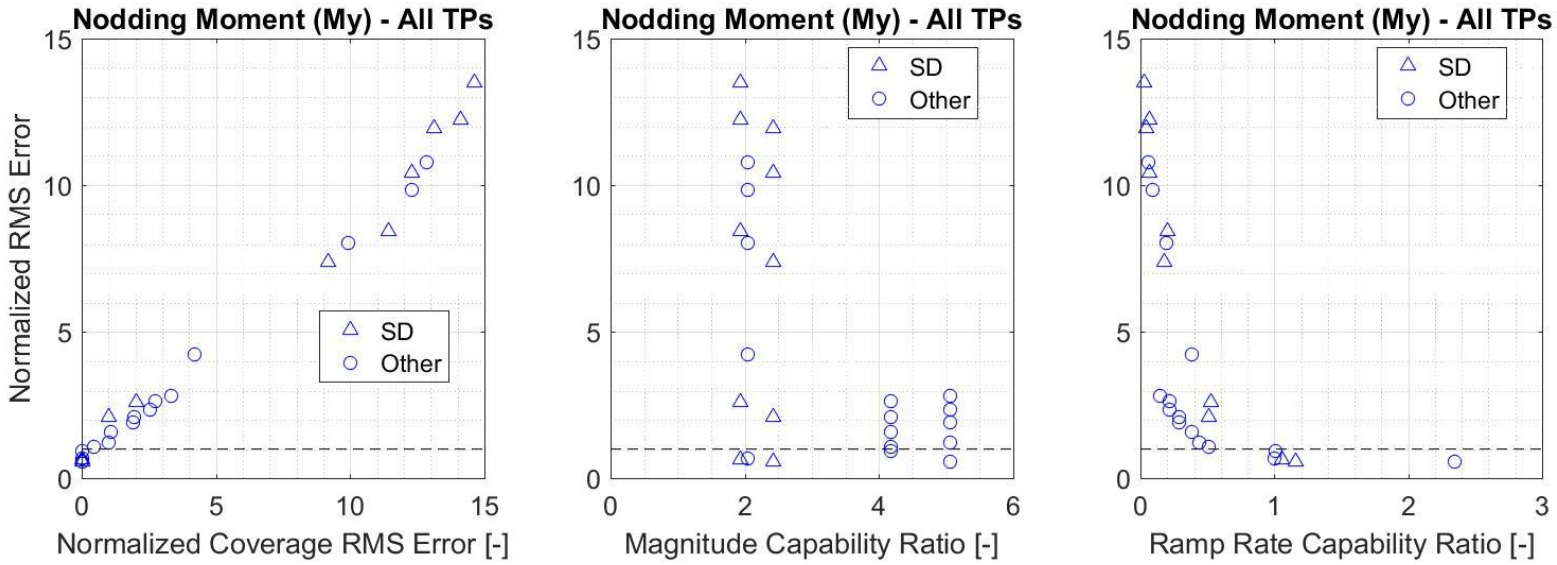

Figure 6.37: Normalized RMS error (E normalization) as a function of the evaluation metrics of test bench coverage, coverage RMS error, magnitude capability ratio, ramp rate capability ratio for the nodding moment for all tests (upper left plot) and the subgroup for extreme events causing the turbine to shut down (SD, right).

The above observations also apply to the results for the SD subgroup as indicated in Figs. 6.38-6.41. These figures are the same as Figs. 6.27 and 6.28 replacing the ramp rate limits with the evaluation metrics. The capability ratio for magnitude is excluded due to the test bench having capability for magnitude that exceeds the commanded magnitude of the yawing and nodding moments by at least a factor of 1.8. Overall, the subgrouping yields clearer trends between the coverage and capability ratio metrics and the actual RMS error. Also, the crossing of the actual RMS error above unity is for a ramp rate capability ratio below one. Both of these observations apply to those made with the measurements made with the 2.3-MW drivetrain.

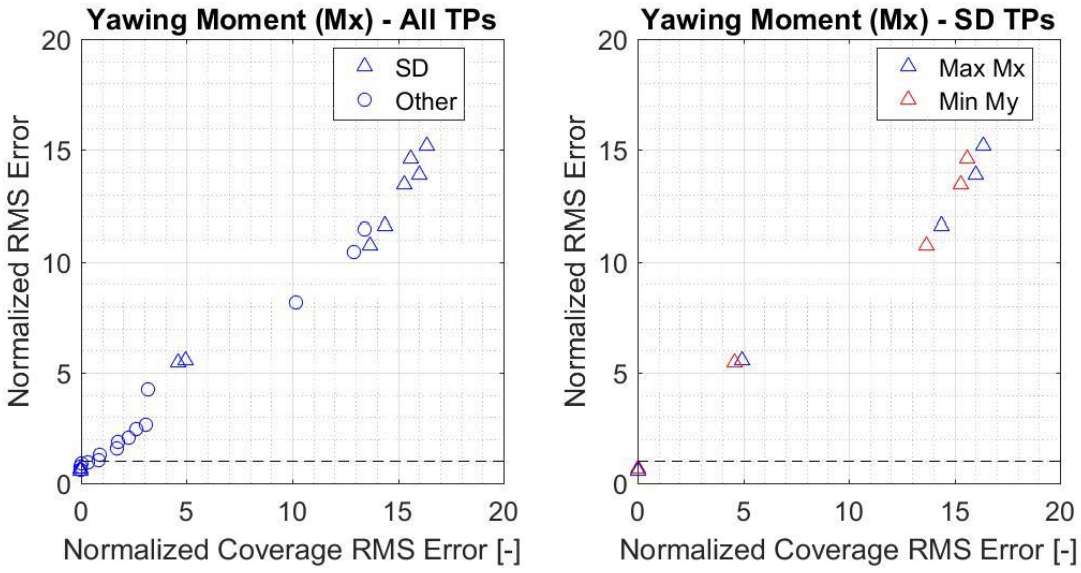

Figure 6.38: Normalized RMS error (E normalization) as a function of the coverage RMS error for the yawing moment for all tests (upper left plot) and the subgroup for extreme events causing the turbine to shut down (SD).

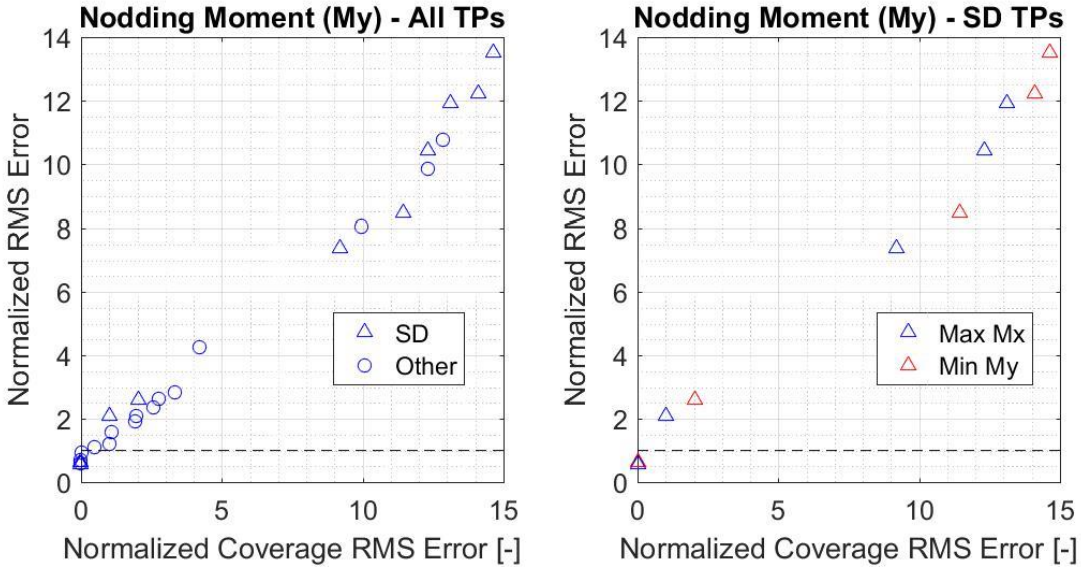

Figure 6.39: Normalized RMS error (E normalization) as a function of the coverage RMS error for the nodding moment for all tests (upper left plot) and the subgroup for extreme events causing the turbine to shut down (SD).

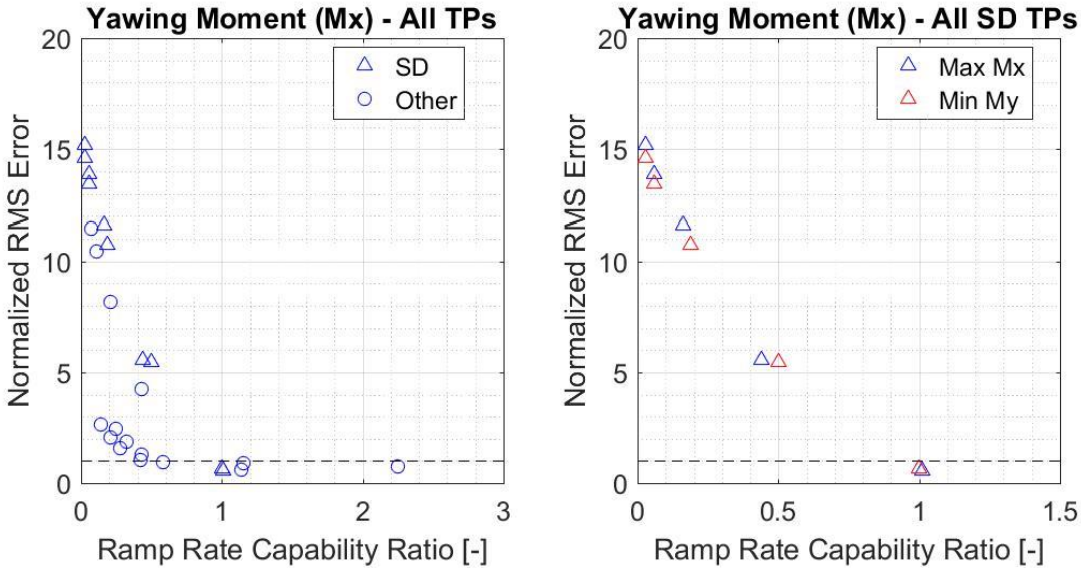

Figure 6.40: Normalized RMS error (E normalization) as a function of the test bench ramp rate capability ratio for the yawing moment for all tests (upper left plot) and the subgroup for extreme events causing the turbine to shut down (SD).

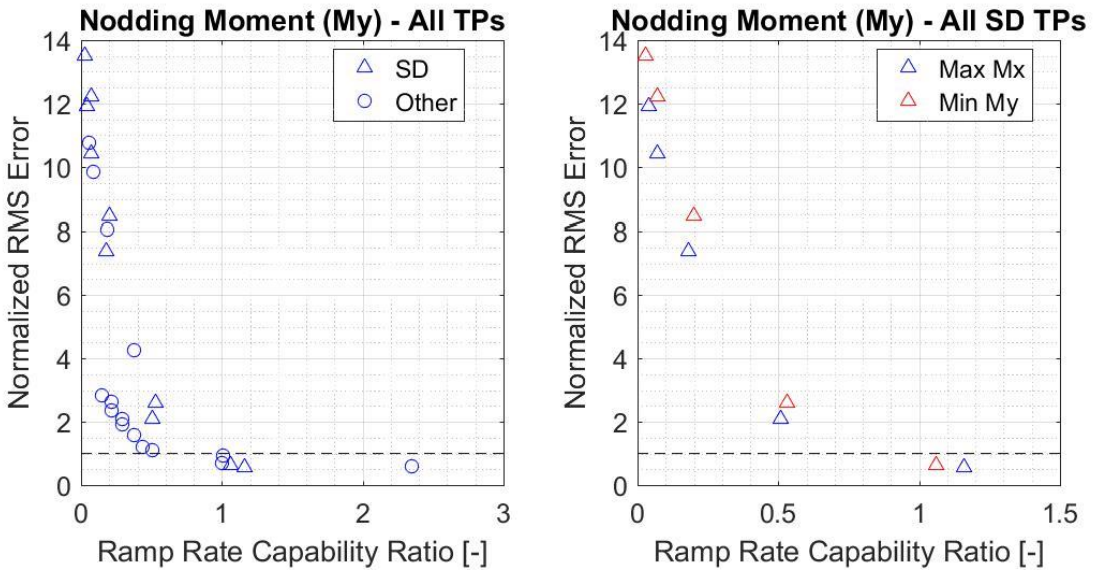

Figure 6.41: Normalized RMS error (E normalization) as a function of the test bench ramp rate capability ratio for the nodding moment for all tests (upper left plot) and the subgroup for extreme events causing the turbine to shut down (SD).

To further demonstrate that large values of capability ratio for magnitude do not improve the predictive capability of the RMS error, Figs. 6.42 and 6.43 present scatter plots of the RMS error as a function of both magnitude and ramp rate capability ratios with the size of the symbols reflecting the magnitude of the RMS error. These figures use the same subgroupings of the test profiles used in Figs. 6.38-6.43. The results from both figures indicate that the RMS error increases with decreasing capability ratio for the ramp rate until a certain value of that metric at which point the RMS error remains relatively constant. The level of increase depends on the type of test profiles with those from the NR subgroup showing essentially no variation in RMS error with decreasing capability ratio for ramp rate.

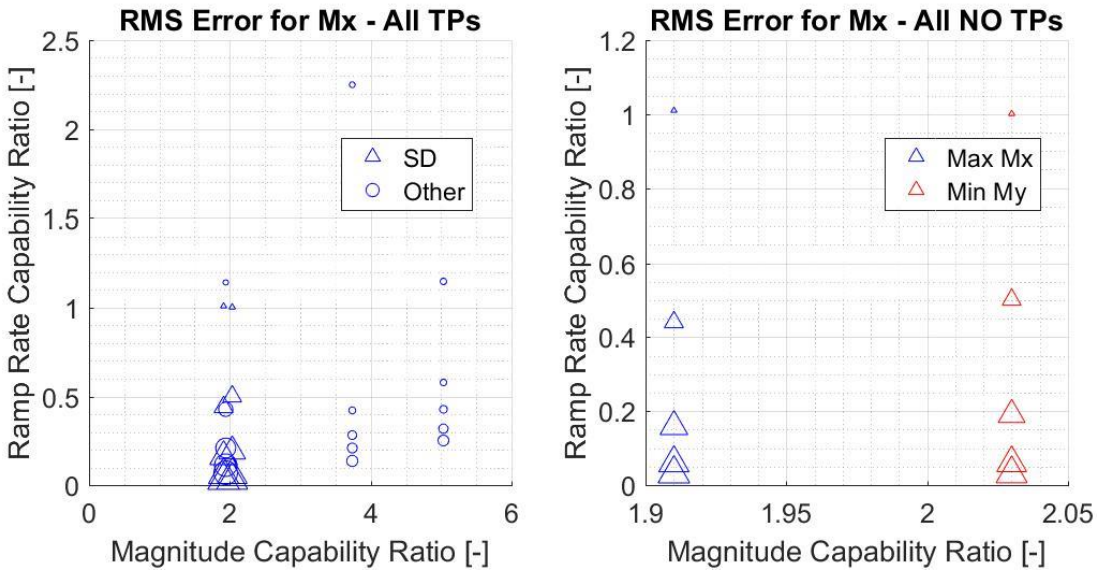

Figure 6.42: Normalized RMS error (E normalization) as a function of the test bench capability ratio for magnitude and ramp rate for the nodding moment for all tests (upper left plot) and the subgroup for extreme events causing the turbine to shut down (SD).

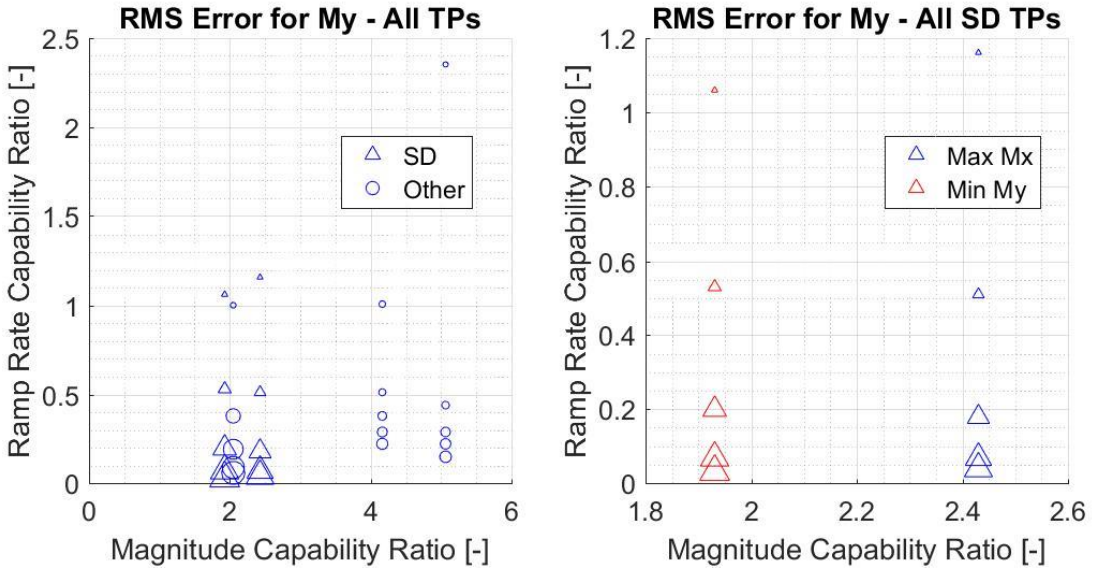

Figure 6.43: Normalized RMS error (E normalization) as a function of the test bench capability ratio for magnitude and ramp rate for the nodding moment for all tests (upper left plot) and the subgroup for extreme events causing the turbine to shut down (SD).

6.2.2 Predictive models from the 2.3-MW test data

The single regression and multiple regressions models presented in Section 4.5.1 were used to predict the RMS error with a total of 41 tests that have been conducted with the 3.2-MW drivetrain. The predictions are presented vs. the measurements in Fig. 6.44 and histograms of the prediction errors are shown in Fig. 6.45.

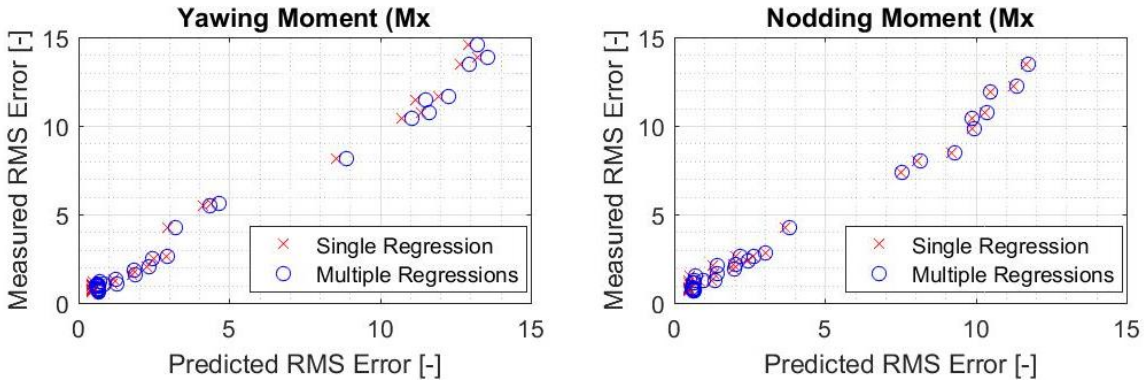

Figure 6.44: Predicted vs. measured RMS error for the yawing moment (Mx) and nodding moment (My) for the 3.2-MW drivetrain test profiles including test with reduced ramp rate limits. The RMS error are normalized with the measurement error (E normalization).

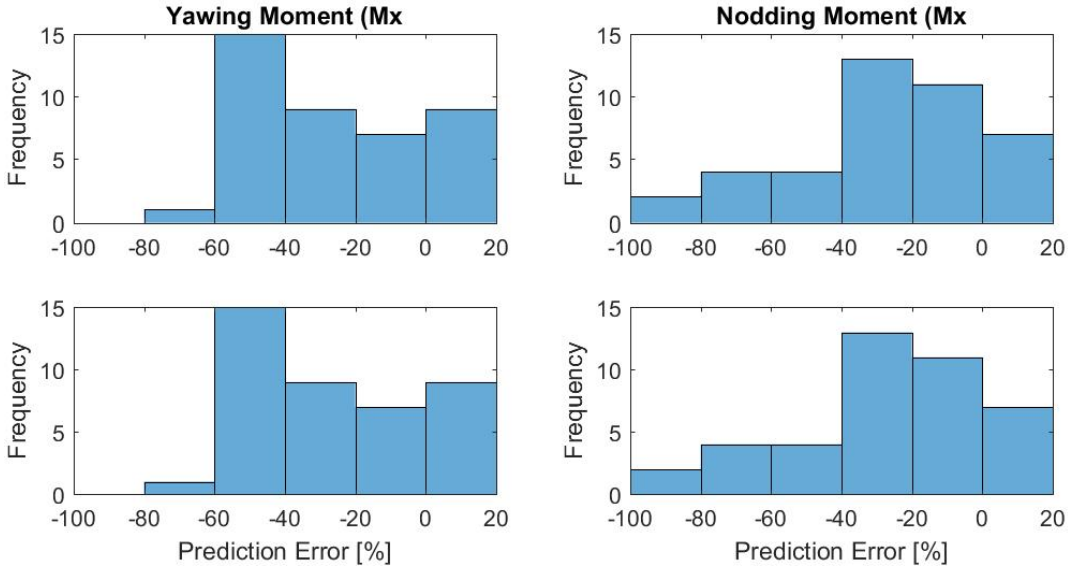

Figure 6.45: Histograms of the prediction errors with the measurements for the RMS error of the yawing moment (Mx) and nodding moment (My) for the 3.2-MW drivetrain test profiles including test with reduced ramp rate limits.

These results show that the good correlations do not result in accurate predictions of the RMS error. The models under predict the measurement error with the multiple regression models having an average error that is approximatively half that of the single regression models. Given the good correlations between the predictions and measurements, an adjustment to the offset would likely improve the accuracy of the predictions. In that respect, the results from the test profiles tested on both drivetrains pointed to a small effect of the drivetrain that does not explain the prediction errors. The tuning of the test bench controller gains is likely a lurking variable in the predictions. Given that the tuning was not tailored for each test profile due to the constraint of using the same gains for all tests with a given drivetrain, the tuning is thus more optimum for some test profiles than others. Nevertheless, the addition of an offset would reduce the prediction error and this offset could be based on one or more characteristics of the test profiles. The focus of this research being on correlating the tracking error with the evaluation metrics, which suffice to determine test profiles that should be replicated with acceptable accuracy, the improvement of the predictive capability of the actual RMS error can build on this research.

6.3 Data analysis

The correlation coefficients between the actual RMS errors for the four evaluation metrics are presented in Fig. 6.46. Results are co-plotted for the yawing and nodding moments and these results are presented for all data together and the SD subgroup. The green and red dotted lines reflect very high and negligible levels of correlation.

The same observations stated in Section 4.3 for the correlation coefficients of the 2.3-MW drivetrain apply to the results presented in Fig. 6.46. The coverage RMS error

continues to provide the best correlation irrespective of the data subgroup and the correlation for the coverage and ramp rate capability improves with the subgrouping. The correlation coefficients presented in 6.46 are sufficiently high to pursue regression analyses. Results from single and multiple regressions are presented in separate sections.

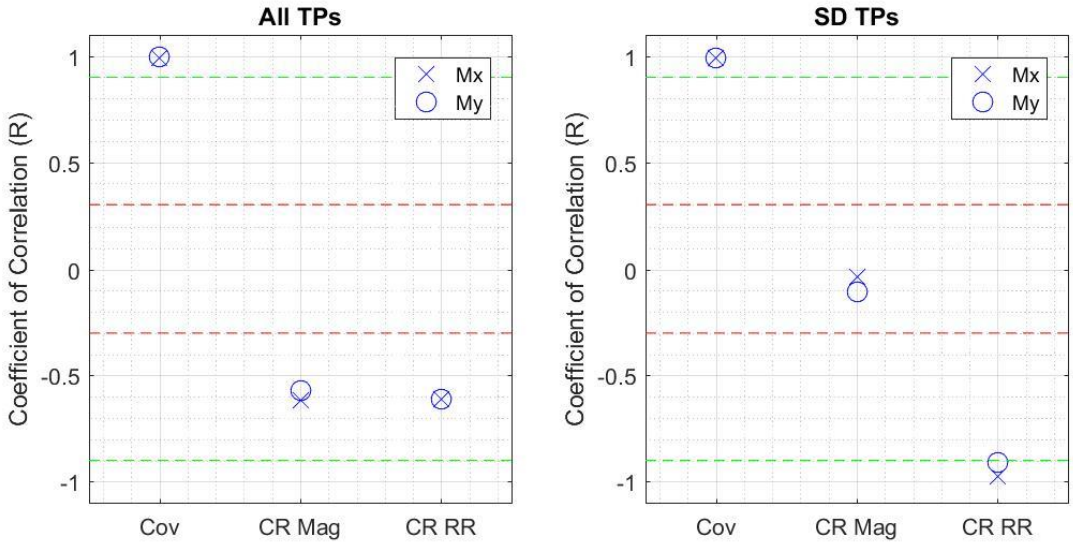

Figure 6.46: Correlation coefficient of the three evaluation metrics for the yawing moment (Mx) and nodding moment (My). All test profiles are considered for the results on the left and those of the right are for the shutdown (SD) subgroup The green and red dotted lines represent the threshold for very high and negligible correlation.

6.3.1 Single regressions

Table 6.7 presents the results from the single regressions obtained with the JMP software for the case of all data grouped together and the SD subgroup using non-linear models to fit the data. Refer to Section 4.3.1 for a description of the approach and selection threshold used for the regression analyses.

Table 6.7: Summary of single regression results for each evaluation metric and data subgroup. The background color reflects the R^2 value with green and yellow used to reflect the range above and below 0.9, respectively.

Subgroup	Yawing Moment (Mx)						Nodding Moment (My)					
	Cov RMS Error		CR Mag		CR RR		Cov RMS Error		CR Mag		CR RR	
	Fit	Adj R^2	Fit	Adj R^2	Fit	Adj R^2	Fit	Adj R^2	Fit	Adj R^2	Fit	Adj R^2
All	Linear	0.985	None	NA	Exp 2P	0.768	Linear	0.987	None	NA	Exp 2P	0.853
SD	Linear	0.976	None	NA	Exp 2P	0.968	Linear	0.980	None	NA	Exp 2P	0.976

The observations from the single regressions results using the measurements with the 2.3-MW drivetrain mostly applies to the 3.2-MW drivetrain measurements. The coverage RMS error provides the best regressions without the need of a non-linear regression, and the subgrouping of the measurements yields better regressions for the ramp rate capability ratio. There is consistency in the mathematical function that best fit the data between the yawing and nodding moments.

6.3.2 Multiple regressions

A total of four multiple regressions were performed to cover the two data groups and both moments (Mx and My). The same approach used for the 2.3-MW data was used for the 3.2-MW measurements. Refer to Section 4.3.2 for a description of the approach. Table 6.8 and Fig. 6.47 present the outcome of the multiple regressions. The significant terms of the multiple regressions are indicated in Table 6.9. Figure 6.47 also includes the adjusted R^2 for the single (linear) regression for the coverage RMS error, which is used as baseline.

Table 6.8: Summary of the significant (S) and non-significant (NS) main effects and interactions from the multiple regressions.

	Yawing Moment (Mx)						
Subgroup	**Main Effects**			**Interactions**			
	Cov (1)	CR Mag (2)	CR RR (3)	1&2	1&3	2&3	1&2&3
All	S	NS	NS	NS	NS	NS	NS
SD	S	NS	S	NS	S	NS	NS
	Nodding Moment (My)						
Subgroup	**Main Effects**			**Interactions**			
	Cov (1)	CR Mag (2)	CR RR (3)	1&2	1&3	2&3	1&2&3
All	S	S	S	NS	S	S	NS
SD	S	NS	S	NS	S	NS	NS

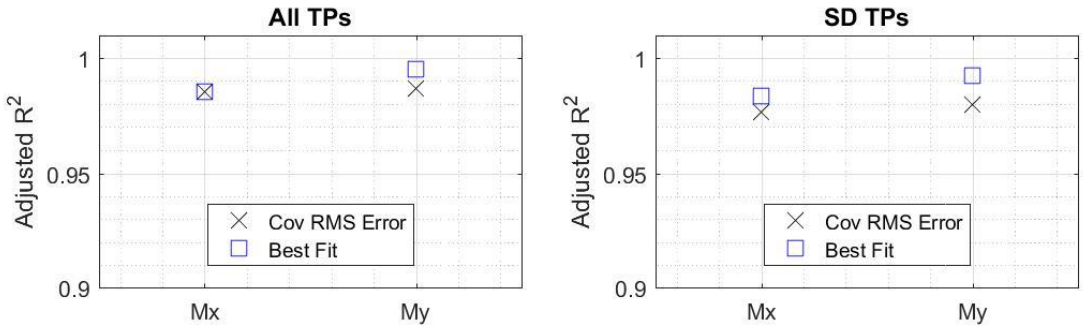

Figure 6.47: Comparison of the adjusted R^2 of the single regression model based on the coverage RMS error and the multiple regression models for the yawing moment (Mx) and nodding moment (My). All test profiles are considered for the results on the left and those of the right are for the shutdown (SD) subgroup.

The only significant term for the case of the yawing moment and considering all data is the coverage RMS error, and thus no improvement in from the multiple regression in that case. Overall, all improvements over the single regression results with the coverage RMS error are approximatively 1% in adjusted R^2.

The observations from the results presented in Table 6.8 and Fig. 6.47 are similar to those from the 2.3-MW drivetrain measurements. The improvement in the adjusted R^2 is marginal and only the interaction between the coverage RMS error and the capability ratio for ramp rate was found to be significant more than once.

6.4 Correlation of tracking error with test profile characteristics

The results presented for the 2.3-MW drivetrain included the correlation of actual RMS error with test profile characteristics such as the standard deviation of the magnitude and ramp rate of the loads and speed. Figures 6.48-6.51 present results from the same analyses using the test profiles and measurements of the 3.2-MW drivetrain.

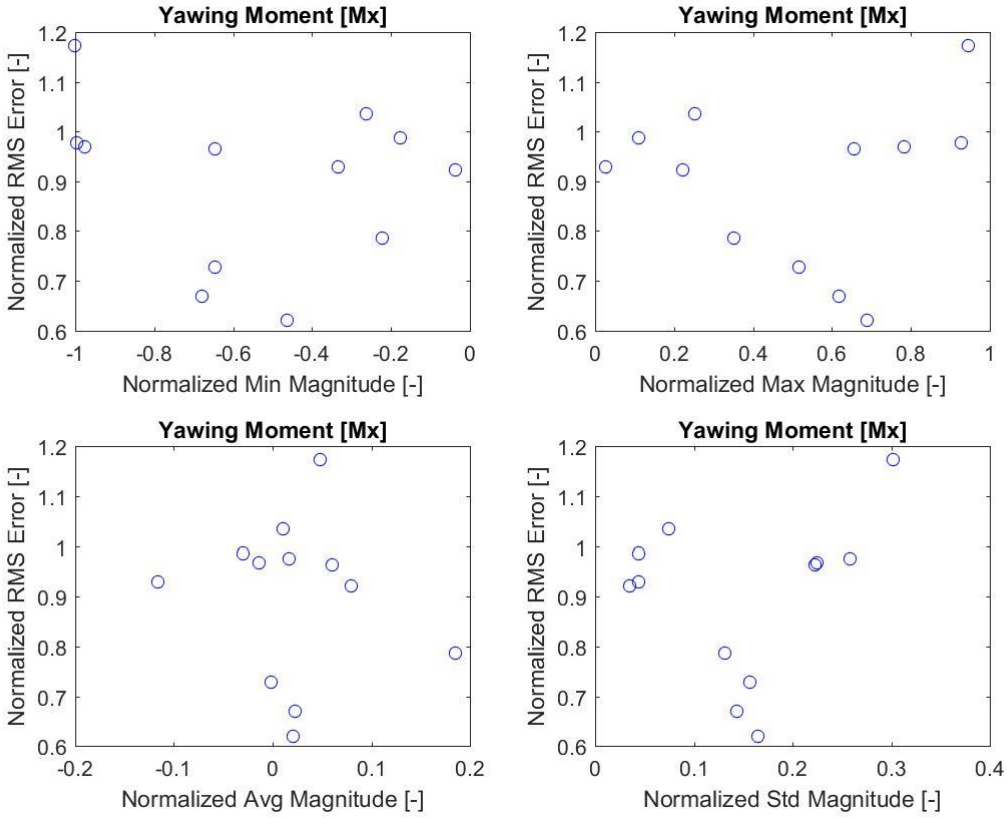

Figure 6.48: Actual RMS error (E normalization) as a function of the normalized minimum (Min), maximum (Max), average (Avg), and standard deviation (Std) of the magnitude of the yawing moment (Mx). The normalization of the RMS error is with the measurement error (E normalization) and Mx is normalized with the maximum peak value from all test profiles.

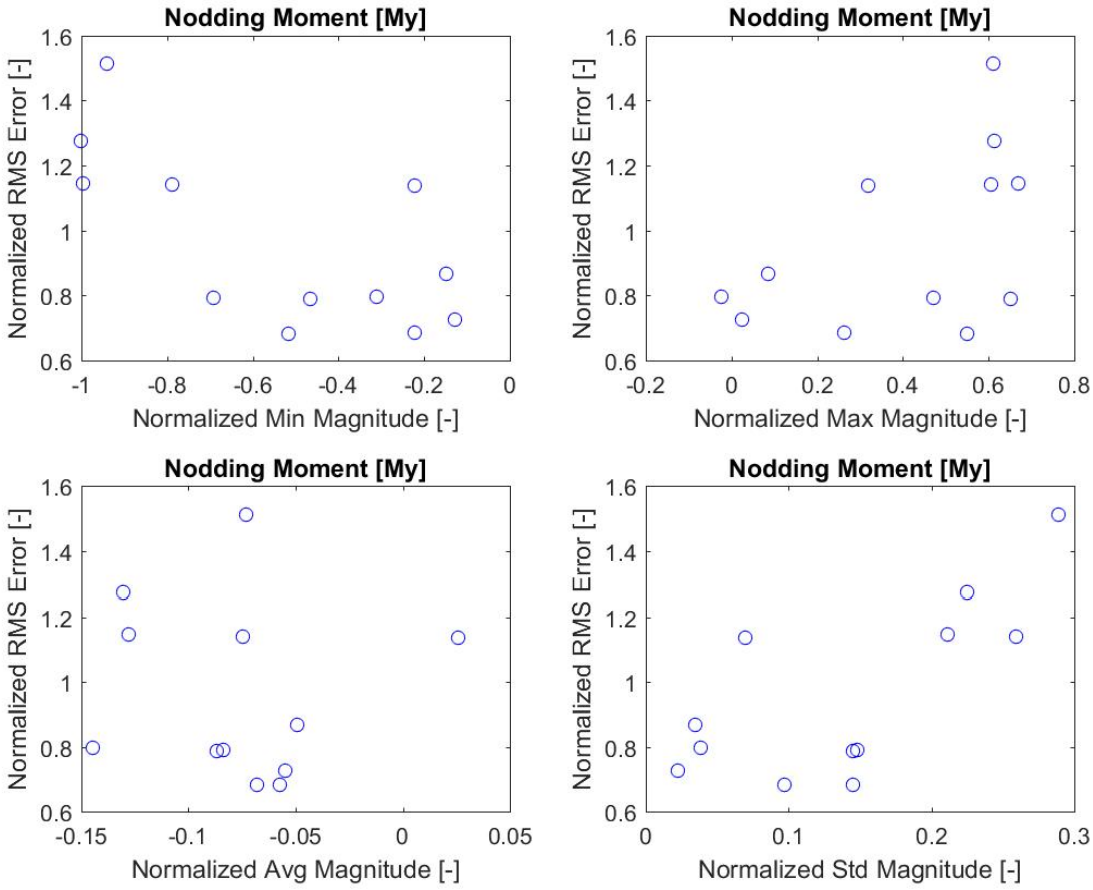

Figure 6.49: Actual RMS error (E normalization) as a function of the normalized minimum (Min), maximum (Max), average (Avg), and standard deviation (Std) of the magnitude of the nodding moment (My). The normalization of the RMS error is with the measurement error (E normalization) and My is normalized with the maximum peak value from all test profiles.

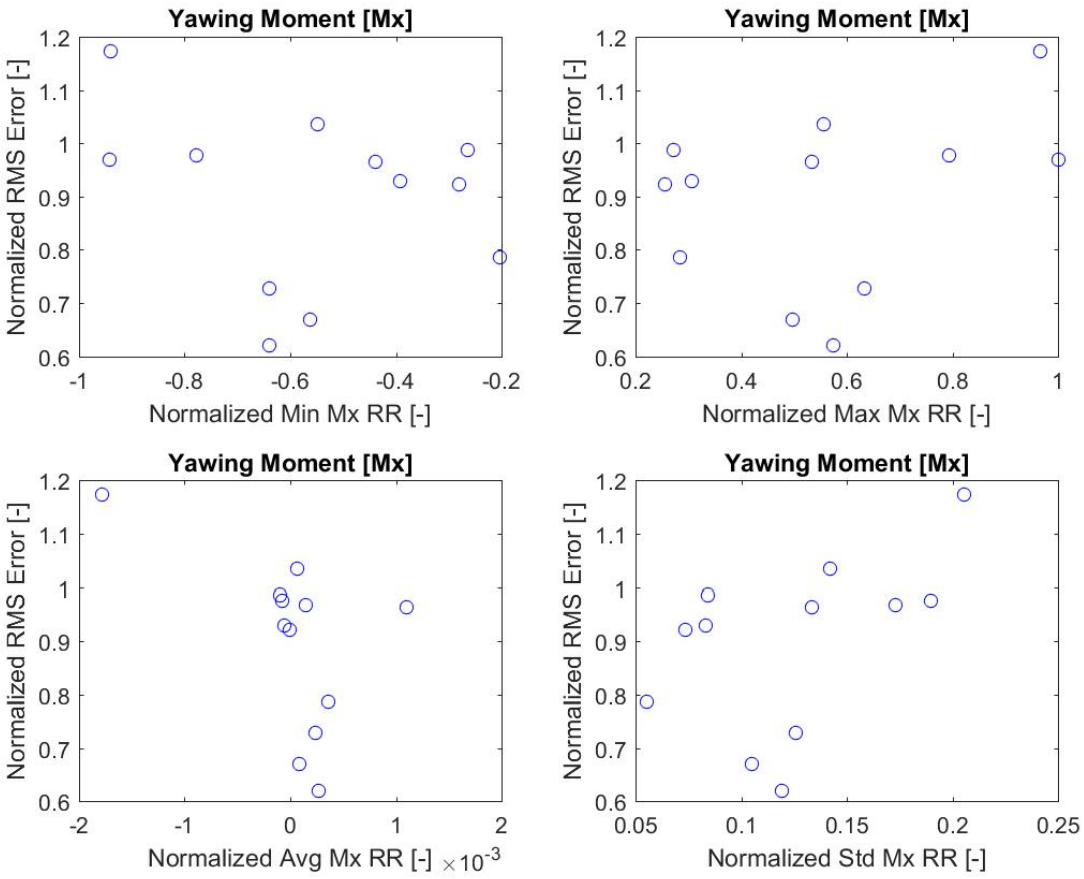

Figure 6.50: Actual RMS error (E normalization) as a function of the normalized minimum (Min), maximum (Max), average (Avg), and standard deviation (Std) of the ramp rate of the yawing moment (Mx). The normalization of the RMS error is with the measurement error (E normalization) and Mx is normalized with the maximum peak value from all test profiles.

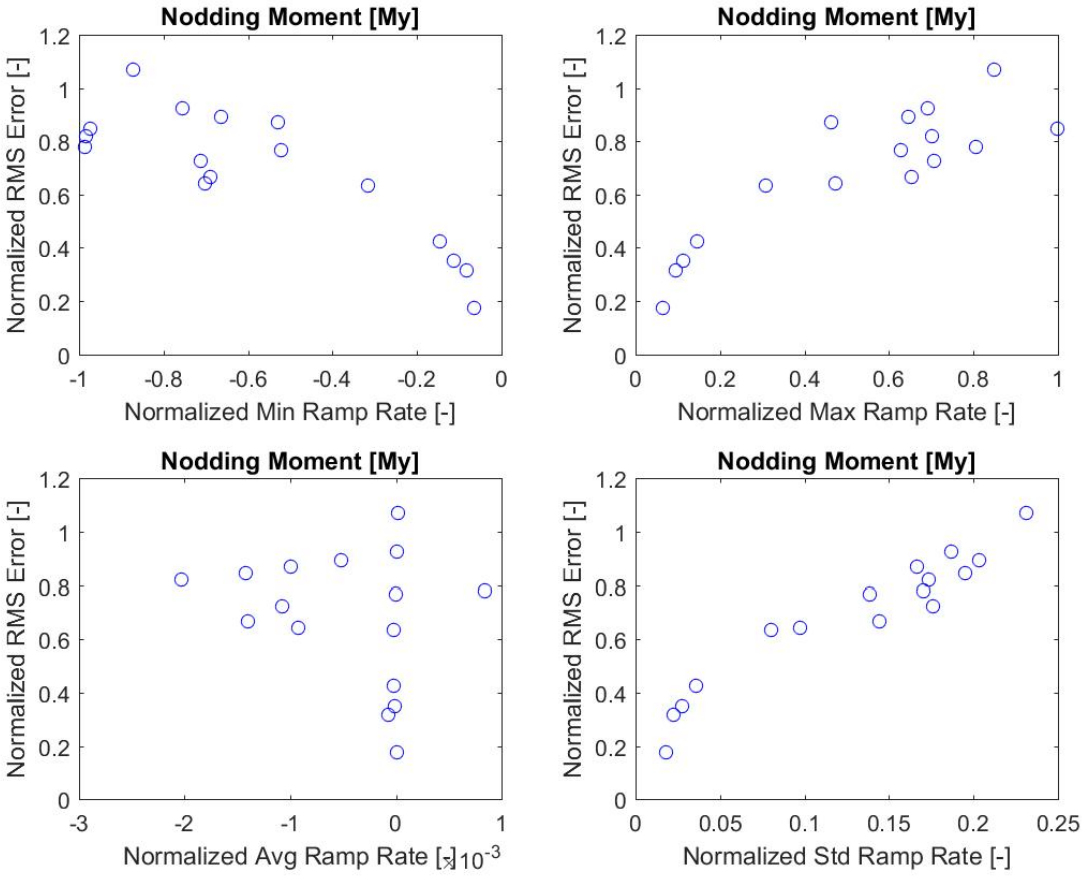

Figure 6.51: Actual RMS error (E normalization) as a function of the normalized minimum (Min), maximum (Max), average (Avg), and standard deviation (Std) of the ramp rate of the nodding moment (My). The normalization of the RMS error is with the measurement error (E normalization) and My is normalized with the maximum peak value from all test profiles.

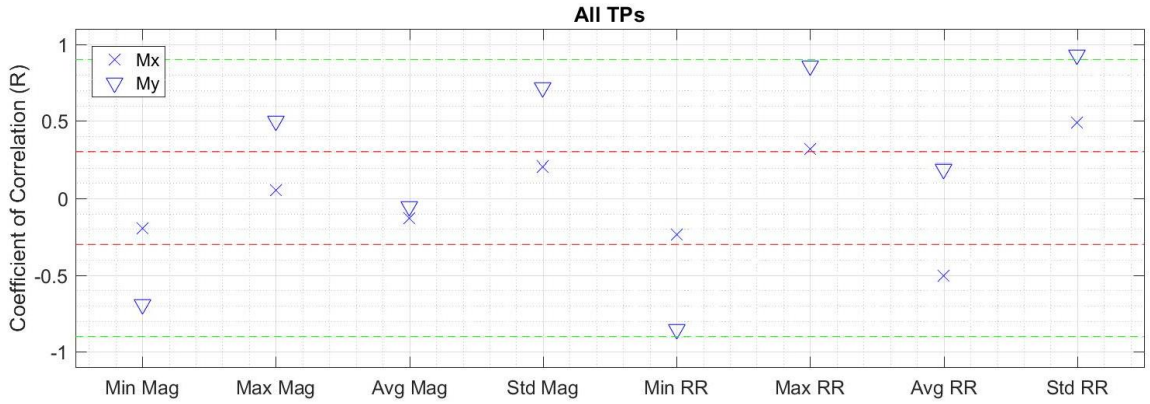

Figure 6.52: Correlation coefficient of test profile characteristics for the yawing moment (Mx) and nodding moment (My) considering the tests done with the nominal test bench limits. The green and red dotted lines represent the threshold for very high and negligible correlation.

The results presented in Figs. 6.48-6.51 and summarized in Fig. 6.52 point to similar observations than those made for the 2.3-MW drivetrain for the nodding moment, but the correlations for the yawing moment are marginal at best.

6.5 Combined data

The combination of the data from both drivetrain is a logical next step to determine if the high level of the correlation observed thus far is preserved and if the drivetrain emerges as a significant factor in the multiple regression. The two drivetrains are captured purely as a binary factor given that they were unchanged over their respective tests.

6.5.1 Single regressions

The adjusted R^2 values for the single regressions are presented in Table 6.9 for the same subgroups considered for the 3.2-MW drivetrain. Combining the data from both drivetrains negatively impacted the correlation with the CR for ramp rate. The correlation with Cov error is essentially unchanged to the results presented when considering the test data set of both turbines individually. This is a sign of robustness of the Cov error metric

and that the drivetrain itself is not a significant factor in predicting the tracking (RMS) error. This may not be surprising given that the results from the test profiles tested with both drivetrains indicated a relatively consistent effect of the drivetrain stiffness and mass on the actual RMS error. To investigate this further, the slopes and offsets of the linear regressions for the cases of the combined data from both drivetrains and each individual drivetrain are presented in Fig. 6.53. The results point to the drivetrain mainly impacting the offset rather than the slope. This is an important finding suggesting that adding additional complexity to the evaluation method to account for the effect of the drivetrain may not be necessary. It may actually be more beneficial to focus on determining the effect of the drivetrain characteristics on the ramp rate limits of a test bench.

Table 6.9: Summary of single regression results for each evaluation metric and data subgroup. The background color reflects the R^2 value with green and yellow used to reflect the range above and below 0.9, respectively.

	Yawing Moment (Mx)						Nodding Moment (My)					
Subgroup	**Cov RMS Error**		**CR Mag**		**CR RR**		**Cov RMS Error**		**CR Mag**		**CR RR**	
	Fit	**Adj R^2**	**Fit**	**Adj R^2**	**Fit**	**Adj R^2**	**Fit**	**Adj R^2**	**Fit**	**Adj R^2**	**Fit**	**Adj R^2**
All	Linear	0.986	None	NA	None	NA	Linear	0.982	None	NA	Exp 2P	0.572
SD	Linear	0.978	None	NA	Exp 3P	0.885	Linear	0.970	None	NA	Exp 3P	0.937

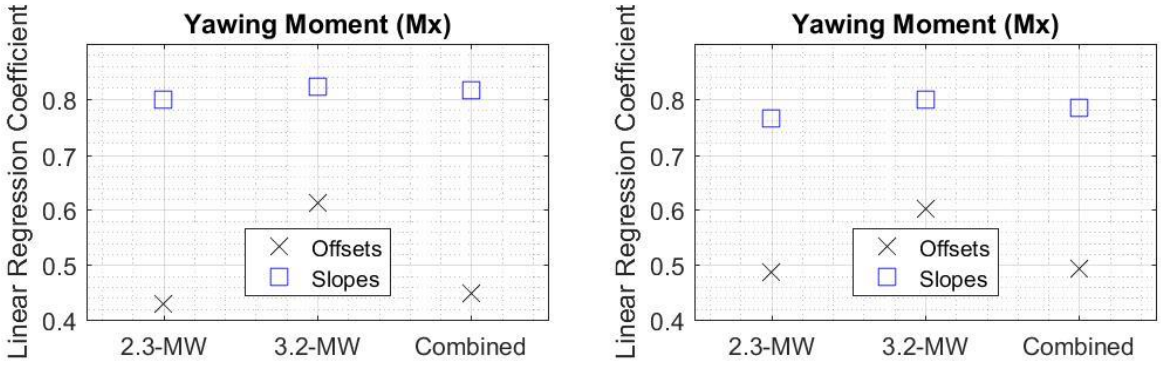

Figure 6.53: Comparison of the linear regression coefficients from the single regressions with the Cov error for the yawing moment (Mx) and the nodding moment (My) when considering the data from each drivetrain individually and when they are combined.

6.5.2 Multiple regressions

The four multiple regressions done with the 3.2-MW drivetrain data were repeated after adding the 2.3-MW data and adding the drivetrain as eligible factor in the multiple regressions. The results are presented in Table 6.10 and Fig. 6.54 with a comparison to the results from the single regression with the Cov error.

Table 6.10: Summary of the significant (S) and non-significant (NS) main effects and two-way interactions from the multiple regressions.

	Yawing Moment (Mx)									
Subgroup	**Main Effects**				**Two-way Interactions**					
	Cov (1)	CR Mag (2)	CR RR (3)	DT (4)	1&2	1&3	1&4	2&3	2&4	3&4
All	S	S	NS	NS	S	NS	NS	NS	NS	NS
SD	S	S	NS	NS	NS	S	NS	NS	NS	NS
	Nodding Moment (My)									
Subgroup	**Main Effects**				**Two-way Interactions**					
	Cov (1)	CR Mag (2)	CR RR (3)	DT (4)	1&2	1&3	1&4	2&3	2&4	3&4
All	S	S	S	NS	S	S	NS	NS	NS	NS
SD	S	NS	S	S	NS	S	NS	NS	NS	NS

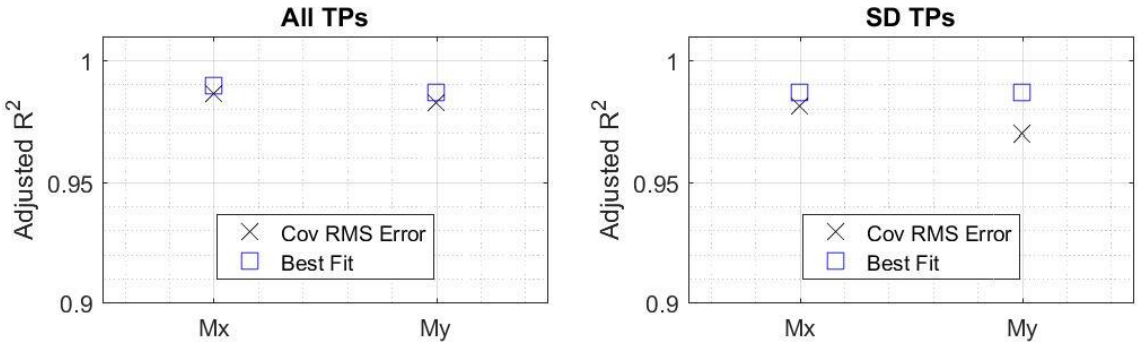

Figure 6.54: Comparison of the adjusted R^2 of the single regression model based on the coverage RMS error and the multiple regression models for the yawing moment (Mx) and nodding moment (My). All test profiles are considered for the results on the left and those of the right are for the shutdown (SD) subgroup.

The differences in correlation is more pronounced with the aggregated data from both drivetrains, but the level of correlation remains high. Although the drivetrain (DT)

was found to be a significant factor for the nodding moment for the SD subgroup, removing this factor from that multiple regressions leaves the adjusted R^2 value essentially unchanged.

6.6 Main findings

The results from the experimental verification with the 3.2-MW drivetrain were found to be in good agreement with those from the 2.3-MW drivetrain. The new findings relate to the effect of the drivetrain on tracking performance and the application of the predictive models derived from the test data from the 2.3-MW drivetrain. The differences in tracking performance between the two drivetrains was found to be small with the tuning of the test bench controller gains being a factor that influenced the results. Applying the predictive models from the 2.3-MW drivetrain to the 3.2-MW drivetrain resulted in large predictive errors suggesting that additional factors of characteristics of the test profiles must be considered to enhance predictive capability. The results presented in this Chapter provides a starting point. Further, the merit of the evaluation methodology to identify dynamic test profiles that a test bench should be able to replicate with an acceptable level is supported by this second experimental verification.

CHAPTER SEVEN

CONCLUSIONS AND RECOMMENDATIONS

Wind turbine drivetrain test facilities are large and impressive laboratory environments. The size of wind turbine drivetrains alone is a challenge and this research focused on perhaps a greater challenge, which is replicating the stochastic loads and speed inputs that wind turbine drivetrains are subjected to from the wind. Applying MN of forces and MNm of bending moments in a consistent and repeatable way is difficult, and the difficulty is much greater when varying loads of that magnitude at rates of MN/s and MNm/s in a stable and safe manner. Wind turbines around the world experience such level of loads variation during their operation and this research sheds light on the capability of a wind turbine drivetrain to replicate such stochastic loads.

This research is the first demonstration of the dynamic capability of a test bench when challenged to replicate the design conditions from the international standard for the design and safety of wind turbines [45]. The conclusions from testing two multi-MW wind turbine drivetrains on the same test bench and modeling one of the two drivetrains are summarized in Section 7.1. Several recommendations emerged over the course of this research and they are presented in Section 7.2. These conclusions and recommendations are the contributions from this research, which are summarized in Section 7.3.

7.1 Conclusions

This research provides answers to two basic questions.

1. What are the design load cases (DLCs) from the International Electrotechnical Commission (IEC) 61400-1 standard that can be tested with sufficient accuracy on a wind turbine drivetrain test bench, and why?

2. What level of accuracy must be achieved when replicating design loads of a wind turbine drivetrain using the LAU of a test bench, and why?

The short answer to the first question is that all DLCs from the IEC 61400-1 standard can be tested as long as the magnitude and rate of change of the loads and speed to be replicated are within the capability of the test bench. In other words, the test bench has the capability to reproduce the frequency content of the loads and speed. This obvious yet important condition directed the focus of this research towards developing and validating the first evaluation method for that purpose.

It is important to note that the conclusion on the ability of a test bench to test a given IEC DLC with sufficient accuracy is based on achieving the expected dynamic response from the combined inputs to the load application unit (LAU) of the test bench. Accordingly, this conclusion should not be interpreted to mean that all LAU inputs are replicated with the same accuracy (tracking error). This research demonstrated that not all LAU inputs are accurately replicated due to the cross-coupling effect between the forces and moments dynamically applied by the LAU, but this research also used modeling to show that the expected dynamic response is achieved despite significant deviations in vertical and lateral forces. Furthermore, the ability of a test bench to test IEC DLCs in which the turbine is parked in extreme winds does not seem to be limited by not capturing the idling motion of the rotor from the LAU at negative speed. This limitation may not apply to all test benches and drivetrains, however, depending on the design of the test bench and the control strategy a wind turbine is using during the parked load cases of the IEC.

The detailed answer to the first question is given in Table 7.1, which list all IEC load cases with the corresponding conclusion about the ability of a test bench to replicate the corresponding loads and speed (rpm) time series.

Table 7.1: IEC design load cases and corresponding capability of a wind turbine drivetrain test bench to replicate with sufficient accuracy.

IEC DLC	Ability to Test with Sufficient Accuracy
Normal power production (DLC # 1.1, 1.2) Power production in extreme wind shear (DLC #1.5)	Can replicate all LAU inputs within the LAU measurement error although not always for Fx and Fy, but the deviations are not significantly changing the dynamic response of the drivetrain. Demonstrated with the 2.3-MW drivetrain.
Power production in extreme turbulence (DLC # 1.3)	Can replicate all LAU inputs slightly above the LAU measurement error except for Fx and Fy. Demonstrated with the 3.2-MW drivetrain.
Power production with extreme direction change (DLC #1.4) Power production with fault from protection system or internal electrical control system fault or loss of electrical network (DLC # 2.2, 2.4)	Can replicate all LAU inputs within the LAU measurement error. Demonstrated with the 3.2-MW drivetrain.
Power production with fault from control system or loss of electrical network (DLC # 2.1, 2.4) Parked turbine in 50-yr extreme wind with loss of electrical network (DLC # 6.2)	Can replicate all LAU inputs within the LAU measurement error although not always for Fx and Fy, but the deviations are not significantly changing the dynamic response of the drivetrain. Demonstrated with the 2.3-MW and 3.2-MW drivetrains.
Power production with internal or external electrical fault or loss of electrical network (DLC # 2.3) Parked turbine in 50-yr extreme wind (DLC # 6.1)	Can replicate all LAU inputs with the LAU measurement error. Demonstrated with the 2.3-MW drivetrain.
Turbine start-up (DLC # 3.1, 3.2, 3.3) Normal shut down (DLC # 4.1, 4.2) Emergency shut down (DLC # 5.1) Parked turbine in 1-yr extreme wind with extreme yaw misalignment (DLC # 6.3) Parked turbine in 1-yr extreme wind and system fault (DLC # 7.1) Turbine transport, assembly, maintenance, and repair (DLC # 8.1, 8.2)	Not tested due to not being a design driver for drivetrains, but no reason to believe these DLCs cannot be tested as the conditions are more benign than those that have been demonstrated with both drivetrains.

Although not all IEC DLCs have been tested, those that were not are typically not design drivers for wind turbine drivetrains because their conditions are more benign than the other DLCs. Accordingly, this research is confident that a conclusion can be drawn for all IEC DLCs with the acknowledgement that this conclusion has not been demonstrated for DLCs 3.1, 3.2, 3.3, 4.1, 4.2, 5.1, 6.3, 7.1, 8.1, and 8.2.

As explained in Chapter Five, answering the second question as worded would certainly make the answer debatable and not useful. Given that this research is very much focused on application rather than fundamentals, the question was reformulated from the context of a test bench operator who should be able to demonstrate that a tracking error up to the LAU measurement error should not significantly change the dynamic response of the drivetrain. Modeling is the only way to demonstrate this and a state-of-the-art multibody simulation software in Simpack was used to make this demonstration based on measurements from testing a 2.3-MW drivetrain onto the 7.5-MW test bench of Clemson University. Although this answer is specific to that test bench, it is expected to be applicable to other drivetrains of similar designs, such as the 3.2-MW that was tested. Also, the method used to arrive at this conclusion is applicable to any test bench, drivetrain, and MBS software.

This research also demonstrated that the excellent correlation between the coverage (RMS) error with the actual RMS error is not specific to a given drivetrain. The effect of the drivetrain on the tracking error was found to be small for the two test profiles considered and could be driven by differences in test bench controller tuning. This secondary contribution can be used as a starting point for improving the predictive capability of the tracking error. Another secondary contribution was to highlight that the vertical force appears to be a contributor to the cross-coupling effect.

7.2 Recommendations

There are several opportunities for advancing the state-of-the-art of testing a wind turbine drivetrain/nacelle on a test bench. Recommended research directions are summarized in Table 7.2 and recommendations relevant to design certification follows.

Table 7.2: Recommended research directions.

Focus Area	Description	Impact
Measurement system and validation	Detailed assessment (bottoms up) of measurement system accuracy under static and dynamic loads.	Increased confidence in the test data and better usage of the data.
	Development of more sophisticated MBS models.	Aid in the planning of a test and complement the testing.
	Drivetrain model validation using test bench data.	Increased confidence in the simulation results and further optimization of drivetrains.
	Comparison between test bench data and data from installed wind turbines.	Improve the understanding of the effect of abstraction on test bench results.
Test bench enhancements	Controller enhancements to reduce cross-coupling between the applied forces and moments.	Improved tracking of the vertical and lateral forces.
	Determine the tracking improvements from tuning the controller for a specific test profile.	Understand if such controller tuning can offset tracking error from test bench hardware.
	Investigate the relationship between the cross-coupling effect and the magnitude of the forces.	A better understanding of the cross-coupling effect enables better compensation.
	Modifications to allow testing at idling speeds.	Replicate the speed conditions of test profiles from parked conditions of a wind turbine in extreme winds.
Methods development	Development of a test sequence for determining the test bench magnitude and ramp rate boundary for a given drivetrain.	Systematic assessment of the test bench capability.
	Development of method to estimate the expected ramp rate limit of a drivetrain prior to the actual testing.	Improve the output from the method for evaluating the test bench capability to replicate dynamic loads.
	Predictive model for the tracking error due solely to the test bench controller.	Improve the method for evaluating the test bench capability to replicate dynamic loads.

The experimental demonstration of accurate tracking of dynamic test profiles that are relevant to the design of wind turbine drivetrain components shows promise for the role of test benches for design certification purposes. Specifically, drivetrain test benches that can apply torque and non-torque loads onto the test article offer the following opportunities.

- Demonstrate (validate) that the drivetrain can withstand the design and simulated loads, which are often from design load cases that cannot be replicated in the field. For example, the loads from a 50-yr gust event can be tested with a wind turbine drivetrain test bench.
- Validate the design margins.
- Validate wind turbine drivetrain models used to extrapolate the input loads to the locations of interest for the drivetrain components.
- Promote the role of hardware-in-the-loop capability to reduce the need for field testing.

A static demonstration of the load carrying capability of a wind turbine drivetrain suffice for the design loads because they include a load factor, which accounts for several factors including the dynamic amplification of the loads. Such demonstration should be possible as long as the test bench has a capability ratio for magnitude that is at least equal to the load factor (and preferably higher) to compensate for the finite stiffness of the drivetrain. This research offers a basis for revisiting the load factor applied to the design-driving loads. This can be pursued by commanding scaled-up simulated loads to the LAU of a test bench. These are dynamic tests and the test bench must of course have the capability to replicate these scaled-up loads. If the drivetrain design can withstand such

dynamic tests and multiple designs are tested with positive outcomes, the results could be used to make a case for altering the load factors applicable to drivetrain loads. This opportunity assumes that the effect of abstraction can be compensated (mitigated), which is a position expressed by IEA Wind Task 35 for most abstractions [30,31].

The modeling of wind turbine drivetrain components and of their assembly as a subsystem yields the design margins. Although this modeling can account for the level of variations allowed during manufacturing and assembly, a verification of the expected design margins of a wind turbine drivetrain can confirm the modeling results or identify additional margins or shortcomings. Additional margins can be used in cost-out efforts or expand the application of the component to higher loads. A shortcoming in design margins can trigger mitigation actions prior to the deployment of production units in large numbers to the field. Admittedly, drawing conclusions from a single test on a single drivetrain design is premature, but the aggregation of such tests over time as additional drivetrains are tested should eventually provide sufficient samples to draw conclusions. The reduction in cycle time for exchanging a drivetrain on a test bench or one or more of its components is an enabler for validating design margins.

The prediction of design margins requires models to extrapolate the drivetrain input loads to the locations of interest for each drivetrain component. The measurements of the drivetrain response to the inputs loads made from testing on a test bench provide the basis for the validation of such models. This research indicated that not only the replication of dynamic test profiles can be sufficiently accurate, but it is also repeatable. This provides an advantage over field tests.

The development of hardware-in-the-loop capability using a wind turbine drivetrain/nacelle test bench assumes that the test bench has the capability to apply the

output loads from the model(s) used to generate those input loads. Accordingly, this research is complementary to the development of HIL capability using a wind turbine drivetrain test bench. As long as the HIL capability is found to adequately capture the effects from the wind and that of the missing rotor and tower, a case can be made for using ground-based testing with a full-scale drivetrain/nacelle to reduce the need for field testing.

7.3 Contributions summary

The research contributions are summarized in Tables 7.3 and 7.4 using questions that motivated this research. Answers in Table 7.3 are based on experimental results from the tests conducted with two multi-MW wind turbine drivetrains whereas those in Table 7.4 are based in MBS simulation results.

Table 7.3: Contributions from this research based on experimental results.

Question	2017 Answer	Answer from this Research
What design load case from the IEC 61400-1 standard can be replicated on a wind turbine drivetrain test bench?	Open question.	Acceptable tracking of the yawing and nodding moments as well as speed have been demonstrated for all of the design load cases of the IEC 61400-1 standard that typically drives the design of wind turbine drivetrains.
How to evaluate the capability of a test bench to replicate test profiles of interest for testing a wind turbine on a test bench?	Make decision based on IEA Wind Task 35 summary [9].	Apply the validated evaluation method presented in this dissertation.
What is the correlation between the tracking error and characteristic of a test profile (e.g., standard deviation of a given load input)?	Open question.	The tracking error due to the test bench controller correlates well with the standard deviation and min/max values of the magnitude and ramp rates of the yawing and nodding moments.

Table 7.4: Contributions from this research based on MBS simulation results.

Question	2017 Answer	Answer from this Research
What level of accuracy must be achieved when replicating design loads of a wind turbine drivetrain on a wind turbine drivetrain test bench?	Open question.	A tracking error for the yawing and nodding moments within the measurement error of the load application unit of the test bench (74 kNm in the case of Clemson's 7.5-MW test bench) is sufficiently accurate. The tracking error on the forces is secondary due to their much smaller magnitudes as compared with the moments.
Is the cross-coupling effect between the forces and moments applied by the LAU of a test bench resulting in unacceptable tracking error?	Open question.	The cross-coupling effect of the magnitude measured during this research was found to be acceptable.

In addition, this research provided observations specific to the effect of the drivetrain on the tracking error, which was found to be small for the test profiles considered (refer to Section 6.1.3.2 for more details). The capability of single and multiple regression models for predicting the actual tracking error was also investigated and quantified. The results showed promise and a need for refinement (refer to Sections 4.4, 6.2.2, 6.3, and 6.5). Overall, this research opened a new avenue of research in the wind energy sector that can expanded using the recommendations made in Section 7.2.

REFERENCES

[1] Global Wind Energy Council (GWEC), “Global Wind Report, Annual Market Update 2018”, p. 28, www.gwec.net/wp-content/uploads/2019/04/GWEC-Global-Wind-Report-2018.pdf (Accessed: April 2019).

[2] Center for Wind Power Drives (RWTH), Aachen University, www.cwd.rwth-aachen.de/1/infrastructure (Accessed: April 2019).

[3] Averous, N.R., Stieneker, M., Kock, S., Andrei, C., Helmedag, A., De Doncker, R.W., Hameyer, K., Jacobs, G., and Monti, A., “Development of a 4 MW Full-Size Wind-Turbine Test Bench”, IEE Journal of Emerging and Selected Topics in Power Electronics, Vol. 5, No. 2, June 2017.

[4] Schkoda, R., and Fox, C., “Integration of Mechanical and Electrical Hardware for Testing Full Scale Wind Turbine Nacelles”, Proceedings of the Power Systems Conference, Clemson University, Clemson, SC, March 11-14, 2014.

[5] Fraunhofer Institute of Wind Energy and Energy System Technology (IWES), Dynamic Nacelle Testing Laboratory (DYNALAB), www.iwes.fraunhofer.de/content/dam/windenergie/de/documents/aktuelleDatenblaetter/DB%20DyNaLab_2017_en%20print.pdf (Accessed: April 2019).

[6] Lindoe Offshore Renewables Center (LORC), Nacelle Testing, www.lorc.dk/test-facilities#lindo-nacelle-testing (Accessed: April 2019).

[7] National Renewable Energy Laboratory (NREL), Dynamometer Research Facilities, http://www.nrel.gov/wind/facilities-dynamometer.html (Accessed: April 2019).

[8] National Renewables Energy Center (NaREC), ore.catapult.org.uk/testing-validation/facilities/powertrains (Accessed: April 2019).

[9] IEA Task Force 35 – Ground Based Testing for Wind Turbines and Their Components, “Test Center Capabilities”, Fact sheet, May 2016 www.cwd.rwth-aachen.de/iea-wind/downloads (Accessed: April 2019).

[10] Holierhoek, J.G. (editor), “PROTEST Final Report: Project Results and Recommendations for Standardisation”, Energy Center of the Netherlands report ECN-E-10-100, Oct. 2010.

[11] PROTEST project, http://www.protest-fp7.eu (Accessed: April 2019).

[12] Schkoda, R., “Sliding Mode Control of a Hydraulically Actuated Load Application Unit with Application to Wind Turbine Drivetrain Testing”, IEEE Control Systems Technology Journal, Vol. 23, No. 6, Nov. 2015.

[13] Jassmann, U., Reiter, and M., Abel D., “Driving Torque Control for a Nacelle Test Bench”, *Journal of Physics: Conference Series* 524 012068, 2014, Science of Making Torque from Wind Conference (TORQUE 2014).

[14] Georg, S., Heyde, S., and Schulte, H., “Sensor Fault-Tolerant Control of a Drivetrain Test Rig an Observer-Based Approach within a Wind Turbine Simulation Model”, Proceedings of the European Workshop on Advanced Control and Diagnosis, Berlin, Germany, November 13-14, 2014.

[15] Leithead, W.E., Rogers, M.C.M., Connor, B., Pierik, J.T.E, Van Engelen, T.G., and O’Reilly, J., “Design of a Controller for a Test-Rig for a Variable Speed Wind Turbine”, Proceedings of the Third IEEE Conference on Control Applications, pp. 239-244, Vol. 1, Glasgow, UK, 1994.

[16] Neshati, M., Jersch, T, and Wenske, J., “Model Based Active Damping of Drive Train Torsional Oscillation for a Full-Scale Wind Turbine Nacelle Test Rig”, Proceedings of the American Control Conference (ACC), pp. 2283-2288, Boston, MA, July 6-8, 2016.

[17] Jassmann, U., Hakenberg, M., and Abel, D., “An Extended Inertia and Eigenfrequency Emulation for Full-Scale Wind Turbine Nacelle Test Benches”, IEEE International Conference on Advanced Intelligent Mechatronics (AIM), Busan, Korea, July 7-11, 2015.

[18] Leisten, C., Jassmann, U., Balshüsemann, J., and Abel, D., “Model Predictive Speed Control of a Wind Turbine System Test Bench”, IFAC Workshop on Control Applications of Optimization CAO, Yekaterinburg, Russia, *IFAC-PapersOnLine*, Vol. 51, Issue 32, pp. 349-354, Oct. 15-19, 2018.

[19] Schkoda, R., and Hall, T., “Hydraulic Spool Valve Modeling for System Level Analysis”, Proceedings of the American Control Conference, Portland, OR, June 4-6, 2014.

[20] Schkoda, R., “Geartrain Reduction for Real-Time Simulation of a Multibody Wind Turbine Gearbox Model”, Proceedings of the ASME Dynamic Systems and Control Conference, San Antonio, TX, Oct. 22-24, 2014.

[21] Panyam, M., Bibo, A., and Roach, S., “On the Multi-Body Modeling and Validation of a Full Scale Wind Turbine Nacelle Test Bench”, Proceedings of the ASME Dynamic Systems and Control Conference (DSCC), Atlanta, GA, Sep. 30 – Oct. 3, 2018.

[22] Bi, L., Schelenz, R., and Jacobs, G., “Dynamic Simulation of Full-Scale Nacelle Test Rig with Focus on Drivetrain Response Under Emulated Loads”, 2nd Conference for Wind Power Drives, Center for Wind Power Drives, Aachen University, March 3-4, 2015.

[23] Matzke, D., Jacobs, G., and Schelenz, R., “Full Scale System Simulation of a 2.7 MW Wind Turbine on a System Test Bench”, Proceedings of the Wind Power Drives Conference, Aachen, Germany, March 7-8, 2017.

[24] Helsen, J., Vanhollebeke, F., De Coninck, F., Vandepitte, D., and Desmet, W., “Insights in Wind Turbine Drive Train Dynamics Gathered by Validating Advanced Models on a Newly Developed 13.2 MW Dynamically Controlled Test-Rig”, *Mechatronics Journal*, Vol. 21, No. 4, pp. 737-752, June 2011.

[25] Guo, Y., Keller, J., Moan, T., and Xing, Y., “Model Fidelity Study of Dynamic Transient Loads in a Wind Turbine Gearbox”, Proceedings of the American Wind Energy Conference (WindPower), Chicago, May 2013.

[26] Marrant, B, Vanhollebeke, and F., Peeters, J., “Comparison of Multibody Simulations and Measurements of Wind Turbine Gearboxes at Hansen’s 13 MW Test Facility”, Proceedings of the European Wind Energy Conference and Exhibition, pp. 2337-2360, Warsaw, April 2010.

[27] Liewen, C., Jacobs, G., and Bosse, D., “Validation of Planetary Bearing Loads in Wind Turbine Gearboxes on a 4 MW System Test Bench’, Proceedings of the Wind Power Drives Conference, Aachen, Germany, March 7-8, 2017.

[28] Matzke, D., Schelenz, R., and Jacobs, G., ”Validation of MBS Modeling Methods to Calculate Bearing and Tooth Loads in the Planetary Gear Stage of a Wind Turbine”, Proceedings of the 2019 Wind Power Drive Conference, Aachen, Germany, March 12-13, 2019.

[29] Schkoda, R., Bibo, A., Guo, Y., Lambert, S., and Wallen, R., “Characterizing the Influence of Abstraction in Full-Scale Wind Turbine Nacelle Testing”, Proceedings of the ASME International Design Engineering Technical Conference and Computer and Information in Engineering Conference (IDTEC/CIE), Charlotte, NC, Aug. 21-24, 2016.

[30] Duda, T., Jacobs, G., and Bosse, D., “IEA Wind task 35 – Full Size Ground Testing of Wind Turbine Nacelles”, Poster presented at the Wind Europe Summit (Turbine Technology), Hamburg, Germany, Sept. 27-29, 2016.

[31] Bosse, D., Duda, T., and Hughes, S., “Final Management Report – IEA Wind TCP Task 35 Full Size Ground Testing for Wind Turbines and their Components”, International Energy Agency, www.community.ieawind.org/viewdocument/task-35-final-management-report (Accessed: April 2019).

[32] Schkoda, R., and Bibo, A., “A Hardware-in-the-loop Strategy for Control of a Wind Turbine Test Bench”, Proceedings of the ASME Dynamic Systems and Control Conference, Columbus, OH, Oct. 28-30, 2015.

[33] Franzen, S., Radner, D., Jacobs, G., Schelenz, R., and Bosse, D., “Hardware in the Loop Operating Mode for Full Size Nacelle Testing”, Proceedings of the European Wind Energy Conference and Exhibition, Barcelona, March 2014.

[34] Helmedag, A., Isermann, T., Jassmann, U., Radner, D., Abel, D., Jacobs, G., and Monti, A., “Testing Nacelles of Wind Turbines with a Hardware in the Loop Test Bench”, IEEE Instrumentation & Measurement Magazine, Vol. 17, Issue 5, pp. 26-33, Oct. 2014.

[35] Neshato, M., Zuga, A., Jersch, T., and Wenske, J., “Hardware-in-the-Loop Drive Train Control for Realistic Emulation of Rotor Torque in A Full-Scale Wind Turbine Nacelle Test Rig”, European Control Conference (ECC), Ålborg, Denmark, pp. 1481-1486, June 29-July 1, 2016.

[36] Neshati, M., Zuga, A., Mehler, C., ”Hard-in-the-Loop Framework with Emulation of Rotor Dynamics for Electrical Certification on a Nacelle System Test Bench”, Proceedings of the 2019 Wind Power Drive Conference, Aachen, Germany, March 12-13, 2019.

[37] Vestas Offshore Wind (2017) *U.S. Leads the World in Offshore Wind Turbine Testing* [Press release]. 27 Oct. Available at www.mhivestasoffshore.com/us-leads-the-world-in-offshore-wind-turbine-testing (Accessed: April 2019).

[38] Catapult, Offshore Renewable Energy (2018*) GE Renewable Energy And ORE Catapult Sign Five-Year R&D Agreement To Advance Offshore Wind Technologies In The UK* [Press release]. 24 April. Available at ore.catapult.org.uk/press-releases/ge-renewable-energy-and-ore-catapult-sign-five-year-rd-agreement-to-advance-offshore-wind-technologies-in-the-uk (Accessed: April 2019).

[39] GE Renewable Energy (2019) *GE Renewable Energy To Test Cypress Onshore Wind Turbine Platform at IWES Lab in Germany* [Press release]. 1 April. Available at www.genewsroom.com/press-releases/ge-renewable-energy-test-cypress-onshore-wind-turbine-platform-iwes-lab-germany (Accessed: April 2019).

[40] Häckerl, M., Fiedmann, H., and Nuber, A., "Observer-based Condition Monitoring for Drive Trains of Offshore Wind Energy Converters – Application to a Large-Scale Test at the CWD", Proceedings of the 2019 Wind Power Drive Conference, Aachen, Germany, March 12-13, 2019.

[41] Giguère, P., and Wagner, J.R., "A Case Study of Evaluating and Augmenting Test Bench Capability for IEC Dynamic Load Cases", Proceedings of the Wind Power Drives Conference, Aachen, Germany, March 7-8, 2017.

[42] Giguère, P., and Wagner, J.R., "Wind Turbine Drivetrain Test Bench Capability to Replicate Design Loads – Part I: Evaluation Methodology", Proceedings of the ASME 11th International Conference on Energy Sustainability, Charlotte, NC, June 27-29, 2017.

[43] Giguère, P., and Wagner, J.R., "Wind Turbine Drivetrain Test Bench Capability to Replicate Design Loads – Part II: Case Study of a Multi-MW Drivetrain", Proceedings of the ASME 11th International Conference on Energy Sustainability, Charlotte, NC, June 27-29, 2017.

[44] Giguère, P., Bibo A., Panyam M., and Wagner, J.R., "Application of a Test Bench to Wind Turbine Drivetrains Subject to Dynamic Loads: Learnings and Recommendations", Proceedings of the 2019 Wind Power Drive Conference, Aachen, Germany, March 12-13, 2019.

[45] International Electrotechnical Commission (IEC) Wind Turbines – Part 1: Design requirements, IEC 61400-1, Third Edition, 2005-08.

[46] Germanisher Lloyd (GL) Guidelines for the Certification of Wind Turbines, Edition 2010, 2010.

[47] Schkoda, R., ”Static Uncertainty Analysis of a Wind Turbine Test Bench’s Load Application Unit”, Proceedings of the American Control Conference, pp. 3150-3155, Chicago, IL, July 2015.

[48] International Electrotechnical Commission (IEC) Wind Turbines – Part 1: Design requirements, IEC 61400-1, Second Edition, 1999-2002.

[49] Baumer Ltd., Technical data sheet for incremental encoders HOG 163, www.baumer.com/asset/medias/__secure__/OADM_12U6460_S35A_web_EN.pdf?mediaPK=8799794233374 (Accessed in April 2019).

[50] Simpack Multibody Simulation Software, http://www.simpack.com (Accessed April 2019).

[51] Baumer Ltd., Technical data sheet for distance sensors OADM 12U6460/S35A, www.baumer.com/asset/medias/__secure__/Baumer_HOG163_DS_EN.pdf?mediaPK=8801023918110 (Accessed in April 2019).

APPENDIX

SUPPLEMENTAL TEST PROFILE INFORMATION

The 28 test profiles considered in this research cover a wide range of magnitude of ramp rate. The peak magnitude of the three forces, two moments and the speed for these 28 test profiles are presented in Fig. A.1 using the maximum value for each load or speed to normalize the data (OP normalization). The test profile number used in this Figure is described in Table A.1. Figure A.2 gives the same information for the peak ramp rate of each load and speed.

Table A.1: Test profile labels used in Figs. A.1 and A.2.

TP #	Drivetrain [MW]	Label	Description
1	2.3	NO 8	Normal operation, 8 m/s average wind speed
2	2.3	NO 12	Normal operation, 12 m/s average wind speed
3	2.3	NO 16	Normal operation, 16 m/s average wind speed
4	2.3	Fx min	Minimum vertical force (Fx)
5	2.3	Fx max	Maximum vertical force (Fx)
6	2.3	Fy min	Minimum lateral force (Fy)
7	2.3	Fy max	Maximum lateral force (Fy)
8	2.3	Fz min	Minimum longitudinal force (Fz)
9	2.3	Fz max	Maximum longitudinal force (Fz)
10	2.3	Fr max	Maximum resultant force (Fr) - resultant from Fx and Fy
11	2.3	Mx min	Minimum yawing moment (Mx)
12	2.3	Mx max	Maximum yawing moment (Mx)
13	2.3	My min	Minimum nodding moment (My)
14	2.3	My max	Maximum nodding moment (My)
15	2.3	Mr min	Minimum resultant moment (Mr) - resultant from Mx and My
16	2.3	Mr max	Maximum resultant moment (Mr) - resultant from Mx and My
17	3.2	Fx min	Minimum vertical force (Fx)
18	3.2	Fx max	Maximum vertical force (Fx)
19	3.2	Fy min	Minimum lateral force (Fy)
20	3.2	Fy max	Maximum lateral force (Fy)
21	3.2	Fz max	Maximum longitudinal force (Fz)
22	3.2	Fr max	Maximum resultant force (Fr) - resultant from Fx and Fy
23	3.2	Mx min	Minimum yawing moment (Mx)
24	3.2	Mx max	Maximum yawing moment (Mx)
25	3.2	My min	Minimum nodding moment (My)
26	3.2	My max case 1	Maximum nodding moment (My) case 1
27	3.2	My max case 2	Maximum nodding moment (My) case 2
28	3.2	Mr max	Maximum resultant moment (Mr) - resultant from Mx and My

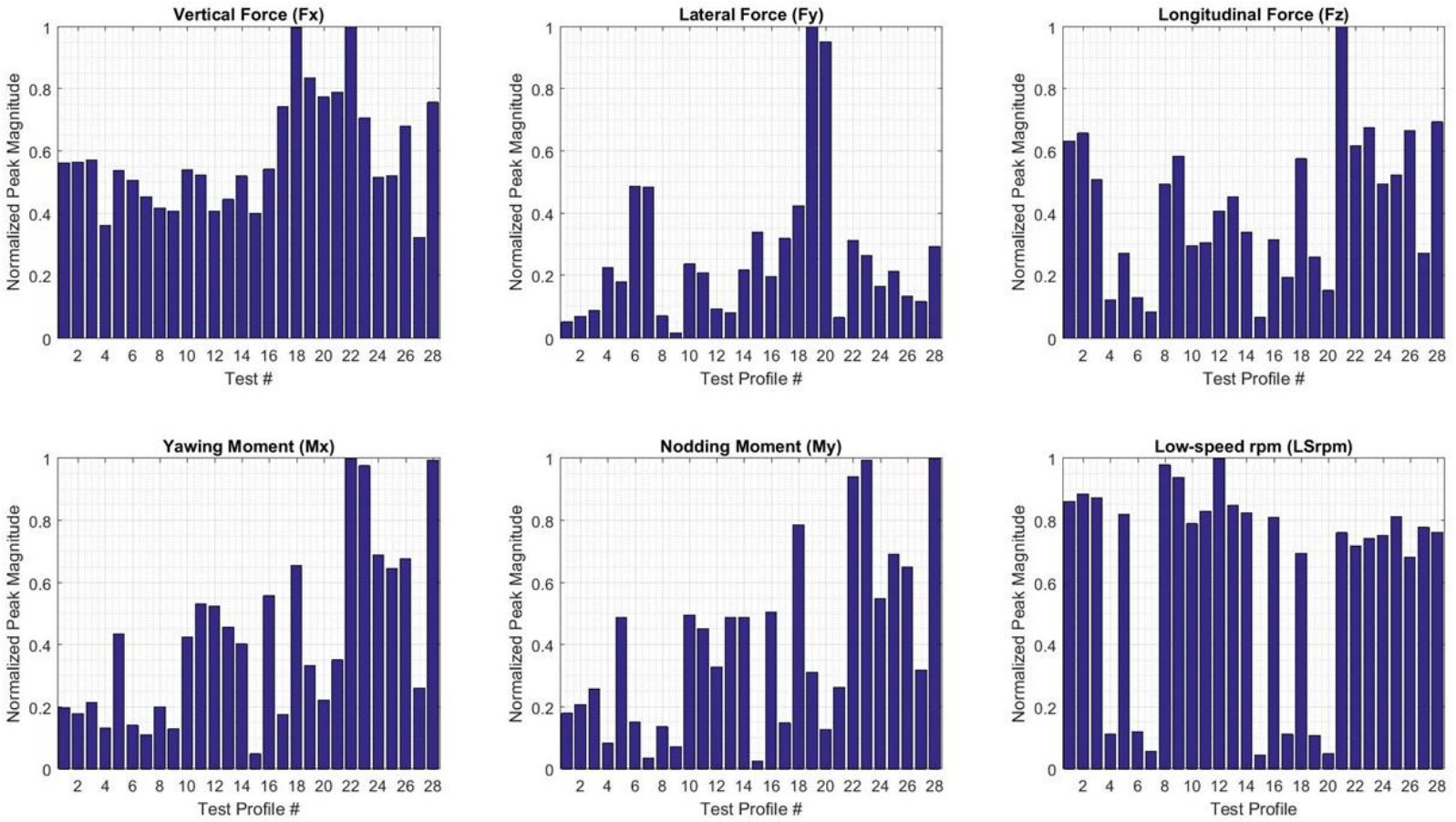

Figure A.1: Peak magnitude of the loads and speed for all test profiles considered in this research (OP norm). Test profiles 1-16 are from the 2.3-MW drivetrain, test profiles 17-28 are from the 3.2-MW drivetrain. Refer to Table A.1 for details.

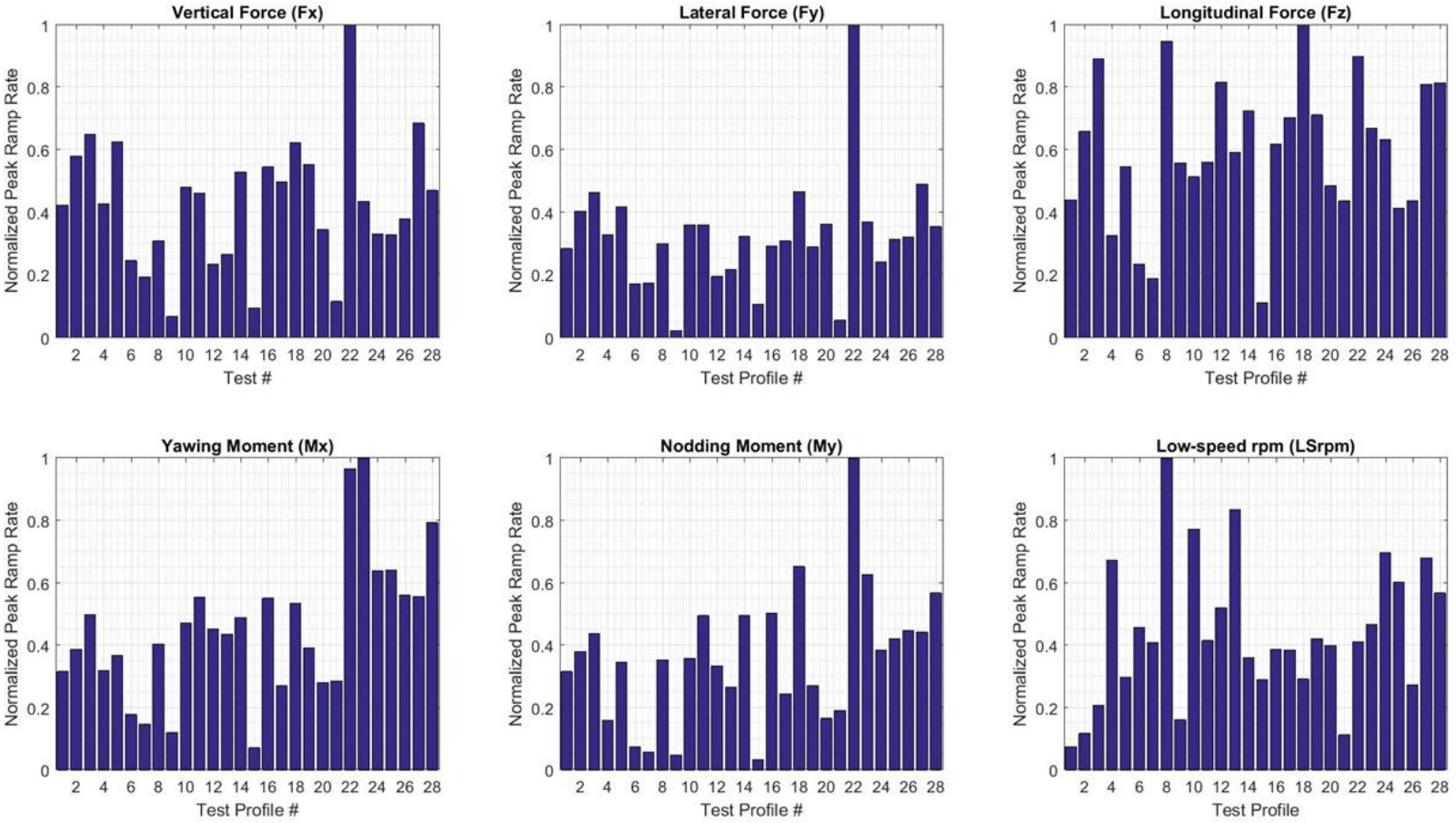

Figure A.2: Peak ramp rate of the loads and speed for all test profiles considered in this research (OP norm). Test profiles 1-16 are from the 2.3-MW drivetrain, test profiles 17-28 are from the 3.2-MW drivetrain. Refer to Table A.1 for details.